

# **Energy-Based Modeling and Tracking Control of Rigid Body Systems with Practical Multicopter Applications**

DISSERTATION  
zur Erlangung des Grades  
**des Doktors der Ingenieurwissenschaften**  
(Dr.-Ing.)  
der Naturwissenschaftlich-Technischen Fakultät II  
– Physik und Mechatronik –  
der Universität des Saarlandes

von

MATTHIAS KONZ

Saarbrücken  
October 22, 2023

# Abstract

Many machines, vehicles and robots may be modeled as rigid body systems, i.e. a number of interconnected, undeformable bodies subject to inertia, gravity, and other forces. Energy-based methods for derivation of their equations of motion, like the Lagrange formalism, are standard in engineering education and well established in the dedicated literature. These algorithms commonly rely on the use of a minimal set of generalized coordinates. This is appropriate for many applications, e.g. machines containing only one-dimensional joints. For systems whose configuration space is nonlinear, e.g. mobile robots whose configuration space contains the rigid body attitude, the use of minimal coordinates necessarily leads to singularities. From the point of view of differential geometry, this is a well known fact.

This work resolves this problem by the use of (possibly) redundant configuration coordinates and (possibly) nonholonomic velocity coordinates. The second chapter reviews several established formalisms of analytical mechanics and states them in terms of these more general coordinates. The third chapter applies these results to rigid body systems. Though inertia is the crucial part of the dynamics, this work also investigates dissipation and stiffness. Finally, it presents an algorithm for the derivation of global equations of motion of general rigid body systems.

The literature states computed-torque is a standard approach for tracking control of fully actuated mechanical systems. However, this recipe relies on minimal coordinates and consequently suffers from the problems mentioned above. There is no established “standard” approach for the control of underactuated systems.

This work presents three slightly different algorithms for tracking control of general rigid body systems by means of static state feedback. These essentially minimize the distance between the actual realizable acceleration of the model and a desired acceleration computed from a stable prototype system. The prototype system shares the geometry and kinematics of the actual model, but may have different constitutive properties (inertia, damping, stiffness). The resulting control law can be computed globally and explicitly for any rigid body system. The resulting closed loop system (which may differ from the prototype in the underactuated case), is invariant to the chosen coordinates, i.e. its formulation is covariant. However, so far, there is no general proof of stability. The performance of the proposed approaches are discussed on several examples and simulation results.

The last chapter of this work discusses the experimental realization of the control approach to two small UAVs. The performance is demonstrated on tracking control for several aerobatic maneuvers.

# Contents

<b>1</b>	<b>Introduction</b>	<b>1</b>
1.1	context and state of the art . . . . .	1
1.2	Motivation example . . . . .	3
1.3	Goal and outline of this work . . . . .	5
<b>2</b>	<b>Calculus with redundant coordinates</b>	<b>7</b>
2.1	Redundant configuration coordinates . . . . .	7
2.2	Minimal velocity coordinates . . . . .	8
2.3	Directional derivative and Hessian . . . . .	10
2.4	Commutation coefficients . . . . .	11
2.5	Linearization about a trajectory . . . . .	13
2.6	Calculus of variations . . . . .	14
<b>3</b>	<b>Analytical mechanics of particle systems</b>	<b>16</b>
3.1	A single free particle . . . . .	16
3.2	Systems of constrained particles . . . . .	18
3.2.1	First principles . . . . .	18
3.2.2	Coordinates . . . . .	19
3.2.3	Inertia . . . . .	22
3.2.4	Gravitation . . . . .	22
3.2.5	Stiffness . . . . .	22
3.2.6	Dissipation . . . . .	23
3.3	A single free rigid body . . . . .	25
3.3.1	Coordinates . . . . .	25
3.3.2	Inertia . . . . .	26

3.3.3	Gravitation . . . . .	29
3.3.4	Stiffness . . . . .	29
3.3.5	Dissipation . . . . .	32
3.3.6	Summary . . . . .	33
3.4	Rigid body systems . . . . .	34
3.4.1	Configuration . . . . .	34
3.4.2	Velocity . . . . .	38
3.4.3	Inertia . . . . .	40
3.4.4	Gravitation . . . . .	41
3.4.5	Stiffness . . . . .	41
3.4.6	Dissipation . . . . .	42
3.4.7	Summary . . . . .	43
3.5	General constraints . . . . .	44
3.6	Energy . . . . .	45
<b>4</b>	<b>Tracking control of rigid body systems</b>	<b>46</b>
4.1	Approach 1: Inspired by particle distribution . . . . .	47
4.1.1	Particle system . . . . .	47
4.1.2	Free rigid body . . . . .	49
4.1.3	Rigid body systems . . . . .	51
4.2	Approach 2: Body based approach . . . . .	53
4.2.1	Free rigid body . . . . .	53
4.2.2	Rigid body systems . . . . .	54
4.3	Approach 3: Inspired by total energy . . . . .	55
4.3.1	Overall structure . . . . .	55
4.3.2	Special cases . . . . .	59
4.3.3	Free rigid body . . . . .	60
4.3.4	Rigid body systems . . . . .	61
4.4	Constant reference and Linearization . . . . .	62
4.5	Underactuated systems . . . . .	63
4.5.1	Control law through static optimization . . . . .	63

4.5.2	Matching condition . . . . .	64
4.5.3	Approximations . . . . .	65
4.5.4	Systems with input constraints . . . . .	66
4.6	Summary and recipe . . . . .	66
4.7	Examples of fully actuated systems . . . . .	69
4.7.1	Prismatic joint . . . . .	69
4.7.2	Revolute joint . . . . .	70
4.7.3	Rigid body orientation . . . . .	72
4.7.4	Planar rigid body . . . . .	74
4.7.5	Decoupling of translational and rotational motion . . . . .	77
4.7.6	SCARA robot . . . . .	80
4.7.7	Robot arm . . . . .	83
4.8	Examples of underactuated systems . . . . .	88
4.8.1	Two masses connected by a spring . . . . .	88
4.8.2	PVTOL . . . . .	90
4.8.3	Quadcopter . . . . .	93
4.8.4	Bicopter . . . . .	95
<b>5</b>	<b>Multicopter control realization</b>	<b>100</b>
5.1	Hardware & software realization . . . . .	101
5.2	Multicopter Models . . . . .	102
5.2.1	Actuator models . . . . .	102
5.2.2	Propeller aerodynamics . . . . .	103
5.2.3	Dissipative forces . . . . .	104
5.2.4	Rigid body model . . . . .	104
5.2.5	Parameter identification . . . . .	107
5.2.6	Model validation and simplification . . . . .	112
5.3	Controller Structure . . . . .	114
5.4	Control of the generalized force . . . . .	114
5.4.1	Servo simulation . . . . .	116
5.4.2	Propeller tracking control . . . . .	117

5.4.3	Tricopter force control . . . . .	118
5.4.4	Quadcopter force vector control . . . . .	121
5.5	State estimation . . . . .	124
5.5.1	IMU model and misalignment correction . . . . .	125
5.5.2	Angular velocity and torque bias . . . . .	127
5.5.3	Configuration measurement delay . . . . .	127
5.5.4	Attitude . . . . .	129
5.5.5	Position, velocity and accelerometer bias . . . . .	131
5.5.6	Force bias . . . . .	133
5.6	Experimental results . . . . .	133
<b>A</b>	<b>Some math</b>	<b>141</b>
A.1	Linear algebra . . . . .	141
A.1.1	Matrix sets . . . . .	141
A.1.2	Trace . . . . .	141
A.1.3	Inner product . . . . .	142
A.1.4	Vee & wedge . . . . .	143
A.2	SVD and polar decomposition . . . . .	144
A.2.1	Singular value decomposition (SVD) . . . . .	144
A.2.2	Polar decomposition . . . . .	144
A.2.3	Special singular decomposition . . . . .	144
A.2.4	Special polar decomposition . . . . .	145
A.3	Attitude potential . . . . .	145
A.4	On error coordinates . . . . .	148
A.5	A possible generalization of the rigid body energies . . . . .	149
<b>B</b>	<b>Templates</b>	<b>155</b>
B.1	Math fonts . . . . .	155

# Chapter 1

## Introduction

### 1.1 context and state of the art

**Modeling.** As the title suggests this work deals with modeling and control of rigid body systems. The procedure of physical modeling is illustrated in Figure 1.1. It starts by approximating the system under consideration by a mechanical model. The mathematical part requires the choice of coordinates  $\mathbf{z}$  to capture the state (positions and velocities) of the model. Combining this with principles of mechanics, we may derive a set of ordinary differential equations that capture its motion. This work mainly deals with this second part, i.e. the derivation of *equations of motion*.

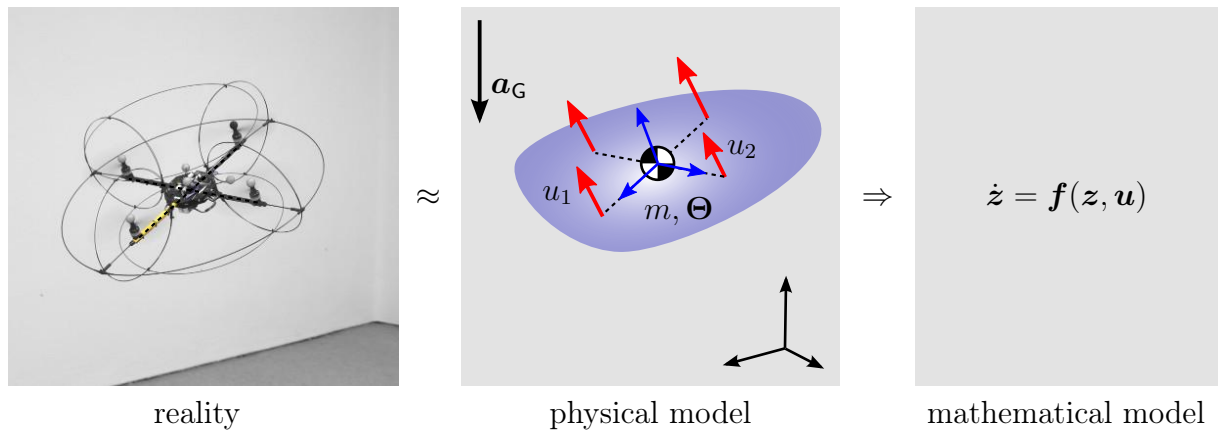


Figure 1.1: Modeling illustration

A very common approach for deriving equations of motion of finite-dimensional, holonomic mechanical systems is the so called *Lagrange formalism*: First, the system is parameterized by so called *generalized coordinates*  $\mathbf{q}$ . Then the kinetic energy  $\mathcal{T}$ , the potential energy  $\mathcal{V}$  and virtual work  $\delta\mathcal{W}$  of external forces are formulated in terms of these coordinates and their derivatives  $\dot{\mathbf{q}} = d\mathbf{q}/dt$ :

$$\mathcal{L}(\mathbf{q}, \dot{\mathbf{q}}) = \mathcal{T}(\mathbf{q}, \dot{\mathbf{q}}) - \mathcal{V}(\mathbf{q}), \quad \delta\mathcal{W}^E = (\delta\mathbf{q})^\top \mathbf{f}^E. \quad (1.1)$$

The equations of motion are derived from the Lagrangian  $\mathcal{L}$  as

$$\frac{d}{dt} \frac{\partial \mathcal{L}}{\partial \dot{\mathbf{q}}} - \frac{\partial \mathcal{L}}{\partial \mathbf{q}} = \mathbf{f}^E. \quad (1.2)$$

The kinetic energy for a time-invariant, mechanical system is always strictly quadratic  $\mathcal{T} = \frac{1}{2} \dot{\mathbf{q}}^\top \mathbf{M}(\mathbf{q}) \dot{\mathbf{q}}$ . Furthermore, we assume that the external forces  $\mathbf{f}^E$  is an affine function of the control inputs  $\mathbf{u}$ . Then the equations of motion take the structure

$$\mathbf{M}(\mathbf{q})\ddot{\mathbf{q}} + \mathbf{b}(\mathbf{q}, \dot{\mathbf{q}}) = \mathbf{B}(\mathbf{q})\mathbf{u} \quad \Leftrightarrow \quad \underbrace{\frac{d}{dt} \begin{bmatrix} \mathbf{q} \\ \dot{\mathbf{q}} \end{bmatrix}}_z = \underbrace{\begin{bmatrix} \dot{\mathbf{q}} \\ \mathbf{M}^{-1}(\mathbf{q})(\mathbf{B}(\mathbf{q})\mathbf{u} - \mathbf{b}(\mathbf{q}, \dot{\mathbf{q}})) \end{bmatrix}}_{\mathbf{f}(z, \mathbf{u})} \quad (1.3)$$

The right hand side of (1.3) is a standard form for simulation, i.e. numerical solution, or general control design. However, the structure of the left hand side of (1.3) can be exploited for a particular control design.

**Feedback Control.** From a mathematical point of view, a feedback controller is some map  $\mathbf{u} = \mathbf{g}(\mathbf{z}, \mathbf{r})$  that computes the control input  $\mathbf{u}$  based on the measured system state  $\mathbf{z}$  and some reference input  $\mathbf{r}$ . The goal is that the resulting controlled system  $\dot{\mathbf{z}} = \mathbf{f}(\mathbf{z}, \mathbf{g}(\mathbf{z}, \mathbf{r})) = \bar{\mathbf{f}}(\mathbf{z}, \mathbf{r})$  has desirable properties.

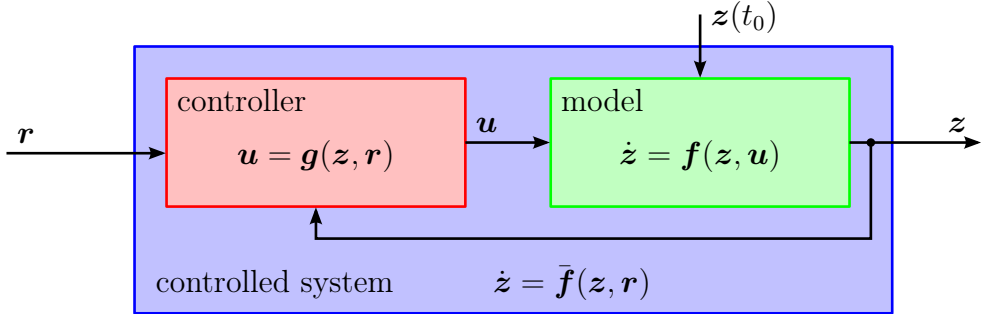


Figure 1.2: Model, controller and controlled system

For a system of the structure (1.3), a typical control objective is, that a given reference trajectory  $t \mapsto \mathbf{q}_R(t)$  is a stable trajectory of the controlled system. If there are as many control inputs as degrees of freedom  $\dim \mathbf{u} = \dim \mathbf{q} = n$  and the input matrix  $\mathbf{B}$  is invertible, there is a popular control approach, commonly called *computed torque*: Defining the error dynamics as

$$\ddot{\mathbf{e}} + \Lambda_1 \dot{\mathbf{e}} + \Lambda_0 \mathbf{e} = \mathbf{0}, \quad \mathbf{e} = \mathbf{q} - \mathbf{q}_R \quad (1.4)$$

with the symmetric, positive definite matrices  $\Lambda_0, \Lambda_1$  as tuning parameters. Combining this with the model (1.3) yields the control law

$$\mathbf{u} = \mathbf{B}^{-1}(\mathbf{M}(\mathbf{q})(\ddot{\mathbf{q}}_R - \Lambda_1 \dot{\mathbf{e}} - \Lambda_0 \mathbf{e}) + \mathbf{b}(\mathbf{q}, \dot{\mathbf{q}})) = \mathbf{g}(\underbrace{\mathbf{q}, \dot{\mathbf{q}}}_z, \underbrace{\mathbf{q}_R, \dot{\mathbf{q}}_R, \ddot{\mathbf{q}}_R}_r) \quad (1.5)$$

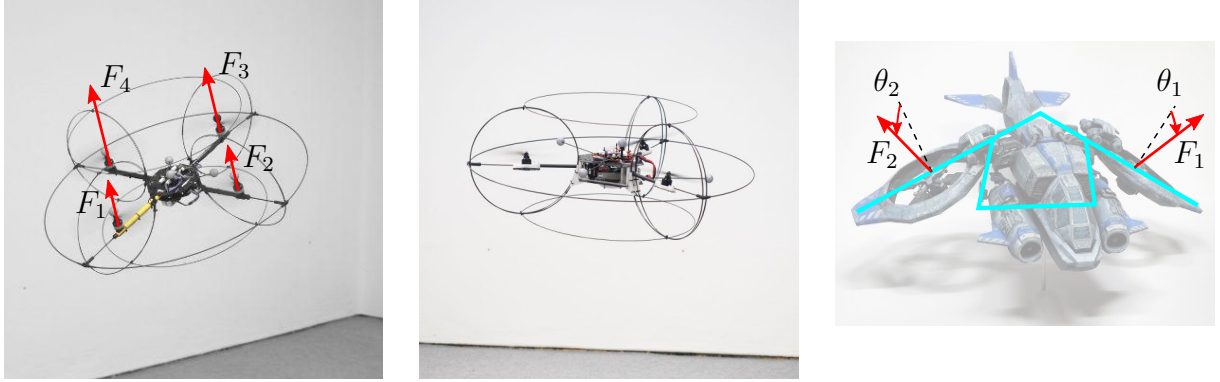


Figure 1.3: lsr-quadcopter (left), lsr-tricopter (middle) and a concept of a bicopter

**Multicopters.** In contrast to conventional helicopters, multicopters are aerial vehicles that use several rigid (fixed pitch) propellers to generate lift and maneuver. They are usually small and unmanned and are used to carry cameras or other sensors. In particular, the four propeller quadcopter configuration has became quite popular over the last two decades.

The *Chair of Systems Theory and Control Engineering* at Saarland University has developed realizations of a quadcopter and a tricopter with three tilttable propellers (see Figure 1.3). A bicopter with two titlable and inclined propellers has been studied through simulations.

From a mechanical point of view, these multicopters may be modelled as a free rigid body moving within Earth's gravity. The difference between them is only the placement of the actuators: the tricopter is fully-actuated, so it poses the easiest control task. The quadcopter only has four actuators for its six degrees of freedom, i.e. it is underactuated. However, its model is well known to be a configuration flat system and corresponding standard control design approaches may be applied. The bicopter is (probably) not a flat system and consequently, poses the toughest control task.

## 1.2 Motivation example

Consider a free rigid body as illustrated in the middle of Figure 1.1, but fixed at its center of mass, i.e. it may only rotate about this point. For simplicity, we also assume that the chosen frame coincides with its principle axis and there are three independent control torques about these axis. Then the coefficients of inertia are  $\boldsymbol{\Theta} = \text{diag}(\Theta_x, \Theta_y, \Theta_z)$ .

**Lagrange's equation.** For application of the Lagrange formalism we need to parameterize the system by minimal generalized coordinates. A popular choice for the rigid body

orientation are Euler angles in the *roll-pitch-yaw* convention:

$$\mathbf{R}(\mathbf{q}) = \begin{bmatrix} c_\varphi c_\beta & -s_\varphi c_\alpha + c_\varphi s_\beta s_\alpha & s_\varphi s_\alpha + c_\varphi s_\beta c_\alpha \\ s_\varphi c_\beta & c_\varphi c_\alpha + s_\varphi s_\beta s_\alpha & -c_\varphi s_\alpha + s_\varphi s_\beta c_\alpha \\ -s_\beta & c_\beta s_\alpha & c_\beta c_\alpha \end{bmatrix}, \quad (1.6a)$$

$$\boldsymbol{\omega}(\mathbf{q}, \dot{\mathbf{q}}) = \underbrace{\begin{bmatrix} 1 & 0 & -s_\beta \\ 0 & c_\alpha & c_\beta s_\alpha \\ 0 & -s_\alpha & c_\beta c_\alpha \end{bmatrix}}_{\mathbf{Y}(\mathbf{q})} \underbrace{\begin{bmatrix} \dot{\alpha} \\ \dot{\beta} \\ \dot{\varphi} \end{bmatrix}}_{\dot{\mathbf{q}}}. \quad (1.6b)$$

The shortcut notation  $s_\varphi := \sin(\varphi)$  and  $c_\varphi := \cos(\varphi)$  used here, will be used throughout this text. With this, we may formulate the kinetic energy  $\mathcal{T}(\mathbf{q}, \dot{\mathbf{q}}) = \frac{1}{2}(\boldsymbol{\omega}(\mathbf{q}, \dot{\mathbf{q}}))^\top \boldsymbol{\Theta} \boldsymbol{\omega}(\mathbf{q}, \dot{\mathbf{q}})$  which coincides with the Lagrangian since there is no potential energy. Evaluation of Lagrange's equation (1.2) yields the equations of motion

$$\underbrace{\begin{bmatrix} \Theta_x & 0 & -\Theta_x s_\beta \\ 0 & \Theta_y c_\alpha^2 + \Theta_z s_\alpha^2 & (\Theta_y - \Theta_z) c_\alpha s_\alpha c_\beta \\ -\Theta_x s_\beta & (\Theta_y - \Theta_z) c_\alpha s_\alpha c_\beta & \Theta_x s_\beta^2 + (\Theta_y s_\alpha^2 + \Theta_z c_\alpha^2) c_\beta^2 \end{bmatrix}}_{\mathbf{M}(\mathbf{q})} \underbrace{\begin{bmatrix} \ddot{\alpha} \\ \ddot{\beta} \\ \ddot{\varphi} \end{bmatrix}}_{\ddot{\mathbf{q}}} + \underbrace{\begin{bmatrix} (\Theta_y - \Theta_z) c_\alpha s_\alpha \dot{\beta}^2 + \dots \\ 2(\Theta_z - \Theta_y) s_\alpha c_\alpha \dot{\beta} \dot{\alpha} + \dots \\ (2(\Theta_y - \Theta_z) c_\alpha^2 - \Theta_x - \Theta_y + \Theta_z) c_\beta \dot{\beta} \dot{\alpha} + \dots \end{bmatrix}}_{\mathbf{b}(\mathbf{q}, \dot{\mathbf{q}})} = \underbrace{\begin{bmatrix} 1 & 0 & 0 \\ 0 & c_\alpha & -s_\alpha \\ -s_\beta & c_\beta s_\alpha & c_\beta c_\alpha \end{bmatrix}}_{\mathbf{Y}^\top(\mathbf{q})} \underbrace{\begin{bmatrix} \tau_x \\ \tau_y \\ \tau_z \end{bmatrix}}_u. \quad (1.7)$$

The entries in  $\mathbf{b}$  are not displayed here since they would fill several lines and are actually not of relevance here. What is crucial here is that the model has singularities at  $\beta = \pm \frac{\pi}{2}$ :  $\det \mathbf{M} = \Theta_x \Theta_y \Theta_z c_\beta^2$  and  $\det \mathbf{Y} = c_\beta$ . Consequently this model is neither suited for a global simulation nor for application of computed torque control.

**Euler's rotation equations.** For this particular example one finds another formulation of the equations of motion directly in most textbooks on mechanics, e.g. [Arnold, 1989, p. 143] or [Roberson and Schwertassek, 1988, p. 145]:

$$\underbrace{\frac{d}{dt} \begin{bmatrix} R_x^x & R_y^x & R_z^x \\ R_x^y & R_y^y & R_z^y \\ R_x^z & R_y^z & R_z^z \end{bmatrix}}_{\mathbf{R}} = \underbrace{\begin{bmatrix} R_x^x & R_y^x & R_z^x \\ R_x^y & R_y^y & R_z^y \\ R_x^z & R_y^z & R_z^z \end{bmatrix}}_{\mathbf{R}} \underbrace{\begin{bmatrix} 0 & -\omega_z & \omega_y \\ \omega_z & 0 & -\omega_x \\ -\omega_y & \omega_x & 0 \end{bmatrix}}_{\text{wed } \boldsymbol{\omega}}, \quad (1.8a)$$

$$\underbrace{\begin{bmatrix} \Theta_x & 0 & 0 \\ 0 & \Theta_y & 0 \\ 0 & 0 & \Theta_z \end{bmatrix}}_{\boldsymbol{\Theta}} \underbrace{\begin{bmatrix} \dot{\omega}_x \\ \dot{\omega}_y \\ \dot{\omega}_z \end{bmatrix}}_{\dot{\boldsymbol{\omega}}} + \underbrace{\begin{bmatrix} 0 & -\omega_z & \omega_y \\ \omega_z & 0 & -\omega_x \\ -\omega_y & \omega_x & 0 \end{bmatrix}}_{\text{wed } \boldsymbol{\omega}} \underbrace{\begin{bmatrix} \Theta_x & 0 & 0 \\ 0 & \Theta_y & 0 \\ 0 & 0 & \Theta_z \end{bmatrix}}_{\boldsymbol{\Theta}} \underbrace{\begin{bmatrix} \omega_x \\ \omega_y \\ \omega_z \end{bmatrix}}_{\boldsymbol{\omega}} = \underbrace{\begin{bmatrix} \tau_x \\ \tau_y \\ \tau_z \end{bmatrix}}_u. \quad (1.8b)$$

The 9 coefficients of the matrix  $\mathbf{R}$  have to obey the constraint  $\mathbf{R}^\top \mathbf{R} = \mathbf{I}_3$ . However, it can be shown that if this is fulfilled for the initial condition  $\mathbf{R}(t_0)$ , then the kinematic equation (1.8a) ensures that the condition remains fulfilled. This formulation has no singularities and is well suited for global simulation. Moreover, loosely speaking, its mathematical

structure reflects the physical symmetries of the model. The obvious draw-back is that due to the lack of generalized coordinates, its unclear how a method like computed torque could be applied.

**Discussion.** Euler's equations (1.8) and (1.7) describe the same system. In fact one may plug (1.6b) into (1.8b) and multiply it by  $\mathbf{Y}^\top$  to obtain (1.7).

Each of these formulations has its advantages and draw-backs: Euler's equations are more compact and have a symmetric structure in contrast to (1.7). The downside is that they require 9 coordinates, the coefficients of the rotation matrix  $\mathbf{R}$ , to parameterize the attitude, whereas the Euler-angles  $\mathbf{q}$  only require 3. The crucial advantage of Lagrange's equation (1.2) is, that it holds for *any* finite dimensional and holonomic mechanical system, whereas Euler's equations only hold for this particular example. However, for this example, the equations (1.7) are quite cumbersome and lack an obvious structure. Probably the worst fact is that the inertia matrix  $\mathbf{M}(\mathbf{q})$  is singular at the point  $\beta = \pm\frac{\pi}{2}$  and consequently  $\ddot{\mathbf{q}}$  is undefined at these points.

It should be stressed that there is no physical reason for the singularity in Example [Example:EulerAngles], it is rather a consequence of an unsuitable parameterization of the system. The problem arises from the fact the the configuration space  $\mathfrak{X}$  determined by the geometric constraints [eq:ThreeParticleConstraint], though having  $\dim \mathfrak{X} = 3$ , is not homeomorphic to  $\mathbb{R}^3$ .

The problem is brought to the point in [Roberson and Schwertassek, 1988, sec. 1.1.1]:

*[The scientists of the Eighteenth Century] recognized that there was something about rotation [...] which somehow made the analysis of rotation a problem of higher order difficulty. We now know that the problem is in the mathematics, not the physics, but the problem is still with us.*

## 1.3 Goal and outline of this work

The first chapter reviews established methods of analytical mechanics with the addition of allowing redundant coordinates (like the coefficients of a rotation matrix  $\mathbf{R}$ ) and non-holonomic velocity coordinates (like the coefficients of the angular velocity  $\boldsymbol{\omega}$ ). It will present a formulation that can derive both of the presented equations of motion for the motivation example, but holds for general finite-dimensional mechanical systems.

The second chapter specializes to rigid body systems, i.e. systems that consist of several interconnected rigid bodies. It presents an algorithm that derives the equations of motion based on chosen coordinates and given constitutive parameters. Furthermore, natural formulations of stiffness, dissipation and inertia for a rigid body are established.

The third chapter proposes tracking control algorithms for rigid body systems. Based on the findings of the second chapter it will present three control algorithms motivated by defining desired stiffness, damping and inertia of the resulting controlled system. Further-

more, these algorithms are extended to tackle underactuated systems. These algorithms are discussed through several examples.

The fourth chapter presents the developed quadcopter and tricopter and their performance for real control of aerobatic maneuvers.

# Chapter 2

## Calculus with redundant coordinates

The example of the rigid body orientation showed that, though its degree of freedom is  $n = 3$ , it cannot be *globally* parameterized by 3 coordinates without having singularities. In other words, the configuration space of the rigid body orientation is not isomorphic to  $\mathbb{R}^3$  and is called a nonlinear manifold.

If interested in a global parameterization of a  $n$  dimensional nonlinear manifold, there are two common approaches:

1. Choose a finite number of overlapping local charts with with *minimal* coordinates  $\mathbf{q} \in \mathbb{R}^n$ , e.g. four distinct sets of Euler angles for the rigid body attitude [Grafarend and Kühnel, 2011]. As this is the common way of defining a smooth manifold, this is always possible.
2. Choose one parameterization with *redundant* coordinates  $\mathbf{x} \in \mathbb{R}^\nu$ , i.e. coordinates that are constrained by smooth equations of the form  $\phi(\mathbf{x}) = \mathbf{0}$ . E.g. the coefficients of the rotation matrix as done in (1.8). *Whitney embedding theorem* states that this is always possible with at least  $\nu = 2n$  coordinates.

Both approaches have benefits and drawbacks depending on the application, but the first approach and the use of minimal coordinates are far more dominant in the literature. This work utilizes the second approach.

This chapter reviews mathematical tools required for analytical mechanics for the context of redundant coordinates.

### 2.1 Redundant configuration coordinates

In the notation of this work, we use  $\nu > 0$  coordinates  $\mathbf{x}(t) = [x^1(t), \dots, x^\nu(t)]^\top \in \mathbb{R}^\nu$  that might be constrained by  $c \geq 0$  smooth functions of the form  $\phi(\mathbf{x}) = [\phi^1(\mathbf{x}), \dots, \phi^c(\mathbf{x})]^\top = \mathbf{0}$ . For  $c > 0$  these coordinates are not independent and are commonly called *redundant*. The set of mutually admissible coordinates is called the configuration space  $\mathbb{X}$ :

$$\mathbb{X} = \{\mathbf{x} \in \mathbb{R}^\nu \mid \phi(\mathbf{x}) = \mathbf{0}\}. \quad (2.1)$$

Assuming that the rank of  $\frac{\partial \phi}{\partial \mathbf{x}}$  is constant, the dimension of the configuration space is

$$n = \dim \mathbb{X} = \nu - \text{rank } \frac{\partial \phi}{\partial \mathbf{x}}. \quad (2.2)$$

For holonomic systems,  $n$  is also called its degree of freedom.

Whitney embedding theorem (see e.g. [Lee, 2003, Theo. 6.14]) states that: *Every smooth manifold of dimension  $n$  can be smoothly embedded in the Euclidean space  $\mathbb{R}^{2n}$ .* The number  $2n$  is a worst case bound, i.e. for a particular example a lower dimension for the embedding space  $\mathbb{R}^\nu$  might work and a higher dimension is permitted anyway. For this work, it essentially guarantees the existence of a global parameterization by the set  $\mathbb{X}$  for any smooth manifold.

## 2.2 Minimal velocity coordinates

For the following it is crucial to note that a geometric constraint is equivalent to its derivative supplemented with a suitable initial condition

$$\phi^\kappa(\mathbf{x}) = 0 \quad (2.3a)$$

$$\Leftrightarrow \frac{\partial \phi^\kappa}{\partial x^\alpha}(\mathbf{x}) \dot{x}^\alpha = 0, \quad \phi^\kappa(\mathbf{x}_0) = 0 \quad (2.3b)$$

$$\Leftrightarrow \frac{\partial \phi^\kappa}{\partial x^\alpha}(\mathbf{x}) \ddot{x}^\alpha + \frac{\partial^2 \phi^\kappa}{\partial x^\alpha \partial x^\beta}(\mathbf{x}) \dot{x}^\beta \dot{x}^\alpha = 0, \quad \phi^\kappa(\mathbf{x}_0) = 0, \quad \frac{\partial \phi^\kappa}{\partial x^\alpha}(\mathbf{x}_0) \dot{x}_0^\alpha = 0 \quad (2.3c)$$

...

where  $\mathbf{x}_0 = \mathbf{x}(t_0)$ . Even though (2.3a) might be nonlinear, its derivative (2.3b) is always *linear* in the velocities  $\dot{\mathbf{x}}$ . So here it is reasonable to choose *minimal velocity coordinates*: Let  $\mathbf{A}(\mathbf{x}) \in \mathbb{R}^{\nu \times n}$  be a matrix with the properties  $\frac{\partial \phi}{\partial \mathbf{x}} \mathbf{A} = \mathbf{0}$  and  $\text{rank } \mathbf{A} = n$ . The first property of  $\mathbf{A}(\mathbf{x})$  is that these columns of  $\mathbf{A}(\mathbf{x})$  are orthogonal to the rows of  $\frac{\partial \phi}{\partial \mathbf{x}}(\mathbf{x})$ . The second property implies that the columns of  $\mathbf{A}(\mathbf{x})$  are linearly independent. So the columns of  $\mathbf{A}(\mathbf{x})$  can be interpreted as a *basis vectors* for the tangent space  $T_{\mathbf{x}} \mathbb{X}$ . We can capture all allowed velocities  $\dot{\mathbf{x}}(t)$  by the minimal velocity coordinates  $\xi(t) \in \mathbb{R}^n$  through

$$\dot{\mathbf{x}} = \mathbf{A}(\mathbf{x}) \xi \quad (2.4)$$

This kinematic relation (2.4) ensures that the time derivative (2.3b) of the geometric constraint is fulfilled, and consequently the geometric constraint only has to be imposed on the initial condition  $\phi(\mathbf{x}(t_0)) = \mathbf{0}$ .

**Example 1.** Consider a single particle constrained to a circle of radius  $\rho$  as illustrated in Figure 2.1.

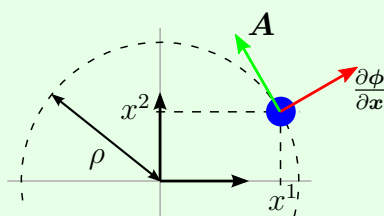


Figure 2.1: Particle on a circle

We use the its Cartesian position  $[x^1, x^2]^\top \in \mathbb{R}^2$  constrained by  $\phi = (x^1)^2 + (x^2)^2 - \rho^2 = 0$  as configuration coordinates. A reasonable choice for the kinematics matrix  $\mathbf{A}$  is motivated from

$$\underbrace{\begin{bmatrix} 2x^1 & 2x^2 \end{bmatrix}}_{\frac{\partial \phi}{\partial \mathbf{x}}} \underbrace{\begin{bmatrix} -x^2 \\ x^1 \end{bmatrix}}_{\mathbf{A}} = 0 \quad (2.5)$$

**Example 2.** Consider again the system from Example [Example:ThreeParticles](#). Instead of parameterizing the rotation matrix  $\mathbf{R}$  by minimal coordinates we now take its 9 coefficients  $\mathbf{x} = [R_x^x, R_y^y, R_z^z, R_x^y, R_y^y, R_z^y, R_x^z, R_y^z, R_z^z]^\top \in \mathbb{R}^9$  as configuration coordinates. The constraints  $\mathbf{R}^\top \mathbf{R} = \mathbf{I}_3$  and  $\det \mathbf{R} = 1$  read

$$\phi(\mathbf{x}) = \begin{bmatrix} (R_x^x)^2 + (R_y^y)^2 + (R_z^z)^2 - 1 \\ (R_x^y)^2 + (R_y^y)^2 + (R_z^y)^2 - 1 \\ (R_x^z)^2 + (R_y^z)^2 + (R_z^z)^2 - 1 \\ R_y^x R_x^x + R_y^y R_z^y + R_y^z R_z^z \\ R_x^x R_z^x + R_x^y R_z^y + R_x^z R_z^z \\ R_x^y R_z^x + R_x^y R_z^y + R_x^z R_z^z \\ R_x^x R_y^x + R_x^y R_y^y + R_x^z R_y^z \\ R_x^x R_y^z + R_y^y R_z^y + R_z^z R_x^z - R_x^y R_z^y - R_y^x R_z^z - R_z^x R_y^z - 1 \end{bmatrix} = \mathbf{0}. \quad (2.6)$$

The 9 conditions  $\mathbf{R}^\top \mathbf{R} = \mathbf{I}_3$  yields due to symmetry only 6 constraints and already imply  $\det \mathbf{R} = \pm 1$ . Since the determinant is a smooth function, the corresponding manifold must consist of two disjoint components, one with  $\det \mathbf{R} = +1$  (proper rotations) and one with  $\det \mathbf{R} = -1$  (rotations with reflection). So the additional constraint  $\det \mathbf{R} = +1$  does not change the dimension of the configuration space. Formally this means  $\text{rank } \frac{\partial \phi}{\partial \mathbf{x}} = 6$  and consequently  $\dim \mathbb{X} = 9 - 6 = 3$ . A kinematics matrix with  $\frac{\partial \phi}{\partial \mathbf{x}} \mathbf{A} = \mathbf{0}$  and  $\text{rank } \mathbf{A} = 3$  is given by

$$\mathbf{A}(\mathbf{x}) = \begin{bmatrix} 0 & -R_z^x & R_y^x \\ 0 & -R_z^y & R_y^y \\ 0 & -R_z^z & R_z^y \\ R_z^x & 0 & -R_x^x \\ R_z^y & 0 & -R_x^y \\ R_z^z & 0 & -R_x^z \\ -R_y^x & R_x^x & 0 \\ -R_y^y & R_x^y & 0 \\ -R_y^z & R_x^z & 0 \end{bmatrix}. \quad (2.7)$$

The resulting kinematic equation  $\dot{\mathbf{x}} = \mathbf{A}(\mathbf{x})\xi$  can be reordered to the matrix equation  $\dot{\mathbf{R}} = \mathbf{R} \text{wed}(\xi)$  by introducing the *wedge operator* defined as

$$\text{wed} \begin{bmatrix} \xi^1 \\ \xi^2 \\ \xi^3 \end{bmatrix} = \begin{bmatrix} 0 & -\xi^3 & \xi^2 \\ \xi^3 & 0 & -\xi^1 \\ -\xi^2 & \xi^1 & 0 \end{bmatrix}. \quad (2.8)$$

**Some identities involving the pseudo-inverse.** For any matrix  $\mathbf{S} \in \mathbb{R}^{m \times n}$  there exists a unique (*Moore-Penrose*) pseudoinverse  $\mathbf{S}^+ \in \mathbb{R}^{n \times m}$  determined by the following conditions [Penrose, 1955, Theo. 1]:

$$\mathbf{S}\mathbf{S}^+\mathbf{S} = \mathbf{S}, \quad (2.9a)$$

$$\mathbf{S}^+\mathbf{S}\mathbf{S}^+ = \mathbf{S}^+, \quad (2.9b)$$

$$(\mathbf{S}\mathbf{S}^+)^\top = \mathbf{S}\mathbf{S}^+, \quad (2.9c)$$

$$(\mathbf{S}^+\mathbf{S})^\top = \mathbf{S}^+\mathbf{S}. \quad (2.9d)$$

If the matrix  $\mathbf{S}$  has linearly independent columns, its pseudoinverse is  $\mathbf{S}^+ = (\mathbf{S}^\top \mathbf{S})^{-1} \mathbf{S}^\top$ . Similarly, if  $\mathbf{S}$  has linearly independent rows, its pseudoinverse is  $\mathbf{S}^+ = \mathbf{S}^\top (\mathbf{S} \mathbf{S}^\top)^{-1}$ .

Define  $\mathbf{Y}(\mathbf{x}) \in \mathbb{R}^{n \times \nu}$  as  $\mathbf{Y} = \mathbf{A}^+ = (\mathbf{A}^\top \mathbf{A})^{-1} \mathbf{A}^\top$ , i.e. the pseudoinverse of the kinematics matrix  $\mathbf{A}$ . Note that this implies  $\mathbf{Y}\mathbf{A} = \mathbf{I}_n$ , but  $\mathbf{A}\mathbf{Y} \neq \mathbf{I}_\nu$ . We also introduce the matrices  $\boldsymbol{\Phi} = \frac{\partial \phi}{\partial \mathbf{x}}$  and  $\boldsymbol{\Psi} = \boldsymbol{\Phi}^+$ . With  $\boldsymbol{\Phi}\mathbf{A} = \mathbf{0}$  and the Penrose conditions (2.9), we can show<sup>1</sup> that  $\boldsymbol{\Psi}^\top \mathbf{A} = \mathbf{0}$  and  $\mathbf{Y}^\top \boldsymbol{\Phi} = \mathbf{0}$ . Furthermore, since  $\text{rank } \boldsymbol{\Psi} = \text{rank } \boldsymbol{\Phi} = \nu - n$  the columns of  $\boldsymbol{\Psi}(\mathbf{x})$  span the complementary space  $(T_{\mathbf{x}}\mathbb{X})^\perp$  though they might not be a basis since the columns might not be linearly independent.

The matrix  $\mathbf{P} = \mathbf{A}\mathbf{Y}$  is an *orthogonal projector*, i.e.  $\mathbf{P}^2 = \mathbf{P}$  and  $\mathbf{P}^\top = \mathbf{P}$  which result directly from the Penrose conditions (2.9). It is in fact the unique orthogonal projector from  $\mathbb{R}^\nu$  to the tangent space  $T_{\mathbf{x}}\mathbb{X}$ . The unique orthogonal projector to the complementary space  $(T_{\mathbf{x}}\mathbb{X})^\perp$  is  $\mathbf{P}^\perp = \mathbf{I}_\nu - \mathbf{P}$ . On the other hand, since  $\boldsymbol{\Psi}$  spans the complementary space the complementary projector can also be expressed as  $\mathbf{P}^\perp = \boldsymbol{\Psi}\boldsymbol{\Phi}$ . This leads to the identity

$$\underbrace{\mathbf{AY}}_{\mathbf{P}} + \underbrace{\boldsymbol{\Psi}\boldsymbol{\Phi}}_{\mathbf{P}^\perp} = \mathbf{I}_\nu. \quad (2.10)$$

In summary: for  $\boldsymbol{\Phi}$  and  $\mathbf{A}$  with  $\boldsymbol{\Phi}\mathbf{A} = \mathbf{0}$  we have

$$\mathbf{S}^+\mathbf{S}\mathbf{S}^+ = \mathbf{S}^+, \quad (2.11a)$$

$$(\mathbf{S}\mathbf{S}^+)^\top = \mathbf{S}\mathbf{S}^+, \quad (2.11b)$$

$$(\mathbf{S}^+\mathbf{S})^\top = \mathbf{S}^+\mathbf{S}. \quad (2.11c)$$

## 2.3 Directional derivative and Hessian

Consider a function  $\mathcal{V} : \mathbb{R}^\nu \rightarrow \mathbb{R}$  and a curve  $\mathbf{x} : \mathbb{R} \rightarrow \mathbb{X}$ . Since  $\mathbb{X} \subset \mathbb{R}^\nu$ , their composition  $\mathcal{V} \circ \mathbf{x} = f : \mathbb{R} \rightarrow \mathbb{R}$  is a scalar function and has the Taylor expansion

$$\begin{aligned} \underbrace{\mathcal{V}(\mathbf{x}(t))}_{f(t)} &= \underbrace{\mathcal{V}(\mathbf{x}(0))}_{f(0)} + t \underbrace{\frac{\partial \mathcal{V}}{\partial x^\alpha}(\mathbf{x}(0)) \dot{x}^\alpha(0)}_{\dot{f}(0)} \\ &\quad + \underbrace{\frac{1}{2} t^2 \left( \frac{\partial^2 \mathcal{V}}{\partial x^\beta \partial x^\alpha}(\mathbf{x}(0)) \dot{x}^\alpha(0) \dot{x}^\beta(0) + \frac{\partial \mathcal{V}}{\partial x^\alpha}(\mathbf{x}(0)) \ddot{x}^\alpha(0) \right)}_{\ddot{f}(0)} + \mathcal{O}(t^3). \end{aligned} \quad (2.12)$$

---

<sup>1</sup> $\boldsymbol{\Psi}^\top \mathbf{A} = (\boldsymbol{\Psi}\boldsymbol{\Phi}\boldsymbol{\Psi})^\top \mathbf{A} = \boldsymbol{\Psi}^\top (\boldsymbol{\Psi}\boldsymbol{\Phi})^\top \mathbf{A} = \boldsymbol{\Psi}^\top \boldsymbol{\Psi}\boldsymbol{\Phi}\mathbf{A} = \mathbf{0}$

Now let the curve be parameterized by  $\dot{\mathbf{x}}(t) = \mathbf{A}(\mathbf{x}(t))\xi(t)$  and we use the shorthand notations  $\bar{\mathbf{x}} = \mathbf{x}(0)$ ,  $\bar{\xi} = \xi(0)$  and  $\bar{\mathbf{A}} = \mathbf{A}(\mathbf{x}(0))$  to write

$$\begin{aligned}\mathcal{V}(\mathbf{x}(t)) &= \mathcal{V}(\bar{\mathbf{x}}) + t \frac{\partial \mathcal{V}}{\partial x^\alpha}(\bar{\mathbf{x}}) \bar{A}_i^\alpha \bar{\xi}^i \\ &\quad + \frac{1}{2} t^2 \left( \frac{\partial^2 \mathcal{V}}{\partial x^\beta \partial x^\alpha}(\bar{\mathbf{x}}) \bar{A}_i^\alpha \bar{A}_j^\beta \bar{\xi}^i \bar{\xi}^j + \frac{\partial \mathcal{V}}{\partial x^\alpha}(\bar{\mathbf{x}}) \left( \frac{\partial A_i^\alpha}{\partial x^\beta}(\bar{\mathbf{x}}) \bar{A}_j^\beta \bar{\xi}^i \bar{\xi}^j + \bar{A}_i^\alpha \dot{\xi}^i \right) \right) + \mathcal{O}(t^3)\end{aligned}\quad (2.13)$$

Introducing the notation

$$\partial_i = A_i^\alpha \frac{\partial}{\partial x^\alpha}, \quad i = 1, \dots, n \quad (2.14)$$

for the derivative in the direction of the  $i$ -th basis vector, we can state the Taylor expansion as

$$\mathcal{V}(\mathbf{x}(t)) = \mathcal{V}(\bar{\mathbf{x}}) + t \partial_i \mathcal{V}(\bar{\mathbf{x}}) \bar{\xi}^i + \frac{1}{2} t^2 (\partial_i \partial_j \mathcal{V}(\bar{\mathbf{x}}) \bar{\xi}^i \bar{\xi}^j + \partial_i \mathcal{V}(\bar{\mathbf{x}}) \dot{\xi}^i) + \mathcal{O}(t^3). \quad (2.15)$$

There are two more things we can derive from this equation:

- If  $\partial_i \mathcal{V}(\bar{\mathbf{x}}) = 0, i = 1, \dots, n$  then  $\bar{\mathbf{x}}$  is called a *critical point* of  $\mathcal{V}$ . At a critical point the expansion (2.15) reduces to

$$\mathcal{V}(\mathbf{x}(t)) = \mathcal{V}(\bar{\mathbf{x}}) + \frac{1}{2} t^2 \underbrace{(\partial_i \partial_j \mathcal{V})(\bar{\mathbf{x}})}_{\bar{H}_{ij}} \bar{\xi}^i \bar{\xi}^j + \mathcal{O}(t^3). \quad (2.16)$$

This relation holds for any sufficiently smooth curve  $t \mapsto \mathbf{x}(t)$  through  $\bar{\mathbf{x}}$  and consequently for any velocity vector  $\bar{\xi}$  at the critical point. So if the matrix  $\bar{\mathbf{H}}$  is positive (negative) definite, then  $\bar{\mathbf{x}}$  is a local minimum (maximum) of  $\mathcal{V}$ .

- Assume the curve  $t \mapsto \mathbf{x}(t)$  is a *geodesic*, i.e.  $\dot{\xi}^i = -\Gamma_{jk}^i \xi^j \xi^k$  with the connection coefficients  $\Gamma_{jk}^i$  that will be discussed later. Plugging this into (2.15) we find a coordinate form of the *Hessian tensor*  $\nabla^2 \mathcal{V}$  of the potential:

$$\mathcal{V}(\mathbf{x}(t)) = \mathcal{V}(\bar{\mathbf{x}}) + t (\partial_i \mathcal{V})(\bar{\mathbf{x}}) \bar{\xi}^i + \frac{1}{2} t^2 \underbrace{(\partial_i \partial_j \mathcal{V} - \Gamma_{ij}^k \partial_k \mathcal{V})(\bar{\mathbf{x}})}_{(\nabla^2 \mathcal{V})_{ij}} \bar{\xi}^i \bar{\xi}^j + \mathcal{O}(t^3). \quad (2.17)$$

At a critical point  $\bar{\mathbf{x}}$ , the Hessian of the potential is independent of the connection coefficients  $\Gamma_{jk}^i$  and consequently of the underlying metric. There it coincides with the matrix  $\bar{\mathbf{H}}$  defined in (2.16).

## 2.4 Commutation coefficients

For a function  $\mathcal{V} : \mathbb{R}^\nu \rightarrow \mathbb{R}$  we are used to the fact that partial derivatives commute, i.e.  $\partial^2 \mathcal{V} / \partial x^\alpha \partial x^\beta = \partial^2 \mathcal{V} / \partial x^\beta \partial x^\alpha$ . Unfortunately this is (in general) not the case for a

directional derivatives like  $\partial_i$  defined in (2.14). Consequently we investigate the following commutation relation

$$\begin{aligned}\partial_i \partial_j \mathcal{V} - \partial_j \partial_i \mathcal{V} &= A_i^\alpha \frac{\partial}{\partial x^\alpha} \left( A_j^\beta \frac{\partial \mathcal{V}}{\partial x^\beta} \right) - A_j^\beta \frac{\partial}{\partial x^\beta} \left( A_i^\alpha \frac{\partial \mathcal{V}}{\partial x^\alpha} \right) \\ &= A_i^\alpha \frac{\partial A_j^\beta}{\partial x^\alpha} \frac{\partial \mathcal{V}}{\partial x^\beta} - A_j^\beta \frac{\partial A_i^\alpha}{\partial x^\beta} \frac{\partial \mathcal{V}}{\partial x^\alpha} + A_i^\alpha A_j^\beta \underbrace{\left( \frac{\partial^2 \mathcal{V}}{\partial x^\alpha \partial x^\beta} - \frac{\partial^2 \mathcal{V}}{\partial x^\beta \partial x^\alpha} \right)}_{=0} \\ &= \left( A_i^\beta \frac{\partial A_j^\alpha}{\partial x^\beta} - A_j^\beta \frac{\partial A_i^\alpha}{\partial x^\beta} \right) \frac{\partial \mathcal{V}}{\partial x^\alpha}.\end{aligned}\quad (2.18)$$

Now using the identity (2.10) with  $\Phi_\alpha^\kappa = \frac{\partial \phi^\kappa}{\partial x^\alpha}$  and  $\Phi_\alpha^\kappa A_i^\alpha = 0 \Rightarrow \Phi_\alpha^\kappa \frac{\partial A_i^\alpha}{\partial x^\beta} = -\frac{\partial \Phi_\alpha^\kappa}{\partial x^\beta} A_i^\alpha$  to shape this expressions a bit further

$$\begin{aligned}\partial_i \partial_j \mathcal{V} - \partial_j \partial_i \mathcal{V} &= \left( A_i^\beta \frac{\partial A_j^\alpha}{\partial x^\beta} - A_j^\beta \frac{\partial A_i^\alpha}{\partial x^\beta} \right) \overbrace{\left( A_k^\sigma Y_\alpha^k + \Psi_\kappa^\sigma \Phi_\alpha^\kappa \right)}^{\delta_\alpha^\sigma} \frac{\partial \mathcal{V}}{\partial x^\sigma} \\ &= \left( A_i^\beta \frac{\partial A_j^\alpha}{\partial x^\beta} - A_j^\beta \frac{\partial A_i^\alpha}{\partial x^\beta} \right) Y_\alpha^k A_k^\sigma \frac{\partial \mathcal{V}}{\partial x^\sigma} - \left( A_i^\beta A_j^\alpha \frac{\partial \Phi_\alpha^\kappa}{\partial x^\beta} - A_j^\beta A_i^\alpha \frac{\partial \Phi_\alpha^\kappa}{\partial x^\beta} \right) \Psi_\kappa^\sigma \frac{\partial \mathcal{V}}{\partial x^\sigma} \\ &= \underbrace{\left( A_i^\beta \frac{\partial A_j^\alpha}{\partial x^\beta} - A_j^\beta \frac{\partial A_i^\alpha}{\partial x^\beta} \right)}_{\gamma_{ij}^k} \underbrace{Y_\alpha^k A_k^\sigma \frac{\partial \mathcal{V}}{\partial x^\sigma}}_{\partial_k \mathcal{V}} - A_j^\beta A_i^\alpha \underbrace{\left( \frac{\partial^2 \phi^\kappa}{\partial x^\alpha \partial x^\beta} - \frac{\partial^2 \phi^\kappa}{\partial x^\beta \partial x^\alpha} \right)}_{=0} \Psi_\kappa^\sigma \frac{\partial \mathcal{V}}{\partial x^\sigma}.\end{aligned}\quad (2.19)$$

Since this relation holds for any function  $\mathcal{V}$  we can state it in operator form and introduce the *commutation coefficients*  $\gamma_{ij}^k$  as

$$\partial_i \partial_j - \partial_j \partial_i = \gamma_{ij}^k \partial_k, \quad \gamma_{ij}^k = (\partial_i A_j^\alpha - \partial_j A_i^\alpha)(A^+)_\alpha^k. \quad (2.20)$$

It is interesting to note that the commutation coefficients are *invariant* to the choice of configuration coordinates  $\mathbf{x}$ , even though the coordinates appear explicitly in the definition: For a change of configuration coordinates  $\mathbf{x} = f(\hat{\mathbf{x}})$  the commutation symbols transform like  $\hat{\gamma}_{ij}^k(\hat{\mathbf{x}}) = \gamma_{ij}^k(f(\hat{\mathbf{x}}))$ . This might be obvious from a geometric point of view, but the explicit calculation of the coordinate transformation is shown in see (??). It will even turn out that for most of our examples the coefficients will be constants.

The right hand side of (2.20) appears in the context of Lagrange's equation in [Boltzmann, 1902] and [Hamel, 1904] for the case of minimal configuration coordinates and consequently with square matrices  $\mathbf{Y}$  and  $\mathbf{A}$ . In the contemporary literature on this context these quantities  $\gamma_{ij}^k$  are sometimes called the *Boltzmann three-index symbols* [Lurie, 2002, sec. 1.8] or *Hamel coefficients* [Bremer, 2008, p. 75]. The left hand side of (2.20) appears in the context of tensor algebra in [Misner et al., 1973, Box 8.4] where  $\gamma_{ij}^k$  are called the *commutation coefficients*. From the way  $\gamma_{ij}^k$  is defined here (2.20), this naming seems most fitting.

The commutation coefficients  $\gamma_{jk}^i$  vanish if the corresponding velocity coordinates  $\xi^i$  are *integrable*, i.e.

$$\begin{aligned}\exists \pi^i : \dot{\pi}^i = \xi^i = Y_\alpha^i \dot{x}^\alpha &\Rightarrow Y_\alpha^i = \frac{\partial \pi^i}{\partial x^\beta} \\ &\Rightarrow \frac{\partial Y_\alpha^i}{\partial x^\alpha} = \frac{\partial^2 \pi^i}{\partial x^\beta \partial x^\alpha} = \frac{\partial Y_\beta^i}{\partial x^\alpha}, \quad \Rightarrow \quad \gamma_{jk}^i = 0\end{aligned}\quad (2.21)$$

which is not the case in general. Nevertheless the quantities  $\pi$  are commonly introduced as *nonholonomic coordinates* in [Boltzmann, 1902] (also called *quasi coordinates* in [Lurie, 2002, sec. 1.5]). Then we could write  $\partial_i(\partial_j f) - \partial_j(\partial_i f) = \partial^2 f / \partial \pi^i \partial \pi^j - \partial^2 f / \partial \pi^j \partial \pi^i \neq 0$  what might lead to the conception that partial derivatives do not commute. The commutativity clearly holds, the issue is rather that the coordinates  $\pi$  do not exist. To avoid confusion of this kind we do not pick up this notation here.

**Example 3.** The commutation coefficients  $\gamma_{ij}^k$  associated with the kinematics matrix  $\mathbf{A}$  from (2.7) are

$$\gamma_{ij}^k = \begin{cases} +1, & (i, j, k) \text{ even permutation of } (1, 2, 3) \\ -1, & (i, j, k) \text{ odd permutation of } (1, 2, 3) \\ 0, & \text{else} \end{cases}. \quad (2.22)$$

This coincides with the three dimensional Levi-Civita symbol. It is related to the 3 dimensional *cross product* by  $\mathbf{a}, \mathbf{b} \in \mathbb{R}^3 : [\gamma_{ij}^k a^i b^j]_{k=1..3} = \mathbf{a} \times \mathbf{b}$ .

## 2.5 Linearization about a trajectory

Let  $\bar{\mathbf{x}} : [t_1, t_2] \rightarrow \mathbb{X}$  be a smooth curve with the velocity coordinates  $\bar{\boldsymbol{\xi}} : [t_1, t_2] \rightarrow \mathbb{R}^n : t \mapsto \mathbf{A}^+(\bar{\mathbf{x}}(t))\dot{\bar{\mathbf{x}}}(t)$ . For a small deviation  $\mathbf{x} \approx \bar{\mathbf{x}}$  with  $\mathbf{x} \in \mathbb{X}$  we may approximate the geometric constraint as

$$\phi(\mathbf{x}) \approx \underbrace{\phi(\bar{\mathbf{x}})}_{=0} + \frac{\partial \phi}{\partial \mathbf{x}}(\bar{\mathbf{x}})(\mathbf{x} - \bar{\mathbf{x}}) = 0. \quad (2.23)$$

Since this constraint is affine w.r.t.  $\mathbf{x}$  it is reasonable to use a the basis  $\boldsymbol{\varepsilon}(t) \in \mathbb{R}^n$  for the deviated configuration coordinates:

$$\mathbf{x} = \bar{\mathbf{x}} + \mathbf{A}(\bar{\mathbf{x}})\boldsymbol{\varepsilon}, \quad \boldsymbol{\varepsilon} = \mathbf{A}^+(\bar{\mathbf{x}})(\mathbf{x} - \bar{\mathbf{x}}), \quad (2.24)$$

For the velocity coordinates  $\boldsymbol{\xi}$  of the deviated curve  $\mathbf{x}$  we use again the first order approximation and  $\mathbf{Y} = \mathbf{A}^+$ :

$$\begin{aligned} \xi^i &= Y_\alpha^i(\mathbf{x})\dot{x}^\alpha \\ &\approx Y_\alpha^i(\bar{\mathbf{x}} + \mathbf{A}(\bar{\mathbf{x}})\boldsymbol{\varepsilon}) \frac{d}{dt} (\bar{x}^\alpha + A_j^\alpha(\bar{\mathbf{x}})\varepsilon^j) \\ &\approx Y_\alpha^i(\bar{\mathbf{x}}) \left( \dot{x}_R^\alpha + \frac{\partial A_j^\alpha}{\partial x^\beta}(\bar{\mathbf{x}}) \dot{x}_R^\beta \varepsilon^j + A_j^\alpha(\bar{\mathbf{x}}) \dot{\varepsilon}^j \right) + \frac{\partial Y_\alpha^i}{\partial x^\beta}(\bar{\mathbf{x}}) A_j^\beta(\bar{\mathbf{x}}) \varepsilon^j \dot{x}_R^\alpha \\ &= \bar{\xi}^i + \dot{\varepsilon}^i + \gamma_{kj}^i(\bar{\mathbf{x}}) \bar{\xi}^k \varepsilon^j \end{aligned} \quad (2.25)$$

Using these results we may formulate an approximation of a general smooth function  $f$  along the trajectory  $t \mapsto \bar{\mathbf{x}}(t)$  as

$$\begin{aligned} f(\mathbf{x}, \boldsymbol{\xi}, \dot{\boldsymbol{\xi}}) &\approx f(\bar{\mathbf{x}}, \bar{\boldsymbol{\xi}}, \dot{\bar{\boldsymbol{\xi}}}) + \frac{\partial f}{\partial x^\alpha}(\bar{\mathbf{x}}, \bar{\boldsymbol{\xi}}, \dot{\bar{\boldsymbol{\xi}}})(x^\alpha - \bar{x}^\alpha) + \frac{\partial f}{\partial \xi^i}(\bar{\mathbf{x}}, \bar{\boldsymbol{\xi}}, \dot{\bar{\boldsymbol{\xi}}})(\xi^i - \bar{\xi}^i) \\ &\quad + \frac{\partial f}{\partial \dot{\xi}^i}(\bar{\mathbf{x}}, \bar{\boldsymbol{\xi}}, \dot{\bar{\boldsymbol{\xi}}})(\dot{\xi}^i - \dot{\bar{\xi}}^i) \\ &\approx f(\bar{\mathbf{x}}, \bar{\boldsymbol{\xi}}, \dot{\bar{\boldsymbol{\xi}}}) + (\partial_i f)(\bar{\mathbf{x}}, \bar{\boldsymbol{\xi}}, \dot{\bar{\boldsymbol{\xi}}})\varepsilon^i + \frac{\partial f}{\partial \xi^i}(\bar{\mathbf{x}}, \bar{\boldsymbol{\xi}}, \dot{\bar{\boldsymbol{\xi}}})(\dot{\varepsilon}^i + \gamma_{kj}^i(\bar{\mathbf{x}})\bar{\xi}^k\varepsilon^j) \\ &\quad + \frac{\partial f}{\partial \dot{\xi}^i}(\bar{\mathbf{x}}, \bar{\boldsymbol{\xi}}, \dot{\bar{\boldsymbol{\xi}}})(\ddot{\varepsilon}^i + \gamma_{kj}^i(\bar{\mathbf{x}})\bar{\xi}^k\dot{\varepsilon}^j + \gamma_{kj}^i(\bar{\mathbf{x}})\dot{\bar{\xi}}^k\varepsilon^j + \partial_l\gamma_{kj}^i(\bar{\mathbf{x}})\bar{\xi}^l\bar{\xi}^k\varepsilon^j) \\ &= \bar{f} + \bar{F}_i^0\varepsilon^i + \bar{F}_i^1\dot{\varepsilon}^i + \bar{F}_i^2\ddot{\varepsilon}^i \end{aligned} \tag{2.26}$$

where

$$\begin{aligned} \bar{f} &= f(\bar{\mathbf{x}}, \bar{\boldsymbol{\xi}}, \dot{\bar{\boldsymbol{\xi}}}), \\ \bar{F}_i^0 &= (\partial_i f)(\bar{\mathbf{x}}, \bar{\boldsymbol{\xi}}, \dot{\bar{\boldsymbol{\xi}}}) + \frac{\partial f}{\partial \xi^j}(\bar{\mathbf{x}}, \bar{\boldsymbol{\xi}}, \dot{\bar{\boldsymbol{\xi}}})\gamma_{ki}^j(\bar{\mathbf{x}})\bar{\xi}^k + \frac{\partial f}{\partial \dot{\xi}^j}(\bar{\mathbf{x}}, \bar{\boldsymbol{\xi}}, \dot{\bar{\boldsymbol{\xi}}})(\gamma_{ki}^j(\bar{\mathbf{x}})\dot{\bar{\xi}}^k + \partial_l\gamma_{ki}^j(\bar{\mathbf{x}})\bar{\xi}^l\bar{\xi}^k), \\ \bar{F}_i^1 &= \frac{\partial f}{\partial \xi^i}(\bar{\mathbf{x}}, \bar{\boldsymbol{\xi}}, \dot{\bar{\boldsymbol{\xi}}}) + \frac{\partial f}{\partial \dot{\xi}^j}(\bar{\mathbf{x}}, \bar{\boldsymbol{\xi}}, \dot{\bar{\boldsymbol{\xi}}})\gamma_{ki}^j(\bar{\mathbf{x}})\bar{\xi}^k, \\ \bar{F}_i^2 &= \frac{\partial f}{\partial \dot{\xi}^i}(\bar{\mathbf{x}}, \bar{\boldsymbol{\xi}}, \dot{\bar{\boldsymbol{\xi}}}). \end{aligned}$$

Evidently, the expressions simplify significantly if the velocity coordinates are holonomic, i.e.  $\gamma = 0$ , or if the approximation is about a static point  $\bar{\mathbf{x}} = \text{const.} \Rightarrow \boldsymbol{\xi} = \mathbf{0}$ .

## 2.6 Calculus of variations

The calculus of variations is concerned with the extremals of functionals, i.e. functions of functions. For the particular context of classical mechanics we are interested in the curves  $t \mapsto \mathbf{x}(t)$  for which the functional

$$\mathcal{J}[\mathbf{x}] = \int_{t_1}^{t_2} \mathcal{L}(\mathbf{x}(t), \boldsymbol{\xi}(t), t) dt \tag{2.27}$$

for given boundary conditions  $\mathbf{x}(t_1)$  and  $\mathbf{x}(t_2)$  is *stationary*. The *Lagrangian*  $\mathcal{L}$  is here a function of the configuration coordinates  $\mathbf{x}$ , its derivatives  $\dot{\mathbf{x}} = \mathbf{A}\boldsymbol{\xi}$  parameterized in the velocity coordinates  $\boldsymbol{\xi}$  and may depend explicitly on the time  $t$  as well.

For the standard case,  $\mathbf{x} = \mathbf{q}$  and  $\boldsymbol{\xi} = \dot{\mathbf{q}}$ , a derivation may be found in e.g. [Lanczos, 1986, ch. II], [Arnold, 1989, sec. 12] or [Courant and Hilbert, 1924, chap. 4, §3]. For the present case we modify the well known derivation slightly: Suppose that  $\mathbf{x} : [t_1, t_2] \mapsto \mathbb{X}$  is the solution to the variational problem. With the function  $\boldsymbol{\chi}(t) \in \mathbb{R}^\nu$  and the parameter  $\varepsilon \in \mathbb{R}$  we define a perturbation to it by

$$\bar{\mathbf{x}} = \mathbf{x} + \varepsilon\boldsymbol{\chi}. \tag{2.28}$$

We need  $\bar{\mathbf{x}}(t) \in \mathbb{X}$  and consequently  $\phi(\bar{\mathbf{x}}) = \mathbf{0}$ . Assuming  $\varepsilon$  to be sufficiently small, we may use the first order approximation analog to section 2.5: With the *variation coordinates*  $\mathbf{h} : [t_1, t_2] \rightarrow \mathbb{R}^n$  we parameterize  $\boldsymbol{\chi} = \mathbf{A}(\mathbf{x})\mathbf{h}$ . Using the inverse kinematic relation  $\boldsymbol{\xi} = \mathbf{Y}(\mathbf{x})\dot{\mathbf{x}}$  we can write the functional for the varied path as

$$\mathcal{J}[\bar{\mathbf{x}}] = \int_{t_1}^{t_2} \mathcal{L}(\mathbf{x} + \varepsilon \mathbf{A}(\mathbf{x})\mathbf{h}, \mathbf{Y}(\mathbf{x} + \varepsilon \mathbf{A}(\mathbf{x})\mathbf{h}) \frac{d}{dt}(\mathbf{x} + \varepsilon \mathbf{A}(\mathbf{x})\mathbf{h}), t) dt =: \mathcal{P}(\varepsilon) \quad (2.29)$$

Now if  $\mathbf{x}(t)$  is indeed the solution to the variational problem, then  $\mathcal{P}(\varepsilon)$  must have a minimum at  $\mathcal{P}(0)$  and consequently  $\partial\mathcal{P}/\partial\varepsilon(0) = 0$ . Evaluation of this “ordinary” differentiation yields

$$\begin{aligned} 0 &= \frac{\partial\mathcal{P}}{\partial\varepsilon}\Big|_{\varepsilon=0} = \int_{t_1}^{t_2} \left( \frac{\partial\mathcal{L}}{\partial x^\alpha} A_i^\alpha h^i + \frac{\partial\mathcal{L}}{\partial \xi^i} \left( \frac{\partial Y_\alpha^i}{\partial x^\beta} A_j^\beta h^j \dot{x}^\alpha + Y_\alpha^i \frac{\partial A_j^\alpha}{\partial x^\beta} h^j \dot{x}^\beta + \dot{h}^i \right) \right) dt \\ &= \int_{t_1}^{t_2} \left( \partial_i \mathcal{L} h^i + \frac{\partial\mathcal{L}}{\partial \xi^i} (\gamma_{kj}^i h^j \xi^k + \dot{h}^i) \right) dt \end{aligned} \quad (2.30)$$

where we have found again the commutation coefficients  $\gamma_{kj}^i$  previously derived in (2.20). Integrating by parts with the boundary conditions  $\mathbf{h}(t_1) = \mathbf{h}(t_2) = \mathbf{0}$  gives

$$\int_{t_0}^{t_1} h^i \left( A_i^\alpha \frac{\partial\mathcal{L}}{\partial x^\alpha} - \frac{d}{dt} \frac{\partial\mathcal{L}}{\partial \xi^i} - \gamma_{ij}^k \xi^j \frac{\partial\mathcal{L}}{\partial \xi^k} \right) dt = 0. \quad (2.31)$$

Since the variation coordinates  $h^i, i = 1, \dots, n$  are independent by definition, the *fundamental lemma of the calculus of variations* (see e.g. [Arnold, 1989, p. 57] or [Courant and Hilbert, 1924, p. 166]) states that, for the integral to vanish, the terms in the brackets have to vanish, i.e.

$$\frac{d}{dt} \frac{\partial\mathcal{L}}{\partial \xi^i} + \gamma_{ij}^k \xi^j \frac{\partial\mathcal{L}}{\partial \xi^k} - A_i^\alpha \frac{\partial\mathcal{L}}{\partial x^\alpha} = 0, \quad i = 1, \dots, n. \quad (2.32)$$

This, combined with the kinematic relation  $\dot{x}^\alpha = A_i^\alpha \xi^i, \alpha = 1 \dots \nu$ , is the necessary condition for the functional (2.27) to be stationary.

For the special case  $\mathbf{x}(t) = \mathbf{q}(t) \in \mathbb{R}^n$  and  $\boldsymbol{\xi}(t) = \dot{\mathbf{q}}(t)$  we have  $\mathbf{A} = \mathbf{I}_n$  and  $\gamma = 0$ . Then (2.32) coincides with the *Euler-Lagrange equation*.

**Example 4.** Consider the configuration coordinates  $\mathbf{x} = [\mathbf{R}_x^\top, \mathbf{R}_y^\top, \mathbf{R}_z^\top]^\top$  and the velocity coordinates  $\boldsymbol{\xi} = \boldsymbol{\omega}$  related by  $\dot{\mathbf{R}} = \mathbf{R} \operatorname{wed}(\boldsymbol{\omega})$ . For the Lagrangian

$$\mathcal{L} = \frac{1}{2} \boldsymbol{\omega}^\top \boldsymbol{\Theta} \boldsymbol{\omega} + \operatorname{tr}(\boldsymbol{\Pi}' (\mathbf{I}_3 - \mathbf{R})) \quad (2.33)$$

and taking into account the results from Example (??) and 3 we obtain

$$\left[ \frac{d}{dt} \frac{\partial\mathcal{L}}{\partial \xi^i} + \gamma_{ij}^k \xi^j \frac{\partial\mathcal{L}}{\partial \xi^k} - A_i^\alpha \frac{\partial\mathcal{L}}{\partial x^\alpha} \right]_{i=1,2,3} = \boldsymbol{\Theta} \dot{\boldsymbol{\omega}} + \boldsymbol{\omega} \times \boldsymbol{\Theta} \boldsymbol{\omega} + \operatorname{vee2}(\boldsymbol{\Pi}' \mathbf{R}). \quad (2.34)$$

# Chapter 3

## Analytical mechanics of particle systems

**Goal.** Established approaches of analytical mechanics commonly rely on the parameterization of the system in terms of *minimal* generalized coordinates  $\mathbf{q}$  and their derivatives  $\dot{\mathbf{q}}$ . In this section we like to generalize this to handle redundant configuration coordinates  $\mathbf{x}(t) \in \mathbb{X}$  and nonholonomic velocity coordinates  $\boldsymbol{\xi}(t) \in \mathbb{R}^n$  as introduced in the previous section. The resulting formulations might become more cumbersome, but with some examples we like to show that it is worth it.

### 3.1 A single free particle

[Landau and Lifshitz, 1960, §1]: *One of the fundamental concepts of mechanics is that of a particle, also called material point.* This abstracts a body whose dimensions may be neglected and all its mass  $\mathfrak{m}$  is located at a point with the Cartesian coordinates  $\mathbf{r}(t) \in \mathbb{R}^3$  at time  $t$ . Its motion obeys Newton's second law [Newton, 1687, p. 13, lex II], english translation [Newton, 1846, p. 83]: *The alteration of motion is ever proportional to the motive force impressed; and is made in the direction of the right line in which that force is impressed.* The contemporary version reads (e.g. [Lurie, 2002, eq. 6.1.1] or [Goldstein, 1951, eq. 1.3])

$$\mathfrak{m}\ddot{\mathbf{r}} = \mathfrak{F}^A. \quad (3.1)$$

where  $\ddot{\mathbf{r}} \equiv d^2\mathbf{r}/dt^2$  is Newton's notation of differentiation and the applied force  $\mathfrak{F}^A$  collects all other (non inertial) influences on the particle. In this work we will investigate three sources of applied forces, gravity, linear springs and viscous friction.

**Gravity.** For far most engineering applications we are dealing with systems that move close to the surface of the earth and where Galilei's gravitation principle [Galilei, 1638, Day 3] holds. In a contemporary formulation it states that a particle with mass  $\mathfrak{m}_p$  is subject to the gravitational force

$$\mathfrak{F}^G = \mathfrak{m}\mathbf{a}_G \quad (3.2)$$

where  $\mathbf{a}_G$  are the coefficients of the gravitational acceleration of the earth w.r.t. the chosen inertial frame. Commonly the inertial frame is chosen such that the  $e_z$  axis is opposing gravity and we have  $\mathbf{a}_G = [0, 0, -g]^\top$  with the *gravity of earth*  $g = 9.8 \frac{\text{m}}{\text{s}^2}$ .

**Linear spring.** Let the particle be connected with a spring to a point  $\mathbf{r}_0$ . The simplest model of a spring is that of Hooke's law [Hooke, 1678]: The force  $\mathfrak{F}^K$  on the particle is opposite and proportional by a factor  $k$  to the spring displacement  $\mathbf{r} - \mathbf{r}_0$ , i.e.

$$\mathfrak{F}^K = -k(\mathbf{r} - \mathbf{r}_0). \quad (3.3)$$

**Viscous friction.** [Rayleigh, 1877, §81]: *There is another group of forces whose existence is often advantageous to recognize specially, namely those arising from friction or viscosity. [...] we suppose that each particle is retarded by forces proportional to its component velocities.* We may think of the particle to be immersed in a viscous fluid which, at the particle position, has the velocity  $\mathbf{v}_0$ . The force on the particle is

$$\mathfrak{F}^D = -\delta(\dot{\mathbf{r}} - \mathbf{v}_0) \quad (3.4)$$

with the damping parameter  $\delta \in \mathbb{R}^+$ .

**Equation of motion.** A single free particle that is subject to all the aforementioned forces and a general, not further specified external force  $\mathfrak{F}^E$ , i.e.  $\mathfrak{F}^A = \mathfrak{F}^G + \mathfrak{F}^K + \mathfrak{F}^D + \mathfrak{F}^E$ , has the equation of motion

$$m(\ddot{\mathbf{r}} - \mathbf{a}_G) + \delta(\dot{\mathbf{r}} - \mathbf{v}_0) + k(\mathbf{r} - \mathbf{r}_0) = \mathfrak{F}^E. \quad (3.5)$$

**Control engineering.** From a control engineering perspective the structure of this system is already nice enough to consider it as a desired closed loop dynamics: If we want the particle to track a sufficiently smooth reference trajectory  $t \mapsto \mathbf{r}_R(t)$  a reasonable desired closed loop dynamics is

$$m(\ddot{\mathbf{r}} - \ddot{\mathbf{r}}_R) + \bar{\delta}(\dot{\mathbf{r}} - \dot{\mathbf{r}}_R) + \bar{k}(\mathbf{r} - \mathbf{r}_R) = \mathbf{0}. \quad (3.6)$$

This is essentially the same as above (3.5), but we replaced the spring origin  $\mathbf{r}_0$  with the reference position  $\mathbf{r}_R$ , the fluid velocity  $\mathbf{v}_0$  with the reference velocity  $\dot{\mathbf{r}}_R$  and the free-fall acceleration  $\mathbf{a}_G$  with the reference acceleration  $\ddot{\mathbf{r}}_R$ . Furthermore, we replaced the spring stiffness  $k$  and viscosity  $\delta$  by analog tuning parameters  $\bar{k}, \bar{\delta} \in \mathbb{R}^+$ . Plugging the desired dynamics (3.6) into the plant dynamics (3.5) yields the required control law

$$\mathfrak{F}^E = m(\ddot{\mathbf{r}}_R - \mathbf{a}_G) + \delta(\dot{\mathbf{r}} - \mathbf{v}_0) + k(\mathbf{r} - \mathbf{r}_0) - \bar{\delta}(\dot{\mathbf{r}} - \dot{\mathbf{r}}_R) - \bar{k}(\mathbf{r} - \mathbf{r}_R) - m\mathbf{a}_G. \quad (3.7)$$

As this control approach is closely related to familiar to mechanics, it should be more intuitive for an engineer than other generic mathematical approaches.

## 3.2 Systems of constrained particles

**System under consideration.** For this chapter we consider a system of  $\mathfrak{N}$  particles under geometric constraints: The *position* of a particle with respect to a given inertial frame at a given time  $t$  is  $\mathbf{r}_p(t) \in \mathbb{R}^3, p = 1, \dots, \mathfrak{N}$  and the collection of all particle positions is  $\mathbf{x} = [\mathbf{r}_1^\top, \dots, \mathbf{r}_{\mathfrak{N}}^\top]^\top \in \mathbb{R}^{3\mathfrak{N}}$ . *Geometric constraints* on the particles are captured in  $\mathfrak{H} \geq 0$  smooth functions of the form  $\mathbf{c}(\mathbf{x}) = [\mathbf{c}^1(\mathbf{x}), \dots, \mathbf{c}^{\mathfrak{H}}(\mathbf{x})]^\top = \mathbf{0}$ . The set of all mutually admissible particle positions

$$\mathfrak{X} = \{\mathbf{x} \in \mathbb{R}^{3\mathfrak{N}} \mid \mathbf{c}(\mathbf{x}) = \mathbf{0}\} \quad (3.8)$$

is called the *configuration space*. We require  $\frac{\partial \mathbf{c}}{\partial \mathbf{x}}(\mathbf{x})$  to have a constant, though not necessarily full rank.

### 3.2.1 First principles

**principle of constraint release.** (see e.g. [Lurie, 2002, sec. 6.1], [Hamel, 1949, sec. 32]) states that the motion of system of geometrically constrained particles is governed by

$$\mathbf{c}(\mathbf{x}) = \mathbf{0}, \quad m_p \ddot{\mathbf{r}}_p = \mathfrak{F}_p^A + \lambda_\kappa \frac{\partial \mathbf{c}^\kappa}{\partial \mathbf{r}_p}, \quad p = 1, \dots, \mathfrak{N}. \quad (3.9)$$

**Lagrange-d'Alembert principle.** for a system of geometrically constrained particles states (e.g. [Goldstein, 1951, sec. 1.4] or [Lurie, 2002, sec. 6.3]):

$$\sum_{p=1}^{\mathfrak{N}} \langle \delta \mathbf{r}_p, \mathfrak{F}_p^A - m_p \ddot{\mathbf{r}}_p \rangle = 0 \quad \forall \quad \frac{\partial \mathbf{c}}{\partial \mathbf{x}} \delta \mathbf{x} = \mathbf{0}. \quad (3.10)$$

The *virtual displacements*  $\delta \mathbf{r}_p$  are tangents to possible motions: For particle positions constrained by  $\mathbf{c}(\mathbf{x}) = \mathbf{0}$  the displacements have to fulfill  $\frac{\partial \mathbf{c}}{\partial \mathbf{x}} \delta \mathbf{x} = \mathbf{0}$ .

**Gauß principle.** For this work we use the formulation from [Päsler, 1968, sec. 7] of Gauß principle:

$$\begin{aligned} \min_{\ddot{\mathbf{x}} \in \mathbb{R}^{3\mathfrak{N}}} \quad & \mathcal{G} = \frac{1}{2} \sum_{p=1}^{\mathfrak{N}} m_p \|\ddot{\mathbf{r}}_p - \ddot{\mathbf{r}}_p^f\|^2 \\ \text{s. t.} \quad & \ddot{\mathbf{c}}(\mathbf{x}, \dot{\mathbf{x}}, \ddot{\mathbf{x}}) = \mathbf{0} \end{aligned} \quad (3.11)$$

where  $\mathbf{x} = [\mathbf{r}_1^\top, \dots, \mathbf{r}_{\mathfrak{N}}^\top]^\top$  and  $\ddot{\mathbf{r}}_p^f$  are the particle accelerations of the unconstrained system and we call  $\mathcal{G}$  the Gaussian constraint. Its crucial to note that the constraint equations  $\ddot{\mathbf{c}}(\mathbf{x}, \dot{\mathbf{x}}, \ddot{\mathbf{x}}) = \mathbf{0}$  are *linear* in the accelerations  $\ddot{\mathbf{x}}$ . Consequently, as stressed in [Gauß, 1829], the principle (3.11) can be regarded as a (static) quadratic optimization problem with linear constraints.

**Hamilton's principle.** Another principle can be stated as [Lurie, 2002, sec. 12.2] or [Szabó, 1956, sec. I.3]:

$$\int_{t_1}^{t_2} (\delta \mathcal{T} - \delta' \mathcal{W}) dt = 0, \quad \mathcal{T} = \frac{1}{2} \sum_p \mathfrak{m}_p \|\dot{\mathbf{r}}_p\|^2, \quad \delta' \mathcal{W} = \langle \delta \mathbf{r}_p, \mathfrak{F}_p^A \rangle \quad (3.12)$$

### 3.2.2 Coordinates

**Generalized coordinates.** In most cases we are not really interested in the motion of the individual particles but rather in the system as a whole. Using the constraint equations it is possible to capture the configuration of the system by  $\dim \mathfrak{X} = 3\mathfrak{N} - \text{rank } \frac{\partial \mathfrak{c}}{\partial \mathbf{r}} = n$  coordinates, commonly called *generalized coordinates* and commonly denoted by  $\mathbf{q}$ . Its components, in contrast to the Cartesian particle coordinates, may be lengths, angles or some completely generic quantity stressed by the term “generalized”. What is more crucial but usually implicit is that they have to be independent from another to parameterize the  $n$  dimensional configuration space with its  $n$  components. Whenever used in this work, these coordinates are referred to as *minimal generalized coordinates*  $\mathbf{q} \in \mathbb{R}^n$ .

**Redundant generalized coordinates.** As shown in the introduction [link], in some cases it might be useful to use a slightly larger number of *redundant* generalized coordinates  $\mathbf{x} \in \mathbb{R}^\nu, \nu \geq n$ . For  $\nu > n$  the components cant be independent, but are themselves constrained by smooth equations of the form  $\phi(\mathbf{x}) = \mathbf{0}$ . The set of all mutually admissible coordinates is

$$\mathbb{X} = \{\mathbf{x} \in \mathbb{R}^\nu \mid \phi(\mathbf{x}) = \mathbf{0}\}. \quad (3.13)$$

As discussed in the previous chapter, it is always possible to choose coordinates such that  $\mathbb{X}$  is isomorphic to  $\mathfrak{X}$ .

**Velocity coordinates.** As discussed in the previous chapter [link], we assume that the derivative of the possible redundant configuration coordinates  $\mathbf{x}(t) \in \mathbb{X}$  may be parameterized by a minimal set of velocity coordinates  $\xi(t) \in \mathbb{R}^n$  through the relations

$$\dot{\mathbf{x}}(t) = \mathbf{A}(\mathbf{x}(t))\xi(t), \quad (3.14)$$

where  $\mathbf{A} \in \mathbb{R}^{\nu \times n}$  with  $\frac{\partial \phi}{\partial \mathbf{x}} \mathbf{A} \equiv \mathbf{0}$  and  $\text{rank } \mathbf{A} = n$ .

Note that the common minimal parameterization  $\mathbf{x} = \mathbf{q} \in \mathbb{R}^n$  and  $\xi = \dot{\mathbf{q}} \in \mathbb{R}^n$  is of course included as the special case  $\mathbb{X} = \mathbb{R}^n$  and  $\mathbf{A} = \mathbf{I}_n$ .

**Particle parameterization.** Let the admissible particle positions  $\mathbf{r} \in \mathfrak{X}$  be parameterized  $\mathbf{r}_p = \mathbf{r}_p(\mathbf{x}, t)$  by possibly redundant coordinates  $\mathbf{x} \in \mathbb{X}$ . This means  $\phi(\mathbf{x}) = \mathbf{0} \Rightarrow \mathfrak{c}(\mathbf{r}(\mathbf{x}, t)) = \mathbf{0}$  and consequently  $\mathbf{x} \in \mathbb{X} \Rightarrow \mathbf{r}(\mathbf{x}) \in \mathfrak{X}$ . The particle velocities and

accelerations in terms of the coordinates we have

$$\dot{\mathbf{r}}_p = \partial_i \mathbf{r}_p \xi^i + \frac{\partial \mathbf{r}_p}{\partial t} \quad (3.15a)$$

$$\ddot{\mathbf{r}}_p = \partial_i \mathbf{r}_p \dot{\xi}^i + \partial_j \partial_i \mathbf{r}_p \xi^i \xi^j + \underbrace{\left( \partial_i \frac{\partial \mathbf{r}_p}{\partial t} + \frac{\partial}{\partial t} \partial_i \mathbf{r}_p \right) \xi^i}_{\mathbf{a}_p^E} + \frac{\partial^2 \mathbf{r}_p}{\partial t^2}. \quad (3.15b)$$

There are two relations which will be useful in the following derivations: Firstly, from (3.15) it is evident that

$$\partial_i \mathbf{r}_p = \frac{\partial \dot{\mathbf{r}}_p}{\partial \xi^i} = \frac{\partial \ddot{\mathbf{r}}_p}{\partial \dot{\xi}^i}. \quad (3.16)$$

Secondly, taking the time derivative of the constraint equations we have

$$\frac{d}{dt} \mathbf{c}^\kappa = \sum_p \frac{\partial \mathbf{c}^\kappa}{\partial \mathbf{r}_p} \dot{\mathbf{r}}_p = \sum_p \frac{\partial \mathbf{c}^\kappa}{\partial \mathbf{r}_p} \left( \partial_i \mathbf{r}_p \xi^i + \frac{\partial \mathbf{r}_p}{\partial t} \right) = 0, \quad \kappa = 1, \dots, \mathfrak{H}. \quad (3.17)$$

Since this has to hold for any  $\xi$  we must have

$$\sum_p \frac{\partial \mathbf{c}^\kappa}{\partial \mathbf{r}_p} \partial_i \mathbf{r}_p = 0, \quad \sum_p \frac{\partial \mathbf{c}^\kappa}{\partial \mathbf{r}_p} \frac{\partial \mathbf{r}_p}{\partial t} = 0, \quad \kappa = 1, \dots, \mathfrak{H}, \quad i = 1, \dots, n. \quad (3.18)$$

**Application to the principle of constraint release.** Summing up the projections of (3.9) on  $\partial_i \mathbf{r}_p$  eliminates the constraint forces  $\boldsymbol{\lambda}$  due to (3.18):

$$\sum_p \mathfrak{m}_p \langle \partial_i \mathbf{r}_p, \ddot{\mathbf{r}}_p \rangle = \sum_p \langle \partial_i \mathbf{r}_p, \mathfrak{F}_p^A \rangle + \underbrace{\sum_p \langle \partial_i \mathbf{r}_p, \lambda_\kappa \frac{\partial \mathbf{c}^\kappa}{\partial \mathbf{r}_p} \rangle}_0, \quad i = 1, \dots, n. \quad (3.19)$$

Parameterizing the particle accelerations  $\ddot{\mathbf{r}}_p$  in terms of the chosen coordinates (3.15b) yields

$$\sum_p \mathfrak{m}_p \langle \partial_i \mathbf{r}_p, \partial_j \mathbf{r}_p \dot{\xi}^j + \partial_k \partial_j \mathbf{r}_p \xi^k \xi^j + \mathbf{a}_p^E \rangle = \sum_p \langle \partial_i \mathbf{r}_p, \mathfrak{F}_p^A \rangle \quad i = 1, \dots, n. \quad (3.20)$$

These are  $n$  equations linear in the  $n$  acceleration coordinates  $\dot{\xi}$ .

**Application to the Lagrange-d'Alembert principle.** Analog to the velocity, we may parameterize virtual displacements as  $\delta \mathbf{r}_p = \partial_i \mathbf{r}_p h^i, p = 1, \dots, \mathfrak{N}$  with  $\mathbf{h} \in \mathbb{R}^n$ . Plugging this into (3.10) we get

$$h^i \sum_p \langle \partial_i \mathbf{r}_p, \mathfrak{F}_p^A - \mathfrak{m}_p \ddot{\mathbf{r}}_p \rangle = 0 \quad \forall \quad \mathbf{h} \in \mathbb{R}^n. \quad (3.21)$$

Since this has to hold for any  $\mathbf{h}$  we have the identical result as above (3.19).

**Application to the Gauß principle.** Parameterizing the particle accelerations  $\ddot{\mathbf{r}}_p$  in terms of the chosen coordinates (3.15b) in Gauß' principle (3.11) essentially transforms it to an *unconstrained* minimization problem:

$$\min_{\dot{\boldsymbol{\xi}} \in \mathbb{R}^n} \mathcal{G} = \frac{1}{2} \sum_p m_p \|\partial_j \mathbf{r}_p \dot{\xi}^j + \partial_k \partial_j \mathbf{r}_p \xi^k \xi^j + \mathbf{a}_p^E - \frac{\mathbf{f}_p^A}{m_p}\|^2 \quad (3.22)$$

The necessary condition for a critical point is

$$\frac{\partial \mathcal{G}}{\partial \dot{\xi}^i} = \sum_p m_p \langle \partial_i \mathbf{r}_p, \partial_j \mathbf{r}_p \dot{\xi}^j + \partial_k \partial_j \mathbf{r}_p \xi^k \xi^j + \mathbf{a}_p^E - \frac{\mathbf{f}_p^A}{m_p} \rangle = 0, \quad i = 1, \dots, n \quad (3.23)$$

$$\Leftrightarrow \underbrace{\sum_p m_p \langle \partial_i \mathbf{r}_p, \partial_j \mathbf{r}_p \rangle}_{M_{ij}} \dot{\xi}^j = \underbrace{\sum_p \langle \mathbf{f}_p^A - m_p (\partial_i \mathbf{r}_p, \partial_k \partial_j \mathbf{r}_p \xi^k \xi^j + \mathbf{a}_p^E) \rangle}_{b_i}, \quad i = 1, \dots, n \quad (3.24)$$

Which is, again, the same result as above. The solution  $\dot{\boldsymbol{\xi}} = \mathbf{M}^{-1} \mathbf{b}$  is a minimum if  $\partial^2 \mathcal{G} / \partial \dot{\boldsymbol{\xi}} \partial \dot{\boldsymbol{\xi}} = \mathbf{M}$  is positive definite.

**Application to Hamilton's principle.** To evaluate Hamilton's principle (3.12) we have to formulate the kinetic energy  $\mathcal{T}$  in terms of the chosen coordinates

$$\mathcal{T}(\mathbf{x}, \boldsymbol{\xi}, t) = \frac{1}{2} \sum_p m_p \|\partial_i \mathbf{r}_p(\mathbf{x}) \xi^i + \frac{\partial \mathbf{r}_p}{\partial t}(\mathbf{x}, t)\|^2 \quad (3.25)$$

Using the result (2.32) from the calculus of variations we obtain

$$\underbrace{\frac{d}{dt} \frac{\partial \mathcal{T}}{\partial \xi^i} + \gamma_{ij}^k \xi^j \frac{\partial \mathcal{T}}{\partial \xi^k} - \partial_i \mathcal{T}}_{-f_i^M} = \underbrace{\langle \partial_i \mathbf{r}_p, \mathbf{f}_p^A \rangle}_{f_i^A}, \quad i = 1, \dots, n. \quad (3.26)$$

Evaluation and some rearrangement of the left hand term  $f_i^M$  shows that it indeed is the generalized inertia force previously defined in [eq:PrinciplesForceBalance]:

$$\begin{aligned} -f_i^M &= \sum_p m_p \left( \frac{d}{dt} \langle \partial_i \mathbf{r}_p, \partial_j \mathbf{r}_p \dot{\xi}^j \rangle + \gamma_{ij}^k \xi^j \langle \partial_k \mathbf{r}_p, \partial_l \mathbf{r}_p \xi^l \rangle - \langle \partial_i \partial_j \mathbf{r}_p \xi^j, \partial_k \mathbf{r}_p \xi^k \rangle \right) \\ &= \sum_p m_p \left( \langle \partial_i \mathbf{r}_p, \partial_j \mathbf{r}_p \dot{\xi}^j + \partial_k \partial_j \mathbf{r}_p \xi^j \xi^k \rangle + \langle \partial_l \mathbf{r}_p \xi^l, \underbrace{(\partial_j \partial_i \mathbf{r}_p - \partial_i \partial_j \mathbf{r}_p + \gamma_{ij}^k \partial_k \mathbf{r}_p)}_0 \xi^j \rangle \right). \end{aligned} \quad (3.27)$$

**Conclusion** Evaluation of the principles above with the coordinates leads to

$$\underbrace{\sum_p m_p \langle \partial_i \mathbf{r}_p, \partial_j \mathbf{r}_p \rangle}_{M_{ij}} \dot{\xi}^j = \underbrace{\sum_p \langle \mathbf{f}_p^A - m_p (\partial_i \mathbf{r}_p, \partial_k \partial_j \mathbf{r}_p \xi^k \xi^j + \mathbf{a}_p^E) \rangle}_{b_i}, \quad i = 1, \dots, n \quad (3.28)$$

### 3.2.3 Inertia

several forms:

$$f_i^M = \sum_p \langle \partial_i \mathbf{r}_p, \mathbf{m}_p \ddot{\mathbf{r}}_p \rangle, \quad i = 1, \dots, n \quad (3.29a)$$

$$= \sum_p \mathbf{m}_p \langle \partial_i \mathbf{r}_p, \partial_j \mathbf{r}_p \dot{\xi}^j + \partial_k \partial_j \mathbf{r}_p \xi^k \xi^j + \mathbf{a}_p^E \rangle \quad (3.29b)$$

$$= M_{ij} \dot{\xi}^j + \Gamma_{ijk} \xi^j \xi^k + \sum_p \mathbf{m}_p \langle \partial_i \mathbf{r}_p, \mathbf{a}_p^E \rangle, \quad M_{ij} = \sum_p \mathbf{m}_p \langle \partial_i \mathbf{r}_p, \partial_j \mathbf{r}_p \rangle \quad (3.29c)$$

$$= \frac{d}{dt} \frac{\partial \mathcal{T}}{\partial \xi^i} + \gamma_{ij}^k \xi^j \frac{\partial \mathcal{T}}{\partial \xi^k} - \partial_i \mathcal{T}, \quad \mathcal{T} = \frac{1}{2} \sum_p \mathbf{m}_p \|\dot{\mathbf{r}}_p\|^2 \quad (3.29d)$$

$$= \frac{\partial \mathcal{S}}{\partial \dot{\xi}^i}, \quad \mathcal{S} = \frac{1}{2} \sum_p \mathbf{m}_p \|\ddot{\mathbf{r}}_p\|^2 \quad (3.29e)$$

### 3.2.4 Gravitation

The resulting generalized force for a system of particles is

$$f_i^G = \sum_p \langle \partial_i \mathbf{r}_p, \mathfrak{F}_p^G \rangle = \sum_p \mathbf{m}_p \langle \partial_i \mathbf{r}_p, \mathbf{a}_G \rangle. \quad (3.30)$$

We may define the gravitational potential  $\mathcal{V}^G$  of the system though

$$f_i^G = \partial_i \mathcal{V}^G, \quad \mathcal{V}^G(\mathbf{x}, t) = \sum_p \mathbf{m}_p \langle \mathbf{r}_p(\mathbf{x}, t), \mathbf{a}_G \rangle \quad (3.31)$$

### 3.2.5 Stiffness

Assume that the particle with index  $p$  is connected to another particle with index  $q$  by a spring. In the simplest case the resulting spring force obeys Hooke's law [Hooke, 1678]: The force on particle  $p$  connected by a spring, with the spring constant  $\mathfrak{k}_{pq} \in \mathbb{R}^+$ , to particle  $q$  is

$$\mathfrak{F}_{pq}^K = \mathfrak{k}_{pq} (\mathbf{r}_q - \mathbf{r}_p). \quad (3.32)$$

Naturally, the opposing force  $\mathfrak{F}_{qp}^K = -\mathfrak{F}_{pq}^K$  acts on particle  $q$ . For a particle system we can assume that each particle may be connected to each other particle and set  $\mathfrak{k}_{pq} = 0$  if there is no spring. Then the overall force on each particle is

$$\mathfrak{F}_p^K = \sum_{q=1, q \neq p}^N \mathfrak{k}_{pq} (\mathbf{r}_q - \mathbf{r}_p), \quad \mathfrak{k}_{pq} = \mathfrak{k}_{qp}. \quad (3.33)$$

For a parameterized system (??) we have the *generalized stiffness force*:

$$\begin{aligned}
f_i^K &= \sum_{p=1}^{\mathfrak{N}} \langle \partial_i \mathbf{r}_p, \mathfrak{F}_p^K \rangle = \sum_{p=1}^{\mathfrak{N}} \sum_{q=1, q \neq p}^{\mathfrak{N}} \mathfrak{k}_{pq} \langle \partial_i \mathbf{r}_p, \mathbf{r}_q - \mathbf{r}_p \rangle \\
&= \frac{1}{2} \sum_{p=1}^{\mathfrak{N}} \sum_{q=1}^{\mathfrak{N}} \mathfrak{k}_{pq} \langle \partial_i \mathbf{r}_p, \mathbf{r}_q - \mathbf{r}_p \rangle + \frac{1}{2} \sum_{p=1}^{\mathfrak{N}} \sum_{q=1}^{\mathfrak{N}} \mathfrak{k}_{qp} \langle \partial_i \mathbf{r}_q, \mathbf{r}_p - \mathbf{r}_q \rangle \\
&= -\frac{1}{2} \sum_{p=1}^{\mathfrak{N}} \sum_{q=1}^{\mathfrak{N}} \mathfrak{k}_{pq} \langle \partial_i (\mathbf{r}_q - \mathbf{r}_p), \mathbf{r}_q - \mathbf{r}_p \rangle \\
&= -\partial_i \underbrace{\left( \frac{1}{4} \sum_{p=1}^{\mathfrak{N}} \sum_{q=1}^{\mathfrak{N}} \mathfrak{k}_{pq} \|\mathbf{r}_q - \mathbf{r}_p\|^2 \right)}_{\mathcal{V}^K} = -\partial_i \underbrace{\left( \frac{1}{2} \sum_{p=1}^{\mathfrak{N}} \sum_{q=p+1}^{\mathfrak{N}} \mathfrak{k}_{pq} \|\mathbf{r}_q - \mathbf{r}_p\|^2 \right)}_{\mathcal{V}^K} \quad (3.34)
\end{aligned}$$

Since it can be derived from a potential  $\mathcal{V}^K : \mathbb{X} \rightarrow \mathbb{R}$ , it is called a *conservative force*. Note that the non-negativity of the spring constants  $\mathfrak{k}_{pq} \geq 0, p, q = 1, \dots, \mathfrak{N}$  implies the non-negativity of the potential  $\mathcal{V}^K \geq 0$ .

potential energy

$$\mathcal{V}^K = \frac{1}{2} \sum_{p=1}^{\mathfrak{N}} \sum_{q=p+1}^{\mathfrak{N}} \mathfrak{k}_{pq} \|\mathbf{r}_p - \mathbf{r}_q\|^2, \quad f_i^K = \partial_i \mathcal{V}^K \quad (3.35)$$

This identity might not be so obvious so we display the computation explicitly: First note that due to  $\mathfrak{k}_{pq} = \mathfrak{k}_{qp}$  and the obvious fact that the term for  $q = p$  vanishes anyway, the potential can be expressed as

$$\mathcal{V}^K = \frac{1}{4} \sum_{p=1}^{\mathfrak{N}} \sum_{q=1}^{\mathfrak{N}} \mathfrak{k}_{pq} \|\mathbf{r}_p - \mathbf{r}_q\|^2 \quad (3.36)$$

with this the directional derivatives are

$$\begin{aligned}
\partial_i \mathcal{V}^K &= \frac{1}{2} \sum_{p=1}^{\mathfrak{N}} \sum_{q=1}^{\mathfrak{N}} \mathfrak{k}_{pq} \langle \partial_i \mathbf{r}_p - \partial_i \mathbf{r}_q, \mathbf{r}_p - \mathbf{r}_q \rangle \\
&= \frac{1}{2} \sum_{p=1}^{\mathfrak{N}} \sum_{q=1}^{\mathfrak{N}} \mathfrak{k}_{pq} \langle \partial_i \mathbf{r}_p, \mathbf{r}_p - \mathbf{r}_q \rangle + \frac{1}{2} \sum_{p=1}^{\mathfrak{N}} \sum_{q=1}^{\mathfrak{N}} \mathfrak{k}_{pq} \langle \partial_i \mathbf{r}_q, \mathbf{r}_q - \mathbf{r}_p \rangle \\
&= \sum_{p=1}^{\mathfrak{N}} \sum_{q=1, q \neq p}^{\mathfrak{N}} \mathfrak{k}_{pq} \langle \partial_i \mathbf{r}_p, \mathbf{r}_p - \mathbf{r}_q \rangle \quad (3.37)
\end{aligned}$$

### 3.2.6 Dissipation

[Goldstein, 1951, p. 24] "Frictional forces of this type may be derived in terms of a function, known as Rayleigh's dissipation function" [Papastavridis, 2002, p. 519] same as above For

dissipative forces we pick up the concept from [Rayleigh, 1877, §81]: "Suppose that each particle of the system is retarded by forces proportional to its component velocities". So for each particle we assume a damping force

$$\mathfrak{F}_p^D = -\mathfrak{d}_p \dot{\mathbf{r}}_p, \quad p = 1, \dots, \mathfrak{N} \quad (3.38)$$

with the damping parameters  $\mathfrak{d}_p \in \mathbb{R}^+$ . For a parameterized system (??) we have the *generalized dissipation force*:

$$f_i^D = \sum_p \langle \partial_i \mathbf{r}_p, \mathfrak{F}_p^D \rangle = - \underbrace{\sum_p \mathfrak{d}_p \langle \partial_i \mathbf{r}_p, \partial_j \mathbf{r}_p \rangle}_{D_{ij}} \xi^j \quad (3.39)$$

where we introduced the *system dissipation matrix*  $\mathbf{D}(\mathbf{x}) \in \mathbb{SYM}_0^+(n)$ . Furthermore, these quantities can be derived from the so-called *Rayleigh dissipation function*  $\mathcal{R} : \mathbb{T}\mathbb{X} \rightarrow \mathbb{R}$  using the rules (3.16):

$$\mathcal{R} = \sum_p \frac{1}{2} \mathfrak{d}_p \|\dot{\mathbf{r}}_p\|^2 = \frac{1}{2} D_{ij} \xi^i \xi^j, \quad f_i^D = -\frac{\partial \mathcal{R}}{\partial \xi^i}, \quad D_{ij} = \frac{\partial^2 \mathcal{R}}{\partial \xi^i \partial \xi^j}. \quad (3.40)$$

Note that the non-negativity of the damping parameters  $\mathfrak{d}_p \geq 0, p = 1, \dots, \mathfrak{N}$  implies non-negativity of the dissipation function  $\mathcal{R} \geq 0$  and positive semi-definiteness of the dissipation matrix  $\mathbf{D} \geq 0$ . General dissipation

$$\mathcal{R} = \frac{1}{2} \sum_{p,q=1}^{\mathfrak{N}} \mathfrak{d}_{pq} \|\dot{\mathbf{r}}_p - \dot{\mathbf{r}}_q\|^2 \quad (3.41)$$

$$= \frac{1}{2} \left( \underbrace{\sum_{p,q=1}^{\mathfrak{N}} \mathfrak{d}_{pq} \langle \partial_i \mathbf{r}_p - \partial_i \mathbf{r}_q, \partial_j \mathbf{r}_p - \partial_j \mathbf{r}_q \rangle}_{D_{ij}} \right) \xi^j \xi^i \quad (3.42)$$

### 3.3 A single free rigid body

Established textbooks on physics (e.g. [Goldstein, 1951, chap. 4], [Landau and Lifshitz, 1960, §31] or [Boltzmann, 1897, §44]) define a *rigid body* as a system of a *finite* number  $\mathfrak{N}$  particles such that the distances  $d_{pq} = \|\mathbf{r}_p - \mathbf{r}_q\|$  between their positions  $\mathbf{r}_p$  are constant. Textbooks that are more focused on engineering like [Hamel, 1949, sec. 8, § 1], [Bremer, 2008, sec. 4.1] or [Roberson and Schwertassek, 1988, sec. 6.1.1] rather define a rigid body as a rigid volume over which infinitesimal mass increments are distributed. Both modeling assumptions eventually lead to the same equations of motion when using the same generalized coordinates. They differ in the computation of the inertial parameters of total mass, center of mass and moment of inertia: The physics perspective has a finite sum over the particles, whereas the engineering point of view requires an integral over the body volume.

In this section we will not only consider inertia, but also stiffness and damping of the rigid body. The model with a finite number of particles is simply easier to analyze.

#### 3.3.1 Coordinates

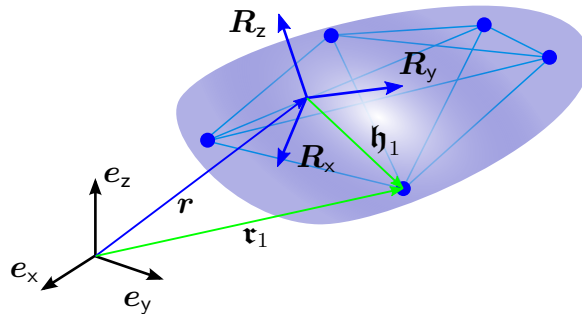


Figure 3.1: body fixed frame and particle positions

A common approach for modeling the rigid body (in both the physics and engineering perspective mentioned above) is the use of a *body fixed frame*. This is the choice of a position  $\mathbf{r} \in \mathbb{R}^3$  and a triple of orthonormal, right handed vectors  $[\mathbf{R}_x, \mathbf{R}_y, \mathbf{R}_z] = \mathbf{R} \in \mathbb{SO}(3)$  which are rigidly attached to the body, i.e. move with it. The position of any particle of the body may then be written as (see Figure 3.1)

$$\mathbf{r}_p = \mathbf{r} + \mathbf{R}\mathbf{h}_p, \quad p = 1, \dots, \mathfrak{N} \quad (3.43)$$

where the relative position  $\mathbf{h}_p$  to the body fixed frame is *constant*. Consequently, the motion of the rigid body is completely captured by the position  $\mathbf{r}(t) \in \mathbb{R}^3$  and orientation  $\mathbf{R}(t) \in \mathbb{SO}(3)$  of the body fixed frame.

For parameterization of the velocity of the rigid body we will use the body fixed velocity  $\mathbf{v}(t) \in \mathbb{R}^3$  and the angular velocity  $\boldsymbol{\omega}(t) \in \mathbb{R}^3$  which are related to the configuration by

$$\dot{\mathbf{r}} = \mathbf{R}\mathbf{v}, \quad \dot{\mathbf{R}} = \mathbf{R} \operatorname{wed}(\boldsymbol{\omega}). \quad (3.44)$$

With this we may express the velocity and accelerations of the body particles as

$$\dot{\mathbf{r}}_p = \mathbf{R}(\mathbf{v} - \text{wed}(\mathbf{h}_p)\boldsymbol{\omega}), \quad (3.45a)$$

$$\ddot{\mathbf{r}}_p = \mathbf{R}(\dot{\mathbf{v}} - \text{wed}(\mathbf{h}_p)\dot{\boldsymbol{\omega}} + \text{wed}(\boldsymbol{\omega})(\mathbf{v} - \text{wed}(\mathbf{h}_p)\boldsymbol{\omega})), \quad p = 1, \dots, \mathfrak{N} \quad (3.45b)$$

In order to comply to the framework from the previous chapter we may group the configuration coordinates as  $\mathbf{x} = [\mathbf{r}^\top, \mathbf{R}_x^\top, \mathbf{R}_y^\top, \mathbf{R}_z^\top]^\top \in \mathbb{X} \subset \mathbb{R}^{12}$  and their geometric constraint as  $\phi(\mathbf{x}) = \mathbf{0}$  are the constraints of  $\mathbb{SO}(3)$  as discussed in [REF]. The kinematic relation to the chosen velocity coordinates  $\boldsymbol{\xi}$  is

$$\underbrace{\begin{bmatrix} \dot{\mathbf{r}} \\ \dot{\mathbf{R}}_x \\ \dot{\mathbf{R}}_y \\ \dot{\mathbf{R}}_z \end{bmatrix}}_{\dot{\mathbf{x}}} = \underbrace{\begin{bmatrix} \mathbf{R}_x & \mathbf{R}_y & \mathbf{R}_z & 0 & 0 & 0 \\ 0 & 0 & 0 & 0 & -\mathbf{R}_z & \mathbf{R}_y \\ 0 & 0 & 0 & \mathbf{R}_z & 0 & -\mathbf{R}_x \\ 0 & 0 & 0 & -\mathbf{R}_y & \mathbf{R}_x & 0 \end{bmatrix}}_{\mathbf{A}} \underbrace{\begin{bmatrix} v_x \\ v_y \\ v_z \\ \omega_x \\ \omega_y \\ \omega_z \end{bmatrix}}_{\boldsymbol{\xi}}. \quad (3.46)$$

Plugging the kinematic matrix  $\mathbf{A}$  from into the definition (2.20) of the commutation symbols  $\gamma$  yields

$$\begin{aligned} \gamma_{26}^1 &= \gamma_{53}^1 = \gamma_{34}^2 = \gamma_{61}^2 = \gamma_{15}^3 = \gamma_{42}^3 = \gamma_{56}^4 = \gamma_{64}^5 = \gamma_{45}^6 = 1, \\ \gamma_{62}^1 &= \gamma_{35}^1 = \gamma_{43}^2 = \gamma_{16}^2 = \gamma_{51}^3 = \gamma_{24}^3 = \gamma_{65}^4 = \gamma_{46}^5 = \gamma_{54}^6 = -1 \end{aligned} \quad (3.47)$$

and the remaining coefficients vanish. With this we have

$$[\gamma_{ij}^k \xi^j]_{i=1 \dots 6}^{k=1 \dots 6} = \begin{bmatrix} \text{wed}(\boldsymbol{\omega}) & 0 \\ \text{wed}(\mathbf{v}) & \text{wed}(\boldsymbol{\omega}) \end{bmatrix} = -\text{ad}_{\boldsymbol{\xi}}^\top \quad (3.48)$$

whose naming will be discussed later.

### 3.3.2 Inertia

The previous section derived several formulations for the generalized inertial force  $\mathbf{f}^M$ . These will now be applied to the the rigid body and the chosen coordinates.

**Kinetic energy.** Expressing the particle velocities  $\dot{\mathbf{r}}_p$  in terms of the chosen coordinates (3.45a) the kinetic energy  $\mathcal{T}$  of a free rigid body is

$$\begin{aligned} \mathcal{T} &= \frac{1}{2} \sum_p m_p \left\| \overbrace{\mathbf{R}(\mathbf{v} - \text{wed}(\mathbf{h}_p)\boldsymbol{\omega})}^{\dot{\mathbf{r}}_p} \right\|^2 \\ &= \frac{1}{2} \underbrace{\sum_p m_p \|\mathbf{v}\|^2}_{m} - \mathbf{v}^\top \underbrace{\sum_p m_p \text{wed}(\mathbf{h}_p) \boldsymbol{\omega}}_{m \text{wed}(\mathbf{s})} + \frac{1}{2} \boldsymbol{\omega}^\top \underbrace{\sum_p m_p \text{wed}(\mathbf{h}_p)^\top \text{wed}(\mathbf{h}_p)}_{\boldsymbol{\Theta}} \boldsymbol{\omega} \\ &= \frac{1}{2} \underbrace{[\mathbf{v}^\top \boldsymbol{\omega}^\top]}_{\boldsymbol{\xi}^\top} \underbrace{\begin{bmatrix} m \mathbf{I}_3 & m \text{wed}(\mathbf{s})^\top \\ m \text{wed}(\mathbf{s}) & \boldsymbol{\Theta} \end{bmatrix}}_{\mathbf{M}} \underbrace{[\mathbf{v} \ \boldsymbol{\omega}]}_{\boldsymbol{\xi}}. \end{aligned} \quad (3.49)$$

Here we have substituted some well established inertia parameters: the total mass  $m$ , the center of mass  $\mathbf{s} = m^{-1} \sum_p \mathfrak{m}_p \mathbf{h}_p$  and the moment of inertia  $\Theta = \Theta^\top$ . Assuming that the particle masses are positive  $\mathfrak{m}_p > 0, p = 1, \dots, \mathfrak{N}$  implies that the total mass is positive  $m > 0$ . Furthermore, if the rigid body has at least three particles that do not lie on a line, the inertia matrix is positive definite  $\Theta > 0$ . It is important to notice that the inertia matrix  $\mathbf{M}$  for the chosen coordinates is *constant*<sup>1</sup>.

Plugging the the kinetic energy (3.49) into the corresponding formulation (3.29d) of the generalized inertia force and using the commutation symbols from (3.48) yields

$$\mathbf{f}^M = \underbrace{\begin{bmatrix} m\mathbf{I}_3 & m \text{wed}(\mathbf{s})^\top \\ m \text{wed}(\mathbf{s}) & \Theta \end{bmatrix}}_{\mathbf{M}} \underbrace{\begin{bmatrix} \dot{\mathbf{v}} \\ \dot{\boldsymbol{\omega}} \end{bmatrix}}_{\dot{\xi}} + \underbrace{\begin{bmatrix} \text{wed}(\boldsymbol{\omega}) & 0 \\ \text{wed}(\mathbf{v}) & \text{wed}(\boldsymbol{\omega}) \end{bmatrix}}_{-\text{ad}_{\dot{\xi}}^\top} \underbrace{\begin{bmatrix} m\mathbf{I}_3 & m \text{wed}(\mathbf{s})^\top \\ m \text{wed}(\mathbf{s}) & \Theta \end{bmatrix}}_{\mathbf{M}} \underbrace{\begin{bmatrix} \mathbf{v} \\ \boldsymbol{\omega} \end{bmatrix}}_{\xi} \quad (3.50)$$

**Acceleration energy.** Expressing the particle accelerations  $\ddot{\mathbf{r}}_p$  in terms of the coordinates (3.45b) we find the acceleration energy  $\mathcal{S}$  for the free rigid body as<sup>2</sup>

$$\begin{aligned} \mathcal{S} &= \frac{1}{2} \sum_p \mathfrak{m}_p \left\| \overbrace{\mathbf{R}(\dot{\mathbf{v}} - \text{wed}(\mathbf{h}_p)\dot{\boldsymbol{\omega}} + \text{wed}(\boldsymbol{\omega})(\mathbf{v} - \text{wed}(\mathbf{h}_p)\boldsymbol{\omega}))}^{\ddot{\mathbf{r}}_p} \right\|^2 \\ &= \underbrace{\frac{1}{2} \sum_p \mathfrak{m}_p \|\dot{\mathbf{v}}\|^2}_{m} - \dot{\mathbf{v}}^\top \underbrace{\sum_p \mathfrak{m}_p \text{wed}(\mathbf{h}_p) \dot{\boldsymbol{\omega}}}_{m \text{wed}(\mathbf{s})} + \frac{1}{2} \dot{\boldsymbol{\omega}}^\top \underbrace{\sum_p \mathfrak{m}_p \text{wed}(\mathbf{h}_p)^\top \text{wed}(\mathbf{h}_p)}_{\Theta} \dot{\boldsymbol{\omega}} \\ &\quad + \dot{\mathbf{v}}^\top \text{wed}(\boldsymbol{\omega}) \left( \underbrace{\sum_p \mathfrak{m}_p \mathbf{v}}_{m} - \underbrace{\sum_p \mathfrak{m}_p \text{wed}(\mathbf{h}_p) \boldsymbol{\omega}}_{m \text{wed}(\mathbf{s})} \right) \\ &\quad + \dot{\boldsymbol{\omega}}^\top \left( \underbrace{\sum_p \mathfrak{m}_p \text{wed}(\mathbf{h}_p) \text{wed}(\boldsymbol{\omega}) \mathbf{v}}_{m \text{wed}(\mathbf{s})} + \text{wed}(\boldsymbol{\omega}) \underbrace{\sum_p \mathfrak{m}_p \text{wed}(\mathbf{h}_p)^\top \text{wed}(\mathbf{h}_p)}_{\Theta} \boldsymbol{\omega} \right) \\ &\quad + \frac{1}{2} \underbrace{\sum_p \mathfrak{m}_p \|\text{wed}(\boldsymbol{\omega})\mathbf{v}\|^2}_{m} + \mathbf{v}^\top \text{wed}(\boldsymbol{\omega})^2 \underbrace{\sum_p \mathfrak{m}_p \text{wed}(\mathbf{h}_p) \boldsymbol{\omega}}_{m \text{wed}(\mathbf{s})} \\ &\quad + \frac{1}{2} \text{tr} \left( \underbrace{\sum_p \mathfrak{m}_p \mathbf{h}_p \mathbf{h}_p^\top}_{\Theta'} \text{wed}(\boldsymbol{\omega})^4 \right) \end{aligned} \quad (3.51)$$

---

<sup>1</sup>One reason for the choice of  $\mathbf{v}$  as velocity coordinates it the fact that the inertia matrix  $\mathbf{M}$  is *constant*. If we choose instead  $\dot{\mathbf{r}}$  as velocity coordinates we have

$$\mathcal{T} = \frac{1}{2} [\dot{\mathbf{r}}^\top, \boldsymbol{\omega}^\top] \begin{bmatrix} m\mathbf{I}_3 & m\mathbf{R} \text{wed}(\mathbf{s})^\top \\ m \text{wed}(\mathbf{s})\mathbf{R}^\top & \Theta \end{bmatrix} \begin{bmatrix} \dot{\mathbf{r}} \\ \boldsymbol{\omega} \end{bmatrix}.$$

Obviously the body inertia matrix depends on the orientation  $\mathbf{R}$  of the body and is not constant unless the reference position  $\mathbf{r}$  coincides with the *center of mass*, i.e.  $\mathbf{s} = 0$ . Actually many textbooks, e.g. [Murray et al., 1994, p. 167] or [Shabana, 2005, p. 153], restrict to this case for their expressions of the kinetic energy. In the next section on rigid body systems we will see that it can be quite useful to use *geometrically* meaningful body fixed frames rather than restricting to the center of mass.

<sup>2</sup>using the Jacobi identity  $\mathbf{a}, \mathbf{b}, \mathbf{c} \in \mathbb{R}^3$ :  $\text{wed}(\mathbf{a}) \text{wed}(\mathbf{b})\mathbf{c} + \text{wed}(\mathbf{b}) \text{wed}(\mathbf{c})\mathbf{a} + \text{wed}(\mathbf{c}) \text{wed}(\mathbf{a})\mathbf{b} = \mathbf{0}$

Not at all surprisingly, we found the same inertia parameters  $(m, \mathbf{s}, \boldsymbol{\Theta})$  as for the kinetic energy  $\mathcal{T}$ . Collecting these further in the inertia matrix  $\mathbf{M}$  we have

$$\begin{aligned} \mathcal{S} = & \underbrace{\frac{1}{2} [\dot{\mathbf{v}}^\top \dot{\boldsymbol{\omega}}^\top]}_{\dot{\xi}^\top} \underbrace{\left[ \begin{array}{cc} m\mathbf{I}_3 & m \text{wed}(\mathbf{s})^\top \\ m \text{wed}(\mathbf{s}) & \boldsymbol{\Theta} \end{array} \right]}_{\mathbf{M}} \underbrace{[\dot{\mathbf{v}} \dot{\boldsymbol{\omega}}]}_{\dot{\xi}} \\ & + \underbrace{[\dot{\mathbf{v}}^\top \dot{\boldsymbol{\omega}}^\top]}_{\dot{\xi}^\top} \underbrace{\left[ \begin{array}{cc} \text{wed}(\boldsymbol{\omega}) & \mathbf{0} \\ \text{wed}(\mathbf{v}) & \text{wed}(\boldsymbol{\omega}) \end{array} \right]}_{-\text{ad}_{\dot{\xi}}^\top} \underbrace{\left[ \begin{array}{cc} m\mathbf{I}_3 & m \text{wed}(\mathbf{s})^\top \\ m \text{wed}(\mathbf{s}) & \boldsymbol{\Theta} \end{array} \right]}_{\mathbf{M}} \underbrace{[\mathbf{v} \boldsymbol{\omega}]}_{\xi} \\ & + \underbrace{\frac{1}{2} m \|\text{wed}(\boldsymbol{\omega})\mathbf{v}\|^2 + \mathbf{v}^\top \text{wed}(\boldsymbol{\omega})^2 m \text{wed}(\mathbf{s})\boldsymbol{\omega} + \frac{1}{2} \text{tr}(\boldsymbol{\Theta}' \text{wed}(\boldsymbol{\omega})^4)}_{\mathcal{S}_0}. \end{aligned} \quad (3.52)$$

Plugging this into the corresponding formulation (3.29e) of the generalized inertia force, i.e.  $\mathbf{f}^M = \partial \mathcal{S} / \partial \dot{\xi}$ , we obviously find the same expression as above (3.50). Note that  $\mathcal{S}_0$  is independent of the generalized acceleration  $\dot{\xi}$  and consequently does not contribute to the inertia force.

**Connection coefficients.** As the inertia matrix  $\mathbf{M}$  in (3.49) is constant, the corresponding connection coefficients  $\Gamma_{ijk}$  only consist of the terms with the commutation coefficients  $\gamma$ :

$$\Gamma_{ijk} = \frac{1}{2} (\gamma_{ij}^s M_{sk} + \gamma_{ik}^s M_{sj} - \gamma_{jk}^s M_{si}) = -\Gamma_{jik}. \quad (3.53)$$

Using the commutation coefficients  $\gamma$  given in (3.47) and taking into account the skew symmetry above, the non-zero connection coefficients are

$$\Gamma_{324} = \Gamma_{135} = \Gamma_{216} = m, \quad (3.54a)$$

$$\Gamma_{254} = \Gamma_{364} = \Gamma_{515} = \Gamma_{616} = ms_x, \quad (3.54b)$$

$$\Gamma_{424} = \Gamma_{145} = \Gamma_{365} = \Gamma_{626} = ms_y, \quad (3.54c)$$

$$\Gamma_{434} = \Gamma_{535} = \Gamma_{146} = \Gamma_{256} = ms_z, \quad (3.54d)$$

$$\Gamma_{654} = \Theta'_{xx} = \frac{1}{2} (\Theta_{yy} + \Theta_{zz} - \Theta_{xx}), \quad (3.54e)$$

$$\Gamma_{465} = \Theta'_{yy} = \frac{1}{2} (\Theta_{xx} + \Theta_{zz} - \Theta_{yy}), \quad (3.54f)$$

$$\Gamma_{546} = \Theta'_{zz} = \frac{1}{2} (\Theta_{xx} + \Theta_{yy} - \Theta_{zz}), \quad (3.54g)$$

$$\Gamma_{464} = \Gamma_{655} = \Theta'_{xy} = -\Theta_{xy}, \quad (3.54h)$$

$$\Gamma_{544} = \Gamma_{656} = \Theta'_{xz} = -\Theta_{xz}, \quad (3.54i)$$

$$\Gamma_{545} = \Gamma_{466} = \Theta'_{yz} = -\Theta_{yz}. \quad (3.54j)$$

Note that the quantity  $\boldsymbol{\Theta}' = \frac{1}{2} \text{tr}(\boldsymbol{\Theta})\mathbf{I}_3 - \boldsymbol{\Theta}$  also appeared above in (3.51). Simply assembling the terms  $f_i^M = M_{ij}\dot{\xi}^j + \Gamma_{ijk}\dot{\xi}^j\xi^k$  we may check that this is indeed again (3.50).

### 3.3.3 Gravitation

The potential energy  $\mathcal{V}^G$  of a rigid body due to a gravitational acceleration  $\mathbf{a}_G$  according to (3.31) in terms of the chosen coordinates is

$$\mathcal{V}^G = \sum_p \underbrace{\langle \mathbf{r} + \mathbf{R}\mathbf{h}_p, \mathbf{m}_p \mathbf{a}_G \rangle}_{m \mathbf{a}_G} = \langle \underbrace{\sum_p \mathbf{m}_p \mathbf{r}}_m + \mathbf{R} \underbrace{\sum_p \mathbf{m}_p \mathbf{h}_p}_{m \mathbf{s}}, m \mathbf{a}_G \rangle = \langle \mathbf{r} + \mathbf{R}\mathbf{s}, m \mathbf{a}_G \rangle. \quad (3.55)$$

Note that the parameters of total mass  $m$  and center of mass  $\mathbf{s}$  are the same as found above for the inertia matrix. The resulting generalized force is

$$\mathbf{f}^G = \nabla \mathcal{V}^G = \begin{bmatrix} \mathbf{R}^\top m \mathbf{a}_G \\ \text{wed}(\mathbf{s}) \mathbf{R}^\top m \mathbf{a}_G \end{bmatrix}. \quad (3.56)$$

### 3.3.4 Stiffness

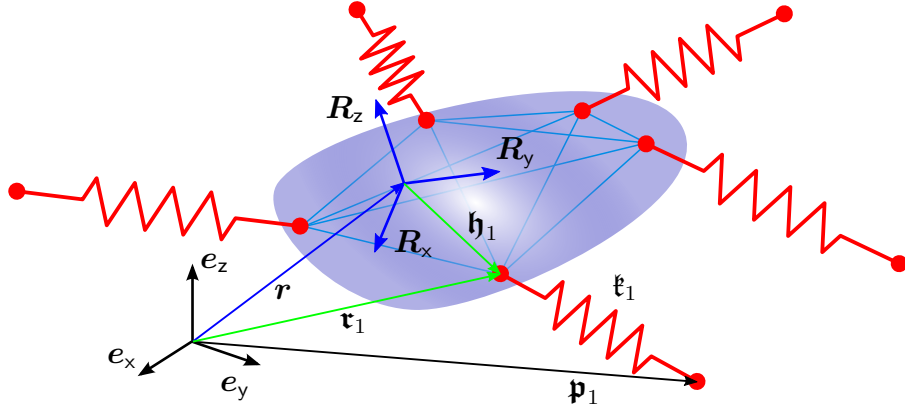


Figure 3.2: springs attached to a rigid body

Assume that every particle of the rigid body with position  $\mathbf{r}_p$  is connected to a position  $\mathbf{p}_p \in \mathbb{R}^3$  by a linear spring with stiffness  $\mathbf{k}_p \in \mathbb{R}^{(+)}$ , see Figure 3.2. The resulting potential energy in terms of the rigid body coordinates  $\mathbf{x} \cong (\mathbf{r}, \mathbf{R})$  is

$$\mathcal{V}^K(\mathbf{x}) = \frac{1}{2} \sum_p \mathbf{k}_p \|\mathbf{r} + \mathbf{R}\mathbf{h}_p - \mathbf{p}_p\|^2. \quad (3.57)$$

**Some identities.** In the following we use some basic identities

$$\mathbf{a}, \mathbf{b} \in \mathbb{R}^n : \mathbf{a}^\top \mathbf{b} = \text{tr}(\mathbf{a}\mathbf{b}^\top) \quad (3.58a)$$

$$\mathbf{a}, \mathbf{b} \in \mathbb{R}^3 : \text{wed}(\mathbf{a})\mathbf{b} = \text{vee2}(\mathbf{b}\mathbf{a}^\top) \quad (3.58b)$$

$$\text{wed}(\mathbf{a}) \text{wed}(\mathbf{b}) = \mathbf{b}\mathbf{a}^\top - (\mathbf{b}^\top \mathbf{a})\mathbf{I}_3 \quad (3.58c)$$

$$\mathbf{A} \in \mathbb{R}^{3 \times 3}, \mathbf{b} \in \mathbb{R}^3 : \text{tr}(\mathbf{A} \text{wed}(\mathbf{b})) = -\mathbf{b}^\top \text{vee2}(\mathbf{A}) \quad (3.58d)$$

$$\text{vee2}(\text{wed}(\mathbf{b})\mathbf{A}) = (\text{tr}(\mathbf{A})\mathbf{I}_3 - \mathbf{A})\mathbf{b} \quad (3.58e)$$

Each may be checked by direct computation.

**Stiffness parameters.** Using the identities above we may rearrange (3.57) to

$$\begin{aligned}\mathcal{V}^K(\mathbf{x}) &= \frac{1}{2} \sum_p \mathbf{\mathfrak{k}}_p \|\mathbf{r} + \mathbf{R}\mathbf{h}_p - \mathbf{p}_p\|^2 \\ &= \frac{1}{2} \sum_p \mathbf{\mathfrak{k}}_p (\|\mathbf{r}\|^2 + \underbrace{\|\mathbf{R}\mathbf{h}_p\|^2}_{\text{const.}} + \underbrace{\|\mathbf{p}_p\|^2}_{\text{const.}} + 2\langle \mathbf{r}, \mathbf{R}\mathbf{h}_p \rangle - 2\langle \mathbf{r}, \mathbf{p}_p \rangle - 2\langle \mathbf{R}\mathbf{h}_p, \mathbf{p}_p \rangle) \\ &= \frac{1}{2} k \|\mathbf{r}\|^2 + k \langle \mathbf{r}, \mathbf{R}\mathbf{h} \rangle - k \langle \mathbf{r}, \mathbf{p} \rangle - \text{tr}(\mathbf{P}\mathbf{R}) + \underbrace{\frac{1}{2} \sum_p \mathbf{\mathfrak{k}}_p (\|\mathbf{h}_p\|^2 + \|\mathbf{p}_p\|^2)}_{\mathcal{V}_c^K = \text{const.}} \quad (3.59)\end{aligned}$$

with substitution of the constant parameters

$$k = \sum_p \mathbf{\mathfrak{k}}_p, \quad \mathbf{h} = k^{-1} \sum_p \mathbf{\mathfrak{k}}_p \mathbf{h}_p, \quad \mathbf{p} = k^{-1} \sum_p \mathbf{\mathfrak{k}}_p \mathbf{p}_p, \quad \mathbf{P} = \sum_p \mathbf{\mathfrak{k}}_p \mathbf{h}_p \mathbf{p}_p^\top. \quad (3.60)$$

Note that there was no specific assumption for the particle and spring distribution, i.e. on the values of  $\mathbf{h}_p$ ,  $\mathbf{p}_p$  and  $\mathbf{\mathfrak{k}}_p$ . Consequently, any constellation may be captured by the  $1 + 3 + 3 + 9 + 1 = 17$  parameters within  $(k, \mathbf{h}, \mathbf{p}, \mathbf{P}, \mathcal{V}_c^K)$ .

**Critical points.** The time derivatives of the potential may be written as

$$\begin{aligned}\frac{d}{dt} \mathcal{V}^K &= k \langle \mathbf{r}, \mathbf{R}\mathbf{v} \rangle + k \langle \mathbf{R}\mathbf{v}, \mathbf{R}\mathbf{h} \rangle + k \langle \mathbf{r}, \mathbf{R} \text{wed}(\boldsymbol{\omega}) \mathbf{h} \rangle - k \langle \mathbf{R}\mathbf{v}, \mathbf{p} \rangle - \text{tr}(\mathbf{P}\mathbf{R} \text{wed}(\boldsymbol{\omega})) \\ &= \boldsymbol{\xi}^\top \underbrace{\left[ \begin{array}{c} k(\mathbf{R}^\top(\mathbf{r} - \mathbf{p}) + \mathbf{h}) \\ k \text{wed}(\mathbf{h}) \mathbf{R}^\top \mathbf{r} + \text{vee2}(\mathbf{P}\mathbf{R}) \end{array} \right]}_{\nabla \mathcal{V}^K} \quad (3.61)\end{aligned}$$

$$\frac{d^2}{dt^2} \mathcal{V}^K = \boldsymbol{\xi}^\top \nabla \mathcal{V}^K + \boldsymbol{\xi}^\top \underbrace{\left[ \begin{array}{cc} k \mathbf{I}_3 & k \text{wed}(\mathbf{R}^\top(\mathbf{r} - \mathbf{p})) \\ k \text{wed}(\mathbf{h}) & k \text{wed}(\mathbf{h}) \text{wed}(\mathbf{R}^\top \mathbf{r}) + \text{tr}(\mathbf{P}\mathbf{R}) \mathbf{I}_3 - (\mathbf{P}\mathbf{R})^\top \end{array} \right]}_{\nabla^2 \mathcal{V}^K} \boldsymbol{\xi} \quad (3.62)$$

We are interested in configurations  $\mathbf{x}_R \cong (\mathbf{r}_R, \mathbf{R}_R)$  at which the potential is stationary  $\nabla \mathcal{V}^K(\mathbf{x}_R) = \mathbf{0}$ : From the upper part of (3.61) we get the condition

$$\mathbf{r}_R = \mathbf{p} - \mathbf{R}_R \mathbf{h}. \quad (3.63)$$

Plugging this into the lower part of (3.61) we obtain

$$k \text{wed}(\mathbf{h}) \mathbf{R}_R^\top (\mathbf{p} - \mathbf{R}_R \mathbf{h}) + \text{vee2}(\mathbf{P}\mathbf{R}_R) = \text{vee2}(\underbrace{(\mathbf{P} - k \mathbf{h} \mathbf{p}^\top) \mathbf{R}_R}_{\mathbf{P}_s}) = \mathbf{0}. \quad (3.64)$$

The solution to this subproblem  $\text{vee2}(\mathbf{P}_s \mathbf{R}_R) = \mathbf{0}$ ,  $\mathbf{R}_R \in \mathbb{SO}(3)$  is discussed in great detail in section A.3: Let  $\mathbf{P}_s^\top = \mathbf{X} \text{Wed}(\boldsymbol{\Pi}_s)$  with  $\mathbf{X} \in \mathbb{SO}(3)$ ,  $\boldsymbol{\Pi}_s \in \mathbb{SYM}_0^+(3)$  be a *special polar decomposition*. Then  $\mathbf{R}_R = \mathbf{X}$  is clearly a critical point. Plugging  $\mathbf{P} = \text{Wed}(\boldsymbol{\Pi}_s) \mathbf{R}_R^\top + k \mathbf{h} \mathbf{p}^\top$  into the Hessian matrix, we have

$$\begin{aligned}\nabla^2 \mathcal{V}^K(\mathbf{x}_R) &= \begin{bmatrix} k \mathbf{I}_3 & k \text{wed}(\mathbf{h})^\top \\ k \text{wed}(\mathbf{h}) & \boldsymbol{\Pi}_s - k \text{wed}(\mathbf{h})^2 \end{bmatrix} \\ &= \begin{bmatrix} \mathbf{I}_3 & \mathbf{0} \\ \text{wed}(\mathbf{h}) & \mathbf{I}_3 \end{bmatrix} \begin{bmatrix} k \mathbf{I}_3 & \mathbf{0} \\ \mathbf{0} & \boldsymbol{\Pi}_s \end{bmatrix} \begin{bmatrix} \mathbf{I}_3 & \text{wed}(\mathbf{h})^\top \\ \mathbf{0} & \mathbf{I}_3 \end{bmatrix} \quad (3.65)\end{aligned}$$

By Sylvester's law of inertia, the definiteness of  $\nabla^2 \mathcal{V}^K(\mathbf{x}_R)$  coincides with the definiteness of  $k \geq 0$  and  $\boldsymbol{\Pi}_s \geq 0$ . Using the results from section A.3 we may conclude that  $\mathbf{x}_R$  is a minimum, and it is strict and global, if, and only if,  $k > 0$  and  $\boldsymbol{\Pi}_s > 0$ .

**Stiffness parameters cont'd.** We may express the parameters  $\mathbf{p}$  and  $\mathbf{P}$  in terms of the minimum configuration  $(\mathbf{r}_R, \mathbf{R}_R)$  and the moment of stiffness matrix  $\boldsymbol{\Pi}_s$  as

$$\mathbf{p} = \mathbf{r}_R + \mathbf{R}_R \mathbf{h}, \quad \mathbf{P} = \text{Wed}(\boldsymbol{\Pi}_s) \mathbf{R}_R^\top + k \mathbf{h} (\mathbf{r}_R + \mathbf{R}_R \mathbf{h})^\top \quad (3.66)$$

Plugging this into (3.59) yields

$$\begin{aligned} \mathcal{V}^K(\mathbf{x}) &= \frac{1}{2}k\|\mathbf{r}\|^2 + k\langle \mathbf{r}, \mathbf{R}\mathbf{h} \rangle - k\langle \mathbf{r}, \mathbf{r}_R + \mathbf{R}_R \mathbf{h} \rangle - k\langle \mathbf{r}_R + \mathbf{R}_R \mathbf{h}, \mathbf{R}\mathbf{h} \rangle \\ &\quad - \text{tr}(\text{Wed}(\boldsymbol{\Pi}_s) \mathbf{R}_R^\top \mathbf{R}) + \frac{1}{2} \sum_p \mathfrak{k}_p (\|\mathbf{h}_p\|^2 + \|\mathbf{p}_p\|^2) \\ &= \frac{1}{2}k\|\mathbf{r} + \mathbf{R}\mathbf{h} - (\mathbf{r}_R + \mathbf{R}_R \mathbf{h})\|^2 + \text{tr}(\text{Wed}(\boldsymbol{\Pi}_s)(\mathbf{I}_3 - \mathbf{R}_R^\top \mathbf{R})) \\ &\quad - \underbrace{\frac{1}{2}k\|\mathbf{r}_R + \mathbf{R}_R \mathbf{h}\|^2 - \frac{1}{2}k\|\mathbf{h}\|^2 - \text{tr}(\text{Wed}(\boldsymbol{\Pi}_s)) + \frac{1}{2} \sum_p \mathfrak{k}_p (\|\mathbf{h}_p\|^2 + \|\mathbf{p}_p\|^2)}_{\mathcal{V}_0^K = \mathcal{V}^K(\mathbf{x}_R)} \end{aligned} \quad (3.67)$$

The first two parts vanish at the minimum  $\mathbf{x}_R$  and  $\mathcal{V}_0^K$  is the potential of the residual displacement of the springs.

$$\begin{aligned} \frac{d}{dt} \mathcal{V}^K &= k\langle \mathbf{R}\mathbf{v} + \mathbf{R} \text{wed}(\boldsymbol{\omega})\mathbf{h}, \mathbf{r} + \mathbf{R}\mathbf{h} - (\mathbf{r}_R + \mathbf{R}_R \mathbf{h}) \rangle - \text{tr}(\text{Wed}(\boldsymbol{\Pi}_s) \mathbf{R}_R^\top \mathbf{R} \text{wed}(\boldsymbol{\omega})) \\ &= k\langle \mathbf{v} - \text{wed}(\mathbf{h})\boldsymbol{\omega}, \mathbf{R}^\top(\mathbf{r} + \mathbf{R}\mathbf{h} - (\mathbf{r}_R + \mathbf{R}_R \mathbf{h})) \rangle + \boldsymbol{\omega}^\top \text{vee2}(\text{Wed}(\boldsymbol{\Pi}_s) \mathbf{R}_R^\top \mathbf{R}) \\ &= \dot{\boldsymbol{\xi}}^\top \underbrace{\left[ \begin{array}{c} k(\mathbf{R}^\top(\mathbf{r} - \mathbf{p}) + \mathbf{h}) \\ k \text{wed}(\mathbf{h}) \mathbf{R}^\top \mathbf{r} + \text{vee2}(\mathbf{P}\mathbf{R}) \end{array} \right]}_{\nabla \mathcal{V}^K} \end{aligned} \quad (3.68)$$

$$\frac{d^2}{dt^2} \mathcal{V}^K = \dot{\boldsymbol{\xi}}^\top \nabla \mathcal{V}^K + \dot{\boldsymbol{\xi}}^\top \underbrace{\left[ \begin{array}{cc} k\mathbf{I}_3 & k \text{wed}(\mathbf{h}) \mathbf{R}^\top(\mathbf{r} - \mathbf{p}) \\ k \text{wed}(\mathbf{h}) & k \text{wed}(\mathbf{h}) \text{wed}(\mathbf{R}^\top \mathbf{r}) + \text{tr}(\mathbf{P}\mathbf{R})\mathbf{I}_3 - (\mathbf{P}\mathbf{R})^\top \end{array} \right]}_{\nabla^2 \mathcal{V}^K} \boldsymbol{\xi} \quad (3.69)$$

The differential may be written as

$$\nabla \mathcal{V}^K(\mathbf{x}) = \left[ \begin{array}{c} k\mathbf{R}^\top(\mathbf{r} - \mathbf{r}_R) + (\mathbf{I}_3 - \mathbf{R}^\top \mathbf{R}_R)k\mathbf{h} \\ k \text{wed}(\mathbf{h}) \mathbf{R}^\top(\mathbf{r} - \mathbf{r}_R) + \text{vee2}(\boldsymbol{\Pi}' \mathbf{R}_R^\top \mathbf{R}) \end{array} \right] \quad (3.70)$$

and the Hessian at the minimum is

$$\nabla^2 \mathcal{V}^K(\mathbf{x}_R) = \left[ \begin{array}{cc} k\mathbf{I}_3 & k \text{wed}(\mathbf{h})^\top \\ k \text{wed}(\mathbf{h}) & \boldsymbol{\Pi} \end{array} \right] \geq 0 \quad (3.71)$$

where  $\boldsymbol{\Pi} = \text{tr}(\boldsymbol{\Pi}')\mathbf{I}_3 - \boldsymbol{\Pi}' = \boldsymbol{\Pi}_s + k \text{wed}(\mathbf{h}) \text{wed}(\mathbf{h})^\top \in \text{SYM}_0^+(\mathbf{3})$ .

**Conclusion.** The conclusion of this subsection is that any constellation of linear springs attached to a rigid body may be captured by the potential  $\mathcal{V}^K$  from (3.67) and the resulting force  $\mathbf{f}^K = \nabla \mathcal{V}^K$  from (3.70). It is parameterized by 6 parameters within  $(\mathbf{r}_R, \mathbf{R}_R) \in \mathbb{R}^3 \times \text{SO}(3)$  which describe the minimum, the  $1+3+6=10$  parameters within the total stiffness  $k \in \mathbb{R}_0^+$ , the center of stiffness  $\mathbf{h} \in \mathbb{R}^3$  and the moment of stiffness  $\boldsymbol{\Pi} \in \text{SYM}_0^+(\mathbf{3})$  and the offset  $\mathcal{V}_0^K$ :  $\mathcal{V}^K(\mathbf{x}) \geq \mathcal{V}_0^K \geq 0$ . The naming is due to the obvious analogy to the inertia parameters from the previous section. The minimum is strict and global if, and only if,  $k > 0$  and  $\boldsymbol{\Pi}_s > 0$ .

### 3.3.5 Dissipation

As motivated in the previous section we may motivate damping as particles moving within a viscous fluid which produce a drag force proportional to the particles velocity  $\dot{\mathbf{r}}_p$ . Different volumes of the particles may motivate different drag coefficients  $\mathfrak{d}_p$ , see ??.

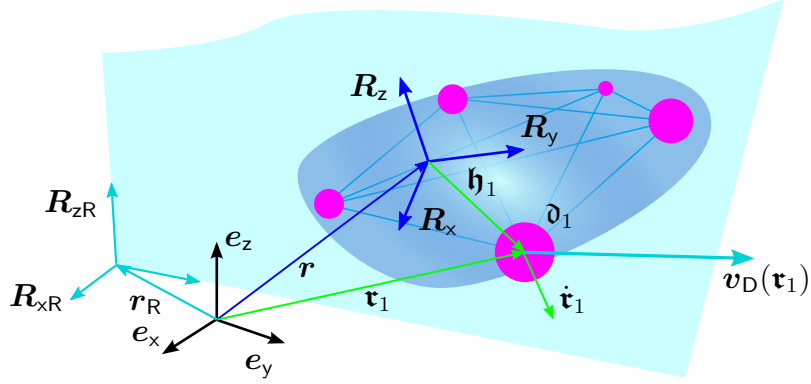


Figure 3.3: rigid body within viscous fluid

**General fluid motion.** Let the fluid at the position of  $p$ -th particle position have the velocity  $\mathbf{v}_{Dp}(t) \in \mathbb{R}^3$  and let its drag coefficient be  $\mathfrak{d}_p \in \mathbb{R}_0^+$ . Overall, the dissipation function is

$$\begin{aligned} \mathcal{R} &= \frac{1}{2} \sum_p \mathfrak{d}_p \| \overbrace{\mathbf{R}(\mathbf{v} - \text{wed}(\mathfrak{h}_p)\boldsymbol{\omega})}^{\dot{\mathbf{r}}_p} - \mathbf{v}_{Dp} \|^2 \\ &= \underbrace{\frac{1}{2} \sum_p \mathfrak{d}_p \|\mathbf{v}\|^2}_{d} - \mathbf{v}^\top \underbrace{\sum_p \mathfrak{d}_p \text{wed}(\mathfrak{h}_p) \boldsymbol{\omega}}_{\mathbf{d} \text{ wed}(\mathbf{l})} + \frac{1}{2} \boldsymbol{\omega}^\top \underbrace{\sum_p \mathfrak{d}_p \text{wed}(\mathfrak{h}_p)^\top \text{wed}(\mathfrak{h}_p) \boldsymbol{\omega}}_{\mathbf{r}} \\ &\quad - \mathbf{v}^\top \sum_p \mathfrak{d}_p \mathbf{R}^\top \mathbf{v}_{Dp} + \boldsymbol{\omega}^\top \sum_p \mathfrak{d}_p \text{wed}(\mathfrak{h}_p) \mathbf{R}^\top \mathbf{v}_{Dp} + \frac{1}{2} \sum_p \mathfrak{d}_p \|\mathbf{v}_{Dp}\|^2 \end{aligned} \quad (3.72)$$

The resulting generalized force is

$$\mathbf{f}^D = \frac{\partial \mathcal{R}}{\partial \xi} = \underbrace{\begin{bmatrix} d\mathbf{I}_3 & d \text{ wed}(\mathbf{l})^\top \\ d \text{ wed}(\mathbf{l}) & \boldsymbol{\gamma} \end{bmatrix}}_{\mathbf{D}} \underbrace{\begin{bmatrix} \mathbf{v} \\ \boldsymbol{\omega} \end{bmatrix}}_{\xi} + \sum_p \mathfrak{d}_p \begin{bmatrix} -\mathbf{I}_3 \\ \text{wed}(\mathfrak{h}_p) \end{bmatrix} \mathbf{R}^\top \mathbf{v}_{Dp}. \quad (3.73)$$

Again we found parameters similar to the established inertia parameters. In analogy to them we call  $d \in \mathbb{R}_0^+$  the total damping,  $\mathbf{l} \in \mathbb{R}^3$  the center of damping, and  $\boldsymbol{\gamma} \in \text{SYM}_0^+(3)$  the moment of damping.

**Rigid fluid motion.** Let us consider a special case in which the fluid velocity also obeys a rigid body motion parameterized by  $(\mathbf{r}_R, \mathbf{R}_R)$  and the velocity  $(\mathbf{v}_R, \boldsymbol{\omega}_R)$ , see Figure 3.3. The absolute fluid velocity at the particle position is then  $\mathbf{v}_{Dp} = \mathbf{R}_R(\mathbf{v}_R + \text{wed}(\boldsymbol{\omega}_R)\mathbf{R}_R^\top(\mathbf{r}_p -$

$\mathbf{r}_R)$ . Then we have the dissipation function

$$\begin{aligned} \mathcal{R} &= \frac{1}{2} \sum_p \mathfrak{d}_p \left\| \overbrace{\mathbf{R}(\mathbf{v} - \text{wed}(\mathbf{h}_p)\boldsymbol{\omega})}^{\dot{\mathbf{r}}_p} - \overbrace{\mathbf{R}_R(\mathbf{v}_R + \text{wed}(\boldsymbol{\omega}_R)\mathbf{R}_R^\top(\mathbf{r} + \mathbf{R}\mathbf{h}_p - \mathbf{r}_R))}^{v_{Dp}} \right\|^2 \\ &= \frac{1}{2} \sum_p \mathfrak{d}_p \left\| \underbrace{\mathbf{v} - \mathbf{R}^\top(\mathbf{R}_R\mathbf{v}_R - \text{wed}(\mathbf{r} - \mathbf{r}_R)\mathbf{R}_R\boldsymbol{\omega}_R)}_{\mathbf{v}_E} - \text{wed}(\mathbf{h}_p) \underbrace{(\boldsymbol{\omega} - \mathbf{R}^\top\mathbf{R}_R\boldsymbol{\omega}_R)}_{\boldsymbol{\omega}_E} \right\|^2 \\ &= \frac{1}{2} \underbrace{[\mathbf{v}_E^\top, \boldsymbol{\omega}_E^\top]}_{\boldsymbol{\xi}_E^\top} \underbrace{\begin{bmatrix} d\mathbf{I}_3 & d \text{wed}(\mathbf{l})^\top \\ d \text{wed}(\mathbf{l}) & \boldsymbol{\Upsilon} \end{bmatrix}}_{\mathbf{D}} \underbrace{\begin{bmatrix} \mathbf{v}_E \\ \boldsymbol{\omega}_E \end{bmatrix}}_{\boldsymbol{\xi}_E} \end{aligned} \quad (3.74)$$

The resulting generalized force is

$$\mathbf{f}^D = \frac{\partial \mathcal{R}}{\partial \boldsymbol{\xi}} = \frac{\partial \mathcal{R}}{\partial \boldsymbol{\xi}_E} = \mathbf{D} \boldsymbol{\xi}_E \quad (3.75)$$

### 3.3.6 Summary

Let

$$\underbrace{\begin{bmatrix} \dot{\mathbf{R}} & \dot{\mathbf{r}} \\ \mathbf{0} & 0 \end{bmatrix}}_{\dot{\mathbf{G}}} = \underbrace{\begin{bmatrix} \mathbf{R} & \mathbf{r} \\ \mathbf{0} & 1 \end{bmatrix}}_{\mathbf{G}} \underbrace{\begin{bmatrix} \text{wed}(\boldsymbol{\omega}) & \mathbf{v} \\ \mathbf{0} & 0 \end{bmatrix}}_{\text{wed}(\boldsymbol{\xi})} \quad (3.76)$$

define the scaled Frobenius norm as

$$\langle \mathbf{A}, \mathbf{B} \rangle_{\mathbf{K}} = \text{tr}(\mathbf{A}^\top \mathbf{K} \mathbf{B}), \quad \|\mathbf{A}\|_{\mathbf{K}}^2 = \langle \mathbf{A}, \mathbf{A} \rangle_{\mathbf{K}}. \quad (3.77)$$

Recalling the definitions of the kinetic energy  $\mathcal{T}$  of a free rigid body (3.49), acceleration energy  $\mathcal{S}$  in (3.51), dissipation function  $\mathcal{R}$  in (3.74) and the potential energy  $\mathcal{V}$  due to linear springs (??), we may write them as

$$\mathcal{T} = \frac{1}{2} \sum_p \mathfrak{m}_p \left\| \overbrace{\dot{\mathbf{r}} + \dot{\mathbf{R}}\mathbf{h}_p}^{\dot{\mathbf{r}}_p} \right\|^2 = \frac{1}{2} \|\dot{\mathbf{G}}^\top\|_{\mathbf{M}'}^2 \quad (3.78a)$$

$$\mathcal{S} = \frac{1}{2} \sum_p \mathfrak{m}_p \left\| \overbrace{\ddot{\mathbf{r}} + \ddot{\mathbf{R}}\mathbf{h}_p}^{\ddot{\mathbf{r}}_p} \right\|^2 = \frac{1}{2} \|\ddot{\mathbf{G}}^\top\|_{\mathbf{M}'}^2 \quad (3.78b)$$

$$\mathcal{R} = \frac{1}{2} \sum_p \mathfrak{d}_p \left\| \overbrace{\dot{\mathbf{r}} + \dot{\mathbf{R}}\mathbf{h}_p}^{\dot{\mathbf{r}}_p} \right\|^2 = \frac{1}{2} \|\dot{\mathbf{G}}^\top\|_{\mathbf{D}'}^2 \quad (3.78c)$$

$$\mathcal{V}^K = \frac{1}{2} \sum_p \mathfrak{k}_p \left\| \overbrace{\mathbf{r} + \mathbf{R}\mathbf{h}_p}^{\mathbf{r}_p} - \overbrace{(\mathbf{r}_R + \mathbf{R}_R\mathbf{h}_p)}^{\mathbf{r}_{pR}} \right\|^2 = \frac{1}{2} \|(\mathbf{G} - \mathbf{G}_R)^\top\|_{\mathbf{K}'}^2 \quad (3.78d)$$

$$\mathcal{V}^G = \sum_p \langle \overbrace{\mathbf{r} + \mathbf{R}\mathbf{h}_p}^{\mathbf{r}_p}, \mathfrak{m}_p \mathbf{a}_G \rangle = \langle \mathbf{G}^\top, \text{wed}(\boldsymbol{\alpha}_G)^\top \rangle_{\mathbf{M}'} \quad \boldsymbol{\alpha}_G^\top = [\mathbf{a}_G^\top, \mathbf{0}_{1 \times 3}]. \quad (3.78e)$$

where

$$\mathbf{M}' = \sum_p \mathfrak{m}_p \begin{bmatrix} \mathfrak{h}_p \mathfrak{h}_p^\top & \mathfrak{h}_p^\top \\ \mathfrak{h}_p & 1 \end{bmatrix} = \begin{bmatrix} \boldsymbol{\Theta}' & ms \\ ms^\top & m \end{bmatrix} \quad (3.79a)$$

$$\mathbf{D}' = \sum_p \mathfrak{d}_p \begin{bmatrix} \mathfrak{h}_p \mathfrak{h}_p^\top & \mathfrak{h}_p^\top \\ \mathfrak{h}_p & 1 \end{bmatrix} = \begin{bmatrix} \boldsymbol{\Upsilon}' & dl \\ dl^\top & d \end{bmatrix} \quad (3.79b)$$

$$\mathbf{K}' = \sum_p \mathfrak{k}_p \begin{bmatrix} \mathfrak{h}_p \mathfrak{h}_p^\top & \mathfrak{h}_p^\top \\ \mathfrak{h}_p & 1 \end{bmatrix} = \begin{bmatrix} \boldsymbol{\Pi}' & kh \\ kh^\top & k \end{bmatrix} \quad (3.79c)$$

The corresponding forces

$$\mathbf{f}^M = \frac{\partial \mathcal{S}}{\partial \dot{\xi}} = \text{vee2} ((\text{wed}(\dot{\xi}) + \text{wed}(\xi)^2) \mathbf{M}') \quad (3.80a)$$

$$\mathbf{f}^D = \frac{\partial \mathcal{R}}{\partial \xi} = \text{vee2} (\text{wed}(\xi) \mathbf{D}') \quad (3.80b)$$

$$\mathbf{f}^K = \nabla \mathcal{V}^K = \text{vee2} ((\mathbf{I}_4 - \mathbf{G}^{-1} \mathbf{G}_R) \mathbf{K}') \quad (3.80c)$$

$$\mathbf{f}^G = \nabla \mathcal{V}^G = \text{vee2} (\mathbf{G}^\top \text{wed}(\alpha_G) \mathbf{M}') = \mathbf{M} \text{Ad}_{\mathbf{G}}^{-1} \alpha_G. \quad (3.80d)$$

## 3.4 Rigid body systems

A rigid body system consists of  $N \geq 1$  rigid bodies which may be constrained to each other and/or to the surrounding space. As before, we restrict to geometric constraints. The derivation of equations of motion for such systems is treated in e.g. [Roberson and Schwertassek, 1988], [Murray et al., 1994], [Kane and Levinson, 1985])

The goal of this section is to present an algorithm for the computation of the equations of motion for rigid body systems that allows for a rather flexible parameterization.

### 3.4.1 Configuration

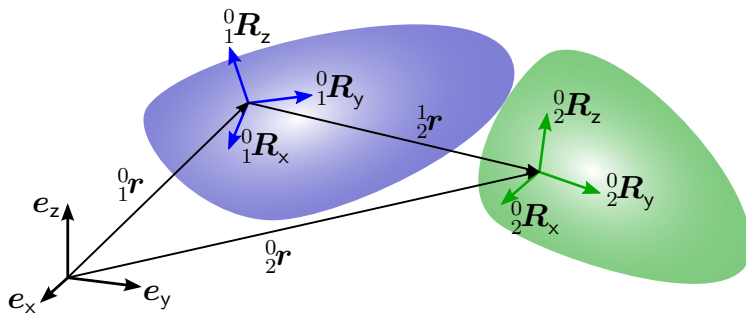


Figure 3.4: inertial frame and body fixed frames

As motivated for the single rigid body, let there be a body fixed frame for each body of the system as illustrated in Figure 3.4. The components of the position of the  $b$ -th body w.r.t. the inertial frame are  ${}_0^b r \in \mathbb{R}^3$  and the components of its attitude are  ${}_0^b R = [{}_b^0 R_x, {}_b^0 R_y, {}_b^0 R_z] \in \mathbb{SO}(3)$ . The configuration can also be expressed w.r.t. any other body:

${}^a_c \mathbf{r}$  is the position of the  $b$ -th frame w.r.t. the frame of the  $a$ -th body and analog of the attitude  ${}^a_b \mathbf{R}$ . The left side indices are used for readability but also to emphasize their different nature compared to the right side indices. The sum convention does not apply to these indices.

For the positions and attitudes we have the following relations

$${}^a_c \mathbf{r} = {}^a_b \mathbf{r} + {}^a_b \mathbf{R} {}^b_c \mathbf{r}, \quad {}^a_c \mathbf{R} = {}^a_b \mathbf{R} {}^b_c \mathbf{R}, \quad (3.81a)$$

$${}^b_a \mathbf{r} = -{}^a_b \mathbf{R}^\top {}^a_b \mathbf{r}, \quad {}^b_a \mathbf{R} = {}^a_b \mathbf{R}^\top, \quad (3.81b)$$

$${}^a_a \mathbf{r} = 0, \quad {}^a_a \mathbf{R} = \mathbf{I}_3, \quad a, b, c = 0, \dots, N. \quad (3.81c)$$

As already motivated in the last section, it will be convenient to merge position  ${}^0_b \mathbf{r} \in \mathbb{R}^3$  and rotation matrix  ${}^0_b \mathbf{R} \in \mathbb{SO}(3)$  into the (rigid body) configuration matrix

$${}^a_b \mathbf{G} = \begin{bmatrix} {}^a_b \mathbf{R} & {}^a_b \mathbf{r} \\ 0 & 1 \end{bmatrix} \in \mathbb{SE}(3). \quad (3.82)$$

Then (3.81) is equivalent to

$${}^a_c \mathbf{G} = {}^a_b \mathbf{G} {}^b_c \mathbf{G}, \quad {}^a_a \mathbf{G} = {}^a_b \mathbf{G}^{-1}, \quad {}^a_a \mathbf{G} = \mathbf{I}_4, \quad a, b, c = 0, \dots, N. \quad (3.83)$$

For a system of  $N$  body fixed frames and a inertial frame there are  $(N+1)^2$  transformations, but due to the rules (3.83), only  $N$  can be independent. So a RBS can have at most  $6N$  degrees of freedom which is the case if there are no constraints (like joints) between the bodies. Constraints of a joint between body  $a$  and  $b$  can be captured inside the corresponding transformation  ${}^a_b \mathbf{G}$ . We will discuss this in the following example.

**Example 5. Tricopter with suspended load: configuration.** Consider the Tricopter with a suspended load as shown in Figure 3.5. The top part of the figure shows the body fixed frames which are attached to geometrically meaningful points. The numbering of the bodies is rather arbitrary.

The Tricopter flies freely in space, i.e. there are no constraints between the inertial frame and any body of the system. So we chose to describe the configuration of the central body w.r.t. the inertial frame as

$${}^0_1 \mathbf{G} = \begin{bmatrix} {}^0_1 R_x^x & {}^0_1 R_y^x & {}^0_1 R_z^x & {}^0_1 r^x \\ {}^0_1 R_x^y & {}^0_1 R_y^y & {}^0_1 R_z^y & {}^0_1 r^y \\ {}^0_1 R_x^z & {}^0_1 R_y^z & {}^0_1 R_z^z & {}^0_1 r^z \\ 0 & 0 & 0 & 1 \end{bmatrix}. \quad (3.84a)$$

The suspended load is a rigid body that is attached by a spherical joint to the central body. The body fixed frame of the load was placed in the center of this spherical joint. As a consequence the position of the load (the position of its body fixed frame not the position of its center of mass) w.r.t. the central body is constant. This is reflected by the configuration

$${}^1_2 \mathbf{G} = \begin{bmatrix} {}^1_2 R_x^x & {}^1_2 R_y^x & {}^1_2 R_z^x & 0 \\ {}^1_2 R_x^y & {}^1_2 R_y^y & {}^1_2 R_z^y & 0 \\ {}^1_2 R_x^z & {}^1_2 R_y^z & {}^1_2 R_z^z & h_L \\ 0 & 0 & 0 & 1 \end{bmatrix}. \quad (3.84b)$$

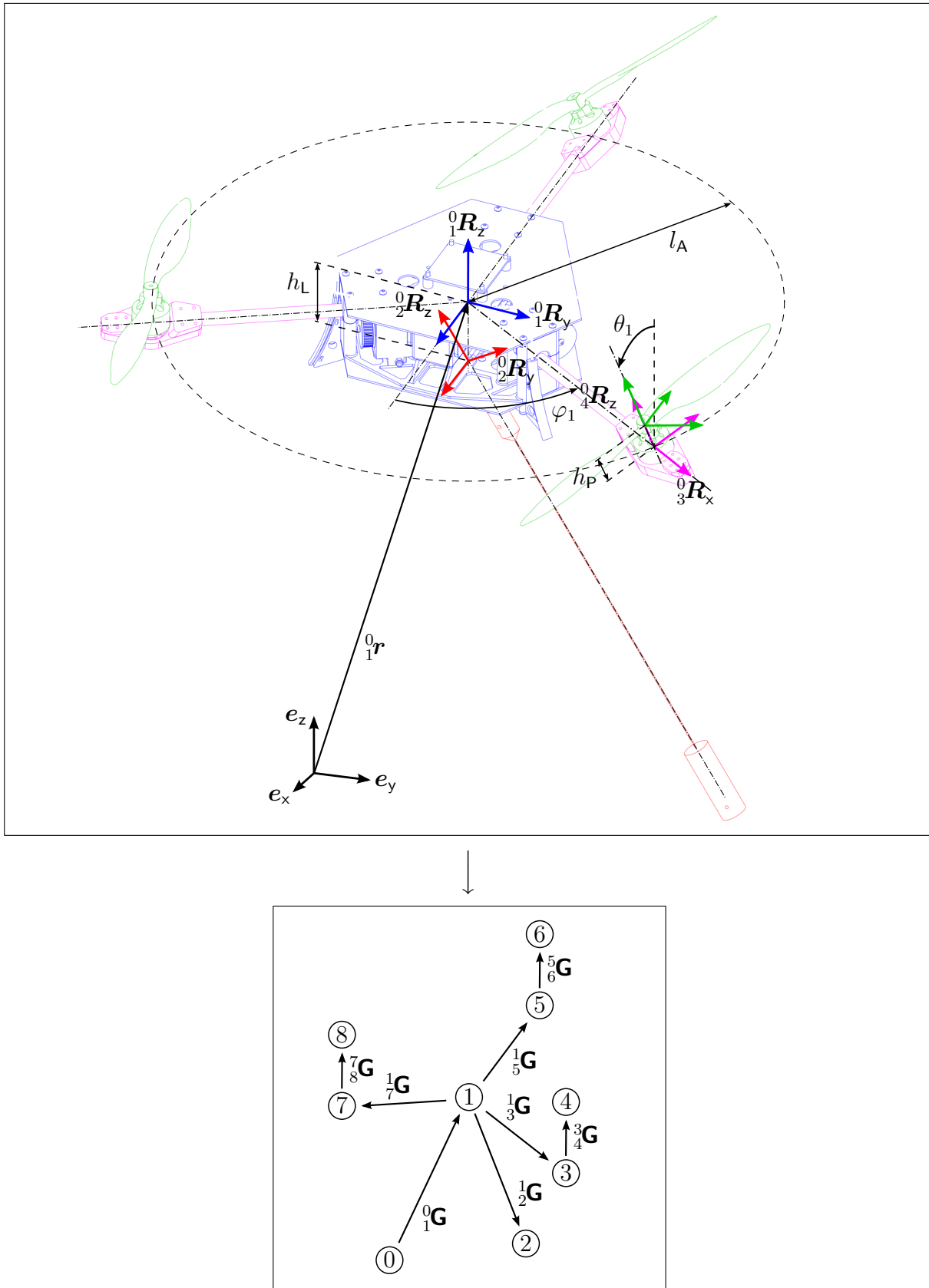


Figure 3.5: Frames attached to the Tricopter bodies (top) and the configuration graph (bottom)

The three arms are connected to the central body each by revolute joints with tilt angles  $\theta_k$ ,  $k = 1, 2, 3$ . The joint axis lie in the plane spanned by  ${}_1^0\mathbf{R}_x$  and  ${}_1^0\mathbf{R}_y$  and their angles to  ${}_1^0\mathbf{R}_x$  are  $\varphi_1 = \frac{\pi}{3}$ ,  $\varphi_2 = \pi$ ,  $\varphi_3 = -\frac{\pi}{3}$ . The body fixed axes are placed such that  ${}_{2k+1}^0\mathbf{R}_x$  coincide with the tilt axis and  ${}_{2k+1}^0\mathbf{R}_z$ ,  $k = 1, 2, 3$  coincide with the propeller spinning axis. The configuration of the  $k$ -th arm w.r.t. the central body is

$${}_{2k+1}^1\mathbf{G} = \begin{bmatrix} \cos \varphi_k & -\sin \varphi_k \cos \theta_k & \sin \varphi_k \sin \theta_k & l_A \cos \varphi_k \\ \sin \varphi_k & \cos \varphi_k \cos \theta_k & -\cos \varphi_k \sin \theta_k & l_A \sin \varphi_k \\ 0 & \sin \theta_k & \cos \theta_k & 0 \\ 0 & 0 & 0 & 1 \end{bmatrix}, \quad k = 1, \dots, 3. \quad (3.84c)$$

The propellers are connected by revolute joints to the arms. The body fixed frame is attached to the geometric center of the propeller (which will be an important point for the aerodynamics). The configuration w.r.t. the corresponding arm is

$${}_{2k+2}^{2k+1}\mathbf{G} = \begin{bmatrix} c_k & -s_k & 0 & 0 \\ s_k & c_k & 0 & 0 \\ 0 & 0 & 1 & h_P \\ 0 & 0 & 0 & 1 \end{bmatrix}, \quad k = 1, \dots, 3. \quad (3.84d)$$

The set of configurations  $\mathcal{G}_0 = \{{}_1^0\mathbf{G}, {}_2^1\mathbf{G}, {}_3^1\mathbf{G}, {}_4^3\mathbf{G}, {}_5^1\mathbf{G}, {}_6^5\mathbf{G}, {}_7^1\mathbf{G}, {}_8^7\mathbf{G}\}$  form a directed graph as shown at the bottom of Figure 3.5. With them and the rules from (3.83) we can compute the configuration  ${}_b^a\mathbf{G}$  of any body w.r.t. any other body or the inertial frame.

The configurations can be seen as functions  ${}_b^a\mathbf{G}(\mathbf{x})$  of the system coordinates

$$\mathbf{x} = [{}^0r^x, {}^0r^y, {}^0r^z, {}^0R_x^x, \dots, {}^0R_z^x, {}^1R_x^x, \dots, {}^1R_z^x, \theta_1, \theta_2, \theta_3, c_1, s_1, c_2, s_2, c_3, s_3]^\top \in \mathbb{R}^{30} \quad (3.85)$$

and the constant parameters  $h_L, l_A, \varphi_1, \varphi_2, \varphi_3, h_P$ . From the rules (3.83) emerge the geometric constraints

$$\boldsymbol{\phi}(\mathbf{x}) = \mathbf{0} \quad \cong \quad \begin{cases} {}^0_1\mathbf{R}^\top {}^0_1\mathbf{R} = \mathbf{I}_3, \det {}^0_1\mathbf{R} = +1, \\ {}^1_2\mathbf{R}^\top {}^1_2\mathbf{R} = \mathbf{I}_3, \det {}^1_2\mathbf{R} = +1, \\ (c_k)^2 + (s_k)^2 = 1, \quad k = 1, 2, 3 \end{cases} \quad (3.86)$$

The configuration space of the rigid body system is

$$\mathbb{X} = \{\mathbf{x} \in \mathbb{R}^{30} \mid \boldsymbol{\phi}(\mathbf{x}) = 0\} \cong \mathbb{SE}(3) \times \mathbb{SO}(3) \times \mathbb{R}^3 \times (\mathbb{S}^1)^3. \quad (3.87)$$

This example was mainly chosen as the Tricopter will be discussed in the following chapters. However, it is also an example of a system that is complex enough that one probably does not want to derive the equations of motion by hand without a formalism. It also covers the most common manifolds encountered in rigid body mechanics. Even though the revolute joints for the propeller tilt and the propeller spinning axes both imply a  $\mathbb{S}^1$  manifold, the local parameterization by the angle  $\theta_k, k = 1, 2, 3$  is chosen. This has a practical motivation: The tilt mechanism also twists the cables to the propeller motor and so  $\theta_k = 0$  and  $\theta_k = 2\pi$  are really different situations in practice. On the other hand it should also show that the following algorithm handles minimal coordinates just as fine.

A generalization of the example states: A rigid body system can be parameterized by a set of  $\nu$  (possibly redundant) coordinates  $\boldsymbol{x}$  which again parameterize a set of configurations  ${}^a_b \mathbf{G}(\boldsymbol{x})$  which form a *connected* graph. The property connected is essential: it ensures that, with the rules (3.83), all remaining configurations of the graph can be computed i.e. the corresponding *complete* graph. Loops in the graph and the property  ${}^a_b \mathbf{G} \in \mathbb{SE}(3)$  may imply geometric constraints.

The use of graph theory in the context of algorithms for rigid body systems is quite common, see e.g. [Roberson and Schwertassek, 1988, sec. 8.2] or [Wittenburg, 2008, sec. 5.3]. However, we will not go any deeper into this. All we need for the following is that any configuration  ${}^a_b \mathbf{G}(\boldsymbol{x})$ ,  $a, b = 0 \dots N$  can be expressed in terms of the configuration coordinates  $\boldsymbol{x}$ .

### 3.4.2 Velocity

In (3.46) we motivated particular velocity coordinates  $\boldsymbol{\xi} = [\boldsymbol{v}^\top, \boldsymbol{\omega}^\top]^\top$  for the free rigid body, which did lead to a convenient mathematical expressions. In the context of rigid body systems we may associate a *body velocity*  ${}^a_b \boldsymbol{\xi} = [{}^a_b \boldsymbol{v}^\top, {}^a_b \boldsymbol{\omega}^\top]^\top$  with any configuration  ${}^a_b \mathbf{G}$ ,  $a, b = 0, \dots, N$  defined by

$${}^a_b \boldsymbol{\xi} = \text{vee}({}^b_a \dot{{}^a_b \mathbf{G}}), \quad a, b = 0, \dots, N. \quad (3.88)$$

From the rules (3.83) for the configurations we can conclude similar rules for their velocities: For the composition  ${}^c_a \mathbf{G} = {}^a_b \mathbf{G} {}^b_c \mathbf{G}$  we get

$${}^a_c \boldsymbol{\xi} = \text{vee}({}^c_b \mathbf{G} {}^b_a \dot{{}^a_b \mathbf{G}} + {}^a_b \mathbf{G} {}^b_c \dot{{}^b_c \mathbf{G}}) = \text{vee}({}^c_b \mathbf{G} \text{wed}({}^a_b \boldsymbol{\xi}) {}^b_c \mathbf{G}) + {}^b_c \boldsymbol{\xi} = \text{Ad}_{\mathbf{g}_b} {}^a_b \boldsymbol{\xi} + {}^b_c \boldsymbol{\xi} \quad (3.89a)$$

Differentiation of the rule for the inverse yields

$$\frac{d}{dt}({}^a_b \mathbf{G} {}^b_a \mathbf{G}) = {}^a_b \dot{\mathbf{G}} {}^b_a \mathbf{G} + {}^a_b \mathbf{G} {}^b_a \dot{\mathbf{G}} = {}^a_b \mathbf{G} \text{wed}({}^a_b \boldsymbol{\xi}) {}^b_a \mathbf{G} + \text{wed}({}^a_b \boldsymbol{\xi}) {}^b_a \mathbf{G} = \mathbf{0} \quad \Leftrightarrow \quad {}^a_b \boldsymbol{\xi} = -\text{Ad}_{\mathbf{g}_b} {}^a_b \boldsymbol{\xi} \quad (3.89b)$$

and obviously

$${}^a_a \boldsymbol{\xi} = \mathbf{0}. \quad (3.89c)$$

**System velocity and body Jacobians.** Based on their definition (3.88), the body velocities  ${}^a_b \boldsymbol{\xi}$  can be seen as a function of the system coordinates  $\boldsymbol{x}$  and their derivatives  $\dot{\boldsymbol{x}} = \mathbf{A}(\boldsymbol{x}) \boldsymbol{\xi}$ . Crucially the velocity is linear in  $\dot{\boldsymbol{x}}$  and consequently linear in the system velocity  $\boldsymbol{\xi}$  and we can write

$${}^a_b \boldsymbol{\xi}(\boldsymbol{x}, \boldsymbol{\xi}) = {}^a_b \mathbf{J}(\boldsymbol{x}) \boldsymbol{\xi}, \quad {}^a_b \mathbf{J}(\boldsymbol{x}) = \frac{\partial {}^a_b \boldsymbol{\xi}}{\partial \boldsymbol{\xi}}(\boldsymbol{x}) = \frac{\partial}{\partial \dot{\boldsymbol{x}}} \text{vee}\left({}^b_a \mathbf{G}(\boldsymbol{x}) \frac{d}{dt}({}^a_b \mathbf{G}(\boldsymbol{x}))\right) \mathbf{A}. \quad (3.90)$$

The matrix  ${}^a_b \mathbf{J}(\boldsymbol{x}) \in \mathbb{R}^{6 \times n}$  that maps the system velocity  $\boldsymbol{\xi}$  to the body velocity  ${}^a_b \boldsymbol{\xi}$  is commonly called the *body Jacobian*. An alternative formula for the body Jacobian, which might give additional geometric insight, is given in (??). The following rules emerge directly from (3.89):

$${}^a_c \mathbf{J} = \text{Ad}_{\mathbf{g}_c} {}^a_b \mathbf{J} + {}^b_c \mathbf{J}, \quad {}^a_a \mathbf{J} = -\text{Ad}_{\mathbf{g}_a} {}^a_b \mathbf{J}, \quad {}^a_a \mathbf{J} = \mathbf{0}. \quad (3.91)$$

**Example 6. Tricopter with suspended load: kinematics.** For the tricopter with load from Example 5 we chose the following velocity coordinates: The components of the body velocity  ${}^0\xi$  of the central body w.r.t. the inertial frame, the components of the angular velocity  ${}^0\omega$  of the load w.r.t. the inertial frame, the angular velocities  $\dot{\theta}_k, k = 1, 2, 3$  of the arm tilt mechanism and the angular velocities  $\varpi_k, k = 1, 2, 3$  of the propellers w.r.t. the arms. These velocity coordinates  $\xi = [{}^0\xi^\top, {}^0\omega^\top, \dot{\theta}_1, \dot{\theta}_2, \dot{\theta}_3, \varpi_1, \varpi_2, \varpi_3]^\top$  are related to the configuration coordinates  $\xi$  by the kinematic equation

$$\dot{x} = A\xi \quad \cong \quad \begin{cases} {}^0\dot{G} = {}^0G \text{ wed}({}^0\xi), \\ {}^1\dot{R} = {}^1R \text{ wed}({}^0\omega) - \text{wed}({}^0\omega){}^1R, \\ \dot{\theta}_k = \dot{\theta}_k, \quad k = 1, 2, 3 \\ \dot{c}_k = -s_k \varpi_k, \quad k = 1, 2, 3 \\ \dot{s}_k = c_k \varpi_k, \quad k = 1, 2, 3 \end{cases}. \quad (3.92)$$

The relative velocity  ${}^1\omega = \text{vee}({}^1R^\top {}^1\dot{R})$  of the load would be another possible and probably more obvious choice. The absolute velocity  ${}^0\omega$  is mainly chosen to demonstrate the flexibility of the presented approach but the use of absolute velocities also leads to less cumbersome terms in the system inertia matrix.

The body velocities associated with the configuration matrices from (3.84) are

$${}^0\xi = \begin{bmatrix} {}^0v^x \\ {}^0v^y \\ {}^0v^z \\ {}^0\omega^x \\ {}^0\omega^y \\ {}^0\omega^z \end{bmatrix}, \quad {}^1\xi = \begin{bmatrix} 0 \\ 0 \\ 0 \\ {}^0\omega^x - \frac{1}{2}R_x^0\omega^x - \frac{1}{2}R_y^0\omega^y - \frac{1}{2}R_z^0\omega^z \\ {}^0\omega^y - \frac{1}{2}R_y^0\omega^x - \frac{1}{2}R_y^0\omega^y - \frac{1}{2}R_y^0\omega^z \\ {}^0\omega^z - \frac{1}{2}R_z^0\omega^x - \frac{1}{2}R_z^0\omega^y - \frac{1}{2}R_z^0\omega^z \end{bmatrix}, \quad (3.93a)$$

$${}^{2k+1}\xi = \begin{bmatrix} 0 \\ 0 \\ 0 \\ \dot{\theta}_k \\ 0 \\ 0 \end{bmatrix}, \quad {}^{2k+2}\xi = \begin{bmatrix} 0 \\ 0 \\ 0 \\ 0 \\ 0 \\ \varpi_k \end{bmatrix}, \quad k = 1, 2, 3. \quad (3.93b)$$

From this it should clear how the corresponding body Jacobians look like, e.g.  ${}^0J = [I_6 \ 0]$ .

For the formulation of the kinetic energy in the following subsection we will need the body Jacobians  ${}^bJ, b = 1, \dots, N$ . From the graph structure and the rules (3.91) we can compute them iteratively as

$${}^0J = \text{Ad}_{{}^0G} {}^0J + {}^1J, \quad (3.94a)$$

$${}^{2k+1}J = \text{Ad}_{{}^{2k+1}G} {}^0J + {}^{2k+1}J, \quad (3.94b)$$

$${}^{2k+2}J = \text{Ad}_{{}^{2k+2}G} {}^{2k+1}J + {}^{2k+2}J. \quad (3.94c)$$

These terms are significantly more cumbersome, so they are not displayed explicitly.

### 3.4.3 Inertia

**Kinetic energy and inertia matrix.** The kinetic energy  $\mathcal{T}$  of a rigid body system is simply the sum of the kinetic energies of its bodies. Recalling the kinetic energy (3.49) for a single free rigid body, and formulation of the absolute body velocities  ${}^0_b\xi$  in terms of the chosen configuration coordinates  $\mathbf{x}$  and velocity coordinates  $\xi$  according to (3.90) yields

$$\mathcal{T}(\mathbf{x}, \xi) = \sum_b \frac{1}{2} ({}^0_b\xi(\mathbf{x}, \xi))^{\top} {}^0_b\mathbf{M} {}^0_b\xi(\mathbf{x}, \xi) = \frac{1}{2} \xi^{\top} \underbrace{\sum_b ({}^0_b\mathbf{J}(\mathbf{x}))^{\top} {}^0_b\mathbf{M} {}^0_b\mathbf{J}(\mathbf{x}) \xi}_{\mathbf{M}(\mathbf{x})} \quad (3.95)$$

with the system inertia matrix  $\mathbf{M}(\mathbf{x}) \in \mathbb{R}^{n \times n}$  computed from the body Jacobians  ${}^0_b\mathbf{J}(\mathbf{x})$  and the body inertia matrices  ${}^0_b\mathbf{M}$  defined in (3.49).

**Connection coefficients.** With a rather cumbersome computation (see (??)), it can be shown that the connection coefficients  $\Gamma_{ijk}$  associated to the system inertia matrix  $\mathbf{M}$  from (3.95) can be expressed in terms of the body Jacobians  ${}^0_b\mathbf{J}$ , the body inertia matrices  ${}^0_b\mathbf{M}$  and the body connection coefficients  ${}^0_b\Gamma_{pqr}$  from (3.54) or the body commutation coefficients  $\gamma_{pq}^h$  from (3.47) as

$$\Gamma_{ijk} = \sum_b {}^0_b J_i^p ({}^0_b\mathbf{M}_{pq} \partial_k {}^0_b J_j^q + \underbrace{\frac{1}{2} (\gamma_{pq}^h {}^0_b\mathbf{M}_{hr} + \gamma_{pr}^h {}^0_b\mathbf{M}_{hq} - \gamma_{qr}^h {}^0_b\mathbf{M}_{hp}) {}^0_b J_j^q {}^0_b J_k^r}_{{}^0_b\Gamma_{pqr}}) \quad (3.96)$$

With this we can state the gyroscopic terms as

$$c_i = \Gamma_{ijk} \xi^j \xi^k = \sum_b {}^0_b J_i^p ({}^0_b\mathbf{M}_{pq} \partial_k {}^0_b J_j^q + {}^0_b J_j^q \gamma_{pq}^h {}^0_b\mathbf{M}_{hr} {}^0_b J_k^r) \xi^j \xi^k \quad (3.97)$$

**Acceleration energy.** Completely analog as above, but based on the acceleration energy (3.51) of a single free rigid body, we express the acceleration energy  $\mathcal{S}$  for a rigid body system as

$$\begin{aligned} \mathcal{S}(\mathbf{x}, \xi, \dot{\xi}) &= \frac{1}{2} \dot{\xi}^{\top} \underbrace{\sum_b ({}^0_b\mathbf{J}(\mathbf{x}))^{\top} {}^0_b\mathbf{M} {}^0_b\mathbf{J}(\mathbf{x}) \dot{\xi}}_{\mathbf{M}(\mathbf{x})} \\ &+ \dot{\xi}^{\top} \underbrace{\sum_b ({}^0_b\mathbf{J}(\mathbf{x}))^{\top} ({}^0_b\mathbf{M} {}^0_b\dot{\mathbf{J}}(\mathbf{x}, \xi) - \text{ad}^{\top} {}^0_b\mathbf{J}(\mathbf{x}) \xi {}^0_b\mathbf{M} {}^0_b\mathbf{J}(\mathbf{x})) \xi}_{c(\mathbf{x}, \xi)} \\ &+ \underbrace{\sum_b \frac{1}{2} \| (\text{wed} ({}^0_b\dot{\mathbf{J}}(\mathbf{x}, \xi) \xi) + \text{wed} ({}^0_b\mathbf{J}(\mathbf{x}) \xi)^2)^{\top} \|_{\text{Wed}({}^0_b\mathbf{M})}^2}_{\mathcal{S}_0(\mathbf{x}, \xi)}. \end{aligned} \quad (3.98)$$

For the explicit form of  $\mathcal{S}_0$ , the formulation (??) is useful.

**Inertia force.** The generalized inertia force  $\mathbf{f}^M$  for a rigid body system can be computed from

- $f_i^M = M_{ij} \dot{\xi}^j + \Gamma_{ijk} \xi^k \dot{\xi}^j$  using the inertia matrix  $M_{ij}$  from (3.95) and the connection coefficients  $\Gamma_{ijk}$  from (3.96).
- $f_i^M = \frac{d}{dt} \frac{\partial \mathcal{T}}{\partial \dot{\xi}^i} + \gamma_{ij}^k \xi^j \frac{\partial \mathcal{T}}{\partial \xi^k} - \partial_i \mathcal{T}$  with the kinetic energy  $\mathcal{T}$  from (3.95).
- $f_i^M = \frac{\partial \mathcal{S}}{\partial \dot{\xi}^i}$  using the acceleration energy  $\mathcal{S}$  from (3.98).

which yield

$$\mathbf{f}^M(\mathbf{x}, \boldsymbol{\xi}, \dot{\boldsymbol{\xi}}) = \mathbf{M}(\mathbf{x}) \dot{\boldsymbol{\xi}} + \mathbf{c}(\mathbf{x}, \boldsymbol{\xi}) \quad (3.99)$$

with the system inertia matrix  $\mathbf{M}$  from (3.95) and the gyroscopic terms  $\mathbf{c}$  from (3.98) or (3.97).

Similar results are called *the projection equation* in [Bremer, 2008, sec. 4.2.5] and *the Kane equations* [Kane and Levinson, 1985, chap. 6]. There is some controversy (starting in [Desloge, 1987]) about the naming, since the equations result rather directly (as shown above) from the Gibbs-Appell formulation. See [Lesser, 1992] or [Papastavridis, 2002, p. 714] for an overview.

In contrast to the derivations in the sources above, the formulation (3.99) poses no restrictions on the body fixed frames and allows redundant configuration coordinates.

### 3.4.4 Gravitation

The potential energy of gravitation of a rigid body system is the sum of the potentials of the individual bodies (3.55). Using the formulation from (??) this is

$$\begin{aligned} \mathcal{V}^G(\mathbf{x}) &= \sum_b {}_b^0 m \langle {}_b^0 \mathbf{r}(\mathbf{x}) + {}_b^0 \mathbf{R}(\mathbf{x}) {}_b^0 \mathbf{s}, \boldsymbol{\alpha}_G \rangle \\ &= \sum_b \langle ({}^0_b \mathbf{G}(\mathbf{x}))^\top, \text{wed}(\boldsymbol{\alpha}_G)^\top \rangle {}_b^0 \mathbf{M}, \quad \boldsymbol{\alpha}_G^\top = [\mathbf{a}_G^\top, \mathbf{0}_{1 \times 3}]. \end{aligned} \quad (3.100)$$

The resulting generalized force on the system may be written as

$$\mathbf{f}^G(\mathbf{x}) = \nabla \mathcal{V}^G(\mathbf{x}) = \sum_b ({}^0_b \mathbf{J}(\mathbf{x}))^\top {}_b^0 \mathbf{M} \text{Ad}_{{}^0_b \mathbf{G}(\mathbf{x})}^{-1} \boldsymbol{\alpha}_G. \quad (3.101)$$

### 3.4.5 Stiffness

Potential energy

$$\mathcal{V}^K(\mathbf{x}) = \sum_{a,b} \frac{1}{2} \|({}^a_b \mathbf{G}(\mathbf{x}) - {}^a_b \mathbf{G}_R)^\top\| {}^a_b \mathbf{K}'^2 \quad (3.102)$$

stiffness force

$$\mathbf{f}^K(\mathbf{x}) = \nabla \mathcal{V}^K(\mathbf{x}) = \sum_{a,b} ({}^a_b \mathbf{J}(\mathbf{x}))^\top \underbrace{\text{vee2}((\mathbf{I}_4 - ({}^a_b \mathbf{G}(\mathbf{x}))^{-1} {}^a_b \mathbf{G}_R) {}^a_b \mathbf{K}')}_{{}^a_b \mathbf{f}^K(\mathbf{x})} \quad (3.103)$$

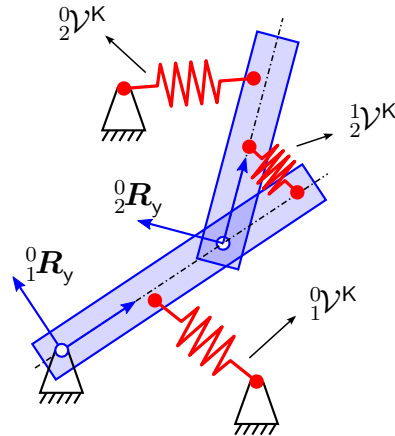


Figure 3.6: MultibodyPotentialIllustration

### 3.4.6 Dissipation

Dissipation function

$$\mathcal{R}(\mathbf{x}, \boldsymbol{\xi}) = \sum_{a,b} \frac{1}{2} \|({}^a_b \dot{\mathbf{G}}(\mathbf{x}, \boldsymbol{\xi}))^\top\|_{{}^a_b \mathbf{D}'}^2 = \underbrace{\frac{1}{2} \boldsymbol{\xi}^\top \sum_{a,b} ({}^a_b \mathbf{J}(\mathbf{x}))^\top {}^a_b \mathbf{D} {}^a_b \mathbf{J}(\mathbf{x}) \boldsymbol{\xi}}_{\mathbf{D}(\mathbf{x})} \quad (3.104)$$

dissipative force

$$\mathbf{f}^D(\mathbf{x}, \boldsymbol{\xi}) = \frac{\partial \mathcal{R}}{\partial \boldsymbol{\xi}}(\mathbf{x}, \boldsymbol{\xi}) = \mathbf{D}(\mathbf{x}) \boldsymbol{\xi} \quad (3.105)$$

### 3.4.7 Summary

There are three ingredients:

1. the chosen parameterization in the configuration coordinates  $\boldsymbol{x}$ , the velocity coordinates  $\boldsymbol{\xi}$  and their relation captured by the kinematics matrix  $\boldsymbol{A}$
2. the rigid body graph  ${}^a_b\mathbf{G}$  that maps the coordinates to the rigid body configuration.
3. the constitutive parameters merged into the inertia matrices  ${}^0_b\mathbf{M}'$ , dissipation matrices  ${}^a_b\mathbf{D}'$ , stiffness matrices  ${}^a_b\mathbf{K}'$ , their corresponding minimum  ${}^a_b\mathbf{G}_R$  and the gravity vector  $\boldsymbol{a}_G$ . It should be stressed that these are independent of the chosen coordinates.

Based on this input we may compute the equations of motion in three steps:

1. compute the body Jacobians for the given configurations:

$${}^a_b\mathbf{J}(\boldsymbol{x}) = \frac{\partial}{\partial \dot{\boldsymbol{x}}} \text{vee} \left( {}^b_a\mathbf{G}(\boldsymbol{x}) \frac{d}{dt} ({}^a_b\mathbf{G}(\boldsymbol{x})) \right) \boldsymbol{A}(\boldsymbol{x}) \quad (3.106)$$

2. use the group rules to compute the missing configurations and Jacobians

$${}^c_a\mathbf{G} = {}^a_b\mathbf{G} {}^b_c\mathbf{G}, \quad {}^b_a\mathbf{G} = {}^a_b\mathbf{G}^{-1}, \quad (3.107a)$$

$${}^a_c\mathbf{J} = \text{Ad}_{\xi} {}^a_b\mathbf{J} + {}^b_c\mathbf{J}, \quad {}^b_a\mathbf{J} = -\text{Ad}_{\xi} {}^a_b\mathbf{J}, \quad (3.107b)$$

$${}^a_c\dot{\mathbf{J}} = \text{Ad}_{\dot{\xi}} ({}^b_a\mathbf{J} + \text{ad}_{\xi} {}^a_b\mathbf{J}) + {}^b_c\dot{\mathbf{J}}, \quad {}^b_a\dot{\mathbf{J}} = -\text{Ad}_{\dot{\xi}} ({}^a_b\mathbf{J} + \text{ad}_{\xi} {}^a_b\mathbf{J}), \quad (3.107c)$$

3. assemble the system matrices

$$\mathbf{M} = \sum_b {}^0_b\mathbf{J}^\top \text{Vee}({}^0_b\mathbf{M}') {}^0_b\mathbf{J}, \quad (3.108a)$$

$$\mathbf{c} = \sum_b {}^0_b\mathbf{J}^\top \text{vee2} ((\text{wed}({}^0_b\mathbf{J}\xi) + \text{wed}({}^0_b\mathbf{J}\xi)^2) {}^0_b\mathbf{M}') \quad (3.108b)$$

$$\mathbf{D} = \sum_{a,b} {}^a_b\mathbf{J}^\top \text{Vee}({}^a_b\mathbf{D}') {}^a_b\mathbf{J} \quad (3.108c)$$

$$\mathbf{f}^K = \sum_{a,b} {}^a_b\mathbf{J}^\top \text{vee2} ((\mathbf{I}_4 - {}^a_b\mathbf{G} {}^a_b\mathbf{G}_R) {}^a_b\mathbf{K}') \quad (3.108d)$$

$$\mathbf{f}^G = \sum_b {}^0_b\mathbf{J}^\top \text{Vee}({}^0_b\mathbf{M}') \text{Ad}_{\xi} \boldsymbol{\alpha}_G, \quad \boldsymbol{\alpha}_G = [\boldsymbol{a}_G^\top, \mathbf{0}_{1 \times 3}]^\top \quad (3.108e)$$

4. explicit equations of motion

$$\dot{\boldsymbol{x}} = \boldsymbol{A}\boldsymbol{\xi}, \quad (3.109a)$$

$$\dot{\boldsymbol{\xi}} = \mathbf{M}^{-1} (\mathbf{f}^E - \mathbf{c} - \mathbf{D}\boldsymbol{\xi} - \mathbf{f}^K - \mathbf{f}^G). \quad (3.109b)$$

The first step (3.106) requires differentiation, so must be performed symbolically. The remaining steps only require basic linear algebra, so can be preformed numerically. For small systems it might be still reasonable to compute  $\mathbf{M}(\boldsymbol{x})$  symbolically, but for larger systems the explicit expressions can be overwhelming even for contemporary computers.

### 3.5 General constraints

In addition to geometric constraints  $\phi(\mathbf{x}) = \mathbf{0}$  that have been incorporated by the chosen coordinates  $\mathbf{x}$  and  $\boldsymbol{\xi}$  we like to incorporate additional constraints of various forms:

- geometric constraints:

$$\begin{aligned} & \psi(\mathbf{x}) = \mathbf{0} \\ \Leftrightarrow & \underbrace{\partial_i \psi^\kappa(\mathbf{x})}_{Z_i^\kappa(\mathbf{x})} \dot{\xi}^i = \underbrace{-\partial_j \partial_i \psi^\kappa(\mathbf{x}) \xi^i \xi^j}_{b^\kappa(\mathbf{x}, \boldsymbol{\xi})}, \quad \psi^\kappa(\mathbf{x}_0) = 0, \quad \partial_i \psi^\kappa(\mathbf{x}_0) \xi_0^i = 0 \end{aligned} \quad (3.110a)$$

- linear kinematic constraints (possibly nonholonomic):

$$\begin{aligned} & \mathbf{N}(\mathbf{x}) \dot{\mathbf{x}} = \underbrace{\mathbf{N}(\mathbf{x}) \mathbf{A}(\mathbf{x})}_{\mathbf{Z}(\mathbf{x})} \boldsymbol{\xi} = \mathbf{0} \\ \Leftrightarrow & Z_i^\kappa(\mathbf{x}) \dot{\xi}^i = \underbrace{-\partial_j Z_i^\kappa(\mathbf{x}) \xi^i \xi^j}_{b^\kappa(\mathbf{x}, \boldsymbol{\xi})}, \quad Z_i^\kappa(\mathbf{x}_0) \xi_0^\kappa = 0 \end{aligned} \quad (3.110b)$$

- general kinematic constraints

$$\begin{aligned} & \boldsymbol{\eta}(\mathbf{x}, \boldsymbol{\xi}, t) = \mathbf{0} \\ \Leftrightarrow & \underbrace{\frac{\partial \eta^\kappa}{\partial \xi^i}(\mathbf{x}, \boldsymbol{\xi}, t)}_{Z_i^\kappa(\mathbf{x}, \boldsymbol{\xi}, t)} \dot{\xi}^i = \underbrace{-\partial_i \eta^\kappa(\mathbf{x}, \boldsymbol{\xi}, t) \xi^i - \frac{\partial \eta^\kappa}{\partial t}(\mathbf{x}, \boldsymbol{\xi}, t)}_{b^\kappa(\mathbf{x}, \boldsymbol{\xi}, t)}, \quad \eta^\kappa(\mathbf{x}_0, \boldsymbol{\xi}_0, t_0) = 0 \end{aligned} \quad (3.110c)$$

- linear<sup>3</sup> acceleration constraints.

$$\mathbf{Z}(\mathbf{x}, \boldsymbol{\xi}, t) \ddot{\boldsymbol{\xi}} = \mathbf{b}(\mathbf{x}, \boldsymbol{\xi}, t) \quad (3.110d)$$

All these constraints can be formulated as *linear acceleration constraints*  $\mathbf{Z} \ddot{\boldsymbol{\xi}} = \mathbf{b}$  possibly supplemented by suitable conditions on the initial coordinates  $\mathbf{x}_0 = \mathbf{x}(t_0)$  and  $\boldsymbol{\xi}_0 = \boldsymbol{\xi}(t_0)$ . Gauß suggested in [Gauß, 1829] also the application to inequality constraints which will not be discussed here. For a contemporary discussion and applications of this see [Pfeiffer and Glocker, 1996, sec. 6.1].

In terms of the chosen coordinates  $\mathbf{x}$  and  $\boldsymbol{\xi}$  the Gaussian constraint  $\mathcal{G}$  can be written as

$$\begin{aligned} \mathcal{G} &= \frac{1}{2} \sum_p \mathfrak{m}_p \left\| \overbrace{\partial_j \mathfrak{r}_p \dot{\xi}^j + \partial_k \partial_j \mathfrak{r}_p \xi^k \xi^j}^{\mathfrak{r}_p} - \frac{\mathfrak{F}_p^A}{\mathfrak{m}_p} \right\|^2 \\ &= \frac{1}{2} \underbrace{\sum_p \mathfrak{m}_p \langle \partial_i \mathfrak{r}_p, \partial_j \mathfrak{r}_p \rangle}_{M_{ij}} \dot{\xi}^i \dot{\xi}^j + \underbrace{\sum_p \mathfrak{m}_p \langle \partial_i \mathfrak{r}_p, \partial_k \partial_j \mathfrak{r}_p \rangle}_{c_i} \xi^j \xi^k \dot{\xi}^i + \underbrace{\sum_p \langle \partial_i \mathfrak{r}_p, \mathfrak{F}_p^A \rangle}_{f_i^A} \dot{\xi}^i + \mathcal{G}_0 \\ &= \frac{1}{2} \dot{\boldsymbol{\xi}}^\top \mathbf{M} \dot{\boldsymbol{\xi}} + (\mathbf{c} - \mathbf{f}^A)^\top \dot{\boldsymbol{\xi}} + \mathcal{G}_0 \end{aligned} \quad (3.111)$$

---

<sup>3</sup>Nonlinear acceleration constraints could be handled as well, but with a more sophisticated solution than (3.113)

where  $\mathcal{G}_0$  collects the terms independent of the acceleration  $\dot{\boldsymbol{\xi}}$ . Overall we can state the Gauß principle with the additional constraints  $\mathbf{Z}\dot{\boldsymbol{\xi}} = \mathbf{b}$  originating from (3.110) as

$$\begin{aligned} \min_{\dot{\boldsymbol{\xi}} \in \mathbb{R}^n} \quad & \mathcal{G} = \frac{1}{2}\dot{\boldsymbol{\xi}}^\top \mathbf{M}\dot{\boldsymbol{\xi}} + \dot{\boldsymbol{\xi}}^\top (\mathbf{c} - \mathbf{f}^A) + \mathcal{G}_0 \\ \text{s. t.} \quad & \mathbf{Z}\dot{\boldsymbol{\xi}} = \mathbf{b} \end{aligned} \quad (3.112)$$

For whatever reason we do not want to eliminate the constraints by a change of coordinates but use the concept of the *Lagrange multipliers* (e.g. [Luenberger and Ye, 2015, ch. 14]): By defining the auxiliary function  $\bar{\mathcal{G}} = \mathcal{G} - \boldsymbol{\lambda}^\top(\mathbf{Z}\dot{\boldsymbol{\xi}} - \mathbf{b})$  the solution to (3.112) can be stated as

$$\begin{bmatrix} \frac{\partial \bar{\mathcal{G}}}{\partial \dot{\boldsymbol{\xi}}} \\ \frac{\partial \bar{\mathcal{G}}}{\partial \boldsymbol{\lambda}} \end{bmatrix} = \mathbf{0} \quad \Leftrightarrow \quad \begin{bmatrix} \mathbf{M} & -\mathbf{Z}^\top \\ \mathbf{Z} & \mathbf{0} \end{bmatrix} \begin{bmatrix} \dot{\boldsymbol{\xi}} \\ \boldsymbol{\lambda} \end{bmatrix} = \begin{bmatrix} \mathbf{f}^A - \mathbf{c} \\ \mathbf{b} \end{bmatrix}. \quad (3.113)$$

The additional quantities  $\boldsymbol{\lambda}$  are called the *Lagrange multipliers* and can be interpreted as reaction forces.

The possibility of handling such a variety of constraints might put Gauß' principle in a superior position compared to other principles as pointed out in [Hamel, 1949, p. 525]. The Lagrange-d'Alembert principle handles linear kinematic constraints  $\mathbf{N}\dot{\mathbf{x}} = \mathbf{0}$  by requiring  $\mathbf{N}\delta\mathbf{x} = \mathbf{0}$ . However, there are no real world examples of nonlinear nonholonomic constraints [Hamel, 1949, p. 499], [Neimark and Fufaev, 1972, ch. IV], [Roberson and Schwertassek, 1988, p. 96] and none of acceleration constraints [Hamel, 1949, p. 505 & 525], so one should be careful with this context. Note for example that for nonlinear kinematic and acceleration constraints the reaction forces  $\boldsymbol{\lambda}$  enter the balance of energy.

Example?

## 3.6 Energy

force balance

$$\underbrace{M_{ij}(\mathbf{x})\dot{\xi}^j + \Gamma_{ijk}(\mathbf{x})\xi^k\xi^j}_{f_i^M} + \underbrace{D_{ij}(\mathbf{x})\xi^j}_{f_i^D} + \underbrace{\partial_i \mathcal{V}(\mathbf{x})}_{f_i^V} = f_i^E(\mathbf{x}, \mathbf{u}), \quad i = 1, \dots, n. \quad (3.114)$$

For the change of kinetic energy  $\mathcal{T}(\mathbf{x}, \boldsymbol{\xi}) = M_{ij}(\mathbf{x})\xi^i\xi^j$  we have

$$\dot{\mathcal{T}} = M_{ij}\xi^i\dot{\xi}^j + \frac{1}{2}\partial_k M_{ij}\xi^i\xi^j\xi^k = \xi^i f_i^M + \underbrace{\left(\frac{1}{2}\partial_k M_{ij} - \Gamma_{ijk}\right)\xi^i\xi^j\xi^k}_0 \quad (3.115)$$

The marked term vanishes due to (??). Furthermore we have similar relations for the potential energy  $\mathcal{V}$ , the dissipation function  $\mathcal{R}$  and we define the external power  $\mathcal{P}^E$  as

$$\dot{\mathcal{V}} = \xi^i f_i^V, \quad 2\mathcal{R} = \xi^i f_i^D, \quad \mathcal{P}^E = \xi^i f_i^E. \quad (3.116)$$

Defining the *total energy*  $\mathcal{W}$  as the sum of kinetic and potential energy and taking into account the kinetic equation  $\mathbf{f}^M + \mathbf{f}^D + \mathbf{f}^V = \mathbf{f}^E$  we find

$$\mathcal{W} = \mathcal{T} + \mathcal{V}, \quad \dot{\mathcal{W}} = \mathcal{P}^E - 2\mathcal{R}. \quad (3.117)$$

# Chapter 4

## Tracking control of rigid body systems

This chapter motivates and discusses several approaches for a model based design of a tracking controller for a rigid body system by static feedback.

**System model.** The previous chapter discussed the equations of motion of rigid body systems: For chosen configuration coordinates  $\mathbf{x}(t) \in \mathbb{X}$ , velocity coordinates  $\boldsymbol{\xi}(t) \in \mathbb{R}^n$  and the control inputs  $\mathbf{u}(t) \in \mathbb{R}^p$  these have the form

$$\dot{\mathbf{x}} = \mathbf{A}(\mathbf{x})\boldsymbol{\xi}, \quad \underbrace{\mathbf{M}(\mathbf{x})\dot{\boldsymbol{\xi}} + \mathbf{c}(\mathbf{x}, \boldsymbol{\xi})}_{\mathbf{f}^M(\mathbf{x}, \boldsymbol{\xi}, \dot{\boldsymbol{\xi}})} + \underbrace{\mathbf{D}(\mathbf{x})\boldsymbol{\xi}}_{\mathbf{f}^D(\mathbf{x}, \boldsymbol{\xi})} + \underbrace{\nabla \mathcal{V}(\mathbf{x})}_{\mathbf{f}^K(\mathbf{x})} = \mathbf{B}(\mathbf{x})\mathbf{u}. \quad (4.1)$$

The forces  $\mathbf{f}^M, \mathbf{f}^D, \mathbf{f}^K$  may be computed from the rigid body configurations  ${}^a_b\mathbf{G}(\mathbf{x})$  and the constitutive parameters  ${}^0_b\mathbf{M}, {}^a_b\mathbf{D}, {}^a_b\mathbf{K}$ . This structure will be the main inspiration for the design of the controlled system.

However, mathematically, the control approach does not rely on the model having this structure. We may assume any model of the form

$$\dot{\mathbf{x}} = \mathbf{A}(\mathbf{x})\boldsymbol{\xi}, \quad \mathbf{M}(\mathbf{x})\dot{\boldsymbol{\xi}} + \mathbf{b}(\mathbf{x}, \boldsymbol{\xi}) = \mathbf{B}(\mathbf{x})\mathbf{u} \quad (4.2)$$

where  $\mathbf{A}(\mathbf{x}) \in \mathbb{R}^{\nu \times n}$  and  $\mathbf{B}(\mathbf{x}) \in \mathbb{R}^{n \times p}$  are full rank, the system inertia matrix  $\mathbf{M}(\mathbf{x}) \in \text{SYM}^+(n)$  is symmetric, positive definite, and  $\mathbf{b}(\mathbf{x}, \boldsymbol{\xi}) \in \mathbb{R}^n$  collects the remaining terms of the kinetic equation. The system is called *fully-actuated* for  $p = n$  and *underactuated* for  $0 < p < n$ . Firstly we will restrict to fully-actuated systems and later try to expand the approach to underactuated systems.

**Reference trajectory and tracking controller.** Let there be a *reference trajectory*  $t \mapsto \mathbf{x}_R(t)$  which is compatible with the model (4.2): It must be feasible, i.e.  $\mathbf{x}_R(t) \in \mathbb{X}$ , and sufficiently smooth, so we can define the reference velocity  $\boldsymbol{\xi}_R = \mathbf{A}^+(\mathbf{x}_R)\dot{\mathbf{x}}_R$  and acceleration  $\dot{\boldsymbol{\xi}}_R$ . For the underactuated case we also require the kinetic equation  $\mathbf{M}(\mathbf{x}_R)\dot{\boldsymbol{\xi}}_R + \mathbf{b}(\mathbf{x}_R, \boldsymbol{\xi}_R) = \mathbf{B}(\mathbf{x}_R)\mathbf{u}_R$  to have a solution for  $\mathbf{u}_R$ .

The design task for a *tracking controller* is: Find a function  $\mathbf{u} = \mathbf{u}(\mathbf{x}, \boldsymbol{\xi}, \mathbf{x}_R, \boldsymbol{\xi}_R, \dot{\boldsymbol{\xi}}_R)$  (the controller) such that  $t \mapsto \mathbf{x}_R(t)$  is a stable and attractive trajectory of the closed loop which is the combination of model (4.2) and controller.

**State of the art.** This is a pretty general task and may be tackled by various standard approaches from control theory, see e.g. [Spong et al., 2006, chap. 7-10] for some overview. For fully actuated systems a popular approach is *computed torque*, see e.g. [Murray et al., 1994, sec. 4.5.2], also called *inverse dynamics* in [Spong et al., 2006, sec. 8.3]. It can be regarded as a particularly simple case of feedback linearization utilizing the fact that any set of minimal generalized coordinates  $\mathbf{q}(t) \in \mathbb{R}^n$  is a *flat output* of a fully actuated mechanical system [Martin et al., 1997, sec. 7.1].

For underactuated systems there is no standard textbook approach. Examples for the flatness-based approach can be found in e.g. [Rathinam and Murray, 1998], [Murray et al., 1995] or [Martin et al., 1997, sec. 7.1]. General Lyapunov designs can be found in [Olfati-Saber, 2001] and a approach called *controlled Lagrangians* is proposed in [Bloch et al., 2000].

**Outline for this chapter.** With the computed torque method one might consider the topic to be solved for fully actuated systems. However, for system whose configuration space is not isomorph to  $\mathbb{R}^n$  it is only local due to the requirement of minimal coordinates  $\mathbf{q}(t) \in \mathbb{R}^n$ . Furthermore, applying linear dynamics in these coordinates may result in intrinsic singularities for the closed loop. Recalling the satellite example from ??, it should be clear that linear dynamics for the Euler angles would probably not be a good choice, also see [Konz and Rudolph, 2016] for further examples.

If linear dynamics are not a general choice, what *is* a good choice for the closed loop dynamics? This chapter motivates three approaches for designing a closed loop for fully actuated systems which rely on the underlying rigid body structure. In addition, the result will be extended to underactuated systems. Finally the approach will be applied to several example systems including the tricopter (fully-actuated), the quadcopter (underactuated but flat) and the bicopter (underactuated and probably not flat).

## 4.1 Approach 1: Inspired by particle distribution

### 4.1.1 Particle system

**The basic idea.** Consider a system of *free* particles with the equations of motion  $\mathfrak{m}_p \ddot{\mathbf{r}}_p = \mathfrak{F}_p^A, p = 1, \dots, \mathfrak{N}$  and the control inputs  $\mathfrak{F}_p^A$ . We want the system to track a smooth reference trajectory  $t \mapsto (\mathbf{r}_{1R}, \dots, \mathbf{r}_{\mathfrak{N}R})(t)$ . Probably the simplest solution is the control law  $\mathfrak{F}_p^A = \underline{\mathfrak{m}}_p \ddot{\mathbf{r}}_{pR} - \bar{\mathfrak{d}}_p \dot{\mathbf{r}}_{pE} - \bar{\mathfrak{k}}_p \mathbf{r}_{pE}$  with the position error  $\mathbf{r}_{pE} = \mathbf{r}_p - \mathbf{r}_{pR}$  and the design parameters  $\bar{\mathfrak{k}}_p, \bar{\mathfrak{d}}_p \in \mathbb{R} > 0$ . The resulting closed loop is

$$\mathfrak{m}_p \ddot{\mathbf{r}}_{pE} + \bar{\mathfrak{d}}_p \dot{\mathbf{r}}_{pE} + \bar{\mathfrak{k}}_p \mathbf{r}_{pE} = \mathbf{0}, \quad p = 1 \dots \mathfrak{N}. \quad (4.3)$$

It is clearly exponentially stable and the *desired stiffness*  $\bar{\mathfrak{k}}_p$  and *desired damping*  $\bar{\mathfrak{d}}_p$  are intuitive tuning parameters.

For a system of particles with geometric constraints  $\mathbf{c}(\mathbf{r}_1, \dots, \mathbf{r}_{\mathfrak{N}}) = \mathbf{0}$  we cannot achieve (4.3) in general. As the next best thing we can get as close as possible by formulation of

the following constrained optimization problem

$$\begin{aligned} \underset{\ddot{\mathbf{x}} \in \mathbb{R}^{3\mathfrak{N}}}{\text{minimize}} \quad & \bar{\mathcal{G}} = \frac{1}{2} \sum_p \frac{1}{\bar{\mathfrak{m}}_p} \|\bar{\mathfrak{m}}_p \ddot{\mathbf{r}}_{pE} + \bar{\mathfrak{d}}_p \dot{\mathbf{r}}_{pE} + \bar{\mathfrak{k}}_p \mathbf{r}_{pE}\|^2 \\ \text{subject to} \quad & \mathbf{c}(\mathbf{r}_1, \dots, \mathbf{r}_{\mathfrak{N}}) = \mathbf{0} \end{aligned} \quad (4.4)$$

Note that we also replaced the particle masses  $\mathfrak{m}_p$  by *desired masses*  $\bar{\mathfrak{m}}_p$  as additional design parameters. This will turn out crucial for control of underactuated systems.

**The controlled system.** The constrained problem (4.4) can be transformed to an unconstrained one by formulating the particle accelerations  $\ddot{\mathbf{r}}_p = \ddot{\mathbf{r}}_p(\mathbf{x}, \xi, \dot{\xi})$ ,  $p = 1 \dots \mathfrak{N}$  in terms of minimal acceleration coordinates  $\dot{\xi}$ . Analogous, let the reference particle positions be formulated in terms of the reference coordinates  $\mathbf{x}_R, \xi_R, \dot{\xi}_R$ , i.e.  $\mathbf{r}_{pR} = \mathbf{r}_p(\mathbf{x}_R)$ ,  $\dot{\mathbf{r}}_{pR} = \dot{\mathbf{r}}_p(\mathbf{x}_R, \xi_R)$ ,  $\ddot{\mathbf{r}}_{pR} = \ddot{\mathbf{r}}_p(\mathbf{x}_R, \xi_R, \dot{\xi}_R)$ , and the position error  $\mathbf{r}_{pE} = \mathbf{r}_{pE}(\mathbf{x}, \mathbf{x}_R) = \mathbf{r}_p(\mathbf{x}) - \mathbf{r}_p(\mathbf{x}_R)$ , etc.. With this, the solution of (4.4) can be computed from

$$\begin{aligned} \frac{\partial \bar{\mathcal{G}}}{\partial \dot{\xi}^i} &= \sum_p \langle \bar{\mathfrak{m}}_p \ddot{\mathbf{r}}_{pE} + \bar{\mathfrak{d}}_p \dot{\mathbf{r}}_{pE} + \bar{\mathfrak{k}}_p \mathbf{r}_{pE}, \frac{\partial \ddot{\mathbf{r}}_p}{\partial \dot{\xi}^i} \rangle \\ &= \sum_p \bar{\mathfrak{m}}_p \langle \ddot{\mathbf{r}}_{pE}, \frac{\partial \ddot{\mathbf{r}}_p}{\partial \dot{\xi}^i} \rangle + \sum_p \bar{\mathfrak{d}}_p \langle \dot{\mathbf{r}}_{pE}, \frac{\partial \ddot{\mathbf{r}}_p}{\partial \dot{\xi}^i} \rangle + \sum_p \bar{\mathfrak{k}}_p \langle \mathbf{r}_{pE}, \partial_i \mathbf{r}_p \rangle \\ &= \underbrace{\frac{\partial}{\partial \dot{\xi}^i} \sum_p \frac{1}{2} \bar{\mathfrak{m}}_p \|\ddot{\mathbf{r}}_{pE}\|^2}_{\bar{f}_i^M} + \underbrace{\frac{\partial}{\partial \dot{\xi}^i} \sum_p \frac{1}{2} \bar{\mathfrak{d}}_p \|\dot{\mathbf{r}}_{pE}\|^2}_{\bar{f}_i^D} + \underbrace{\partial_i \sum_p \frac{1}{2} \bar{\mathfrak{k}}_p \|\mathbf{r}_{pE}\|^2}_{\bar{f}_i^K} = 0, \quad i = 1, \dots, n. \end{aligned} \quad (4.5)$$

Here we introduced formulations for the *controlled acceleration energy*  $\bar{\mathcal{S}}(\mathbf{x}, \xi, \dot{\xi}, \mathbf{x}_R, \xi_R, \dot{\xi}_R)$ , the *controlled dissipation function*  $\bar{\mathcal{R}}(\mathbf{x}, \xi, \mathbf{x}_R, \xi_R)$  and the *controlled potential energy*  $\bar{\mathcal{V}}(\mathbf{x}, \mathbf{x}_R)$ . It is worth noting that the inertia force  $\bar{f}^M$  could also be derived from the *controlled kinetic energy*  $\bar{\mathcal{T}}(\mathbf{x}, \xi, \mathbf{x}_R, \xi_R)$  as

$$\bar{f}_i^M = \frac{d}{dt} \frac{\partial \bar{\mathcal{T}}}{\partial \dot{\xi}^i} + \gamma_{ij}^k \xi^j \frac{\partial \bar{\mathcal{T}}}{\partial \xi^k} - \partial_i \bar{\mathcal{T}}, \quad \bar{\mathcal{T}} = \frac{1}{2} \sum_p \bar{\mathfrak{m}}_p \|\dot{\mathbf{r}}_{pE}\|^2. \quad (4.6)$$

Also note that all the defined “energies” are symmetric in the sense that  $\mathcal{V}(\mathbf{x}, \mathbf{x}_R) = \bar{\mathcal{V}}(\mathbf{x}_R, \mathbf{x})$ , etc..

The corresponding forces expressed more explicitly are

$$\begin{aligned} \bar{f}_i^M &= \frac{\partial \bar{\mathcal{S}}}{\partial \dot{\xi}^i} = \underbrace{\sum_p \bar{\mathfrak{m}}_p \langle \partial_i \mathbf{r}_p(\mathbf{x}), \partial_j \mathbf{r}_p(\mathbf{x}) \rangle \dot{\xi}^j}_{\bar{M}_{ij}(\mathbf{x})} + \underbrace{\sum_p \bar{\mathfrak{m}}_p \langle \partial_i \mathbf{r}_p(\mathbf{x}), \partial_k \partial_j \mathbf{r}_p(\mathbf{x}) \rangle \xi^j \xi^k}_{\bar{F}_{ijk}(\mathbf{x})} \\ &\quad - \underbrace{\sum_p \bar{\mathfrak{m}}_p \langle \partial_i \mathbf{r}_p(\mathbf{x}), \partial_j \mathbf{r}_p(\mathbf{x}_R) \rangle \dot{\xi}_R^j}_{\bar{M}'_{ij}(\mathbf{x}, \mathbf{x}_R)} - \underbrace{\sum_p \bar{\mathfrak{m}}_p \langle \partial_i \mathbf{r}_p(\mathbf{x}), \partial_k \partial_j \mathbf{r}_p(\mathbf{x}_R) \rangle \xi_R^j \xi_R^k}_{\bar{F}'_{ijk}(\mathbf{x}, \mathbf{x}_R)}, \end{aligned} \quad (4.7a)$$

$$\bar{f}_i^D = \frac{\partial \bar{\mathcal{R}}}{\partial \dot{\xi}^i} = \underbrace{\sum_p \bar{\mathfrak{d}}_p \langle \partial_i \mathbf{r}_p(\mathbf{x}), \partial_j \mathbf{r}_p(\mathbf{x}) \rangle \xi^j}_{\bar{D}_{ij}(\mathbf{x})} - \underbrace{\sum_p \bar{\mathfrak{d}}_p \langle \partial_i \mathbf{r}_p(\mathbf{x}), \partial_j \mathbf{r}_p(\mathbf{x}_R) \rangle \xi_R^j}_{\bar{D}'_{ij}(\mathbf{x}, \mathbf{x}_R)}, \quad (4.7b)$$

$$\bar{f}_i^K = \partial_i \bar{\mathcal{V}} = \sum_p \bar{\mathfrak{k}}_p \langle \partial_i \mathbf{r}_p(\mathbf{x}), \mathbf{r}_p(\mathbf{x}) - \mathbf{r}_p(\mathbf{x}_R) \rangle. \quad (4.7c)$$

So we can rewrite (4.5) as

$$\begin{aligned} \bar{M}_{ij}(\mathbf{x})\dot{\xi}^j - \bar{M}'_{ij}(\mathbf{x}, \mathbf{x}_R)\dot{\xi}_R^j + \bar{\Gamma}_{ijk}(\mathbf{x})\xi^j\xi^k - \bar{\Gamma}'_{ijk}(\mathbf{x}, \mathbf{x}_R)\xi_R^j\xi_R^k \\ + \bar{D}_{ij}(\mathbf{x})\xi^j - \bar{D}'_{ij}(\mathbf{x}, \mathbf{x}_R)\xi_R^j + \partial_i \bar{\mathcal{V}}(\mathbf{x}, \mathbf{x}_R) = 0, \quad i = 1, \dots, n. \end{aligned} \quad (4.8)$$

**Total energy.** Having a definition for a kinetic energy  $\bar{\mathcal{T}}$  and a potential energy  $\bar{\mathcal{V}}$  it is worth investigating the total energy  $\bar{\mathcal{W}} = \bar{\mathcal{T}} + \bar{\mathcal{V}}$  and its change along the solutions of closed loop (4.8). Using the substitutions defined in (4.7) and  $\Psi(\mathbf{x}, \mathbf{x}_R) \in \mathbb{R}^{n \times n}$  defined through  $\bar{M}'_{ij}(\mathbf{x}, \mathbf{x}_R) = \Psi_i^s(\mathbf{x}, \mathbf{x}_R)\bar{M}_{sj}(\mathbf{x})$  we have

$$\bar{\mathcal{W}} = \overbrace{\frac{1}{2}\bar{M}_{ij}(\mathbf{x})\xi^i\xi^j - \bar{M}'_{ij}(\mathbf{x}, \mathbf{x}_R)\xi^i\xi_R^j + \frac{1}{2}\bar{M}_{ij}(\mathbf{x}_R)\xi_R^i\xi_R^j}^{\bar{\mathcal{T}}(\mathbf{x}, \xi, \mathbf{x}_R, \xi_R)} + \bar{\mathcal{V}}(\mathbf{x}, \mathbf{x}_R) \quad (4.9)$$

$$\begin{aligned} \dot{\bar{\mathcal{W}}} &= \xi^i(\bar{M}_{ij}(\mathbf{x})\dot{\xi}^j + \bar{\Gamma}_{ijk}(\mathbf{x})\xi^j\xi^k - \bar{M}'_{ij}(\mathbf{x}, \mathbf{x}_R)\dot{\xi}_R^j - \bar{\Gamma}'_{ijk}(\mathbf{x}, \mathbf{x}_R)\xi_R^j\xi_R^k + \partial_i \bar{\mathcal{V}}(\mathbf{x}, \mathbf{x}_R)) \\ &\quad + \xi_R^i(\bar{M}_{ij}(\mathbf{x}_R)\dot{\xi}_R^j + \bar{\Gamma}_{ijk}(\mathbf{x}_R)\xi_R^j\xi_R^k - \bar{M}'_{ij}(\mathbf{x}_R, \mathbf{x})\dot{\xi}^j - \bar{\Gamma}'_{ijk}(\mathbf{x}_R, \mathbf{x})\xi^j\xi^k + \partial_i \bar{\mathcal{V}}(\mathbf{x}_R, \mathbf{x})) \\ &\stackrel{(4.8)}{=} -(\xi^i - \Psi_s^i(\mathbf{x}, \mathbf{x}_R)\xi_R^s)(\bar{D}_{ij}(\mathbf{x})\xi^j - \bar{D}'_{ij}(\mathbf{x}, \mathbf{x}_R)\xi_R^j) \\ &\quad + \xi_R^i(\partial_i \bar{\mathcal{V}}(\mathbf{x}_R, \mathbf{x}) + \Psi_i^s(\mathbf{x}, \mathbf{x}_R)\partial_s \bar{\mathcal{V}}(\mathbf{x}, \mathbf{x}_R) + (\bar{M}_{ij}(\mathbf{x}_R) - \Psi_i^s(\mathbf{x}, \mathbf{x}_R)\bar{M}'_{sj}(\mathbf{x}, \mathbf{x}_R))\dot{\xi}_R^j \\ &\quad + (\bar{\Gamma}_{ijk}(\mathbf{x}_R) - \Psi_i^s(\mathbf{x}, \mathbf{x}_R)\bar{\Gamma}'_{sjk}(\mathbf{x}, \mathbf{x}_R))\xi_R^j\xi_R^k - (\bar{\Gamma}'_{ijk}(\mathbf{x}_R, \mathbf{x}) - \Psi_i^s(\mathbf{x}, \mathbf{x}_R)\bar{\Gamma}_{sjk}(\mathbf{x}))\xi^j\xi^k) \end{aligned} \quad (4.10)$$

Obviously the total energy  $\bar{\mathcal{W}}$  is not a Lyapunov function for a general reference trajectory. It is, however, for the very special case of  $\xi_R = \mathbf{0}$ , i.e. proves stability for a constant reference configuration  $\mathbf{x}_R = const..$

### 4.1.2 Free rigid body

Consider the free rigid body discussed in section 3.3 as a special case of a particle system. As motivated there we use the position  $\mathbf{r}(t) \in \mathbb{R}^3$  and orientation matrix  $\mathbf{R}(t) \in \mathbb{SO}(3)$  merged into the configuration matrix  $\mathbf{G}(t) = [\begin{smallmatrix} \mathbf{R}(t) & \mathbf{r}(t) \\ \mathbf{0} & 1 \end{smallmatrix}] \in \mathbb{SE}(3)$  as configuration coordinates. Expressing the particle positions as  $\mathbf{r}_p = \mathbf{r} + \mathbf{R}\mathbf{h}_p$  and applying the same calculations as in ?? we can write the energies from (4.5) as

$$\bar{\mathcal{V}} = \sum_p \frac{1}{2}\bar{\mathfrak{k}}_p \|\mathbf{r}_p - \mathbf{r}_{pR}\|^2 = \frac{1}{2}\|(\mathbf{G} - \mathbf{G}_R)^\top\|_{\mathbf{K}'}^2 \quad (4.11a)$$

$$\bar{\mathcal{R}} = \sum_p \frac{1}{2}\bar{\mathfrak{d}}_p \|\dot{\mathbf{r}}_p - \dot{\mathbf{r}}_{pR}\|^2 = \frac{1}{2}\|(\dot{\mathbf{G}} - \dot{\mathbf{G}}_R)^\top\|_{\mathbf{D}'}^2 \quad (4.11b)$$

$$\bar{\mathcal{S}} = \sum_p \frac{1}{2}\bar{\mathfrak{m}}_p \|\ddot{\mathbf{r}}_p - \ddot{\mathbf{r}}_{pR}\|^2 = \frac{1}{2}\|(\ddot{\mathbf{G}} - \ddot{\mathbf{G}}_R)^\top\|_{\mathbf{M}'}^2 \quad (4.11c)$$

$$\bar{\mathcal{T}} = \sum_p \frac{1}{2}\bar{\mathfrak{m}}_p \|\dot{\mathbf{r}}_p - \dot{\mathbf{r}}_{pR}\|^2 = \frac{1}{2}\|(\dot{\mathbf{G}} - \dot{\mathbf{G}}_R)^\top\|_{\bar{\mathbf{M}'}}^2 \quad (4.11d)$$

where

$$\bar{\mathbf{K}}' = \sum_p \bar{\mathbf{k}}_p \begin{bmatrix} \mathbf{h}_p \mathbf{h}_p^\top & \mathbf{h}_p^\top \\ \mathbf{h}_p & 1 \end{bmatrix} = \begin{bmatrix} \bar{\mathbf{H}}' & \bar{k} \bar{\mathbf{h}} \\ \bar{k} \bar{\mathbf{h}}^\top & \bar{k} \end{bmatrix}, \quad (4.12a)$$

$$\bar{\mathbf{D}}' = \sum_p \bar{\mathbf{d}}_p \begin{bmatrix} \mathbf{h}_p \mathbf{h}_p^\top & \mathbf{h}_p^\top \\ \mathbf{h}_p & 1 \end{bmatrix} = \begin{bmatrix} \bar{\mathbf{Y}}' & \bar{d} \bar{\mathbf{l}} \\ \bar{d} \bar{\mathbf{l}}^\top & \bar{d} \end{bmatrix}, \quad (4.12b)$$

$$\bar{\mathbf{M}}' = \sum_p \bar{\mathbf{m}}_p \begin{bmatrix} \mathbf{h}_p \mathbf{h}_p^\top & \mathbf{h}_p^\top \\ \mathbf{h}_p & 1 \end{bmatrix} = \begin{bmatrix} \bar{\Theta}' & \bar{m} \bar{\mathbf{s}} \\ \bar{m} \bar{\mathbf{s}}^\top & \bar{m} \end{bmatrix}. \quad (4.12c)$$

As before we can interpret the entries of the *desired inertia matrix*  $\bar{\mathbf{M}} = \text{Vee}(\bar{\mathbf{M}}')$  as the *desired total mass*  $\bar{m}$ , *desired center of mass*  $\bar{\mathbf{s}}$  and the *desired moment of inertia*  $\bar{\Theta} = \text{Vee}(\bar{\Theta}')$ . The analog holds for the entries of the *desired damping matrix*  $\bar{\mathbf{D}} = \text{Vee}(\bar{\mathbf{D}}')$  and the *desired stiffness matrix*  $\bar{\mathbf{K}} = \text{Vee}(\bar{\mathbf{K}}')$ .

Introduce the translational  $\mathbf{v}(t) \in \mathbb{R}^3$  and angular velocity  $\boldsymbol{\omega}(t) \in \mathbb{R}^3$  merged into  $\boldsymbol{\xi} = [\mathbf{v}^\top, \boldsymbol{\omega}^\top]^\top = \text{vee}(\mathbf{G}^{-1}\dot{\mathbf{G}})$  as velocity coordinates. Furthermore, we introduce the *configuration error*  $\mathbf{G}_E = \mathbf{G}_R^{-1}\mathbf{G}$  and exploit the invariance (??) of the norm to left translation of the argument to express the desired energies (4.11) as

$$\bar{\mathcal{V}} = \frac{1}{2} \| (\mathbf{I}_4 - \mathbf{G}_E^{-1})^\top \|_{\bar{\mathbf{K}}'}^2 \quad (4.13a)$$

$$\bar{\mathcal{R}} = \frac{1}{2} \| (\text{wed}(\boldsymbol{\xi}) - \mathbf{G}_E^{-1} \text{wed}(\boldsymbol{\xi}_R))^\top \|_{\bar{\mathbf{D}}'}^2 \quad (4.13b)$$

$$\bar{\mathcal{S}} = \frac{1}{2} \| (\text{wed}(\dot{\boldsymbol{\xi}}) + \text{wed}(\boldsymbol{\xi})^2 - \mathbf{G}_E^{-1} (\text{wed}(\boldsymbol{\xi}_R) + \text{wed}(\boldsymbol{\xi}_R)^2))^\top \|_{\bar{\mathbf{M}}'}^2 \quad (4.13c)$$

$$\bar{\mathcal{T}} = \frac{1}{2} \| (\text{wed}(\boldsymbol{\xi}) - \mathbf{G}_E^{-1} \text{wed}(\boldsymbol{\xi}_R))^\top \|_{\bar{\mathbf{M}}'}^2 \quad (4.13d)$$

Using the vee2-operator defined in (A.12) the resulting forces can be expressed as

$$\bar{\mathbf{f}}^K = \nabla \bar{\mathcal{V}} = \text{vee2} ((\mathbf{I}_4 - \mathbf{G}_E^{-1}) \bar{\mathbf{K}}'), \quad (4.14a)$$

$$\bar{\mathbf{f}}^D = \frac{\partial \bar{\mathcal{R}}}{\partial \boldsymbol{\xi}} = \text{vee2} ((\text{wed}(\boldsymbol{\xi}) - \mathbf{G}_E^{-1} \text{wed}(\boldsymbol{\xi}_R)) \bar{\mathbf{D}}'), \quad (4.14b)$$

$$\bar{\mathbf{f}}^M = \frac{\partial \bar{\mathcal{S}}}{\partial \dot{\boldsymbol{\xi}}} = \text{vee2} ((\text{wed}(\dot{\boldsymbol{\xi}}) + \text{wed}(\boldsymbol{\xi})^2 - \mathbf{G}_E^{-1} (\text{wed}(\boldsymbol{\xi}_R) + \text{wed}(\boldsymbol{\xi}_R)^2)) \bar{\mathbf{M}}') \quad (4.14c)$$

or more explicitly

$$\bar{\mathbf{f}}^K = \begin{bmatrix} \bar{k} \mathbf{R}_E^\top (\mathbf{r}_E + (\mathbf{R}_E - \mathbf{I}_3) \bar{\mathbf{h}}) \\ \bar{k} \text{wed}(\bar{\mathbf{h}}) \mathbf{R}_E^\top \mathbf{r}_E + 2 \text{vee} (\text{Vee}(\bar{\mathbf{H}})(\mathbf{R}_E - \mathbf{I}_3)) \end{bmatrix} \quad (4.15a)$$

$$\bar{\mathbf{f}}^D = \underbrace{\begin{bmatrix} \bar{d} \mathbf{I}_3 & \bar{d} \text{wed}(\bar{\mathbf{l}})^\top \\ \bar{d} \text{wed}(\bar{\mathbf{l}}) & \bar{\mathbf{Y}} \end{bmatrix}}_{\bar{\mathbf{D}}} \underbrace{\begin{bmatrix} \mathbf{v} \\ \boldsymbol{\omega} \end{bmatrix}}_{\boldsymbol{\xi}} - \underbrace{\begin{bmatrix} \bar{d} \mathbf{R}_E^\top & \mathbf{R}_E^\top \bar{d} \text{wed}(\bar{\mathbf{l}})^\top \\ \bar{d} \text{wed}(\bar{\mathbf{l}}) \mathbf{R}_E^\top & \text{Wed}(\mathbf{R}_E^\top \text{Vee}(\bar{\mathbf{Y}})) \mathbf{R}_E^\top \end{bmatrix}}_{\boldsymbol{\xi}_R} \underbrace{\begin{bmatrix} \mathbf{v}_R \\ \boldsymbol{\omega}_R \end{bmatrix}}_{\boldsymbol{\xi}_R} \quad (4.15b)$$

$$\begin{aligned} \bar{\mathbf{f}}^M = & \underbrace{\begin{bmatrix} \bar{m} \mathbf{I}_3 & \bar{m} \text{wed}(\bar{\mathbf{s}})^\top \\ \bar{m} \text{wed}(\bar{\mathbf{s}}) & \bar{\Theta} \end{bmatrix}}_{\bar{\mathbf{M}}} \underbrace{\begin{bmatrix} \dot{\mathbf{v}} \\ \dot{\boldsymbol{\omega}} \end{bmatrix}}_{\dot{\boldsymbol{\xi}}} + \begin{bmatrix} \bar{m} \text{wed}(\boldsymbol{\omega}) & -\bar{m} \text{wed}(\boldsymbol{\omega}) \text{wed}(\bar{\mathbf{s}}) \\ \bar{m} \text{wed}(\bar{\mathbf{s}}) \text{wed}(\boldsymbol{\omega}) & \text{wed}(\text{Vee}(\bar{\Theta})) \boldsymbol{\omega} \end{bmatrix} \begin{bmatrix} \mathbf{v} \\ \boldsymbol{\omega} \end{bmatrix} \\ & - \begin{bmatrix} \bar{m} \mathbf{R}_E^\top & \mathbf{R}_E^\top \bar{m} \text{wed}(\bar{\mathbf{s}})^\top \\ \bar{m} \text{wed}(\bar{\mathbf{s}}) \mathbf{R}_E^\top & \text{Wed}(\mathbf{R}_E^\top \text{Vee}(\bar{\Theta})) \mathbf{R}_E^\top \end{bmatrix} \begin{bmatrix} \dot{\mathbf{v}}_R \\ \dot{\boldsymbol{\omega}}_R \end{bmatrix} \\ & - \begin{bmatrix} \bar{m} \mathbf{R}_E^\top \text{wed}(\boldsymbol{\omega}_R) & -\bar{m} \mathbf{R}_E^\top \text{wed}(\boldsymbol{\omega}_R) \text{wed}(\bar{\mathbf{s}}) \\ \bar{m} \text{wed}(\bar{\mathbf{s}}) \mathbf{R}_E^\top \text{wed}(\boldsymbol{\omega}_R) & \text{Wed}(\mathbf{R}_E^\top \text{wed}(\boldsymbol{\omega}_R) \text{Vee}(\bar{\Theta})) \mathbf{R}_E^\top \end{bmatrix} \begin{bmatrix} \mathbf{v}_R \\ \boldsymbol{\omega}_R \end{bmatrix} \end{aligned} \quad (4.15c)$$

The closed loop kinetic equation  $\bar{\mathbf{f}}^M + \bar{\mathbf{f}}^D + \bar{\mathbf{f}}^K = \mathbf{0}$  contains 30 tuning parameters within the matrices  $\bar{\mathbf{M}}'$ ,  $\bar{\mathbf{D}}'$ ,  $\bar{\mathbf{K}}' \in \text{SYM}^+(4)$ . The characteristic polynomial of the first order approximation of the system about any constant configuration  $\mathbf{x}_R = \text{const.}$  is  $\det(\bar{\mathbf{M}}\lambda^2 + \bar{\mathbf{D}}\lambda + \bar{\mathbf{K}})$  where  $\bar{\mathbf{M}} = \text{Vee}(\bar{\mathbf{M}}')$ , etc..

blah

In contrast to this, the characteristic polynomial resulting from the computed torque method (see subsection 4.3.2) for this system is  $\det(\mathbf{I}_6\lambda^2 + \mathbf{K}_1\lambda + \mathbf{K}_2)$ , which has  $n(n+1) = 42$  tuning parameters within the matrixes  $\mathbf{K}_1, \mathbf{K}_2 \in \text{SYM}^+(6)$ .

blah

A possible generalization of the rigid body potential  $\bar{\mathcal{V}}$  which works with all  $\frac{1}{2}n(n+1) = 21$  tuning parameters in a matrix  $\mathbf{K} \in \text{SYM}^+(6)$  is given in section A.5.

### 4.1.3 Rigid body systems

Let the particles belong to a system of  $N$  rigid bodies with the body configurations  ${}^b\mathbf{G}$  as discussed in section 3.4. The potential energy from (4.5) may be formulated as  $\bar{\mathcal{V}} = \sum_{b=1}^N \frac{1}{2} \|({}^0\mathbf{G} - {}^b\mathbf{G}_R)^\top\|_{{}^b\bar{\mathbf{K}}}^2$ , with a body stiffness matrix  ${}^b\bar{\mathbf{K}}'$  resulting from (4.12) for each body. This potential only captures stiffness w.r.t. the absolute configurations  ${}^0\mathbf{G}$ . Depending on the control objective it may be equally reasonable to consider a stiffness associated with the relative configurations  ${}^a\mathbf{G}$  as illustrated in Figure 4.1. Considering

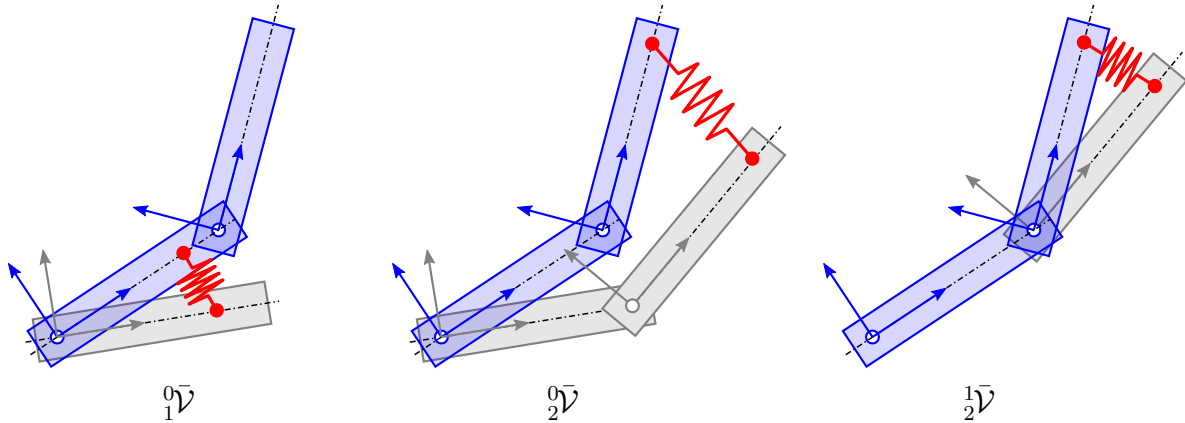


Figure 4.1: Different parts of the potential  $\bar{\mathcal{V}}$  for a double pendulum

the same argument for damping and inertia, we propose the following energies for the

control of a rigid body system:

$$\bar{\mathcal{V}} = \sum_{a,b=0}^N \overbrace{\frac{1}{2} \| ({}^a_b \mathbf{G} - {}^a_b \mathbf{G}_R)^\top \|_{{}^a_b \bar{\mathbf{K}}'}^2}^{{}^a_b \bar{\mathcal{V}}}, \quad {}^a_b \bar{\mathbf{K}}' \in \mathbb{SYM}_0^+(4) \quad (4.16a)$$

$$\bar{\mathcal{R}} = \sum_{a,b=0}^N \overbrace{\frac{1}{2} \| ({}^a_b \dot{\mathbf{G}} - {}^a_b \dot{\mathbf{G}}_R)^\top \|_{{}^a_b \bar{\mathbf{D}}'}^2}^{{}^a_b \bar{\mathcal{R}}}, \quad {}^a_b \bar{\mathbf{D}}' \in \mathbb{SYM}_0^+(4) \quad (4.16b)$$

$$\bar{\mathcal{S}} = \sum_{a,b=0}^N \overbrace{\frac{1}{2} \| ({}^a_b \ddot{\mathbf{G}} - {}^a_b \ddot{\mathbf{G}}_R)^\top \|_{{}^a_b \bar{\mathbf{M}}'}^2}^{{}^a_b \bar{\mathcal{S}}}, \quad {}^a_b \bar{\mathbf{M}}' \in \mathbb{SYM}_0^+(4) \quad (4.16c)$$

$$\bar{\mathcal{T}} = \sum_{a,b=0}^N \overbrace{\frac{1}{2} \| ({}^a_b \dot{\mathbf{G}} - {}^a_b \dot{\mathbf{G}}_R)^\top \|_{{}^a_b \bar{\mathbf{M}}'}^2}^{{}^a_b \bar{\mathcal{T}}}. \quad (4.16d)$$

Note that  ${}^a_b \bar{\mathbf{K}}' = {}^b_a \bar{\mathbf{K}}'$  implies  ${}^b_a \bar{\mathcal{V}} = {}^a_b \bar{\mathcal{V}}$  and  ${}^a_a \bar{\mathcal{V}} = 0$  since  ${}^a_b \mathbf{G} = {}^a_a \mathbf{G}_R = \mathbf{I}_4$  and analog for damping and inertia.

Let the body configurations  ${}^b_a \mathbf{G}(\mathbf{x})$  and the body velocities  ${}^b_a \xi = {}^b_a \mathbf{J}(\mathbf{x})\xi$  be formulated in terms of suitable system coordinates  $\mathbf{x}$  and  $\xi$ , as discussed in section 3.4. With the shorthand notations  ${}^a_b \mathbf{G}_E = {}^a_b \mathbf{G}_E(\mathbf{x}, \mathbf{x}_R) = {}^a_b \mathbf{G}^{-1}(\mathbf{x}_R) {}^a_b \mathbf{G}(\mathbf{x})$  and  ${}^a_b \mathbf{J} = {}^a_b \mathbf{J}(\mathbf{x})$ ,  ${}^a_b \mathbf{J}_R = {}^a_b \mathbf{J}(\mathbf{x}_R)$  we can express (4.16) as

$$\bar{\mathcal{V}} = \sum_{a,b} \frac{1}{2} \| (\mathbf{I}_4 - {}^a_b \mathbf{G}_E^{-1})^\top \|_{{}^a_b \bar{\mathbf{K}}'}^2, \quad (4.17a)$$

$$\bar{\mathcal{R}} = \sum_{a,b} \frac{1}{2} \| (\text{wed}({}^a_b \mathbf{J} \xi) - {}^a_b \mathbf{G}_E^{-1} \text{wed}({}^a_b \mathbf{J}_R \xi_R))^\top \|_{{}^a_b \bar{\mathbf{D}}'}^2, \quad (4.17b)$$

$$\begin{aligned} \bar{\mathcal{S}} = \sum_{a,b} \frac{1}{2} & \| (\text{wed}({}^a_b \mathbf{J} \dot{\xi} + {}^a_b \dot{\mathbf{J}} \xi) + \text{wed}({}^a_b \mathbf{J} \xi)^2 \\ & - {}^a_b \mathbf{G}_E^{-1} (\text{wed}({}^a_b \mathbf{J}_R \dot{\xi}_R + {}^a_b \dot{\mathbf{J}}_R \xi_R) + \text{wed}({}^a_b \mathbf{J}_R \xi_R)^2))^\top \|_{{}^a_b \bar{\mathbf{M}}'}^2 \end{aligned} \quad (4.17c)$$

$$\bar{\mathcal{T}} = \sum_{a,b} \frac{1}{2} \| (\text{wed}({}^a_b \mathbf{J} \xi) - {}^a_b \mathbf{G}_E^{-1} \text{wed}({}^a_b \mathbf{J}_R \xi_R))^\top \|_{{}^a_b \bar{\mathbf{M}}'}^2. \quad (4.17d)$$

Plugging this into the original definition of the closed loop (4.7) we find:

The desired closed loop system for the particle based approach is given by

$$\bar{\mathbf{f}}^M + \bar{\mathbf{f}}^D + \bar{\mathbf{f}}^K = \mathbf{0} \quad (4.18a)$$

where

$$\bar{\mathbf{f}}^K = \nabla \bar{\mathcal{V}} = \sum_{a,b} {}^a_b \mathbf{J}^\top \text{vee2} ((\mathbf{I}_4 - {}^a_b \mathbf{G}_E^{-1}) {}^a_b \bar{\mathbf{K}}') \quad (4.18b)$$

$$\bar{\mathbf{f}}^D = \frac{\partial \bar{\mathcal{R}}}{\partial \xi} = \sum_{a,b} {}^a_b \mathbf{J}^\top \text{vee2} ((\text{wed}({}^a_b \mathbf{J} \xi) - {}^a_b \mathbf{G}_E^{-1} \text{wed}({}^a_b \mathbf{J}_R \xi_R)) {}^a_b \bar{\mathbf{D}}') \quad (4.18c)$$

$$\begin{aligned} \bar{\mathbf{f}}^M = \frac{\partial \bar{\mathcal{S}}}{\partial \dot{\xi}} = \sum_{a,b} & {}^a_b \mathbf{J}^\top \text{vee2} ((\text{wed}({}^a_b \mathbf{J} \dot{\xi} + {}^a_b \dot{\mathbf{J}} \xi) + \text{wed}({}^a_b \mathbf{J} \xi)^2 \\ & - {}^a_b \mathbf{G}_E^{-1} (\text{wed}({}^a_b \mathbf{J}_R \dot{\xi}_R + {}^a_b \dot{\mathbf{J}}_R \xi_R) + \text{wed}({}^a_b \mathbf{J}_R \xi_R)^2)) {}^a_b \bar{\mathbf{M}}') \end{aligned} \quad (4.18d)$$

The system inertia matrix  $\bar{\mathbf{M}}$  can be recovered from the first term in (4.18d):

$$\sum_{a,b} {}^a_b \mathbf{J}^\top \text{vee2} \left( \text{wed}({}^a_b \mathbf{J} \dot{\boldsymbol{\xi}}) {}^a_b \bar{\mathbf{M}}' \right) = \underbrace{\sum_{a,b} {}^a_b \mathbf{J}^\top \text{Wed}({}^a_b \bar{\mathbf{M}}') {}^a_b \mathbf{J} \dot{\boldsymbol{\xi}}}_{\bar{\mathbf{M}}} = \frac{\partial^2 \bar{\mathcal{S}}}{\partial \dot{\boldsymbol{\xi}} \partial \dot{\boldsymbol{\xi}}} = \frac{\partial^2 \bar{\mathcal{T}}}{\partial \boldsymbol{\xi} \partial \boldsymbol{\xi}} \quad (4.19)$$

Though the body inertia matrices  ${}^a_b \bar{\mathbf{M}}' \in \mathbb{SYM}_0^+(4)$  from (4.16c) are only required to be positive semi-definite, the resulting system inertia matrix  $\bar{\mathbf{M}}(\mathbf{x}) \in \mathbb{SYM}^+(n)$  is required to be positive definite for the closed loop to be solvable.

## 4.2 Approach 2: Body based approach

The previous approach for the design of a closed loop has a vivid interpretation for the control energies and parameters. However, the total energy  $\mathcal{W}$  does not, in general, serve as a Lyapunov function. In this section we attempt to modify the energies to account for this.

### 4.2.1 Free rigid body

Using the configuration error  $\mathbf{G}_E = \mathbf{G}_R^{-1} \mathbf{G}$  and its velocity  $\dot{\boldsymbol{\xi}}_E = \mathbf{G}_E^{-1} \dot{\mathbf{G}}_E = \dot{\boldsymbol{\xi}} - \text{Ad}_{\mathbf{G}_E}^{-1} \dot{\boldsymbol{\xi}}_R$  we modify the energies from section 4.1 to

$$\bar{\mathcal{V}} = \frac{1}{2} \|(\mathbf{G}_E - \mathbf{I}_4)^\top\|_{\bar{\mathbf{K}}}^2, \quad \bar{\mathbf{K}}' \in \mathbb{SYM}^+(4), \quad (4.20a)$$

$$\bar{\mathcal{R}} = \frac{1}{2} \|\dot{\mathbf{G}}_E^\top\|_{\bar{\mathbf{D}}'}^2 = \frac{1}{2} \|\text{wed}(\dot{\boldsymbol{\xi}}_E)^\top\|_{\bar{\mathbf{D}}'}^2 = \frac{1}{2} \dot{\boldsymbol{\xi}}_E^\top \bar{\mathbf{D}} \dot{\boldsymbol{\xi}}_E, \quad \bar{\mathbf{D}}' \in \mathbb{SYM}^+(4), \quad (4.20b)$$

$$\bar{\mathcal{S}} = \frac{1}{2} \|\ddot{\mathbf{G}}_E^\top\|_{\bar{\mathbf{M}}'}^2 = \frac{1}{2} \|(\text{wed}(\dot{\boldsymbol{\xi}}_E) + \text{wed}(\boldsymbol{\xi}_E)^2)^\top\|_{\bar{\mathbf{M}}'}^2, \quad \bar{\mathbf{M}}' \in \mathbb{SYM}^+(4), \quad (4.20c)$$

$$\bar{\mathcal{T}} = \frac{1}{2} \|\dot{\mathbf{G}}_E^\top\|_{\bar{\mathbf{M}}'}^2 = \frac{1}{2} \|\text{wed}(\dot{\boldsymbol{\xi}}_E)^\top\|_{\bar{\mathbf{M}}'}^2 = \frac{1}{2} \dot{\boldsymbol{\xi}}_E^\top \bar{\mathbf{M}} \dot{\boldsymbol{\xi}}_E \quad (4.20d)$$

with usual substitution  $\bar{\mathbf{M}} = \text{Vee}(\bar{\mathbf{M}}')$ . The closed loop forces are again defined as the derivatives of their corresponding energies. Using  $\partial \boldsymbol{\xi}_E / \partial \boldsymbol{\xi} = \mathbf{I}_6$  we have

$$\bar{\mathbf{f}}^K = \nabla \bar{\mathcal{V}} = \text{vee2} ((\mathbf{I}_4 - \mathbf{G}_E^{-1}) \bar{\mathbf{K}}') \quad (4.21a)$$

$$\bar{\mathbf{f}}^D = \frac{\partial \bar{\mathcal{R}}}{\partial \boldsymbol{\xi}} = \text{vee2} (\text{wed}(\dot{\boldsymbol{\xi}}_E) \bar{\mathbf{D}}') = \bar{\mathbf{D}} \dot{\boldsymbol{\xi}}_E \quad (4.21b)$$

$$\bar{\mathbf{f}}^M = \frac{\partial \bar{\mathcal{S}}}{\partial \dot{\boldsymbol{\xi}}} = \text{vee2} ((\text{wed}(\dot{\boldsymbol{\xi}}_E) + \text{wed}(\boldsymbol{\xi}_E)^2) \bar{\mathbf{M}}') = \bar{\mathbf{M}} \dot{\boldsymbol{\xi}}_E - \text{ad}_{\dot{\boldsymbol{\xi}}_E}^\top \bar{\mathbf{M}} \dot{\boldsymbol{\xi}}_E \quad (4.21c)$$

A crucial result of this approach is that the resulting closed loop equations can be written as *autonomous* equations for the configuration  $\mathbf{G}_E$  and velocity error  $\dot{\boldsymbol{\xi}}_E$  as

$$\dot{\mathbf{G}}_E = \mathbf{G} \text{wed}(\boldsymbol{\xi}_E), \quad \bar{\mathbf{M}} \dot{\boldsymbol{\xi}}_E - \text{ad}_{\dot{\boldsymbol{\xi}}_E}^\top \bar{\mathbf{M}} \dot{\boldsymbol{\xi}}_E + \bar{\mathbf{D}} \dot{\boldsymbol{\xi}}_E + \text{vee2} ((\mathbf{I}_4 - \mathbf{G}_E^{-1}) \bar{\mathbf{K}}') = \mathbf{0}. \quad (4.22)$$

A quite similar (though restricted to  $\mathbf{s} = \mathbf{l} = \mathbf{h} = \mathbf{0}$ ) closed loop for the free rigid body is proposed in [Koditschek, 1989], though motivated from a Lie group point of view.

**Total energy.** The change of the total energy  $\bar{\mathcal{W}} = \bar{\mathcal{T}} + \bar{\mathcal{V}}$  along the solutions of the closed loop (4.22) is

$$\dot{\bar{\mathcal{W}}} = \xi_E^\top (\bar{\mathbf{M}} \dot{\xi}_E + \text{vee2}((\mathbf{I}_4 - \mathbf{G}_E^{-1}) \bar{\mathbf{K}}')) = \underbrace{\xi_E^\top \text{ad}_{\xi_E}^\top \bar{\mathbf{M}} \xi_E}_{=0} - \xi_E^\top \bar{\mathbf{D}} \xi_E = -2\bar{\mathcal{R}}. \quad (4.23)$$

Note that  $\bar{\mathbf{K}}', \bar{\mathbf{D}}', \bar{\mathbf{M}}' \in \mathbb{S}\mathbb{Y}\mathbb{M}^+(4)$  imply the positive definiteness of the total energy  $\bar{\mathcal{W}}$  and the dissipation function  $\bar{\mathcal{R}}$ . Using this with the techniques from [Koditschek, 1989], one can show that “almost” all solutions of (4.22) converge to  $\mathbf{G}_E = \mathbf{I}_4$  and  $\xi_E = \mathbf{0}$ . The remaining solutions are the constant ( $\xi_E = \mathbf{0}$ ) configurations  $\mathbf{G}_E \neq \mathbf{I}_4$  which are critical points of the potential  $\bar{\mathcal{V}}$ , see subsection 3.3.4. Roughly speaking, the configuration in which the body is 180° rotated to its reference.

### 4.2.2 Rigid body systems

For a rigid body system, let the body configurations  ${}^a_b \mathbf{G} = {}^a_b \mathbf{G}(\mathbf{x})$  and the body velocities  ${}^a_b \dot{\xi} = {}^a_b \mathbf{J}(\mathbf{x}) \xi$  be parameterized by the configuration  $\mathbf{x}$  and velocity coordinates  $\xi$ . So the body configuration errors  ${}^a_b \mathbf{G}_E$  and body velocity errors  ${}^a_b \dot{\xi}_E$  may be expressed as

$${}^a_b \mathbf{G}_E(\mathbf{x}, \mathbf{x}_R) = {}^a_b \mathbf{G}^{-1}(\mathbf{x}_R) {}^a_b \mathbf{G}(\mathbf{x}), \quad (4.24a)$$

$${}^a_b \dot{\xi}_E(\mathbf{x}, \xi, \mathbf{x}_R, \xi_R) = {}^a_b \mathbf{J}(\mathbf{x}) \xi - \text{Ad}_{{}^a_b \mathbf{G}_E(\mathbf{x}, \mathbf{x}_R)}^{-1} {}^a_b \mathbf{J}_R(\mathbf{x}_R) \xi_R. \quad (4.24b)$$

As done in subsection 4.1.3, the system energies are simply the sum over the energies associated with the absolute and relative body configurations:

$$\bar{\mathcal{V}} = \sum_{a,b} \frac{1}{2} \|({}^a_b \mathbf{G}_E - \mathbf{I}_4)^\top\|_{{}^a_b \bar{\mathbf{K}}'}^2, \quad (4.25a)$$

$$\bar{\mathcal{R}} = \sum_{a,b} \frac{1}{2} \|\text{wed}({}^a_b \dot{\xi}_E)^\top\|_{{}^a_b \bar{\mathbf{D}}'}^2, \quad (4.25b)$$

$$\bar{\mathcal{S}} = \sum_{a,b} \frac{1}{2} \|(\text{wed}({}^a_b \dot{\xi}_E) + \text{wed}({}^a_b \dot{\xi}_E)^2)^\top\|_{{}^a_b \bar{\mathbf{M}}'}^2, \quad (4.25c)$$

$$\bar{\mathcal{T}} = \sum_{a,b} \frac{1}{2} \|\text{wed}({}^a_b \dot{\xi}_E)^\top\|_{{}^a_b \bar{\mathbf{M}}'}^2. \quad (4.25d)$$

Overall, the desired controlled system for the body based approach takes the form

$$\bar{\mathbf{f}}^M + \bar{\mathbf{f}}^D + \bar{\mathbf{f}}^K = \mathbf{0} \quad (4.26a)$$

where

$$\bar{\mathbf{f}}^K = \nabla \bar{\mathcal{V}} = \sum_{a,b} {}^a_b \mathbf{J}^\top \text{vee2}((\mathbf{I}_4 - {}^a_b \mathbf{G}_E^{-1}) {}^a_b \bar{\mathbf{K}}'), \quad (4.26b)$$

$$\bar{\mathbf{f}}^D = \frac{\partial \bar{\mathcal{R}}}{\partial \xi} = \sum_{a,b} {}^a_b \mathbf{J}^\top {}^a_b \bar{\mathbf{D}} {}^a_b \dot{\xi}_E \quad (4.26c)$$

$$\bar{\mathbf{f}}^M = \frac{\partial \bar{\mathcal{S}}}{\partial \dot{\xi}} = \sum_{a,b} {}^a_b \mathbf{J}^\top ({}^a_b \bar{\mathbf{M}} {}^a_b \dot{\xi}_E - \text{ad}_{{}^a_b \dot{\xi}_E}^\top {}^a_b \bar{\mathbf{M}} {}^a_b \dot{\xi}_E) \quad (4.26d)$$

The change of the total energy  $\bar{\mathcal{W}} = \bar{\mathcal{T}} + \bar{\mathcal{V}}$  along the solutions of (4.26) does *not* take a similar form to (4.23). Consequently there is no simple conclusion about stability.

### 4.3 Approach 3: Inspired by total energy

The previous approaches for the design of a closed loop also motived a total energy  $\bar{\mathcal{W}}$ . Unfortunately, it did, in general, not turn out to be useful for stability analysis. In this section we like to motivate yet another approach for the design of a closed loop dynamics for the tracking problem which is based on the total energy as Lyapunov function.

#### 4.3.1 Overall structure

**Total energy.** Initially we drop the rigid body structure of the system and only consider the coordinates  $\mathbf{x}, \boldsymbol{\xi}$  and their kinematic relation  $\dot{\mathbf{x}} = \mathbf{A}(\mathbf{x})\boldsymbol{\xi}$ . Define the “total error energy” as

$$\bar{\mathcal{W}}(\mathbf{x}, \boldsymbol{\xi}, \mathbf{x}_R, \boldsymbol{\xi}_R) = \underbrace{\frac{1}{2} \|\boldsymbol{\xi} - \mathbf{Q}(\mathbf{x}, \mathbf{x}_R)\boldsymbol{\xi}_R\|_{\bar{\mathbf{M}}(\mathbf{x})}^2}_{\bar{\tau}} + \bar{\mathcal{V}}(\mathbf{x}, \mathbf{x}_R) \quad (4.27)$$

with the positive definite error potential  $\bar{\mathcal{V}} : \mathbb{X} \times \mathbb{X} \rightarrow \mathbb{R}^+$ ,  $\bar{\mathcal{V}}(\mathbf{x}, \mathbf{x}_R) = 0 \Leftrightarrow \mathbf{x} = \mathbf{x}_R$  and the positive definite inertia matrix  $\bar{\mathbf{M}}(\mathbf{x}) \in \text{SYM}^+(n)$ . So far the transport map  $\mathbf{Q} : \mathbb{X} \times \mathbb{X} \rightarrow \mathbb{R}^{n \times n}$  may be any regular matrix with  $\mathbf{Q}(\mathbf{x}, \mathbf{x}) = \mathbf{I}_n$ . Combination of these requirements yields the positive definiteness of the total energy, i.e.

$$\bar{\mathcal{W}}(\mathbf{x}, \boldsymbol{\xi}, \mathbf{x}_R, \boldsymbol{\xi}_R) \geq 0, \quad \bar{\mathcal{W}}(\mathbf{x}, \boldsymbol{\xi}, \mathbf{x}_R, \boldsymbol{\xi}_R) = 0 \Leftrightarrow \mathbf{x} = \mathbf{x}_R, \boldsymbol{\xi} = \boldsymbol{\xi}_R. \quad (4.28)$$

**Change of total energy.** The time derivative of the total energy is

$$\begin{aligned} \dot{\bar{\mathcal{W}}} &= \boldsymbol{\xi}_E^\top (\bar{\mathbf{M}} \dot{\boldsymbol{\xi}}_E + \frac{1}{2} \dot{\bar{\mathbf{M}}} \boldsymbol{\xi}_E) + \boldsymbol{\xi}^\top \nabla \bar{\mathcal{V}} + \boldsymbol{\xi}_R^\top \nabla_R \bar{\mathcal{V}} \\ &= \boldsymbol{\xi}_E^\top (\bar{\mathbf{M}} \dot{\boldsymbol{\xi}}_E + \frac{1}{2} \dot{\bar{\mathbf{M}}} \boldsymbol{\xi}_E + \nabla \bar{\mathcal{V}}) + \boldsymbol{\xi}_R^\top (\nabla_R \bar{\mathcal{V}} + \mathbf{Q}^\top \nabla \bar{\mathcal{V}}). \end{aligned} \quad (4.29)$$

where  $\nabla_R = \mathbf{A}^\top(\mathbf{x}_R) \frac{\partial}{\partial \mathbf{x}_R}$ . The second term vanishes if we require the transport map  $\mathbf{Q}$  to fulfill

$$\nabla_R \bar{\mathcal{V}} = -\mathbf{Q}^\top \nabla \bar{\mathcal{V}}. \quad (4.30)$$

The first term is non-positive if we set the closed loop kinetics as

$$\bar{\mathbf{M}} \dot{\boldsymbol{\xi}}_E + (\frac{1}{2} \dot{\bar{\mathbf{M}}} + \bar{\mathbf{S}}) \boldsymbol{\xi}_E + \bar{\mathbf{D}} \boldsymbol{\xi}_E + \nabla \bar{\mathcal{V}} = \mathbf{0}. \quad (4.31)$$

with the positive definite damping matrix  $\bar{\mathbf{D}} \in \text{SYM}_0^+(n)$  and a skew symmetric matrix  $\bar{\mathbf{S}} = -\bar{\mathbf{S}}^\top \in \mathbb{R}^{n \times n}$ . Plugging the closed loop kinetics (4.31) and the requirement on the transport map (4.30) into the change of energy (4.29) yields

$$\dot{\bar{\mathcal{W}}} = -\boldsymbol{\xi}_E^\top \bar{\mathbf{D}} \boldsymbol{\xi}_E = -\|\boldsymbol{\xi}_E\|_{\bar{\mathbf{D}}}^2 = -2\bar{\mathcal{R}}. \quad (4.32)$$

**Covariance of the closed loop.** The skew symmetric matrix  $\bar{\mathbf{S}}$  cancels out in the balance of energy, so is of no interest for tuning purposes. Instead it is used to ensure that the closed loop (4.31) is *covariant*, i.e. its definition is unchanged under a change of coordinates. While the stiffness force  $\bar{f}_i^K = \partial_i \bar{\mathcal{V}}$  and the dissipative force  $\bar{f}_i^D = \bar{D}_{ij} \xi_E^j$  are tensors, the inertia force  $\bar{f}_i^M = \bar{M}_{ij} \dot{\xi}_E^j + \frac{1}{2} \partial_k \bar{M}_{ij} \xi^k \xi_E^j + \bar{S}_{ij} \xi_E^j$  is not. A universal way is to derive a transformation law and put it as an additional requirement for the closed loop. The rather lengthy computation is given in ???. It shows that there are many co-vectors  $\bar{\mathbf{f}}^M$  such that  $\dot{\bar{\mathcal{T}}} = \xi_E^i \bar{f}_i^M$ .

However, a unique choice can be done by recognizing the kinetic energy  $\bar{\mathcal{T}}$  as a Riemannian metric, respectively the inertia matrix  $\bar{\mathbf{M}}$  as its coefficients, and using the *Levi-Civita connection*. The derivation requires more notation of differential geometry and is done in ???. The result takes the familiar form

$$\dot{\bar{\mathcal{T}}} = \xi_E^i \underbrace{\left( M_{ij} \dot{\xi}_E^j + \Gamma_{ijk} \xi^k \xi_E^j \right)}_{\bar{f}_i^M} \quad (4.33)$$

For the coefficients  $\bar{f}_i^M$  to form a tensor we can derive the transformation rule (under a change of coordinates  $\xi^i = W_{\hat{i}}^i(\mathbf{x}) \hat{\xi}^{\hat{i}}$  see ??)

$$\begin{aligned} \hat{f}_{\hat{i}}^M &= \hat{M}_{\hat{i}\hat{j}} \dot{\hat{\xi}}_E^{\hat{j}} + \frac{1}{2} \partial_{\hat{k}} \hat{M}_{\hat{i}\hat{j}} \hat{\xi}^{\hat{k}} \hat{\xi}_E^{\hat{j}} + \hat{S}_{\hat{i}\hat{j}} \hat{\xi}_E^{\hat{j}} \\ &= W_{\hat{i}}^i M_{ij} W_{\hat{j}}^j (Z_k^{\hat{j}} \dot{\xi}_E^k + \partial_l Z_k^{\hat{j}} \xi^l \xi_E^k) \\ &\quad + \frac{1}{2} (W_{\hat{i}}^i W_{\hat{j}}^j W_k^k \partial_k M_{ij} + (W_{\hat{j}}^j \partial_k W_i^i + W_i^i \partial_k W_{\hat{j}}^j) M_{ij}) Z_l^{\hat{k}} \xi^l Z_s^{\hat{j}} \xi_E^s \\ &\quad + \hat{S}_{\hat{i}\hat{j}} Z_j^{\hat{j}} \xi_E^j \\ &= W_{\hat{i}}^i M_{ij} \dot{\xi}_E^j + W_{\hat{i}}^i M_{ij} W_{\hat{j}}^j \partial_l Z_k^{\hat{j}} \xi^l \xi_E^k \\ &\quad + \frac{1}{2} W_{\hat{i}}^i \partial_k M_{ij} \xi^k \xi_E^j + \frac{1}{2} W_{\hat{i}}^i Z_i^{\hat{k}} \partial_l W_k^l M_{kj} \xi^l \xi_E^j + \frac{1}{2} W_{\hat{i}}^i \partial_k W_{\hat{j}}^j M_{ij} \xi^k Z_s^{\hat{j}} \xi_E^s \\ &\quad + W_{\hat{i}}^i Z_i^{\hat{k}} \hat{S}_{\hat{k}\hat{j}} Z_j^{\hat{j}} \xi_E^j \\ &= W_{\hat{i}}^i \left( M_{ij} \dot{\xi}_E^j + \frac{1}{2} \partial_k M_{ij} \xi^k \xi_E^j \right. \\ &\quad \left. + \underbrace{\left( Z_i^{\hat{k}} \hat{S}_{\hat{k}\hat{j}} Z_j^{\hat{j}} + (\mathbf{M}[il] W_{\hat{j}}^l \partial_k Z_j^{\hat{j}} + \frac{1}{2} Z_i^{\hat{k}} \partial_k W_{\hat{k}}^l \mathbf{M}[lj] + \frac{1}{2} \partial_k W_{\hat{j}}^s M_{is} Z_j^{\hat{j}}) \xi^k \right)}_{S_{ij}} \xi_E^j \right) \quad (4.34) \end{aligned}$$

So

$$\hat{S}'_{\hat{i}\hat{j}} = W_{\hat{i}}^i W_{\hat{j}}^j \bar{S}'_{ij} + \frac{1}{2} \bar{M}_{ij} (W_{\hat{i}}^i \partial_k W_{\hat{j}}^j - W_{\hat{j}}^j \partial_k W_{\hat{i}}^i) \xi^k \quad (4.35)$$

$$\hat{S}_{\hat{i}\hat{j}} = \bar{S}_{ij} W_{\hat{i}}^i W_{\hat{j}}^j + \frac{1}{2} \bar{M}_{ij} (W_{\hat{i}}^i \partial_k W_{\hat{j}}^j - W_{\hat{j}}^j \partial_k W_{\hat{i}}^i) \xi^k, \quad \hat{i}, \hat{j} = 1, \dots, n. \quad (4.36)$$

Recall the coefficients  $\bar{\Gamma}_{ijk}$  of the Levi-Civita connection for the chosen metric  $\bar{\mathbf{M}}$ :

$$\bar{\Gamma}_{ijk} = \frac{1}{2} (\partial_k \bar{M}_{ij} + \partial_j \bar{M}_{ik} - \partial_i \bar{M}_{jk} + \gamma_{ij}^s \bar{M}_{sk} + \gamma_{ik}^s \bar{M}_{sj} - \gamma_{jk}^s \bar{M}_{si}), \quad i, j, k = 1, \dots, n \quad (4.37)$$

and their transformation rule

$$\hat{\bar{\Gamma}}_{\hat{i}\hat{j}\hat{k}} = \bar{\Gamma}_{ijk} W_{\hat{i}}^j W_{\hat{j}}^k + \bar{M}_{ij} W_{\hat{i}}^j \partial_{\hat{k}} W_{\hat{j}}^j, \quad \hat{i}, \hat{j}, \hat{k} = 1, \dots, n. \quad (4.38)$$

With this one definition for  $\bar{S}_{ij}$  that obeys (4.48) is

$$\bar{S}_{ij} = \frac{1}{2} (\bar{\Gamma}_{ijk} - \bar{\Gamma}_{jik}) \xi^k, \quad i, j = 1, \dots, n. \quad (4.39)$$

Plugging this into (4.47) we finally obtain a covariant and energy conserving inertia force as

$$f_i^M = \bar{M}_{ij} \dot{\xi}_E^j + \bar{\Gamma}_{ijk} \xi^k \xi_E^j, \quad i = 1, \dots, n. \quad (4.40)$$

Note that  $\bar{f}^M$  from this definition can not be derived by Lagrange's formulation from the kinetic energy  $\bar{\mathcal{T}}$ . It is however completely determined by given metric coefficients  $\bar{M}$ . The definition of the inertia force  $\bar{f}^M$  is not unique: For any antisymmetric tensor  $S'_{ij} = -S'_{ji}$  the inertia force  $\bar{f}_i^M + S'_{ij} \xi_E^j$  is covariant and energy conserving as well. Define the closed loop kinematics as

$$\underbrace{\bar{M}_{ij} \dot{\xi}_E^j}_{\bar{f}_i^M} + \underbrace{\bar{\Gamma}_{ijk} \xi^k \xi_E^j}_{\bar{f}_i^D} + \underbrace{\bar{D}_{ij} \xi_E^j}_{\bar{f}_i^K} + \underbrace{\partial_i \bar{\mathcal{V}}}_{\bar{f}_i^K} = 0, \quad i = 1, \dots, n. \quad (4.41)$$

**Error potential and velocity.** The first thing we need is a quantification of how far the system configuration  $\mathbf{x}(t) \in \mathbb{X}$  is away from its desired configuration  $\mathbf{x}_R(t) \in \mathbb{X}$ : For this consider the *error potential* as a smooth, positive definite function  $\bar{\mathcal{V}} : \mathbb{X} \times \mathbb{X} \rightarrow \mathbb{R}$ , i.e.

$$\bar{\mathcal{V}}(\mathbf{x}, \mathbf{x}_R) \geq 0, \quad \bar{\mathcal{V}}(\mathbf{x}, \mathbf{x}_R) = 0 \Leftrightarrow \mathbf{x} = \mathbf{x}_R. \quad (4.42)$$

For the following we require the existence of a *transport map* as introduced in [Bullo and Murray, 1999]. That is a smooth function  $\mathbf{Q} : \mathbb{X} \times \mathbb{X} \rightarrow \mathbb{R}^{n \times n}$  such that

$$\underbrace{A_i^\alpha(\mathbf{x}_R) \frac{\partial \bar{\mathcal{V}}}{\partial x_R^\alpha}(\mathbf{x}, \mathbf{x}_R)}_{\partial_i^R \bar{\mathcal{V}}(\mathbf{x}, \mathbf{x}_R)} = -Q_i^j(\mathbf{x}, \mathbf{x}_R) \underbrace{A_j^\alpha(\mathbf{x}) \frac{\partial \bar{\mathcal{V}}}{\partial x^\alpha}(\mathbf{x}, \mathbf{x}_R)}_{\partial_j \bar{\mathcal{V}}(\mathbf{x}, \mathbf{x}_R)}, \quad i = 1, \dots, n. \quad (4.43)$$

From this we obtain the relation

$$\frac{d}{dt} \bar{\mathcal{V}} = \xi^i \partial_j \bar{\mathcal{V}} + \xi_R^i \partial_j^R \bar{\mathcal{V}} = \underbrace{(\xi^i - Q_j^i \xi_R^j)}_{\xi_E^i} \underbrace{\partial_i \bar{\mathcal{V}}}_{\bar{f}_i^K}. \quad (4.44)$$

Essentially the transport map gives a mean to compare the actual velocity  $\xi$  and the reference velocity  $\xi_R$  which live on different tangent spaces, thus giving a reasonable definition for the *error velocity*  $\xi_E$ . Note that  $\mathbf{Q}$  are the coefficients of a tensor, (see (??) and (??)), so the existence of a transport map is independent of the particular choice of coordinates.

**Kinetic error energy and inertia force.** Having a notion for the error velocity, we may define the kinetic error energy

$$\bar{\mathcal{T}}(\mathbf{x}, \boldsymbol{\xi}, \mathbf{x}_R, \boldsymbol{\xi}_R) = \frac{1}{2} \bar{M}_{ij}(\mathbf{x}) \underbrace{(\xi^i - Q_k^i(\mathbf{x}, \mathbf{x}_R)\xi_R^k)}_{\xi_E^i} \underbrace{(\xi^j - Q_l^j(\mathbf{x}, \mathbf{x}_R)\xi_R^l)}_{\xi_E^j} \geq 0 \quad (4.45)$$

with a symmetric and positive definite inertia matrix  $\bar{M}(\mathbf{x}) \in \text{SYM}^+(n)$ . We associate the inertia force  $\bar{\mathbf{f}}^M$  with the kinetic energy through

$$\frac{d}{dt} \bar{\mathcal{T}} = \xi_E^i \underbrace{(\bar{M}_{ij} \dot{\xi}_E^j + \frac{1}{2} \partial_k \bar{M}_{ij} \xi^k \xi_E^j)}_{\neq \bar{f}_i^M} \stackrel{!}{=} \xi_E^i \bar{f}_i^M. \quad (4.46)$$

It is crucial to note that the marked terms are *not* covariant, so do not form a tensor. To resolve this we add the antisymmetric coefficients  $\bar{S}_{ij} = -\bar{S}_{ji}$  and define the inertia force as

$$\bar{f}_i^M = \bar{M}_{ij} \dot{\xi}_E^j + \frac{1}{2} \partial_k \bar{M}_{ij} \xi^k \xi_E^j + \bar{S}_{ij} \xi_E^j, \quad i = 1, \dots, n. \quad (4.47)$$

For the coefficients  $\bar{f}_i^M$  to form a tensor we can derive the transformation rule (under a change of coordinates  $\xi^i = W_{\hat{i}}^i(\mathbf{x}) \hat{\xi}^{\hat{i}}$  see ??)

$$\hat{S}_{\hat{i}\hat{j}} = \bar{S}_{ij} W_{\hat{i}}^i W_{\hat{j}}^j + \frac{1}{2} \bar{M}_{ij} (W_{\hat{i}}^i \partial_{\hat{k}} W_{\hat{j}}^j - W_{\hat{j}}^j \partial_{\hat{k}} W_{\hat{i}}^i) \hat{\xi}^{\hat{k}}, \quad \hat{i}, \hat{j} = 1, \dots, n. \quad (4.48)$$

Recall the coefficients  $\bar{\Gamma}_{ijk}$  of the Levi-Civita connection for the chosen metric  $\bar{M}$ :

$$\bar{\Gamma}_{ijk} = \frac{1}{2} (\partial_k \bar{M}_{ij} + \partial_j \bar{M}_{ik} - \partial_i \bar{M}_{jk} + \gamma_{ij}^s \bar{M}_{sk} + \gamma_{ik}^s \bar{M}_{sj} - \gamma_{jk}^s \bar{M}_{si}), \quad i, j, k = 1, \dots, n \quad (4.49)$$

and their transformation rule

$$\hat{\bar{\Gamma}}_{\hat{i}\hat{j}\hat{k}} = \bar{\Gamma}_{ijk} W_{\hat{i}}^i W_{\hat{j}}^j W_{\hat{k}}^k + \bar{M}_{ij} W_{\hat{i}}^i \partial_{\hat{k}} W_{\hat{j}}^j, \quad \hat{i}, \hat{j}, \hat{k} = 1, \dots, n. \quad (4.50)$$

With this one definition for  $\bar{S}_{ij}$  that obeys (4.48) is

$$\bar{S}_{ij} = \frac{1}{2} (\bar{\Gamma}_{ijk} - \bar{\Gamma}_{jik}) \xi^k, \quad i, j = 1, \dots, n. \quad (4.51)$$

Plugging this into (4.47) we finally obtain a covariant and energy conserving inertia force as

$$f_i^M = \bar{M}_{ij} \dot{\xi}_E^j + \bar{\Gamma}_{ijk} \xi^k \xi_E^j, \quad i = 1, \dots, n. \quad (4.52)$$

Note that  $\bar{\mathbf{f}}^M$  from this definition can not be derived by Lagrange's formulation from the kinetic energy  $\bar{\mathcal{T}}$ . It is however completely determined by given metric coefficients  $\bar{M}$ . The definition of the inertia force  $\bar{\mathbf{f}}^M$  is not unique: For any antisymmetric tensor  $S'_{ij} = -S'_{ji}$  the inertia force  $\bar{f}_i^M + S'_{ij} \xi_E^j$  is covariant and energy conserving as well.

**Total error energy and dissipation.** Define the *total error energy*  $\bar{\mathcal{W}}$  as

$$\bar{\mathcal{W}}(\mathbf{x}, \boldsymbol{\xi}, \mathbf{x}_R, \boldsymbol{\xi}_R) = \bar{\mathcal{T}}(\mathbf{x}, \boldsymbol{\xi}, \mathbf{x}_R, \boldsymbol{\xi}_R) + \bar{\mathcal{V}}(\mathbf{x}, \mathbf{x}_R) \geq 0. \quad (4.53)$$

The definitions of the error potential (4.42) and the kinetic error energy (4.45) imply

$$\bar{\mathcal{W}}(\mathbf{x}, \boldsymbol{\xi}, \mathbf{x}_R, \boldsymbol{\xi}_R) = 0 \Leftrightarrow \mathbf{x} = \mathbf{x}_R, \boldsymbol{\xi} = \boldsymbol{\xi}_R. \quad (4.54)$$

Next we define a dissipative force  $f_i^D = \bar{D}_{ij}\xi_E^j$ , with the symmetric positive semi-definite dissipation matrix  $\bar{D}(\mathbf{x}) \in \mathbb{SYM}_0^+(n)$  and associate it with the change of the total energy by

$$\frac{d}{dt}\bar{\mathcal{W}} = \xi_E^i (\bar{f}_i^M + \bar{f}_i^K) \stackrel{!}{=} -\xi_E^i \bar{f}_i^D. \quad (4.55)$$

As above this implies  $\bar{f}_i^M + \bar{f}_i^K + \bar{f}_i^D = S''_{ij}\xi_E^j$  where  $S''$  can be the coefficients of any skew symmetric tensor. For simplicity we chose  $S'' = \mathbf{0}$  and formulate the resulting controlled kinetics:

The desired error kinetics for the energy based approach have the form

$$\underbrace{\bar{M}_{ij}\dot{\xi}_E^j}_{\bar{f}_i^M} + \underbrace{\bar{\Gamma}_{ijk}\xi^k\xi_E^j}_{\bar{f}_i^D} + \underbrace{\bar{D}_{ij}\xi_E^j}_{\bar{f}_i^K} + \underbrace{\partial_i \bar{\mathcal{V}}}_{\bar{f}_i^K} = 0, \quad i = 1, \dots, n. \quad (4.56)$$

Since  $\frac{d}{dt}\bar{\mathcal{W}}$  is only negative semidefinite, we can only conclude stability but not attractiveness. One can pursue the prove of attractiveness by adding a cross term as done in [Bullo and Murray, 1999].

### 4.3.2 Special cases

**Euclidean space.** The existing literature on control of mechanical systems uses almost exclusively minimal generalized coordinates  $\mathbf{q} \in \mathbb{R}^n$  and the velocity coordinates  $\dot{\mathbf{q}}$ . Then the model can we written as

$$\mathbf{M}(\mathbf{q})\ddot{\mathbf{q}} + \mathbf{C}(\mathbf{q}, \dot{\mathbf{q}})\dot{\mathbf{q}} = \mathbf{f}^A \quad (4.57)$$

where  $C_{ij} = \Gamma_{ijk}\xi^k$  and  $\mathbf{f}^A$  collects the remaining forces. For a fully actuated system there exists an input transformation such that  $\mathbf{f}^A$  can be regarded as virtual inputs.

On the Euclidean space  $\mathbb{R}^n$  it is reasonable to introduce error coordinates  $\mathbf{q}_E = \mathbf{q} - \mathbf{q}_R$  and to use a quadratic error potential

$$\bar{\mathcal{V}} = \frac{1}{2}\mathbf{q}_E^\top \bar{\mathbf{K}} \mathbf{q}_E, \quad \bar{\mathbf{K}} \in \mathbb{SYM}^+(n). \quad (4.58)$$

This error potential obviously has the transport map  $\mathbf{Q} = \mathbf{I}_n$  and the resulting error velocity  $\boldsymbol{\xi}_E = \dot{\mathbf{q}}_E = \dot{\mathbf{q}} - \dot{\mathbf{q}}_R$ . Furthermore it is reasonable to choose a constant dissipation matrix  $\bar{D} \in \mathbb{SYM}^+(n)$ .

**Joint PD-Control.** Choosing the desired inertia identical to the model inertia  $\bar{\mathbf{M}} = \mathbf{M}$ , which also implies  $\bar{\mathbf{C}} = \mathbf{C}$ , yields the closed loop kinetics

$$\mathbf{M}(\mathbf{q})\ddot{\mathbf{q}}_{\text{E}} + \mathbf{C}(\mathbf{q}, \dot{\mathbf{q}})\dot{\mathbf{q}}_{\text{E}} + \bar{\mathbf{D}}\dot{\mathbf{q}}_{\text{E}} + \bar{\mathbf{K}}\mathbf{q}_{\text{E}} = \mathbf{0}. \quad (4.59)$$

The resulting control law is

$$\mathbf{f}^{\text{A}} = \mathbf{M}(\mathbf{q})\ddot{\mathbf{q}}_{\text{R}} + \mathbf{C}(\mathbf{q}, \dot{\mathbf{q}})\dot{\mathbf{q}}_{\text{R}} - \bar{\mathbf{D}}\dot{\mathbf{q}}_{\text{E}} - \bar{\mathbf{K}}\mathbf{q}_{\text{E}}. \quad (4.60)$$

This approach is commonly called *joint proportional derivative controller* [Slotine and Li, 1991, sec. 9.1.1] or *augmented PD control law* [Murray et al., 1994, sec. 4.5.3], [Spong et al., 2006, sec. 8.2].

**Computed torque.** Choosing the desired inertia as  $\bar{\mathbf{M}} = \mathbf{I}_n$ , which implies  $\bar{\mathbf{C}} = \mathbf{0}$  leads to the closed loop kinetics

$$\ddot{\mathbf{q}}_{\text{E}} + \bar{\mathbf{D}}\dot{\mathbf{q}}_{\text{E}} + \bar{\mathbf{K}}\mathbf{q}_{\text{E}} = \mathbf{0}. \quad (4.61)$$

The resulting control law is

$$\mathbf{f}^{\text{A}} = \mathbf{M}(\mathbf{q})(\ddot{\mathbf{q}}_{\text{R}} - \bar{\mathbf{D}}\dot{\mathbf{q}}_{\text{E}} - \bar{\mathbf{K}}\mathbf{q}_{\text{E}}) + \mathbf{C}(\mathbf{q}, \dot{\mathbf{q}})\dot{\mathbf{q}}. \quad (4.62)$$

This approach is commonly called *computed torque* [Murray et al., 1994, sec. 4.5.2], [Slotine and Li, 1991, sec. 9.1.2] or *inverse dynamics control* [Spong et al., 2006, sec. 8.3].

These well established approaches are contained within the derived framework (4.56). However, as argued in the introduction of this chapter, the use of the Euclidean metric (4.58) only makes sense if the configuration space is indeed an Euclidean space. Application of this approach to e.g. the rigid body orientation would lead to quite awkward motion.

### 4.3.3 Free rigid body

Consider a single free rigid body as extensively discussed in section 3.3. We use the position  $\mathbf{r}$  and orientation  $\mathbf{R}$  combined in the matrix  $\mathbf{G} \in \mathbb{SE}(3)$  as configuration coordinates and the linear velocity  $\mathbf{v} = \mathbf{R}^T \dot{\mathbf{r}}$  and angular velocity  $\boldsymbol{\omega} = \text{vee}(\mathbf{R}^T \dot{\mathbf{R}})$  combined in  $[\mathbf{v}^T, \boldsymbol{\omega}^T]^T = \boldsymbol{\xi} = \text{vee}(\mathbf{G}^{-1} \dot{\mathbf{G}})$  as velocity coordinates.

**Potential and transport map.** As for the previous approaches, a reasonable choice (motivated from linear springs in subsection 3.3.4) for the potential energy for a rigid body is

$$\bar{\mathcal{V}} = \frac{1}{2}\|(\mathbf{G} - \mathbf{G}_{\text{R}})^T\|_{\bar{\mathbf{K}}'}^2, \quad \bar{\mathbf{K}}' \in \mathbb{SYM}^+(4). \quad (4.63)$$

The time derivative of the potential is

$$\begin{aligned} \dot{\bar{\mathcal{V}}} &= \text{tr}((\mathbf{G} - \mathbf{G}_{\text{R}})\bar{\mathbf{K}}'(\mathbf{G} \text{ wed}(\boldsymbol{\xi}) - \mathbf{G}_{\text{R}} \text{ wed}(\boldsymbol{\xi}_{\text{R}}))^T) \\ &= \text{tr}((\mathbf{I}_4 - \mathbf{G}^{-1}\mathbf{G}_{\text{R}})\bar{\mathbf{K}}' \text{ wed}(\boldsymbol{\xi} - \text{Ad}_{\mathbf{G}^{-1}\mathbf{G}_{\text{R}}}\boldsymbol{\xi}_{\text{R}})^T) \\ &= \underbrace{(\boldsymbol{\xi} - \text{Ad}_{\mathbf{G}^{-1}\mathbf{G}_{\text{R}}}\boldsymbol{\xi}_{\text{R}})}_{\boldsymbol{\xi}_{\text{E}}}^T \underbrace{\text{vee}2((\mathbf{I}_4 - \mathbf{G}^{-1}\mathbf{G}_{\text{R}})\bar{\mathbf{K}}')}_{\nabla \bar{\mathcal{V}}}. \end{aligned} \quad (4.64)$$

Recalling the identity  $\nabla \bar{\mathcal{V}} = \partial \dot{\mathcal{V}} / \partial \xi$ , it is evident that  $\mathbf{Q} = \text{Ad}_{\mathbf{G}^{-1}\mathbf{G}_R}$  is a transport map for this potential. The potential  $\bar{\mathcal{V}}$  and the resulting force  $\bar{\mathbf{f}}^K = \nabla \bar{\mathcal{V}}$  coincides with the ones given for the previous approaches, already explicitly stated in (4.14a).

**Damping and Inertia.** As for the previous approaches, let the damping and inertia matrices have the structure  $\bar{\mathbf{D}} = \text{Vee } \bar{\mathbf{D}}'$  and  $\bar{\mathbf{M}} = \text{Vee } \bar{\mathbf{M}}'$  with  $\bar{\mathbf{D}}', \bar{\mathbf{M}}' \in \mathbb{SYM}^+(4)$ . The entries may be interpreted as controlled total mass  $\bar{m}$ , controlled center of mass  $\bar{s}$  etc. as stated in (4.12). Plugging these matrices into (4.56) we find the controlled dissipation force  $\bar{\mathbf{f}}^D$  and controlled inertial force  $\bar{\mathbf{f}}^M$  as

$$\bar{\mathbf{f}}^D = \underbrace{\begin{bmatrix} \bar{d} \mathbf{I}_3 & \bar{d}(\text{wed } \bar{\mathbf{l}})^\top \\ \bar{d} \text{wed } \bar{\mathbf{l}} & \bar{\mathbf{r}} \end{bmatrix}}_{\bar{\mathbf{D}}} \underbrace{\begin{bmatrix} \mathbf{v}_E \\ \omega_E \end{bmatrix}}_{\xi_E}, \quad (4.65)$$

$$\bar{\mathbf{f}}^M = \underbrace{\begin{bmatrix} \bar{m} \mathbf{I}_3 & \bar{m}(\text{wed } \bar{s})^\top \\ \bar{m} \text{wed } \bar{s} & \bar{\Theta} \end{bmatrix}}_{\bar{\mathbf{M}}} \underbrace{\begin{bmatrix} \dot{\mathbf{v}}_E \\ \dot{\omega}_E \end{bmatrix}}_{\dot{\xi}_E} + \underbrace{\begin{bmatrix} \bar{m} \text{ wed } \omega & -\bar{m} \text{ wed } \omega \text{ wed } \bar{s} \\ \bar{m} \text{ wed } \bar{s} \text{ wed } \omega & \text{wed(Wed } \bar{\Theta} \omega) \end{bmatrix}}_{\bar{C}(\xi) = -\bar{C}^\top(\xi)} \underbrace{\begin{bmatrix} \mathbf{v}_E \\ \omega_E \end{bmatrix}}_{\xi_E}. \quad (4.66)$$

This result is very similar to the previous body based approach (4.22), only differing by replacing  $\bar{C}(\xi)$  with  $\bar{C}(\xi_E)$ . Consequently with this approach the closed loop dynamics are not autonomous.

**An alternative transport map.** It should be noted that the transport map given in (4.64) is not unique. One can check by direct calculation that the following matrix also fulfills the required relation (4.43):

$$\mathbf{Q} = \begin{bmatrix} \mathbf{R}^\top \mathbf{R}_R & \text{wed } \bar{\mathbf{h}} \mathbf{R}^\top \mathbf{R}_R - \mathbf{R}^\top \mathbf{R}_R \text{ wed } \bar{\mathbf{h}} \\ \mathbf{0} & \mathbf{R}^\top \mathbf{R}_R \end{bmatrix}. \quad (4.67)$$

#### 4.3.4 Rigid body systems

As for the previous approaches we use the rigid body structure, i.e. the configurations  ${}_b^a \mathbf{G}(\mathbf{x})$  and velocities  ${}_b^a \xi(\mathbf{x}, \xi) = {}_b^a \mathbf{J}(\mathbf{x}) \xi$ , as inspiration for controlled kinetics. Assigning stiffness, damping and inertia  ${}_b^K, {}_b^a \bar{\mathbf{D}}', {}_b^a \bar{\mathbf{M}}' \in \mathbb{SYM}_0^+(4)$  to each absolute and relative configuration leads to the following potential energy  $\bar{\mathcal{V}}$ , damping  $\bar{\mathbf{D}}$  and inertia matrix  $\bar{\mathbf{M}}$ :

$$\bar{\mathcal{V}}(\mathbf{x}, \mathbf{x}_R) = \sum_{a,b} \frac{1}{2} \|({}_b^a \mathbf{G}(\mathbf{x}) - {}_b^a \mathbf{G}(\mathbf{x}_R))^\top\|_{b^K}^2, \quad {}_b^K \in \mathbb{SYM}_0^+(4) \quad (4.68a)$$

$$\bar{\mathbf{D}}(\mathbf{x}) = \sum_{a,b} {}_b^a \mathbf{J}^\top(\mathbf{x}) \text{Vee}({}_b^a \bar{\mathbf{D}}') {}_b^a \mathbf{J}(\mathbf{x}), \quad {}_b^a \bar{\mathbf{D}}' \in \mathbb{SYM}_0^+(4) \quad (4.68b)$$

$$\bar{\mathbf{M}}(\mathbf{x}) = \sum_{a,b} {}_b^a \mathbf{J}^\top(\mathbf{x}) \text{Vee}({}_b^a \bar{\mathbf{M}}') {}_b^a \mathbf{J}(\mathbf{x}), \quad {}_b^a \bar{\mathbf{M}}' \in \mathbb{SYM}_0^+(4) \quad (4.68c)$$

Note that the body matrices do not have to be positive definite, only the resulting system matrices and the potential have to be positive definite to ensure stability.

**Transport map.** The potential  $\bar{\mathcal{V}}$  and the resulting force  $\nabla \bar{\mathcal{V}}$  are identical to the previous approaches, see e.g. (4.18b). For this energy based approach we require the existence of a transport map. The condition (4.43) for the transport map  $\mathbf{Q}$  with the given potential (4.68a) is equivalent to

$$\sum_{a,b} \left( {}_b^a \mathbf{J} \mathbf{Q} - \text{Ad}_{g_E^{-1}} {}_b^a \mathbf{J}_R \right)^\top \text{vee2} \left( (\mathbf{I}_4 - {}_b^a \mathbf{G}_E^{-1}) {}_b^a \bar{\mathbf{K}}' \right) = \mathbf{0}. \quad (4.69)$$

with the shorthand notation  ${}_b^a \mathbf{G}_E = {}_b^a \mathbf{G}^{-1}(x_R) {}_b^a \mathbf{G}_E(x)$  and  ${}_b^a \mathbf{J}_R = {}_b^a \mathbf{J}(x_R)$ . There is no general solution for this, the transport map  $\mathbf{Q}$  has to be computed for each example individually.

## 4.4 Constant reference and Linearization

**Constant reference.** For a constant reference configuration  $x_R = \text{const.} \Rightarrow \xi_R, \dot{\xi}_R = \mathbf{0}$ , the three control templates lead identical system

$$\dot{x} = \mathbf{A}(x)\xi, \quad \bar{\mathbf{M}}(x)\dot{\xi} + \bar{\mathbf{c}}(x, \xi) + \bar{\mathbf{D}}(x)\xi + \nabla \bar{\mathcal{V}}(x, x_R) = \mathbf{0} \quad (4.70a)$$

where

$$\bar{\mathbf{M}}(x) = \sum_{a,b} \left( {}_b^a \mathbf{J}(x) \right)^\top {}_b^a \bar{\mathbf{M}} {}_b^a \mathbf{J}(x), \quad (4.70b)$$

$$\bar{\mathbf{c}}(x, \xi) = \sum_{a,b} \left( {}_b^a \mathbf{J}(x) \right)^\top \left( {}_b^a \mathbf{M} {}_b^a \mathbf{J}(x, \xi) - \text{ad}_{g_E^{-1}(x)}^\top {}_b^a \mathbf{M} {}_b^a \mathbf{J}(x) \right) \xi \quad (4.70c)$$

$$\bar{\mathbf{D}}(x) = \sum_{a,b} \left( {}_b^a \mathbf{J}(x) \right)^\top {}_b^a \bar{\mathbf{D}} {}_b^a \mathbf{J}(x), \quad (4.70d)$$

$$\nabla \bar{\mathcal{V}}(x, x_R) = \sum_{a,b} \left( {}_b^a \mathbf{J}(x) \right)^\top \text{vee2} \left( (\mathbf{I}_4 - {}_b^a \mathbf{G}_E^{-1}(x, x_R)) {}_b^a \bar{\mathbf{K}}' \right) \quad (4.70e)$$

The total energy  $\bar{\mathcal{W}} = \frac{1}{2} \xi^\top \bar{\mathbf{M}} \xi + \bar{\mathcal{V}}$  is a Lyapunov function for this system if the system inertia matrix  $\bar{\mathbf{M}}$  and the potential energy  $\bar{\mathcal{V}}$  are positive definite, and the system dissipation matrix  $\bar{\mathbf{D}}$  is positive semi-definite.

**Linearization.** Assuming that the configuration of the system is close to its reference, i.e.  $x \approx x_R$ . The first order approximation (see section 2.5) of (4.70) with  $\varepsilon = \mathbf{A}^+(x_R)(x - x_R)$  is

$$\bar{\mathbf{M}}_0 \ddot{\varepsilon} + \bar{\mathbf{D}}_0 \dot{\varepsilon} + \bar{\mathbf{K}}_0 \varepsilon = \mathbf{0} \quad (4.71a)$$

where

$$\bar{\mathbf{M}}_0 = \bar{\mathbf{M}}(x_R) = \sum_{a,b} \left( {}_b^a \mathbf{J}(x_R) \right)^\top {}_b^a \bar{\mathbf{M}} {}_b^a \mathbf{J}(x_R), \quad (4.71b)$$

$$\bar{\mathbf{D}}_0 = \bar{\mathbf{D}}(x_R) = \sum_{a,b} \left( {}_b^a \mathbf{J}(x_R) \right)^\top {}_b^a \bar{\mathbf{D}} {}_b^a \mathbf{J}(x_R), \quad (4.71c)$$

$$\bar{\mathbf{K}}_0 = \nabla^2 \bar{\mathcal{V}}(x_R, x_R) = \sum_{a,b} \left( {}_b^a \mathbf{J}(x_R) \right)^\top {}_b^a \bar{\mathbf{K}} {}_b^a \mathbf{J}(x_R) \quad (4.71d)$$

## 4.5 Underactuated systems

The first three sections of this chapter motivated different desired closed loop dynamics which share the structure

$$\dot{\boldsymbol{x}} = \mathbf{A}(\boldsymbol{x})\boldsymbol{\xi}, \quad \bar{\mathbf{M}}(\boldsymbol{x})\dot{\boldsymbol{\xi}} + \bar{\mathbf{b}}(\boldsymbol{x}, \boldsymbol{\xi}, \boldsymbol{x}_R, \boldsymbol{\xi}_R, \dot{\boldsymbol{\xi}}_R) = \mathbf{0}. \quad (4.72)$$

The system model has still the form of (4.1):

$$\dot{\boldsymbol{x}} = \mathbf{A}(\boldsymbol{x})\boldsymbol{\xi}, \quad \mathbf{M}(\boldsymbol{x})\dot{\boldsymbol{\xi}} + \mathbf{b}(\boldsymbol{x}, \boldsymbol{\xi}) = \mathbf{B}(\boldsymbol{x})\mathbf{u}. \quad (4.73)$$

For a fully actuated system, i.e.  $\text{rank } \mathbf{B} = n$ , the combination of (4.72) and (4.73) can be solved for the system input  $\mathbf{u}$  yielding the actual control law. For an underactuated system, i.e.  $\text{rank } \mathbf{B} = p < n$ , this is not possible.

### 4.5.1 Control law through static optimization

If the desired closed loop dynamics (4.72) cannot be achieved exactly, the next best thing is to get “as close as possible” while still obeying the model dynamics (4.73). This is done by computing the control input  $\mathbf{u}$  by means of the static optimization problem

$$\begin{aligned} & \text{minimize} \quad \bar{\mathcal{G}} = \frac{1}{2}\|\dot{\boldsymbol{\xi}} + \bar{\mathbf{M}}^{-1}\bar{\mathbf{b}}\|_{\bar{\mathbf{M}}}^2 \\ & \text{subject to} \quad \mathbf{M}\dot{\boldsymbol{\xi}} + \mathbf{b} = \mathbf{B}\mathbf{u}, \quad \mathbf{u} \in \mathbb{R}^p \end{aligned} \quad (4.74)$$

Mathematically we do not have to use the metric coefficients  $\bar{\mathbf{M}}$  here for the optimization, any other symmetric positive definite matrix would serve the purpose as well. However, from the physics point of view, the terms in the norm correspond to an acceleration, so the inertia of the desired closed loop is the reasonable choice. Furthermore, from the control point of view, the additional parameters arising with a different matrix would not turn out to be really useful.

Elimination of the acceleration  $\dot{\boldsymbol{\xi}} = \mathbf{M}^{-1}(\mathbf{B}\mathbf{u} - \mathbf{b})$  from (4.74) leads to

$$\begin{aligned} \bar{\mathcal{G}} &= \frac{1}{2}\|\mathbf{M}^{-1}\mathbf{B}\mathbf{u} - \underbrace{(\mathbf{M}^{-1}\mathbf{b} - \bar{\mathbf{M}}^{-1}\bar{\mathbf{b}})}_{\tilde{\mathbf{a}}}\|_{\bar{\mathbf{M}}}^2 \\ &= \frac{1}{2}\mathbf{u}^\top \underbrace{\mathbf{B}^\top \mathbf{M}^{-1} \bar{\mathbf{M}} \mathbf{M}^{-1} \mathbf{B}}_{\mathbf{H}} \mathbf{u} - \mathbf{u}^\top \mathbf{B}^\top \mathbf{M}^{-1} \bar{\mathbf{M}} \tilde{\mathbf{a}} + \frac{1}{2}\tilde{\mathbf{a}}^\top \bar{\mathbf{M}} \tilde{\mathbf{a}} \\ &= \frac{1}{2}(\mathbf{u} - \underbrace{\mathbf{H}^{-1} \mathbf{B}^\top \mathbf{M}^{-1} \bar{\mathbf{M}} \tilde{\mathbf{a}}}_{\mathbf{u}_0})^\top \mathbf{H} (\mathbf{u} - \underbrace{\mathbf{H}^{-1} \mathbf{B}^\top \mathbf{M}^{-1} \bar{\mathbf{M}} \tilde{\mathbf{a}}}_{\mathbf{u}_0}) \\ &\quad + \frac{1}{2}\tilde{\mathbf{a}}^\top \bar{\mathbf{M}} \underbrace{(\mathbf{I}_n - \mathbf{M}^{-1} \mathbf{B} \mathbf{H}^{-1} \mathbf{B}^\top \mathbf{M}^{-1} \bar{\mathbf{M}})}_{\mathbf{P}^\perp} \tilde{\mathbf{a}} \\ &= \frac{1}{2}\|\mathbf{u} - \mathbf{u}_0\|_{\mathbf{H}}^2 + \underbrace{\frac{1}{2}\|\mathbf{P}^\perp \tilde{\mathbf{a}}\|_{\bar{\mathbf{M}}}^2}_{\bar{\mathcal{G}}_0}. \end{aligned} \quad (4.75)$$

For the formulation of  $\bar{\mathcal{G}}_0$  it is crucial to note that  $\mathbf{P}^\perp$  is a projection matrix, which will be exploited in the next subsection.

The control law, i.e. the solution of the minimization problem, is obviously  $\mathbf{u} = \mathbf{u}_0$ . The resulting closed loop kinetics are

$$\begin{aligned} M\dot{\xi} + b &= B \overbrace{H^{-1}B^\top M^{-1}\bar{M}(M^{-1}b - \bar{M}^{-1}\bar{b})}^{u_0} \\ \Leftrightarrow \dot{\xi} &= M^{-1}BH^{-1}B^\top M^{-1}\bar{M}(M^{-1}b - \bar{M}^{-1}\bar{b}) - M^{-1}b \\ \Leftrightarrow \bar{M}\dot{\xi} + \bar{b} &= \underbrace{\bar{M}P^\perp(\bar{M}^{-1}\bar{b} - M^{-1}b)}_{\tilde{b}}. \end{aligned} \quad (4.76)$$

This result means that there is an additional vector<sup>1</sup>  $\tilde{b}(\mathbf{x}, \xi, \mathbf{x}_R, \xi_R, \dot{\xi}_R) \in \mathbb{R}^n$  in the closed loop which allows for the closed loop (4.76) to be realizable with the available controls.

For the special case of a fully actuated system, i.e.  $B$  is invertible, the control law simplifies to  $\mathbf{u}_0 = B^{-1}(b - M\bar{M}^{-1}\bar{b})$ . Furthermore we have  $P^\perp = \mathbf{0}$  and consequently  $\tilde{b} = \mathbf{0}$  and  $\bar{G}_0 = 0$ .

In general, the value  $\bar{G}_0$  is a measure of how much the resulting closed loop differs from the original desired system (4.72). One main goal when parameterizing the controller is to make  $\bar{G}_0$  as small as possible. Unfortunately the form of  $\bar{G}_0$  in (4.76) is not handy, mainly due to  $\text{rank } P^\perp = n - p$ . In the following we like to find a more handy formulation.

### 4.5.2 Matching condition

The matrices  $P = M^{-1}BH^{-1}B^\top M^{-1}\bar{M}$  and its complementary  $P = I_n - P^\perp$  from (4.75) are projection matrices, i.e.  $P^2 = P$  and  $(P^\perp)^2 = P^\perp$ . Furthermore they are orthogonal w.r.t. the inner product  $\langle \cdot, \cdot \rangle_{\bar{M}}$ , i.e.  $\langle P\xi, P^\perp\eta \rangle_{\bar{M}} = 0 \forall \xi, \eta \in \mathbb{R}^n$ . The image of the projector  $P$  is the subspace of  $\mathbb{R}^n$  that is spanned by the columns of  $M^{-1}B$ . Consequently we have  $\text{rank } P = p$  and  $\text{rank } P^\perp = n - p$ . So  $\tilde{b}$  lies in a  $(n - p)$ -dimensional subspace. The goal of this subsection is to construct a basis for this subspace.

Let  $B^\perp \in \mathbb{R}^{n-p}$  be any orthogonal complement to  $B$ , i.e.  $\text{rank } B^\perp = n - p$  and  $B^\top B^\perp = \mathbf{0}$ . The columns of  $\bar{M}^{-1}MB^\perp$  are orthogonal to the columns of  $M^{-1}B$  under the metric  $\langle \cdot, \cdot \rangle_{\bar{M}}$  and span the image of  $P^\perp$ . Using some basic properties of orthogonal projectors (see ??) we can formulate

$$P^\perp = \bar{M}^{-1}MB^\perp \underbrace{((B^\perp)^\top M\bar{M}^{-1}MB^\perp)^{-1}}_{= S \in \text{SYM}^+(n-p)}(B^\perp)^\top M, \quad (4.77)$$

Plugging this into the expressions from the previous subsection, we find

$$\tilde{b} = MB^\perp S \underbrace{(B^\perp)^\top(M\bar{M}^{-1}\bar{b} - b)}_{=\lambda \in \mathbb{R}^{n-p}}. \quad \bar{G}_0 = \frac{1}{2}\|\boldsymbol{\lambda}\|_S^2. \quad (4.78)$$

It is much simpler to analyse  $\boldsymbol{\lambda}$  which has only the dimension of the underactuation  $n - p$  instead of  $\tilde{b}$  which has the full dimension  $n$  of the configuration space. Though it should be stressed that the values of  $\bar{G}_0$  and  $\tilde{b}$  are, as derived above, independent of the choice of

---

<sup>1</sup>The coefficients  $\tilde{b}$  do indeed transform like a tensor, even though  $b$  and  $\bar{b}$  do not.

$\mathbf{B}^\perp$ . The naming  $\boldsymbol{\lambda}$  is because we could have derived the same expressions by applying an acceleration constraint  $\mathbf{B}^\perp(\mathbf{M}\dot{\boldsymbol{\xi}} + \mathbf{b}) = \mathbf{0}$  to the desired closed loop and using the method of *Lagrangian multipliers*.

The best case is, of course, if we achieve

$$\boldsymbol{\lambda} = (\mathbf{B}^\perp)^\top (\mathbf{M}\bar{\mathbf{M}}^{-1}\bar{\mathbf{b}} - \mathbf{b}) = \mathbf{0} \quad \Rightarrow \quad \tilde{\mathbf{b}} = \mathbf{0}, \quad \bar{\mathcal{G}}_0 = 0 \quad (4.79)$$

i.e. the desired closed loop is realized exactly. An approach based on this is discussed in [Bloch et al., 2000]. A condition similar to (4.79) is therein called the *the matching condition* and is required to be fulfilled exactly. However, the examples for which this approach is demonstrated restricts to stabilization tasks  $\boldsymbol{\xi}_R = \mathbf{0}$  for small academic systems.

An advantage of the presented approach is that the control law  $\mathbf{u} = \mathbf{u}_0$  is defined independently of whether the matching condition is fulfilled or not. Instead the quantity  $\boldsymbol{\lambda}$ , which we will call the *matching force* in the following, ensures that the control law is realizable.

### 4.5.3 Approximations

The matching force (4.79) may become very cumbersome for complex systems and might even be impossible to vanish with the given parameters. It might be instructive to analyse it for particular situations.

**Zero error.** Assume that the controller tracks the reference perfectly, i.e.  $\mathbf{x} = \mathbf{x}_R$  and  $\dot{\boldsymbol{\xi}} = \dot{\boldsymbol{\xi}}_R$ . One may check that for this case the three approaches all yield  $\bar{\mathbf{b}} = \bar{\mathbf{M}}\dot{\boldsymbol{\xi}}_R$ . The resulting matching force  $\boldsymbol{\lambda}^{\text{ZeroError}}$  for this special case is

$$\boldsymbol{\lambda}^{\text{ZeroError}} = (\mathbf{B}^\perp(\mathbf{x}_R))^\top (\mathbf{M}(\mathbf{x}_R)\dot{\boldsymbol{\xi}}_R - \mathbf{b}(\mathbf{x}_R, \dot{\boldsymbol{\xi}}_R)) \quad (4.80)$$

Evidently, this is independent of the closed loop parameters, and should rather be regarded as a constraint on the *reference trajectory*  $t \mapsto \mathbf{x}_R(t)$ . The condition  $\boldsymbol{\lambda}^{\text{ZeroError}} = \mathbf{0}$  is essentially the model equation after elimination of the control inputs.

A very useful approach here is to formulate the reference trajectory in terms of a *flat output* [Fliess et al., 1995] of the model. The first step for a systematic construction of a flat output is commonly the elimination of the control inputs (see e.g. [Schlacher and Schöberl, 2007]) i.e.  $\boldsymbol{\lambda}^{\text{ZeroError}} = \mathbf{0}$ .

**Small error.** Assume that we a small error  $\boldsymbol{\varepsilon} = \mathbf{A}^+(\mathbf{x}_R)(\mathbf{x} - \mathbf{x}_R)$  to a constant reference  $\dot{\boldsymbol{\xi}}_R = \mathbf{0}$  as already considered in section 4.4. Then the model and the closed loop template may be approximated by

$$\mathbf{M}_0\ddot{\boldsymbol{\varepsilon}} + \mathbf{D}_0\dot{\boldsymbol{\varepsilon}} + \mathbf{K}_0\boldsymbol{\varepsilon} = \mathbf{B}(\mathbf{x}_R)\Delta\mathbf{u}, \quad (4.81a)$$

$$\bar{\mathbf{M}}_0\ddot{\boldsymbol{\varepsilon}} + \bar{\mathbf{D}}_0\dot{\boldsymbol{\varepsilon}} + \bar{\mathbf{K}}_0\boldsymbol{\varepsilon} = \mathbf{0} \quad (4.81b)$$

and the matching force  $\boldsymbol{\lambda}^{\text{SmallError}}$  for this special case is

$$\begin{aligned}\boldsymbol{\lambda}^{\text{SmallError}} &= (\mathbf{B}^\perp(\mathbf{x}_R))^\top (\bar{\mathbf{M}}_0^{-1}(\bar{\mathbf{D}}_0\dot{\boldsymbol{\varepsilon}} + \bar{\mathbf{K}}_0\boldsymbol{\varepsilon}) - (\mathbf{D}_0\dot{\boldsymbol{\varepsilon}} + \mathbf{K}_0\boldsymbol{\varepsilon})) \\ &= \underbrace{(\mathbf{B}^\perp(\mathbf{x}_R))^\top (\bar{\mathbf{M}}_0^{-1}\bar{\mathbf{D}}_0 - \mathbf{D}_0)}_{\boldsymbol{\Lambda}_D} \dot{\boldsymbol{\varepsilon}} + \underbrace{(\mathbf{B}^\perp(\mathbf{x}_R))^\top (\bar{\mathbf{M}}_0^{-1}\bar{\mathbf{K}}_0 - \mathbf{K}_0)}_{\boldsymbol{\Lambda}_K} \boldsymbol{\varepsilon}\end{aligned}\quad (4.82)$$

As  $\boldsymbol{\varepsilon}$  and  $\dot{\boldsymbol{\varepsilon}}$  can be arbitrary, the matrices  $\boldsymbol{\Lambda}_K$  and  $\boldsymbol{\Lambda}_D$  have to vanish, for  $\boldsymbol{\lambda}^{\text{SmallError}}$  to vanish. For the following examples it will turn out that we can always find suitable parameters within  $\bar{\mathbf{M}}_0$ ,  $\bar{\mathbf{D}}_0$  and  $\bar{\mathbf{K}}_0$  such that  $\boldsymbol{\Lambda}_K = \boldsymbol{\Lambda}_D = \mathbf{0}$ . Thus ensuring that at least the first order approximation of the actual matching force  $\boldsymbol{\lambda}$  vanishes.

#### 4.5.4 Systems with input constraints

In most control systems the control inputs  $\mathbf{u}$  can not take arbitrary values, but are constrained like e.g.  $-u_a^{\max} \leq u_a \leq u_a^{\max}, a = 1, \dots, p$  due to practical limitations. In general we assume that the constraints can be written as  $\mathbf{W}\mathbf{u} \leq \mathbf{l}$  where the inequality is understood componentwise and the resulting set  $\mathbb{U} = \{\mathbf{u} \in \mathbb{R}^p \mid \mathbf{W}\mathbf{u} \leq \mathbf{l}\}$  is assumed to be convex.

Here we can use just the same arguments as in subsection 4.5.1 to motivate a control law defined by the solution of the optimization problem

$$\begin{aligned}&\text{minimize } \bar{\mathcal{G}} = \frac{1}{2}\|\mathbf{u} - \mathbf{u}_0\|_{\mathbf{H}}^2 + \bar{\mathcal{G}}_0 \\ &\text{subject to } \mathbf{W}\mathbf{u} \leq \mathbf{l}, \mathbf{u} \in \mathbb{R}^p\end{aligned}\quad (4.83)$$

with  $\mathbf{H}$  and  $\mathbf{u}_0$  defined in (4.75). Given that  $\mathbf{H} \in \mathbb{S}\mathbb{Y}\mathbb{M}^+(p)$  is positive definite and  $\mathbb{U}$  is convex, this problem has a unique solution, though it usually has to be computed numerically. For the following simulation results the MATLAB function `quadprog` was used and a C++ implementation of the Active-Set algorithm from [Nocedal and Wright, 2006, Algorithm 16.3] was used for the real-time implementation on the Multicopters.

It should be stressed that this approach does not blah stability

## 4.6 Summary and recipe

We have proposed three approaches for a control law for rigid body systems. Each of them formulated a slightly different template for the desired closed loop dynamics. The actual control law results from its combination with the model dynamics. For a fully actuated system the desired closed loop is achieved exactly. For an underactuated system or in the presence of input constraints one achieves closed loop dynamics that are “as close as possible” to the desired dynamics in the sense that the resulting acceleration differs the least.

The implementation of the controller is determined by the rigid body parameterization  ${}^b\mathbf{G}(\mathbf{x})$ , the kinematics  $\dot{\mathbf{x}} = \mathbf{A}(\mathbf{x})\boldsymbol{\xi}$  and the constitutive parameters  ${}^a_b\mathbf{M}$ ,  ${}^a_b\mathbf{D}$ ,  ${}^a_b\mathbf{K}$ . It is

crucial to note that the resulting controlled system is invariant to the chosen coordinates  $\mathbf{x}, \boldsymbol{\xi}$  in the same way as the system model: Though the describing equations depend explicitly on the coordinates, the resulting motion of the closed loop system is the same for any choice of coordinates. This can be validated by checking the covariance of the closed loop equations.

What does affect the motion of the controlled system are the constitutive parameters, i.e. the values within  ${}_b\mathbf{M}$ ,  ${}_b\mathbf{D}$ ,  ${}_b\mathbf{K}$ . These are associated with the rigid bodies and are completely independent of the system coordinates. For the energy based approach, the choice of a transport map might not be unique and consequently might also affect the motion.

### THE recipe:

- Modeling
  - Choose a set of (possibly redundant) configuration coordinates  $\mathbf{x}(t) \in \mathbb{X} = \{\mathbf{x} \in \mathbb{R}^\nu \mid \phi(\mathbf{x}) = \mathbf{0}\}$  and minimal velocity coordinates  $\boldsymbol{\xi}(t) \in \mathbb{R}^n$ ,  $n = \dim \mathbb{X}$  that are related by the kinematics matrix  $\mathbf{A}(\mathbf{x}) \in \mathbb{R}^{\nu \times n}$  (see ??):
 
$$\dot{\mathbf{x}} = \mathbf{A}\boldsymbol{\xi} \quad (4.84a)$$
  - Formulate the rigid body configurations  ${}_b\mathbf{G}(\mathbf{x}) \in \mathbb{SE}(3)$ ,  $a, b = 0, \dots, N$  in terms of the chosen coordinates. This determines the body Jacobians (see ??)
 
$${}_b\mathbf{J} = \frac{\partial}{\partial \dot{\mathbf{x}}} \text{vee}({}_b\mathbf{G}^{-1} {}_b\dot{\mathbf{G}}) \mathbf{A} \quad (4.84b)$$
  - Compute the model inertia force  $\mathbf{f}^M = \mathbf{M}\dot{\boldsymbol{\xi}} + \mathbf{c}$  from the body inertias  ${}_b\mathbf{M}'$  (see subsection 3.4.3)
 
$$\mathbf{M} = \sum_b {}_b\mathbf{J}^\top \text{Vee}({}_b\mathbf{M}') {}_b\mathbf{J}, \quad \mathbf{c} = \sum_b {}_b\mathbf{J}^\top (\text{Vee}({}_b\mathbf{M}') {}_b\dot{\mathbf{J}} - \text{ad}_{{}_b\mathbf{J}\boldsymbol{\xi}}^\top \text{Vee}({}_b\mathbf{M}') {}_b\mathbf{J}) \boldsymbol{\xi} \quad (4.84c)$$
  - The model kinetics are the balance of the inertia force  $\mathbf{f}^M$ , the force of control inputs  $\mathbf{B}\mathbf{u}$  and whatever other forces  $\mathbf{f}^A$  may act on the system
 
$$\mathbf{M}\dot{\boldsymbol{\xi}} + \underbrace{\mathbf{c} + \mathbf{f}^A}_{b} = \mathbf{B}\mathbf{u} \quad (4.84d)$$

- Closed loop template

- The template is computed from the body configurations  ${}_b\mathbf{G}$ , the body Jacobians  ${}_b\mathbf{J}$  and the control parameters  ${}_b\bar{\mathbf{K}}'$ ,  ${}_b\bar{\mathbf{D}}'$ ,  ${}_b\bar{\mathbf{M}}'$ :

$$\bar{\mathbf{M}} = \sum_{a,b} {}_b\mathbf{J}^\top \text{Vee}({}_b\bar{\mathbf{M}}') {}_b\mathbf{J} \quad (4.85a)$$

$$\bar{\mathbf{f}}^K = \sum_{a,b} {}_b\mathbf{J}^\top \text{vee2}((\mathbf{I}_4 - {}_b\mathbf{G}_E^{-1}) {}_b\bar{\mathbf{K}}') \quad (4.85b)$$

- particle-based approach (see subsection 4.1.3)

$$\bar{\mathbf{f}}^D = \sum_{a,b} {}^a_b \mathbf{J}^\top \text{vee2} \left( \left( \text{wed}({}^a_b \mathbf{J}(\mathbf{x}) \boldsymbol{\xi}) - {}^a_b \mathbf{G}_E^{-1} \text{wed}({}^a_b \mathbf{J}(\mathbf{x}_R) \boldsymbol{\xi}_R) \right) {}^a_b \bar{\mathbf{D}}' \right) \quad (4.85c)$$

$$\begin{aligned} \bar{\mathbf{c}} = & \sum_{a,b} {}^a_b \mathbf{J}^\top \text{vee2} \left( \left( \text{wed}({}^a_b \dot{\mathbf{J}} \boldsymbol{\xi}) + \text{wed}({}^a_b \mathbf{J} \boldsymbol{\xi})^2 \right. \right. \\ & \left. \left. - {}^a_b \mathbf{G}_E^{-1} \left( \text{wed}({}^a_b \mathbf{J}_R \dot{\boldsymbol{\xi}}_R + {}^a_b \dot{\mathbf{J}}_R \boldsymbol{\xi}_R) + \text{wed}({}^a_b \mathbf{J}_R \boldsymbol{\xi}_R)^2 \right) \right) {}^a_b \bar{\mathbf{M}}' \right) \end{aligned} \quad (4.85d)$$

- body-based approach (see subsection 4.2.2)

$$\bar{\mathbf{f}}^D = \sum_{a,b} {}^a_b \mathbf{J}^\top \text{Vee}({}^a_b \bar{\mathbf{D}}') {}^a_b \boldsymbol{\xi}_E, \quad {}^a_b \boldsymbol{\xi}_E = {}^a_b \mathbf{J} \boldsymbol{\xi} - \text{Ad}_{{}^a_b \mathbf{G}_E^{-1}} {}^a_b \mathbf{J}_R \boldsymbol{\xi}_R, \quad (4.85e)$$

$$\begin{aligned} \bar{\mathbf{c}} = & \sum_{a,b} {}^a_b \mathbf{J}^\top \left( {}^a_b \bar{\mathbf{M}}' ({}^a_b \dot{\mathbf{J}} \boldsymbol{\xi} - \text{Ad}_{{}^a_b \mathbf{G}_E^{-1}} ({}^a_b \mathbf{J}_R \dot{\boldsymbol{\xi}}_R + {}^a_b \dot{\mathbf{J}}_R \boldsymbol{\xi}_R) + \text{ad}_{{}^a_b \boldsymbol{\xi}_E} \text{Ad}_{{}^a_b \mathbf{G}_E^{-1}} {}^a_b \mathbf{J}_R \boldsymbol{\xi}_R) \right. \\ & \left. - \text{ad}_{{}^a_b \boldsymbol{\xi}_E}^\top {}^a_b \bar{\mathbf{M}}' {}^a_b \boldsymbol{\xi}_E \right), \end{aligned} \quad (4.85f)$$

- energy-based approach (see subsection 4.3.4, requires the choice of a transport map  $\mathbf{Q}$ )

$$\bar{\mathbf{f}}^D = \bar{\mathbf{D}} \boldsymbol{\xi}_E, \quad \bar{\mathbf{D}} = \sum_{a,b} {}^a_b \mathbf{J}^\top \text{Vee}({}^a_b \bar{\mathbf{D}}') {}^a_b \mathbf{J}, \quad \boldsymbol{\xi}_E = \boldsymbol{\xi} - \mathbf{Q} \boldsymbol{\xi}_R \quad (4.85g)$$

$$\bar{\mathbf{C}} = \sum_{a,b} {}^a_b \mathbf{J}^\top \left( \text{Vee}({}^a_b \bar{\mathbf{M}}') {}^a_b \dot{\mathbf{J}} + {}^a_b \bar{\mathbf{C}} {}^a_b \mathbf{J} \right), \quad {}^a_b \bar{\mathbf{C}}_{pq} = \Gamma_{pqr}({}^a_b \bar{\mathbf{M}}') {}^a_b J_k^r \boldsymbol{\xi}^k \quad (4.85h)$$

$$\bar{\mathbf{c}} = \bar{\mathbf{C}} \boldsymbol{\xi}_E - \bar{\mathbf{M}} (\mathbf{Q} \dot{\boldsymbol{\xi}}_R + \dot{\mathbf{Q}} \boldsymbol{\xi}_R), \quad (4.85i)$$

- The desired closed loop kinetics are

$$\bar{\mathbf{M}} \dot{\boldsymbol{\xi}} + \underbrace{\bar{\mathbf{c}} + \bar{\mathbf{f}}^D + \bar{\mathbf{f}}^K}_{\bar{\mathbf{b}}} = \mathbf{0} \quad (4.85j)$$

- Control law:

- For the fully actuated case, the desired closed loop is realized by

$$\mathbf{u} = \mathbf{B}^{-1}(\mathbf{b} - \bar{\mathbf{M}} \bar{\mathbf{M}}^{-1} \bar{\mathbf{b}}) \quad (4.86a)$$

- In the underactuated case, the acceleration error measured by the Gaussian constraint, is minimized by (see subsection 4.5.1)

$$\mathbf{u} = (\mathbf{B}^\top \mathbf{M}^{-1} \bar{\mathbf{M}} \bar{\mathbf{M}}^{-1} \mathbf{B})^{-1} \mathbf{B}^\top \mathbf{M}^{-1} (\bar{\mathbf{M}} \bar{\mathbf{M}}^{-1} \mathbf{b} - \bar{\mathbf{b}}) \quad (4.86b)$$

Choosing an orthogonal complement  $\mathbf{B}^\perp$  to the input matrix  $\mathbf{B}$ , i.e.  $\text{rank } \mathbf{B}^\perp = n - p$  and  $\mathbf{B}^\top \mathbf{B}^\perp = \mathbf{0}$ , the residual acceleration error can be written as  $\bar{\mathcal{G}}_0 = \frac{1}{2} \|\boldsymbol{\lambda}\|_S^2$  where (see subsection 4.5.2)

$$\boldsymbol{\lambda} = (\mathbf{B}^\perp)^\top (\bar{\mathbf{M}} \bar{\mathbf{M}}^{-1} \bar{\mathbf{b}} - \mathbf{b}) = \mathbf{0}, \quad S = ((\mathbf{B}^\perp)^\top \bar{\mathbf{M}} \bar{\mathbf{M}}^{-1} \bar{\mathbf{M}} \mathbf{B}^\perp)^{-1} \quad (4.86c)$$

By adjusting the control parameters within  $\bar{\mathbf{M}}$  and  $\bar{\mathbf{b}}$  one may try to minimize  $\bar{\mathcal{G}}_0$ .

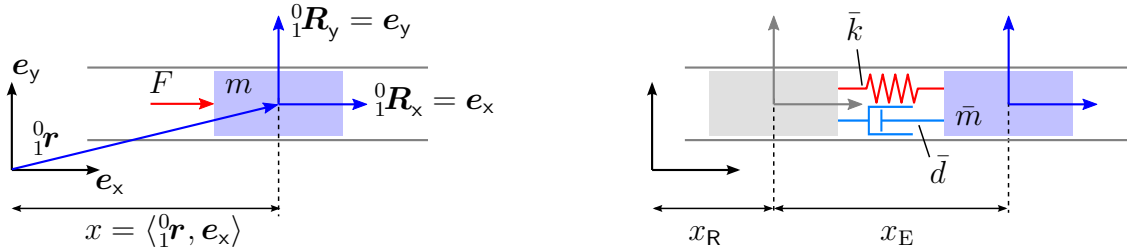


Figure 4.2: Model of a prismatic joint (left) and the closed loop (right)

## 4.7 Examples of fully actuated systems

### 4.7.1 Prismatic joint

**Model.** Probably the simplest example of a rigid body system is a single body moving in a prismatic joint, i.e. can only translate on one axis as illustrated on the left of Figure 4.2. The corresponding rigid body transformation is simply

$${}^0_1\mathbf{G} = \begin{bmatrix} 1 & 0 & 0 & x \\ 0 & 1 & 0 & 0 \\ 0 & 0 & 1 & 0 \\ 0 & 0 & 0 & 1 \end{bmatrix}. \quad (4.87)$$

With the trivial choice of the velocity coordinate  $\xi = \dot{x}$ , i.e.  $\mathbf{A} = 1$ , the equation of motion is

$$m\ddot{x} = F. \quad (4.88)$$

**Closed loop.** Due to the geometry of the model, only the controlled total mass  ${}^0_1m$  within the controlled body inertia matrix  ${}^0_1\mathbf{M}$  contributes to the controlled kinetics and analog for the dissipation and stiffness. For the sake of readability we drop the body indices for the following examples of single bodies. So the only parameters contributing to the controlled kinetics are  $\bar{m}, \bar{d}, \bar{k} \in \mathbb{R} > 0$ .

For this example all three proposed control approaches are identical. With the displacement error  $x_E = x - x_R$  the resulting energies are

$$\bar{\mathcal{V}} = \frac{1}{2}\bar{k}x_E^2, \quad \bar{\mathcal{R}} = \frac{1}{2}\bar{d}\dot{x}_E^2, \quad \bar{\mathcal{T}} = \frac{1}{2}\bar{m}\ddot{x}_E^2, \quad \bar{\mathcal{S}} = \frac{1}{2}\bar{m}\ddot{x}_E^2. \quad (4.89)$$

The potential has the obvious transport map  $\mathbf{Q} = 1$  and the resulting closed loop kinetics are

$$\bar{m}\ddot{x}_E + \bar{d}\dot{x}_E + \bar{k}x_E = 0. \quad (4.90)$$

The corresponding explicit control law is

$$F = m\ddot{x}_R - \frac{m\bar{d}}{\bar{m}}\dot{x}_E - \frac{m\bar{k}}{\bar{m}}x_E. \quad (4.91)$$

An interpretation of the closed loop is given on the right side of Figure 4.2: The controlled body can be thought as being connected by a spring (stiffness  $\bar{k}$ ) and a damper (viscosity  $\bar{d}$ ) to its reference position  $x_R$ . The inertial force  $\bar{m}\ddot{x}_E$  reacts to the error acceleration, i.e. to the acceleration of the body relative to its reference acceleration  $\ddot{x}_R$ . One could say the body has an inertia w.r.t. its reference.

### 4.7.2 Revolute joint

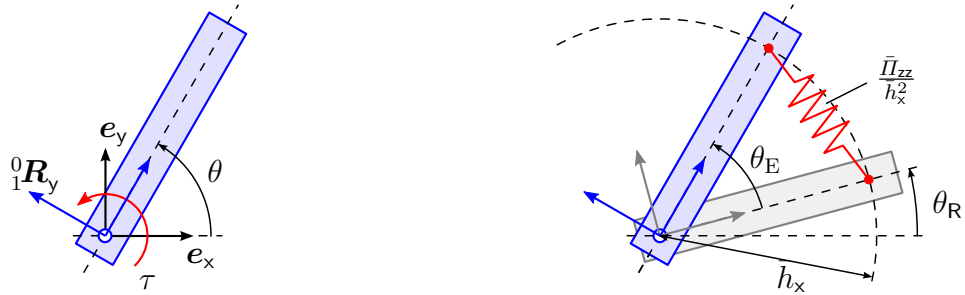


Figure 4.3: Revolute joint: rigid body constrained to rotate about an axis

**Model.** Another elemental case is the revolute joint, i.e. a rigid body constrained to rotate about an axis as illustrated on the left side of Figure 4.3. With the joint angle  $\theta$  the rigid body configuration may be written as

$${}^0\mathbf{G} = \begin{bmatrix} \cos \theta & -\sin \theta & 0 & 0 \\ \sin \theta & \cos \theta & 0 & 0 \\ 0 & 0 & 1 & 0 \\ 0 & 0 & 0 & 1 \end{bmatrix}. \quad (4.92)$$

With the velocity coordinate  $\xi = \dot{\theta}$  the equation of motion is

$$\bar{\Theta}_{zz}\ddot{\theta} = \tau. \quad (4.93)$$

**Potential energy.** Due to the geometry of the model, only the control parameters  $\bar{\Theta}_{zz}, \bar{\Upsilon}_{zz}, \bar{\Pi}_{zz} \in \mathbb{R} > 0$  contribute to the closed loop kinetics. With the angle error  $\theta_E = \theta - \theta_R$  the potential may be written as

$$\bar{\mathcal{V}} = \bar{\Pi}_{zz}(1 - \cos \theta_E). \quad (4.94)$$

It has the obvious transport map  $\mathbf{Q} = 1$ . The potential could be realized by attaching a single linear spring with stiffness  $\bar{\Pi}_{zz}/\bar{h}_z^2$  between desired configuration and actual configuration at a distance  $\bar{h}_z$  as illustrated on the right side of Figure 4.3. This also gives a vivid interpretation of the maximum on the potential at  $\theta_E = \pm\pi$ .

**Approach 1.** The particle based approach leads to the following closed loop kinetics

$$\bar{\Theta}_{zz}(\ddot{\theta} - \ddot{\theta}_R \cos \theta_E - \dot{\theta}_R^2 \sin \theta_E) + \bar{\Upsilon}_{zz}(\dot{\theta} - \dot{\theta}_R \cos \theta_E) + \bar{\Pi}_{zz} \sin \theta_E = 0. \quad (4.95)$$

The total energy  $\bar{\mathcal{W}}$  and its time derivative are

$$\bar{\mathcal{W}} = \frac{1}{2}\bar{\Theta}_z(\dot{\theta}^2 - 2\dot{\theta}\dot{\theta}_R \cos \theta_E + \dot{\theta}_R^2) + \bar{\Pi}_z(1 - \cos \theta_E), \quad (4.96a)$$

$$\begin{aligned} \frac{d}{dt}\bar{\mathcal{W}} = & -\bar{\Upsilon}_z(\dot{\theta} - \dot{\theta}_R \cos \theta_E)^2 + \bar{\Pi}_z \dot{\theta}_R \sin \theta_E (\cos \theta_E - 1) \\ & + \bar{\Theta}_z \dot{\theta}_R (\ddot{\theta}_R(1 - \cos^2 \theta_E) + (\dot{\theta}^2 - \dot{\theta}_R^2 \cos \theta_E) \sin \theta_E) \end{aligned} \quad (4.96b)$$

Without further assumptions on the reference trajectory  $t \mapsto \theta_R(t)$  the total energy is *not* a Lyapunov function for the closed loop. The linear approximation  $\theta \approx \theta_R$  of (4.95) has the characteristic polynomial

$$\lambda^2 + \frac{\bar{Y}_z}{\bar{\Theta}_z} \lambda + \left( \frac{\bar{\Pi}_z}{\bar{\Theta}_z} - \dot{\theta}_R^2 \right). \quad (4.97)$$

So even for the special case of constant reference velocity  $\ddot{\theta}_R(t) = 0$ , we need  $\frac{\bar{\Pi}_z}{\bar{\Theta}_z} > \dot{\theta}_R^2$  to ensure local stability.

**Approach 2 & 3.** For this example the body-based and energy-based approaches lead to identical energies and closed loop kinetics:

$$\bar{\mathcal{R}} = \frac{1}{2} \bar{Y}_{zz} \dot{\theta}_E^2, \quad \bar{\mathcal{T}} = \frac{1}{2} \bar{\Theta}_{zz} \dot{\theta}_E^2, \quad \bar{\Theta}_{zz} \ddot{\theta}_E + \bar{Y}_{zz} \dot{\theta}_E + \bar{\Pi}_{zz} \sin \theta_E = 0. \quad (4.98)$$

The total energy  $\bar{\mathcal{W}} = \bar{\mathcal{T}} + \bar{\mathcal{V}}$ ,  $\dot{\bar{\mathcal{W}}} = -2\bar{\mathcal{R}}$  can be used to conclude that the system converges for *almost* all initial conditions  $(\theta_E(0), \dot{\theta}_E(0))$ . The remaining initial condition  $\dot{\theta}_E(0) = \pm\pi$  and  $\dot{\theta}_E(0) = 0$  is unstable, see Figure 4.4. As a physical interpretation: the controlled dynamics coincide with the dynamics of a damped physical pendulum.

**Linear control.** Since the model (4.93) is a linear differential equation, the following linear closed loop equation might also be reasonable

$$\bar{\Theta}_{zz} \ddot{\theta}_E + \bar{Y}_{zz} \dot{\theta}_E + \bar{\Pi}_{zz} \theta_E = 0. \quad (4.99)$$

The difference between the closed loop (4.98) and (4.99) may be visualized by the corresponding phase plots, see Figure 4.4: The linear control law leads to non-smooth phase curves at  $\theta = \pm\pi$ , which is the consequence of the linear design for a system whose configuration space is actually  $S^1 \not\cong \mathbb{R}$ . See [Konz and Rudolph, 2016, sec. 1.2] for a deeper discussion.

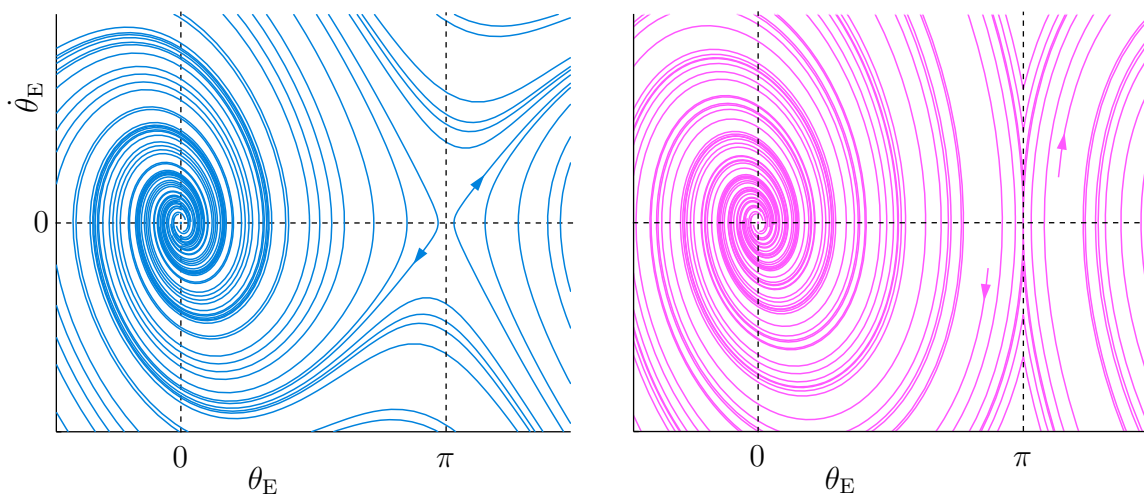


Figure 4.4: Phase plot for (4.98), left, and for (4.99), right

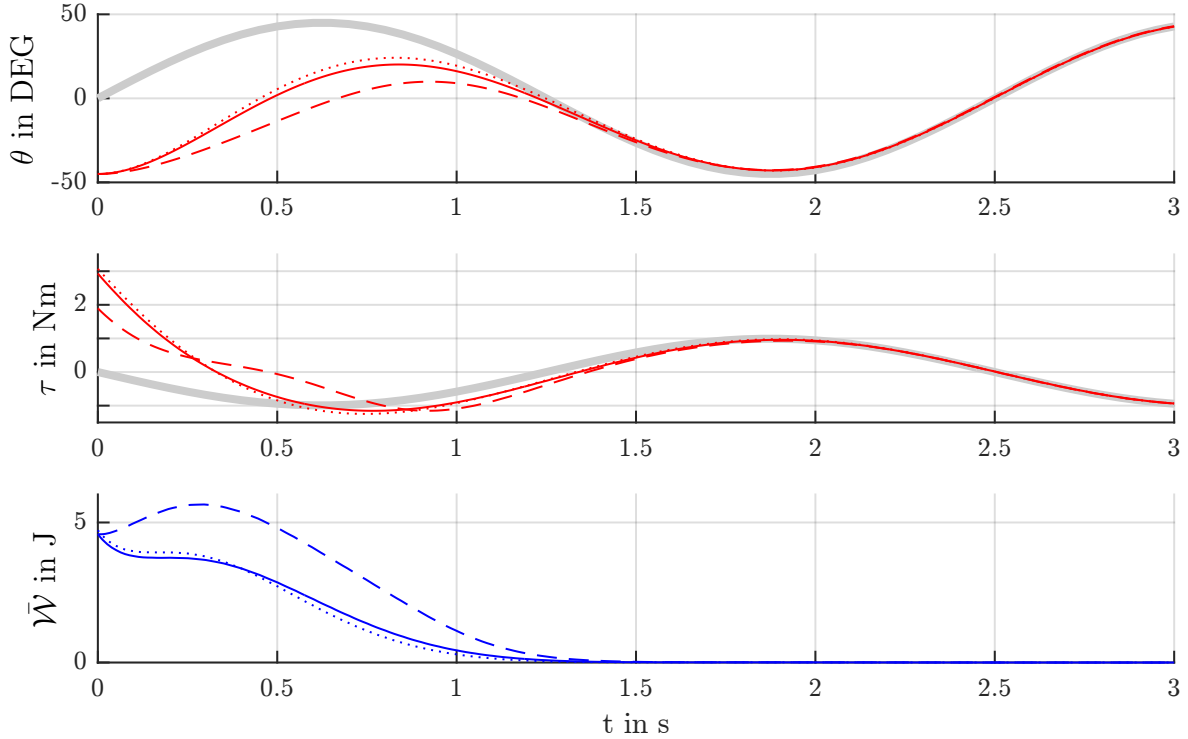


Figure 4.5: Simulation result for the revolute joint: gray line: reference, dashed line: particle-based approach, solid line: energy-based approach, dotted line: linear approach

**Simulation results.** Figure 4.5 shows simulation results comparing the three different approaches (4.95), (4.98) and (4.99) tracking a reference  $\theta_R(t) = \frac{\pi}{2} \sin(\frac{2\pi}{2.5}t)$ . Evidently, all approaches fulfill the control objective, i.e. the joint angle  $\theta$  converges to its reference  $\theta_R$ .

### 4.7.3 Rigid body orientation

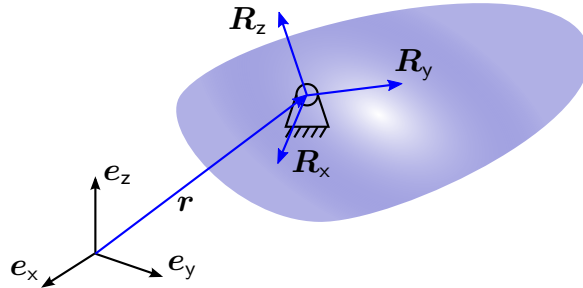


Figure 4.6: rigid body fixed at one point

**Model.** Consider a rigid body fixed at one point  $\mathbf{r} = \text{const.}$  as illustrated in Figure 4.6. Its orientation may be parameterized by the coefficients of the rotation matrix  $\mathbf{R} = [\mathbf{R}_x, \mathbf{R}_y, \mathbf{R}_z] \in \mathbb{SO}(3)$ . With the angular velocity  $\boldsymbol{\omega} = \text{Vee}(\mathbf{R}^\top \dot{\mathbf{R}})$  as velocity coordinates,

the inertia matrix  $\Theta$  and the control torques  $\tau$  about the body fixed axes, the equations of motion may be written as

$$\dot{\mathbf{R}} = \mathbf{R} \text{wed}(\boldsymbol{\omega}) \quad \Theta \dot{\boldsymbol{\omega}} + \text{wed}(\boldsymbol{\omega}) \Theta \boldsymbol{\omega} = \boldsymbol{\tau}. \quad (4.100)$$

**Potential energy.** Only the parameters  $\bar{\Theta}$ ,  $\bar{\Upsilon}$  and  $\bar{\Pi}$  contribute to the closed loop kinetics. Using the attitude error  $\mathbf{R}_E = \mathbf{R}_R^\top \mathbf{R}$  the error potential, its differential and Hessian are

$$\bar{\mathcal{V}} = \text{tr} (\text{Wed}(\bar{\Pi})(\mathbf{I}_3 - \mathbf{R}_E)), \quad (4.101a)$$

$$\bar{\mathbf{f}}^K = \nabla \bar{\mathcal{V}} = \text{vee2}(\text{Wed}(\bar{\Pi}) \mathbf{R}_E), \quad (4.101b)$$

$$(\nabla^2 \bar{\mathcal{V}})|_{\mathbf{R}=\mathbf{R}_R} = \bar{\Pi}. \quad (4.101c)$$

The potential has the transport map  $\mathbf{Q} = \mathbf{R}_E^\top$ , so the velocity error for the energy based approach is  $\boldsymbol{\omega}_E = \boldsymbol{\omega} - \mathbf{R}_E^\top \boldsymbol{\omega}_R$  which coincides with the body velocity error.

**Particle-based approach.** The particle-based approach (4.18) leads to

$$\begin{aligned} \bar{\mathbf{f}}^M &= \bar{\Theta} \dot{\boldsymbol{\omega}} - \text{Vee}(\mathbf{R}_E^\top \text{Wed}(\bar{\Theta})) \mathbf{R}_E^\top \dot{\boldsymbol{\omega}}_R \\ &\quad + \text{wed}(\boldsymbol{\omega}) \bar{\Theta} \boldsymbol{\omega} + \text{vee2}(\text{Wed}(\bar{\Theta}) \text{wed}(\boldsymbol{\omega}_R)^2 \mathbf{R}_E) \end{aligned} \quad (4.102a)$$

$$\bar{\mathbf{f}}^D = \bar{\Upsilon} \boldsymbol{\omega} - \text{Vee}(\mathbf{R}_E^\top \text{Wed}(\bar{\Upsilon})) \mathbf{R}_E^\top \boldsymbol{\omega}_R \quad (4.102b)$$

**Body-based approach.** The body-based approach (4.26) leads to

$$\bar{\mathbf{f}}^M = \bar{\Theta} \dot{\boldsymbol{\omega}}_E + \text{wed}(\boldsymbol{\omega}_E) \bar{\Theta} \boldsymbol{\omega}_E \quad (4.103a)$$

$$\bar{\mathbf{f}}^D = \bar{\Upsilon} \boldsymbol{\omega}_E. \quad (4.103b)$$

The corresponding control law coincides with the one proposed in [Koditschek, 1989]. The total energy  $\bar{\mathcal{W}} = \frac{1}{2} \boldsymbol{\omega}_E^\top \bar{\Theta} \boldsymbol{\omega}_E + \bar{\mathcal{V}}$  with  $\dot{\mathcal{W}} = -\boldsymbol{\omega}_E^\top \bar{\Upsilon} \boldsymbol{\omega}_E$  serves as a Lyapunov function for the closed loop.

**Energy-based approach.** For the energy-based approach (4.56) leads to

$$\bar{\mathbf{f}}^M = \bar{\Theta} \dot{\boldsymbol{\omega}}_E + \text{wed}(\text{Wed}(\bar{\Theta}) \boldsymbol{\omega}) \boldsymbol{\omega}_E \quad (4.104a)$$

$$\bar{\mathbf{f}}^D = \bar{\Upsilon} \boldsymbol{\omega}_E. \quad (4.104b)$$

The corresponding control law coincides with one proposed in [Bullo and Murray, 1999]. The total energy is the same as the one for the body based approach. The two approaches only differ in the gyroscopic terms.

**Linearization.** For a small error to the reference we have

$$\mathbf{R} = \mathbf{R}_R + \mathbf{R}_R \text{wed}(\boldsymbol{\varepsilon}), \quad \boldsymbol{\omega} = \boldsymbol{\omega}_R + \dot{\boldsymbol{\varepsilon}}, \quad \bar{\Theta} \ddot{\boldsymbol{\varepsilon}} + \bar{\Upsilon} \dot{\boldsymbol{\varepsilon}} + \bar{\Pi} \boldsymbol{\varepsilon} = 0. \quad (4.105)$$

#### 4.7.4 Planar rigid body

A planar rigid body is a free rigid body in two dimensional space, i.e. it can translate in two dimensions and rotate about an perpendicular axis as illustrated in Figure 4.7. The model equations as well as the closed loop equations could be directly derived from the three dimensional rigid body by setting e.g.  $v_z = 0$ ,  $\omega_x = \omega_y = 0$  and removing the trivial equations. However it might be still instructive to display the resulting equations.

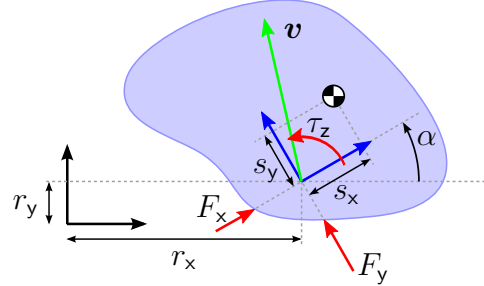


Figure 4.7: model of the planar rigid body

**Coordinates and kinematics.** As configuration coordinates  $\boldsymbol{x}$  we use the position  $r_x, r_y$  and the sine  $s_\alpha$  and cosine  $c_\alpha$  of the angle  $\alpha$ . Consequently we have to impose the constraint  $c_\alpha^2 + s_\alpha^2 - 1 = 0$  on the configuration coordinates. As velocity coordinates  $\boldsymbol{\xi}$  we use the components  $v_x, v_y$  of the translational velocity w.r.t. the body fixed frame as illustrated in Figure 4.7 and the angular velocity  $\omega_z = \dot{\alpha}$ . This kinematic relation is

$$\frac{d}{dt} \underbrace{\begin{bmatrix} r_x \\ r_y \\ s_\alpha \\ c_\alpha \end{bmatrix}}_{\boldsymbol{x}} = \underbrace{\begin{bmatrix} c_\alpha & -s_\alpha & 0 \\ s_\alpha & c_\alpha & 0 \\ 0 & 0 & c_\alpha \\ 0 & 0 & -s_\alpha \end{bmatrix}}_{\boldsymbol{A}} \underbrace{\begin{bmatrix} v_x \\ v_y \\ \omega_z \end{bmatrix}}_{\boldsymbol{\xi}} \quad (4.106)$$

The rigid body configuration  ${}^0_1\mathbf{G}$  and the resulting body Jacobian  ${}^0_1\mathbf{J}$  w.r.t. the chosen velocity coordinates are

$${}^0_1\mathbf{G} = \begin{bmatrix} c_\alpha & -s_\alpha & 0 & r_x \\ s_\alpha & c_\alpha & 0 & r_y \\ 0 & 0 & 1 & 0 \\ 0 & 0 & 0 & 1 \end{bmatrix}, \quad {}^0_1\mathbf{J} = \begin{bmatrix} 1 & 0 & 0 \\ 0 & 1 & 0 \\ 0 & 0 & 0 \\ 0 & 0 & 0 \\ 0 & 0 & 0 \\ 0 & 0 & 1 \end{bmatrix} \quad (4.107)$$

**Kinetic equation.** Let the rigid body have the total mass  $m$ , the moment of inertia  $\Theta_z$  and the coordinates  $s_x, s_y$  of the center of mass w.r.t. the body fixed frame. As control input consider the forces  $F_x, F_y$  and the torque  $\tau_z$  as displayed in Figure 4.7. The resulting

kinetic equation is

$$\underbrace{\begin{bmatrix} m & 0 & -ms_y \\ 0 & m & ms_x \\ -ms_y & ms_x & \Theta_z \end{bmatrix}}_M \underbrace{\begin{bmatrix} \dot{v}_x \\ \dot{v}_y \\ \dot{\omega}_z \end{bmatrix}}_{\dot{\xi}} + \begin{bmatrix} -m(v_y + s_x \omega_z) \omega_z \\ m(v_x - s_y \omega_z) \omega_z \\ m(s_x v_x + s_y v_y) \omega_z \end{bmatrix} = \underbrace{\begin{bmatrix} F_x \\ F_y \\ \tau_z \end{bmatrix}}_u. \quad (4.108)$$

**Control parameters.** For the controlled kinetics we chose the following non-zero parameters

$${}_1^0\bar{m}, {}_1^0d, {}_1^0k \in \mathbb{R}^+, \quad {}_1^0\bar{s}_x, {}_1^0\bar{s}_y, {}_1^0\bar{l}_x, {}_1^0\bar{l}_y, {}_1^0\bar{h}_x, {}_1^0\bar{h}_y \in \mathbb{R}, \quad {}_1^0\bar{\Theta}_z, {}_1^0\bar{\Upsilon}_z, {}_1^0\bar{\Pi}_z \in \mathbb{R}^+. \quad (4.109)$$

Since all parameters are associated with the configuration  ${}_1^0\mathbf{G}$ , we drop the indices in the following, i.e.  $\bar{m} = {}_1^0\bar{m}$ .

**Potential.** The potential, resulting from the chosen parameters (4.109), and its derivatives are

$$\begin{aligned} \bar{\mathcal{V}} = & \frac{1}{2}\bar{k}(r_x - r_{xR})^2 + \frac{1}{2}\bar{k}(r_y - r_{yR})^2 + \bar{\Pi}_z(1 - c_{\alpha_E}) \\ & + \bar{k}\bar{h}_x(c_\alpha - c_{\alpha_R})(r_x - r_{xR}) - \bar{k}\bar{h}_y(s_\alpha - s_{\alpha_R})(r_x - r_{xR}) \\ & + \bar{k}\bar{h}_y(c_\alpha - c_{\alpha_R})(r_y - r_{yR}) - \bar{k}\bar{h}_x(s_\alpha - s_{\alpha_R})(r_y - r_{yR}) \end{aligned} \quad (4.110a)$$

$$\nabla \bar{\mathcal{V}} = \begin{bmatrix} \bar{k}(c_\alpha(r_x - r_{xR}) + s_\alpha(r_y - r_{yR}) + \bar{h}_x(1 - c_{\alpha_E}) - \bar{h}_y s_{\alpha_E}) \\ \bar{k}(-s_\alpha(r_x - r_{xR}) + c_\alpha(r_y - r_{yR}) + \bar{h}_x s_{\alpha_E} + \bar{h}_y(1 - c_{\alpha_E})) \\ \bar{k}((\bar{h}_x c_\alpha + \bar{h}_y s_\alpha)(r_y - r_{yR}) - (\bar{h}_y c_\alpha + \bar{h}_x s_\alpha)(r_x - r_{xR})) + \bar{\Pi}_z s_{\alpha_E} \end{bmatrix} \quad (4.110b)$$

$$\nabla^2 \bar{\mathcal{V}}|_R = \begin{bmatrix} \bar{k} & 0 & -\bar{k}\bar{h}_y \\ 0 & \bar{k} & \bar{k}\bar{h}_x \\ -\bar{k}\bar{h}_y & \bar{k}\bar{h}_x & \bar{\Pi}_z \end{bmatrix} \quad (4.110c)$$

The sine and cosine of the angle error  $\alpha - \alpha_R$  are introduced just for readability

$$c_{\alpha_E} = c_\alpha c_{\alpha_R} + s_\alpha s_{\alpha_R} = \cos(\alpha - \alpha_R), \quad s_{\alpha_E} = s_\alpha c_{\alpha_R} - c_\alpha s_{\alpha_R} = \sin(\alpha - \alpha_R). \quad (4.111)$$

From the Hessian  $\nabla^2 \bar{\mathcal{V}}|_R$  at the critical point  $\mathbf{x} = \mathbf{x}_R$  one can see that (local) positive definiteness requires  $\bar{\Pi}_z > \bar{k}(\bar{h}_x^2 + \bar{h}_y^2)$ . We will encounter the analog requirement for the controlled moment of inertia  $\bar{\Theta}_z$  and damping  $\bar{\Upsilon}_z$ .

A transport map for (4.110a) is given by<sup>2</sup>

$$\underbrace{\begin{bmatrix} v_{xE} \\ v_{yE} \\ \omega_{zE} \end{bmatrix}}_{\xi_E} = \underbrace{\begin{bmatrix} v_x \\ v_y \\ \omega_z \end{bmatrix}}_{\xi} - \underbrace{\begin{bmatrix} c_{\alpha_E} & s_{\alpha_E} & s_\alpha(r_x - r_{xR}) - c_\alpha(r_y - r_{yR}) \\ -s_{\alpha_E} & c_{\alpha_E} & c_\alpha(r_x - r_{xR}) + s_\alpha(r_y - r_{yR}) \\ 0 & 0 & 1 \end{bmatrix}}_Q \underbrace{\begin{bmatrix} v_{xR} \\ v_{yR} \\ \omega_{zR} \end{bmatrix}}_{\xi_R}. \quad (4.112)$$

<sup>2</sup>An alternative transport map corresponding to (4.67) is

$$Q = \begin{bmatrix} c_{\alpha_E} & s_{\alpha_E} & \bar{h}_x s_{\alpha_E} - \bar{h}_y(c_{\alpha_E} - 1) \\ -s_{\alpha_E} & c_{\alpha_E} & \bar{h}_x(c_{\alpha_E} - 1) + \bar{h}_y s_{\alpha_E} \\ 0 & 0 & 1 \end{bmatrix}. \quad (4.113)$$

**Particle-based approach.** The damping and inertia force using the particle based approach are:

$$\bar{\mathbf{f}}^D = \underbrace{\begin{bmatrix} \bar{d} & 0 & -\bar{d}\bar{l}_y \\ 0 & \bar{d} & \bar{d}\bar{l}_x \\ -\bar{d}\bar{l}_y & \bar{d}\bar{l}_x & \bar{\Upsilon}_z \end{bmatrix}}_D \underbrace{\begin{bmatrix} v_x \\ v_y \\ \omega_z \end{bmatrix}}_{\xi} - \underbrace{\begin{bmatrix} \bar{d}c_{\alpha_E} & \bar{d}s_{\alpha_E} & \bar{d}(\bar{l}_x s_{\alpha_E} - \bar{l}_y c_{\alpha_E}) \\ -\bar{d}s_{\alpha_E} & \bar{d}c_{\alpha_E} & \bar{d}(\bar{l}_x c_{\alpha_E} + \bar{l}_y s_{\alpha_E}) \\ -\bar{d}(\bar{l}_x s_{\alpha_E} + \bar{l}_y c_{\alpha_E}) & \bar{d}(\bar{l}_x c_{\alpha_E} - \bar{l}_y s_{\alpha_E}) & \bar{\Upsilon}_z c_{\alpha_E} \end{bmatrix}}_{\dot{\xi}_R} \underbrace{\begin{bmatrix} v_{xR} \\ v_{yR} \\ \omega_{zR} \end{bmatrix}}_{\dot{\xi}_R}, \quad (4.114a)$$

$$\bar{\mathbf{f}}^M = \underbrace{\begin{bmatrix} \bar{m} & 0 & -\bar{m}\bar{s}_y \\ 0 & \bar{m} & \bar{m}\bar{s}_x \\ -\bar{m}\bar{s}_y & \bar{m}\bar{s}_x & \bar{\Upsilon}_z \end{bmatrix}}_D \underbrace{\begin{bmatrix} \dot{v}_x \\ \dot{v}_y \\ \dot{\omega}_z \end{bmatrix}}_{\dot{\xi}} + \underbrace{\begin{bmatrix} -\bar{m}(v_y + \bar{s}_x \omega_z) \omega_z \\ \bar{m}(v_x - \bar{s}_y \omega_z) \omega_z \\ \bar{m}(\bar{s}_x v_x + \bar{s}_y v_y) \omega_z \end{bmatrix}}_{\dot{\xi}} - \underbrace{\begin{bmatrix} \bar{m}c_{\alpha_E} & \bar{m}s_{\alpha_E} & \bar{m}(\bar{s}_x s_{\alpha_E} - \bar{s}_y c_{\alpha_E}) \\ -\bar{m}s_{\alpha_E} & \bar{m}c_{\alpha_E} & \bar{m}(\bar{s}_x c_{\alpha_E} + \bar{s}_y s_{\alpha_E}) \\ -\bar{m}(\bar{s}_x s_{\alpha_E} + \bar{s}_y c_{\alpha_E}) & \bar{m}(\bar{s}_x c_{\alpha_E} - \bar{s}_y s_{\alpha_E}) & \bar{\Upsilon}_z c_{\alpha_E} \end{bmatrix}}_{\dot{\xi}_R} \underbrace{\begin{bmatrix} \dot{v}_{xR} \\ \dot{v}_{yR} \\ \dot{\omega}_{zR} \end{bmatrix}}_{\dot{\xi}_R} - \underbrace{\begin{bmatrix} -\bar{m}((v_y + \bar{s}_x \omega_z) c_{\alpha_E} - (v_{xR} - \bar{s}_y \omega_{zR}) s_{\alpha_E}) \omega_{zR} \\ \bar{m}((v_{yR} + \bar{s}_x \omega_{zR}) s_{\alpha_E} + (v_{xR} - \bar{s}_y \omega_{zR}) c_{\alpha_E}) \omega_{zR} \\ \bar{m}((\bar{s}_x v_{xR} + \bar{s}_y v_{yR}) c_{\alpha_E} - (\bar{s}_y v_{xR} - \bar{s}_x v_{yR}) s_{\alpha_E}) \omega_{zR} + \bar{\Theta}_z s_{\alpha_E} \omega_{zR}^2 \end{bmatrix}}_{\dot{\xi}}. \quad (4.114b)$$

The corresponding total energy as defined in (4.5), is not a Lyapunov function for the closed loop.

**Body-based approach.** The damping and inertia force using the body-based approach are:

$$\bar{\mathbf{f}}^D = \underbrace{\begin{bmatrix} \bar{d} & 0 & -\bar{d}\bar{l}_y \\ 0 & \bar{d} & \bar{d}\bar{l}_x \\ -\bar{d}\bar{l}_y & \bar{d}\bar{l}_x & \bar{\Upsilon}_z \end{bmatrix}}_D \underbrace{\begin{bmatrix} v_{xE} \\ v_{yE} \\ \omega_{zE} \end{bmatrix}}_{\xi_E} \quad (4.115a)$$

$$\bar{\mathbf{f}}^M = \underbrace{\begin{bmatrix} \bar{m} & 0 & -\bar{m}\bar{s}_y \\ 0 & \bar{m} & \bar{m}\bar{s}_x \\ -\bar{m}\bar{s}_y & \bar{m}\bar{s}_x & \bar{\Theta}_z \end{bmatrix}}_M \underbrace{\begin{bmatrix} \dot{v}_{xE} \\ \dot{v}_{yE} \\ \dot{\omega}_{zE} \end{bmatrix}}_{\dot{\xi}_E} + \underbrace{\begin{bmatrix} 0 & -\bar{m}\omega_{zE} & -\bar{m}\bar{s}_x \omega_{zE} \\ \bar{m}\omega_{zE} & 0 & -\bar{m}\bar{s}_y \omega_{zE} \\ \bar{m}\bar{s}_x \omega_{zE} & \bar{m}\bar{s}_y \omega_{zE} & 0 \end{bmatrix}}_{\dot{\xi}_E} \underbrace{\begin{bmatrix} v_{xE} \\ v_{yE} \\ \omega_{zE} \end{bmatrix}}_{\dot{\xi}_E} \quad (4.115b)$$

where the velocity error  $\xi_E$  was defined in (4.112). The total energy  $\bar{\mathcal{W}} = \frac{1}{2}\xi_E^\top \mathbf{M} \xi_E + \bar{\mathcal{V}}$  is a Lyapunov function for the closed loop.

**Energy-based approach.** The damping and inertia forces using the energy-based approach are:

$$\bar{\mathbf{f}}^D = \underbrace{\begin{bmatrix} \bar{d} & 0 & -\bar{d}\bar{l}_y \\ 0 & \bar{d} & \bar{d}\bar{l}_x \\ -\bar{d}\bar{l}_y & \bar{d}\bar{l}_x & \bar{\Upsilon}_z \end{bmatrix}}_{\mathbf{D}} \underbrace{\begin{bmatrix} v_{xE} \\ v_{yE} \\ \omega_{zE} \end{bmatrix}}_{\boldsymbol{\xi}_E}, \quad (4.116a)$$

$$\bar{\mathbf{f}}^M = \underbrace{\begin{bmatrix} \bar{m} & 0 & -\bar{m}\bar{s}_y \\ 0 & \bar{m} & \bar{m}\bar{s}_x \\ -\bar{m}\bar{s}_y & \bar{m}\bar{s}_x & \bar{\Theta}_z \end{bmatrix}}_{\mathbf{M}} \underbrace{\begin{bmatrix} \dot{v}_{xE} \\ \dot{v}_{yE} \\ \dot{\omega}_{zE} \end{bmatrix}}_{\dot{\boldsymbol{\xi}}_E} + \underbrace{\begin{bmatrix} 0 & -\bar{m}\omega_z & -\bar{m}\bar{s}_x\omega_z \\ \bar{m}\omega_z & 0 & -\bar{m}\bar{s}_y\omega_z \\ \bar{m}\bar{s}_x\omega_z & \bar{m}\bar{s}_y\omega_z & 0 \end{bmatrix}}_{\bar{\mathbf{M}}} \underbrace{\begin{bmatrix} v_{xE} \\ v_{yE} \\ \omega_{zE} \end{bmatrix}}_{\boldsymbol{\xi}_E}. \quad (4.116b)$$

The total energy  $\bar{\mathcal{W}} = \frac{1}{2}\boldsymbol{\xi}_E^\top \mathbf{M} \boldsymbol{\xi}_E + \bar{\mathcal{V}}$  coincides with the total energy for the body-based approach and is a Lyapunov function for this closed loop as well. Note that the two approaches do differ in the gyroscopic terms, so do lead to different solutions of the closed loop dynamics.

**Simulation result.** In subsection 4.7.5 we will give and discuss a simulation result for the special parameter choice  $\bar{s}_x = \bar{l}_x = \bar{h}_x = 0$  and  $\bar{s}_y = \bar{l}_y = \bar{h}_y = 0$ .

### 4.7.5 Decoupling of translational and rotational motion

The closed loop equations for a (free) three dimensional rigid body were given in subsection 4.1.2, subsection 4.2.1 and subsection 4.3.3. The reduced equations for the planar case were given in subsection 4.7.4. For most applications we like to *decouple* the translational and the rotational motion of the body.

Observing the closed loop equations one can see immediately that the coupling terms vanish if  $\bar{s} = \bar{l} = \bar{h} = 0$ , i.e. the chosen body fixed point  $\mathbf{r}$  coincides with the center of mass, damping and stiffness. Then the rotational dynamics are identical to the closed loop given in subsection 4.7.3 (subsection 4.7.2 for the planar case), so are indeed decoupled/independent from the translational motion.

**Translational dynamics.** For the translational dynamics the situation is more difficult: Introduce  $\mathbf{e} = \mathbf{r} - \mathbf{r}_R$  as the components of the position error w.r.t. the inertial frame and  $\mathbf{r}_E = \mathbf{R}_R^\top(\mathbf{r} - \mathbf{r}_R)$  as the components w.r.t. the reference frame. The translational dynamics for the different approaches and given transport map are equivalent to

$$\text{particle-based:} \quad \bar{m}\ddot{\mathbf{e}} + \bar{d}\dot{\mathbf{e}} + \bar{k}\mathbf{e} = \mathbf{0} \quad (4.117a)$$

$$\text{body-based:} \quad \bar{m}\ddot{\mathbf{r}}_E + \bar{d}\dot{\mathbf{r}}_E + \bar{k}\mathbf{r}_E = \mathbf{0} \quad (4.117b)$$

$$\text{energy-based:} \quad \bar{m}(\ddot{\mathbf{r}}_E + \text{wed}(\boldsymbol{\omega}_R)\dot{\mathbf{r}}_E) + \bar{d}\dot{\mathbf{r}}_E + \bar{k}\mathbf{r}_E = \mathbf{0} \quad (4.117c)$$

**Translational energy.** For the rigid body we can split the total energy  $\bar{\mathcal{W}} = \bar{\mathcal{W}}_r + \bar{\mathcal{W}}_R$  into a part associated with the position  $\bar{\mathcal{W}}_r$  and one associated with the orientation  $\bar{\mathcal{W}}_R$ .

The rotational energies for the corresponding approaches coincide with the ones given in subsection 4.7.3 (subsection 4.7.2 for the planar case). The translational energies and their derivatives are

$$\text{particle-based: } \bar{\mathcal{W}}_r = \frac{1}{2}\bar{k}\|\boldsymbol{e}\|^2 + \frac{1}{2}\bar{m}\|\dot{\boldsymbol{e}}\|^2, \quad \dot{\bar{\mathcal{W}}}_r = -\bar{d}\|\dot{\boldsymbol{e}}\|^2 \quad (4.118a)$$

$$\text{body-based: } \bar{\mathcal{W}}_r = \frac{1}{2}\bar{k}\|\boldsymbol{r}_E\|^2 + \frac{1}{2}\bar{m}\|\dot{\boldsymbol{r}}_E\|^2, \quad \dot{\bar{\mathcal{W}}}_r = -\bar{d}\|\dot{\boldsymbol{r}}_E\|^2 \quad (4.118b)$$

$$\text{energy-based: } \bar{\mathcal{W}}_r = \frac{1}{2}\bar{k}\|\boldsymbol{r}_E\|^2 + \frac{1}{2}\bar{m}\|\dot{\boldsymbol{r}}_E\|^2, \quad \dot{\bar{\mathcal{W}}}_r = -\bar{d}\|\dot{\boldsymbol{r}}_E\|^2 \quad (4.118c)$$

For their comparison note that

$$\|\boldsymbol{e}\| = \|\boldsymbol{r}_E\|, \quad \|\dot{\boldsymbol{e}}\| = \|\dot{\boldsymbol{r}}_E + \text{wed}(\boldsymbol{\omega}_R)\boldsymbol{r}_E\|. \quad (4.119)$$

The crucial observation is that for all approaches the translational dynamics and energy are indeed independent of the actual orientation  $\boldsymbol{R}$  and its velocity  $\boldsymbol{\omega}$ , but for some approaches they depend on their *reference*  $\boldsymbol{R}_R$  and  $\boldsymbol{\omega}_R$ . For a constant reference orientation  $\boldsymbol{R}_R = \text{const.}$  and consequently  $\boldsymbol{\omega}_R = \mathbf{0}$  all four approaches are equivalent. Furthermore it is worth noting that the error dynamics as well as the energies are invariant to the reference trajectory  $t \mapsto \boldsymbol{r}_R(t)$  for the position.

**Simulation.** The difference between these cases will be discussed on simulation results for the simpler, yet as illustrative, example of a planar rigid body: The reference configuration is  $r_{xR}(t) = r_{yR}(t) = 0$  and  $\alpha_R(t) = \pi t$  which yields the constant reference velocity  $\boldsymbol{\xi}_R(t) = [0, 0, \pi]$ . The control parameters are set to  $\bar{m} = 1$ ,  $\bar{d} = 4$ ,  $\bar{k} = 4$  (neglecting the units). The roots of the characteristic polynomial of (4.117c) are  $\lambda \approx \{-0.5 \pm 0.6i, -3.5 \pm 3.7i\}$ , resulting from the control parameters as well as the constant angular velocity  $\omega_{zR} = \pi$ . The characteristic polynomial for the other approaches is independent of the reference trajectory and has a quadruple root at  $\lambda = -2$ .

Figure 4.8 shows the simulation result for the initial conditions  $r_x(0) = 0, r_y(0) = 1, \alpha(0) = 0$  and  $\boldsymbol{\xi}(0) = \mathbf{0}$ . Observing from the inertial frame, top left of Figure 4.8, for approach 2 the body follows a straight line to its reference position, whereas for the other approaches spiral around it. Observing from the reference frame, top right of Figure 4.8, for approach 3 the body follows a direct path, given the initial velocity. The middle graph in Figure 4.8 shows the evolution of the translational energy  $\bar{\mathcal{W}}_r$ . The difference in the initial values results from  $\dot{\boldsymbol{e}}(0) = \mathbf{0}$ , but  $\dot{\boldsymbol{r}}_E(0) \neq \mathbf{0}$ . The bottom graph in Figure 4.8 shows the evolution of the euclidean distance  $\|\boldsymbol{e}\| = \|\boldsymbol{r}_E\|$ . The rate of convergence for approach 2 and 3 are the same as could be expected from having the same characteristic polynomial.

Even though the energy based approach with the transport map from (4.64) might be mathematically the most elegant solution, its simulation result is not intuitive. Which approach is most desirable, depends given application. For indoor robots (like the multicopters discussed in the next chapter) it is probably most desirable if it corrects its position error following a straight line in the inertial frame.

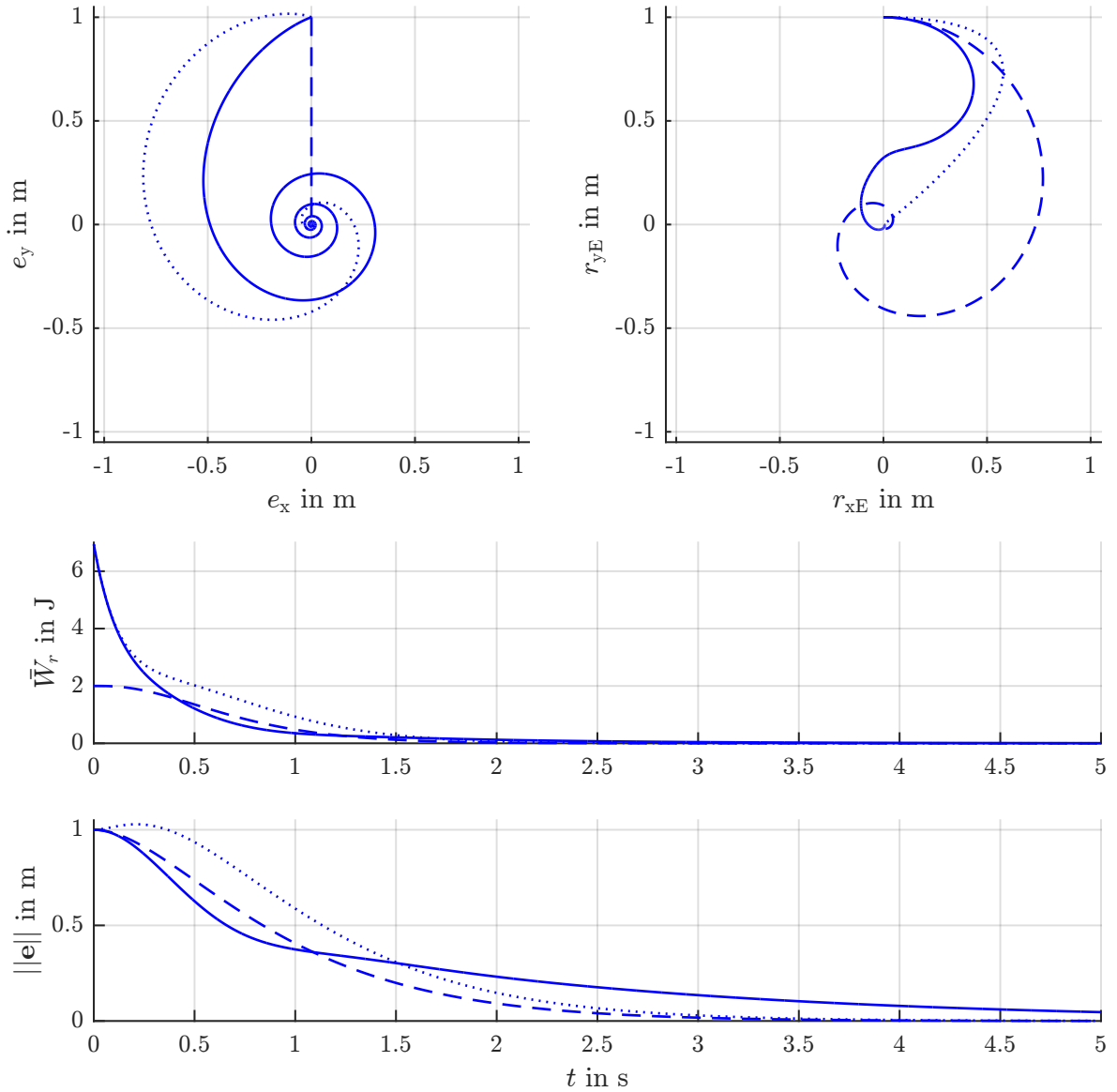


Figure 4.8: Simulation result for the planar rigid body. The solid line: energy-based approach with  $\mathbf{Q} = \text{Ad}_{\mathbf{G}^{-1}\mathbf{G}_R}$ , dashed line: particle-based approach, dotted line: body-based approach.

### 4.7.6 SCARA robot

As a simple example of a multi-body system we consider a SCARA robot as displayed in Figure 4.9. For the sake of demonstration we neglect the vertical axis and the tool orientation. The remaining two axis are sufficient to position a tool (red point in Figure 4.9) in the workspace (green shaded area).

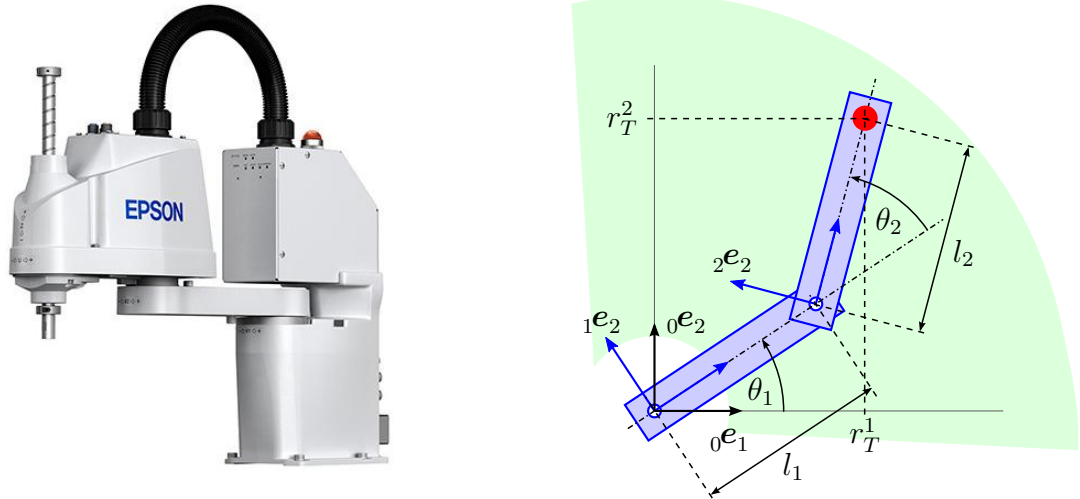


Figure 4.9: A Scara robot and its mechanical model (image [www.epson.com](http://www.epson.com))

**Model.** The model consists of two rigid bodies constraint by two revolute joints. A reasonable choice of coordinates are the relative joint angles  $\boldsymbol{x} = [\theta_1, \theta_2]^\top$  and their derivatives  $\boldsymbol{\xi} = [\dot{\theta}_1, \dot{\theta}_2]^\top$ . The rigid body configurations are

$${}^0\mathbf{G} = \begin{bmatrix} \cos \theta_1 & -\sin \theta_1 & 0 & 0 \\ \sin \theta_1 & \cos \theta_1 & 0 & 0 \\ 0 & 0 & 1 & 0 \\ 0 & 0 & 0 & 1 \end{bmatrix}, \quad {}^0\mathbf{J} = \begin{bmatrix} 0 & 0 \\ 0 & 0 \\ 0 & 0 \\ 0 & 0 \\ 1 & 0 \end{bmatrix} \quad (4.120a)$$

$${}^1\mathbf{G} = \begin{bmatrix} \cos \theta_2 & -\sin \theta_2 & 0 & l_1 \\ \sin \theta_2 & \cos \theta_2 & 0 & 0 \\ 0 & 0 & 1 & 0 \\ 0 & 0 & 0 & 1 \end{bmatrix}, \quad {}^1\mathbf{J} = \begin{bmatrix} 0 & 0 \\ 0 & 0 \\ 0 & 0 \\ 0 & 0 \\ 0 & 1 \end{bmatrix}. \quad (4.120b)$$

Let  ${}_1\Theta_z$  be the moment of inertia of the first body about the first joint and  $l_1$  be the distance between the two joints. The second body has the mass  ${}_2m$ , the center of mass ( ${}_2s_x, {}_2s_y$ ) and the moment of inertia  ${}_2\Theta_z$  about the second joint. The control forces are the joint torques  $\mathbf{u} = [\tau_1, \tau_2]^\top$ . Overall, the equations of motion for the SCARA robot are

$$\begin{bmatrix} {}_1\Theta_z + {}_2\Theta_z + {}_2ml_1^2 + 2a(\theta_2) & {}_2\Theta_z + a(\theta_2) \\ {}_2\Theta_z + a(\theta_2) & {}_2\Theta_z \end{bmatrix} \begin{bmatrix} \ddot{\theta}_1 \\ \ddot{\theta}_2 \end{bmatrix} + \begin{bmatrix} a'(\theta_2)(2\dot{\theta}_1\dot{\theta}_2 + \dot{\theta}_2^2) \\ -a'(\theta_2)\dot{\theta}_1^2 \end{bmatrix} = \begin{bmatrix} \tau_1 \\ \tau_2 \end{bmatrix} \quad (4.121)$$

where

$$a(\theta_2) = {}_2ml_1({}_2s_x \cos \theta_2 - {}_2s_y \sin \theta_2), \quad a'(\theta_2) = -{}_2ml_1({}_2s_x \sin \theta_2 + {}_2s_y \cos \theta_2). \quad (4.122)$$

**Controller parameterization 1.** In the following we will discuss two different controller parameterizations for the SCARA. For the first parameterization the non-zero parameters are

$${}^0\bar{\Pi}_z, {}^0\bar{\Upsilon}_z, {}^0\bar{\Theta}_z, {}^1\bar{\Pi}_z, {}^1\bar{\Upsilon}_z, {}^1\bar{\Theta}_z \in \mathbb{R} > 0. \quad (4.123)$$

These parameters are directly associated with the errors  $\theta_{iE} = \theta_i - \theta_{iR}$ ,  $i = 1, 2$  of the joint angles. The resulting potential is

$$\bar{\mathcal{V}} = {}^0\bar{\Pi}_z(1 - \cos \theta_{1E}) + {}^1\bar{\Pi}_z(1 - \cos \theta_{2E}). \quad (4.124)$$

and obeys the transport map  $\mathbf{Q} = \mathbf{I}_2$ .

The resulting controlled kinetics for the body and energy-based approach are

$${}^{i-1}\bar{\Theta}_z \ddot{\theta}_{iE} + {}^{i-1}\bar{\Upsilon}_z \dot{\theta}_{iE} + {}^{i-1}{}_i\bar{\Pi}_z \sin \theta_{iE} = 0, \quad i = 1, 2. \quad (4.125)$$

The controlled kinetics for the particle based approach yield

$${}^{i-1}\bar{\Theta}_z (\ddot{\theta}_i - \ddot{\theta}_{iR} \cos \theta_{iE} - \dot{\theta}_{iR}^2 \sin \theta_{iE}) + {}^{i-1}\bar{\Upsilon}_z (\dot{\theta}_i - \dot{\theta}_{iR} \cos \theta_{iE}) + {}^{i-1}{}_i\bar{\Pi}_z \sin \theta_{iE} = 0, \quad i = 1, 2. \quad (4.126)$$

With this parameterization the controlled kinetics coincide with two copies of the kinetics of the revolute joint discussed in subsection 4.7.2.

**Controller parameterization 2.** The non-zero parameters for another interesting parameterization of the controller are

$${}^0\bar{k}, {}^0\bar{d}, {}^0\bar{m} \in \mathbb{R} > 0, \quad {}^0\bar{h}_x = {}^0\bar{l}_x = {}^0\bar{s}_x = l_2. \quad (4.127)$$

The resulting potential can be written as

$$\bar{\mathcal{V}}(\mathbf{x}, \mathbf{x}_R) = \frac{1}{2} {}^0\bar{k} \|\mathbf{r}_T(\mathbf{x}) - \mathbf{r}_T(\mathbf{x}_R)\|^2 \quad \mathbf{r}_T(\mathbf{x}) = \begin{bmatrix} l_1 \cos \theta_1 + l_2 \cos(\theta_1 + \theta_2) \\ l_1 \sin \theta_1 + l_2 \sin(\theta_1 + \theta_2) \end{bmatrix}, \quad (4.128)$$

where  $\mathbf{r}_T$  is the position of the tool as illustrated in Figure 4.9. Using the *tool position error*  $\mathbf{e}(\mathbf{x}, \mathbf{x}_R) = \mathbf{r}_T(\mathbf{x}) - \mathbf{r}_T(\mathbf{x}_R)$  as error coordinates, we can apply the rule from (A.35) to compute the transport map as

$$\mathbf{Q}(\mathbf{x}, \mathbf{x}_R) = (\nabla \mathbf{r}_T(\mathbf{x}))^{-1} \nabla \mathbf{r}_T(\mathbf{x}_R). \quad (4.129)$$

The determinant of the differential  $\det \nabla \mathbf{r}_T(\mathbf{x}) = \sin \theta_2$  reflects the well known singularity of the SCARA inverse kinematics, see e.g. [Murray et al., 1994, example 3.6].

The closed loop kinetics for the particle and energy-based approach in terms of the model coordinates  $\boldsymbol{x}$  and the error velocity  $\boldsymbol{\xi}_E = \boldsymbol{\xi} - \mathbf{Q}\boldsymbol{\xi}_R$  are

$$\underbrace{\begin{bmatrix} l_1^2 + 2l_1l_2 \cos \theta_2 + l_2^2 & l_1l_2 \cos \theta_2 + l_2^2 \\ l_1l_2 \cos \theta_2 + l_2^2 & l_2^2 \end{bmatrix}}_{\bar{\mathbf{M}}} \dot{\boldsymbol{\xi}}_E + \underbrace{\begin{bmatrix} -\dot{\theta}_2 & -\dot{\theta}_1 - \dot{\theta}_2 \\ \dot{\theta}_1 & 0 \end{bmatrix}}_{\frac{1}{2}\bar{m}l_1l_2 \sin \theta_2} \boldsymbol{\xi}_E + \underbrace{\begin{bmatrix} l_1^2 + 2l_1l_2 \cos \theta_2 + l_2^2 & l_1l_2 \cos \theta_2 + l_2^2 \\ l_1l_2 \cos \theta_2 + l_2^2 & l_2^2 \end{bmatrix}}_{\bar{\mathbf{D}}} \boldsymbol{\xi}_E + \underbrace{\begin{bmatrix} l_1^2 \sin \theta_{1E} + l_1l_2(\sin(\theta_{1E} - \theta_{2R}) + \sin(\theta_{1E} + \theta_2)) + l_2^2 \sin(\theta_{1E} + \theta_{2E}) \\ l_1l_2(\sin(\theta_{1E} + \theta_2) - \sin(\theta_2)) + l_2^2 \sin(\theta_{1E} + \theta_{2E}) \end{bmatrix}}_{\nabla \bar{\mathcal{V}}} = \mathbf{0}. \quad (4.130a)$$

In terms of the tool position error  $\boldsymbol{e}$  this is equivalent to the much simpler equation

$$\frac{1}{2}\bar{m}\ddot{\boldsymbol{e}} + \frac{1}{2}\bar{d}\dot{\boldsymbol{e}} + \frac{1}{2}\bar{k}\boldsymbol{e} = \mathbf{0}. \quad (4.130b)$$

With the body-based approach we get a similar closed loop that is not displayed or discussed here.

As mentioned above, the transport map  $\mathbf{Q}$  contains terms with  $1/\sin \theta_2$ . Fortunately these terms cancel out in  $\bar{\mathbf{M}}\mathbf{Q}$  and  $\bar{\mathbf{D}}\mathbf{Q}$  in the closed loop equation (4.130a), so this singularity actually does not hurt in practice. This could also be expected since the particle based approach, which does not rely on the transport map, leads to the same closed loop.

A singularity that does hurt, is the inertia matrix with  $\det \bar{\mathbf{M}} = (\frac{1}{2}\bar{m}l_1l_2 \sin \theta_2)^2$ . This means that one can not compute the control law if  $\sin \theta_2 = 0$ . Recalling the mechanical model of the SCARA Figure 4.9, this singularity is evident from a geometric point of view: If  $\sin \theta_2 = 0$  the tool can only move in a tangential direction to the boundary of the workspace but not radial. However, it should be stressed that this singularity is not a consequence of unsuitable configuration coordinates  $\boldsymbol{x} = [\theta_1, \theta_2]^\top$ . It is rather an intrinsic one resulting from forcing dynamics suitable for  $\mathbb{R}^2$  on a system that has the configuration space  $\mathbb{S}^2$ .

**Simulation result.** Figure 4.10 and Figure 4.11 show a simulation results for the SCARA robot with the two proposed parameterizations. The robot starts in a rather random initial configuration. The reference configuration is constant till  $t = 1$  s, then follows a straight line for the tool position till  $t = 4$  s and remains constant thereafter.

For both parameterizations the controlled total energy  $\bar{\mathcal{W}}$  converges. The crucial difference between the two parameterizations is, though the tool position  $\boldsymbol{r}_T$  tracks its reference in both cases, the joint angles  $\theta_1, \theta_2$  do not for the second parameterization. The reason for this is best understood when looking at the controlled potential energy  $\bar{\mathcal{V}}$  illustrated in Figure 4.12: For parameterization 2 the potential has two minima  $\bar{\mathcal{V}} = 0$  for which the tool is at its reference position, but with different joint angles. This holds for any tool position except the ones on the boundary of the workspace where  $\theta_2 = 0$  or  $\theta_2 = \pi$ .

Which of the two parameterizations is “better” probably depends on the practical control task: If the actual joint configuration  $(\theta_1, \theta_2)$  matters then the control parameters

associated with them, i.e.  ${}^0\bar{\Pi}_z, {}^0\bar{\Upsilon}_z, \dots$ , are more suited for the control design. If one is only interested in the tool position  $\mathbf{r}_T$ , then the parameters of the parameterization 2 are useful.

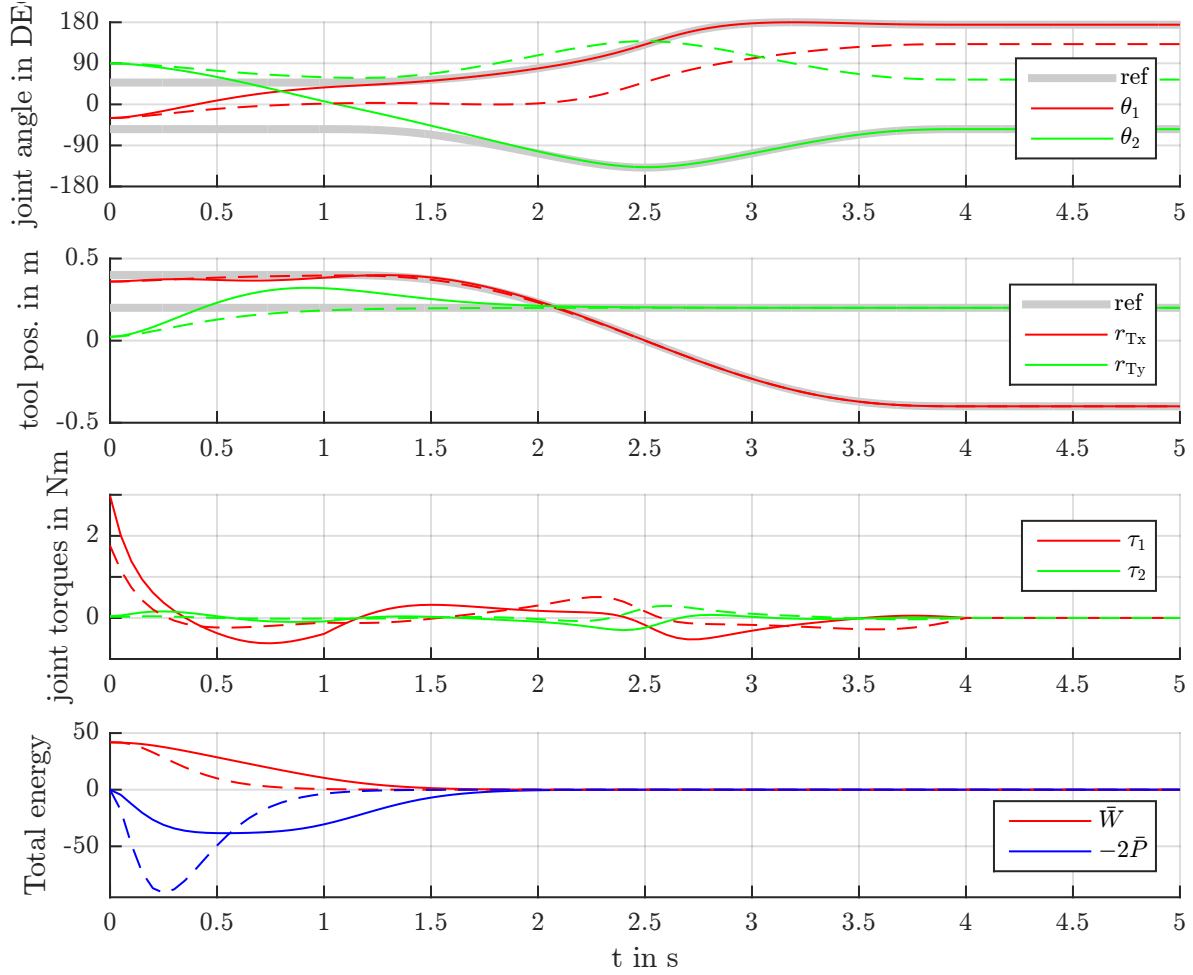


Figure 4.10: Simulation result for the SCARA with parameterization 1 (solid lines) and 2 (dashed lines)

### 4.7.7 Robot arm

As a more complex multibody system we consider a robot arm as illustrated in Figure 4.13. For this example the model equations and the resulting closed loop equations become quite cumbersome and are not displayed explicitly. However this displays some benefits of the proposed control approach: One does not have to look at e.g. the actual system inertia matrix but only at the much less cumbersome body inertia matrices to conclude e.g. stability of the closed loop.

**Model.** A reasonable parameterization of the system are the joint angles  $\mathbf{x} = [\theta_1, \dots, \theta_6]^\top$  as minimal configuration coordinates and trivial kinematics, i.e.  $\xi = \dot{\mathbf{x}}$ . The body con-

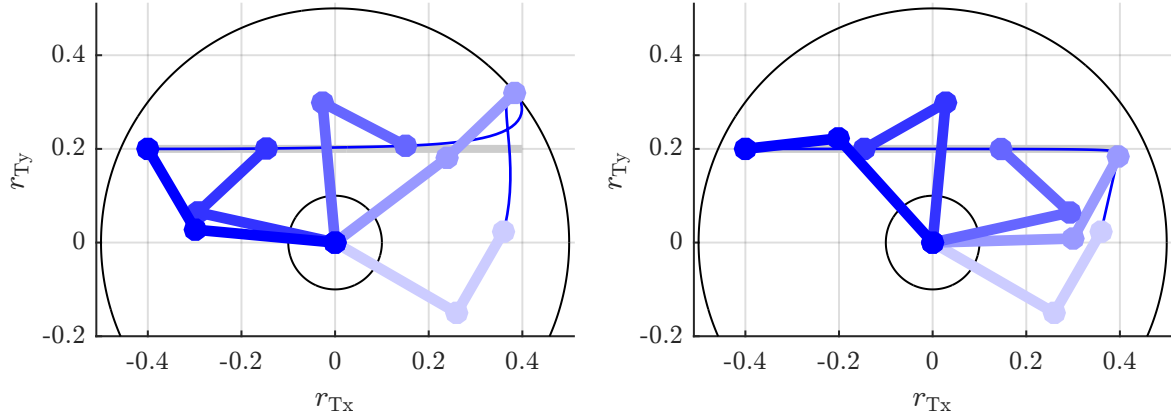


Figure 4.11: Snapshots for the simulation result for the SCARA with parameterization 1 (left) and 2 (right)

figurations can be computed from the following relative transformations

$$\begin{aligned}
 {}^0_1\mathbf{G} &= \begin{bmatrix} \cos \theta_1 & -\sin \theta_1 & 0 & 0 \\ \sin \theta_1 & \cos \theta_1 & 0 & 0 \\ 0 & 0 & 1 & 0 \\ 0 & 0 & 0 & 1 \end{bmatrix}, & {}^1_2\mathbf{G} &= \begin{bmatrix} \cos \theta_2 & 0 & \sin \theta_2 & l_1 \\ 0 & 1 & 0 & 0 \\ -\sin \theta_2 & 0 & \cos \theta_2 & 0 \\ 0 & 0 & 0 & 1 \end{bmatrix}, \\
 {}^2_3\mathbf{G} &= \begin{bmatrix} \cos \theta_3 & 0 & \sin \theta_3 & 0 \\ 0 & 1 & 0 & 0 \\ -\sin \theta_3 & 0 & \cos \theta_3 & l_2 \\ 0 & 0 & 0 & 1 \end{bmatrix}, & {}^3_4\mathbf{G} &= \begin{bmatrix} 1 & 0 & 0 & l_3 \\ 0 & \cos \theta_4 & -\sin \theta_4 & 0 \\ 0 & \sin \theta_4 & \cos \theta_4 & 0 \\ 0 & 0 & 0 & 1 \end{bmatrix}, \\
 {}^4_5\mathbf{G} &= \begin{bmatrix} \cos \theta_5 & 0 & \sin \theta_5 & 0 \\ 0 & 1 & 0 & 0 \\ -\sin \theta_5 & 0 & \cos \theta_5 & 0 \\ 0 & 0 & 0 & 1 \end{bmatrix}, & {}^5_6\mathbf{G} &= \begin{bmatrix} 1 & 0 & 0 & 0 \\ 0 & \cos \theta_6 & -\sin \theta_6 & 0 \\ 0 & \sin \theta_6 & \cos \theta_6 & 0 \\ 0 & 0 & 0 & 1 \end{bmatrix}. \tag{4.131}
 \end{aligned}$$

This together with the body inertia matrices and the gravity coefficients  $\mathbf{a}_G$  and the control forces,  $\mathbf{u} = [\tau_1, \dots, \tau_6]^\top$  determines the equations of motion.

**Controller parameterization 1: Joint space control.** Like above we consider two different sets of controller parameterizations: For the first case, the nonzero control parameters are

$$\begin{aligned}
 {}^0_1\bar{\Pi}_{zz}, {}^1_2\bar{\Pi}_{yy}, {}^2_3\bar{\Pi}_{yy}, {}^3_4\bar{\Pi}_{xx}, {}^4_5\bar{\Pi}_{yy}, {}^5_6\bar{\Pi}_{xx} &\in \mathbb{R} > 0 \\
 {}^0_1\bar{\Upsilon}_{zz}, {}^1_2\bar{\Upsilon}_{yy}, {}^2_3\bar{\Upsilon}_{yy}, {}^3_4\bar{\Upsilon}_{xx}, {}^4_5\bar{\Upsilon}_{yy}, {}^5_6\bar{\Upsilon}_{xx} &\in \mathbb{R} > 0 \\
 {}^0_1\bar{\Theta}_{zz}, {}^1_2\bar{\Theta}_{yy}, {}^2_3\bar{\Theta}_{yy}, {}^3_4\bar{\Theta}_{xx}, {}^4_5\bar{\Theta}_{yy}, {}^5_6\bar{\Theta}_{xx} &\in \mathbb{R} > 0 \tag{4.132}
 \end{aligned}$$

A transport map for the resulting potential energy is  $\mathbf{Q} = \mathbf{I}_6$ . The resulting closed loop kinetics are 6 decoupled equations identical to the ones for the SCARA (4.126) resp. (4.126).

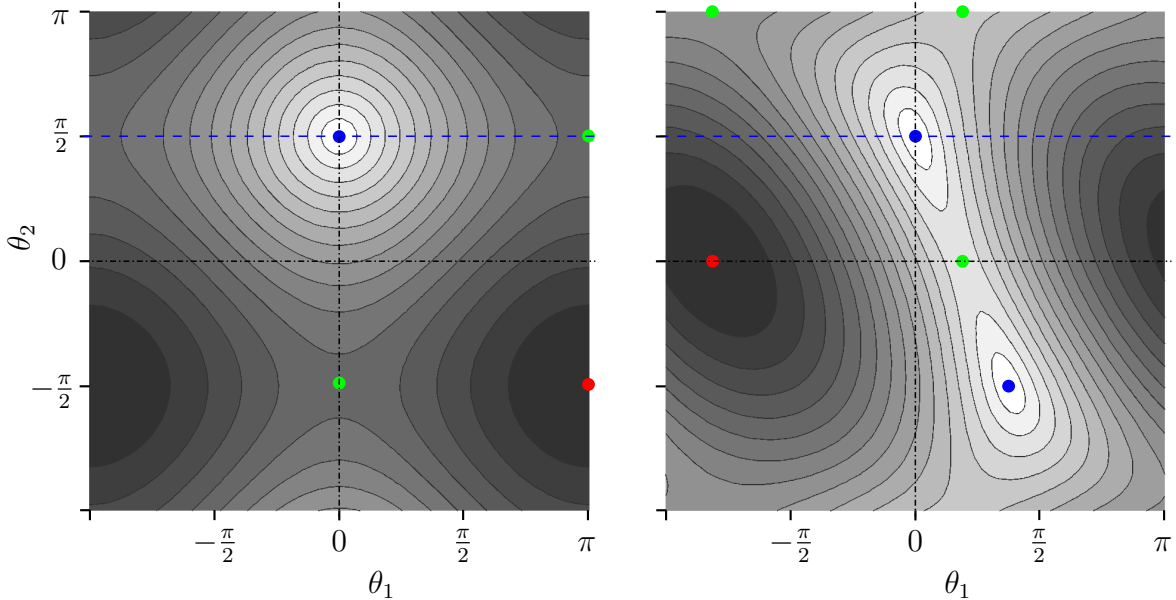


Figure 4.12: The controlled potential energy  $\mathcal{V}$  for parameterization 1 (left) and 2 (right) for  $\theta_{1R} = 0$ ,  $\theta_{2R} = \frac{\pi}{2}$ . Blue dots are minima, red are maxima and green are saddle points.

**Controller parameterization 2: Work space control.** As a second case consider: For many applications the task of the robot arm is to control the position and orientation of a tool mounted at the end of its kinematic chain. This tool might have a particularly meaningful center point (TCP) and principle axis. Let the configuration  ${}^6\mathbf{G} = \text{const.}$  capture these tool specific parameters, for example the tip position and direction of a welding electrode as shown in Figure 4.14.

For this example it could be useful to control the tool as if it is a free rigid body (with its center of mass, damping and stiffness at the TCP) and not care about the particular mechanism that is used to give it this degree of freedom. This is achieved by the following nonzero control parameters

$${}^0\bar{k}, {}^0\bar{d}, {}^0\bar{m} \in \mathbb{R}^+, \quad {}^0\bar{\boldsymbol{\Pi}}, {}^0\bar{\boldsymbol{\Upsilon}}, {}^0\bar{\boldsymbol{\Theta}} \in \mathbb{SYM}^+(3). \quad (4.133)$$

The resulting potential and corresponding transport map are

$$\bar{\mathcal{V}}(\mathbf{x}, \mathbf{x}_R) = \frac{1}{2} \|({}^0\mathbf{G}(\mathbf{x}_R))^{-1} {}^0\mathbf{G}(\mathbf{x}) - \mathbf{I}_4\)^T\|_F^2, \quad \mathbf{Q}(\mathbf{x}, \mathbf{x}_R) = ({}^7\mathbf{J}(\mathbf{x}))^{-1} {}^0\mathbf{J}(\mathbf{x}_R). \quad (4.134)$$

The resulting closed loop dynamics of the robot arm may be written by plugging the absolute tool configuration  ${}^0\mathbf{G}(\mathbf{x})$  and its reference  ${}^0\mathbf{G}(\mathbf{x}_R)$  into the dynamics of a single rigid body for either of the three proposed approaches (4.14), (4.21) or (4.65).

The determinant of the transport map is

$$\det \mathbf{Q}(\mathbf{x}, \mathbf{x}_R) = \frac{\det {}^0\mathbf{J}(\mathbf{x}_R)}{\det {}^0\mathbf{J}(\mathbf{x})}, \quad \det {}^0\mathbf{J}(\mathbf{x}) = -l_2 l_3 (l_1 + l_2 \sin \theta_2 + l_3 \cos(\theta_2 + \theta_3)) \cos \theta_3 \sin \theta_5 \quad (4.135)$$

If the term in the brackets vanishes means that the wrist lies on the axis of  $\theta_1$  and  $\cos \theta_3 = 0$  is the case if the arm is completely straight which is the singularity we already encountered

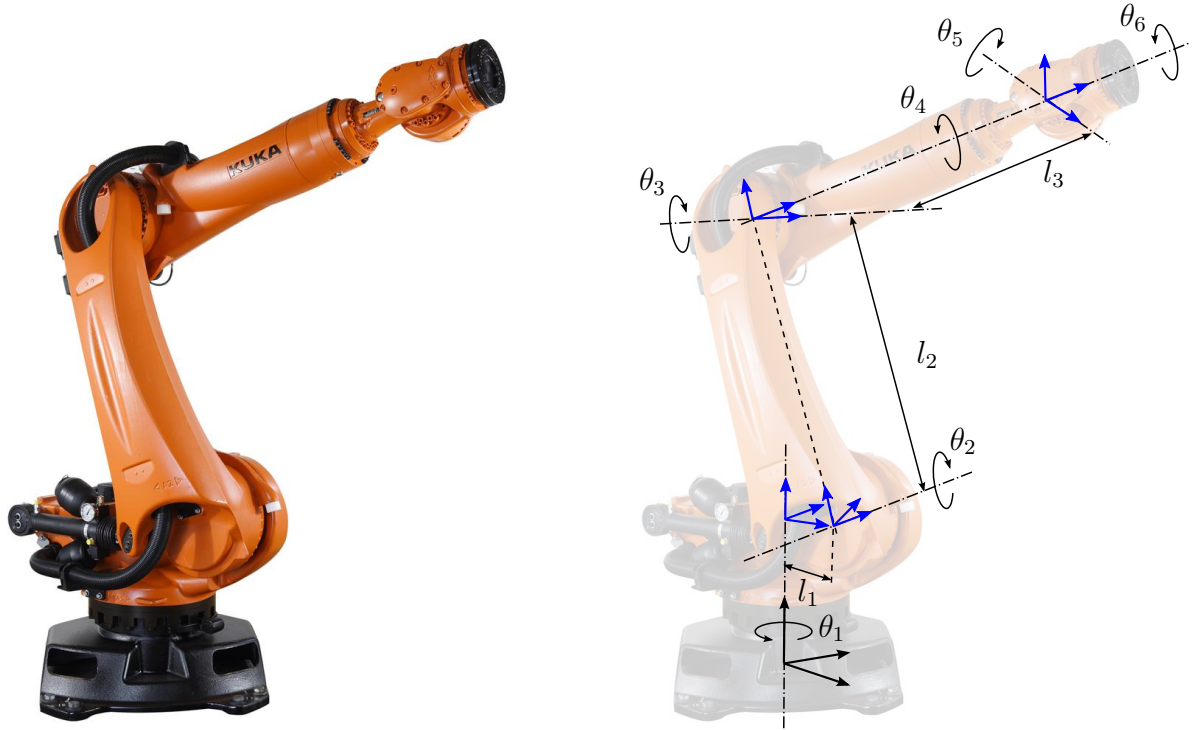


Figure 4.13: A model of a robot arm (background image from [www.kuka.de](http://www.kuka.de))

with the SCARA robot. The last three axis with angles  $\theta_4, \theta_5, \theta_6$  can be regarded as Euler angles in the sequence XYX and  $\sin \theta_5 = 0$  is their singularity. Comparing this to the motivation example in ?? we have the same problem but the other way around: The Euler angles are an absolutely appropriate choice of coordinates since the mechanism is realized like this. Consequently the configuration manifold of this part is  $\mathbb{S}^1 \times \mathbb{S}^1 \times \mathbb{S}^1$  and we are assigning a control that was designed for  $\mathbb{SO}(3)$ .

**Conclusion.** The behavior of the two different parameterizations are quite analog to the two parameterizations of the SCARA robot. Which one is more suitable depends on the actual control task. Furthermore, the two presented parameterizations are just two special cases of which dynamics can be achieved with the more general approach of control of this work.

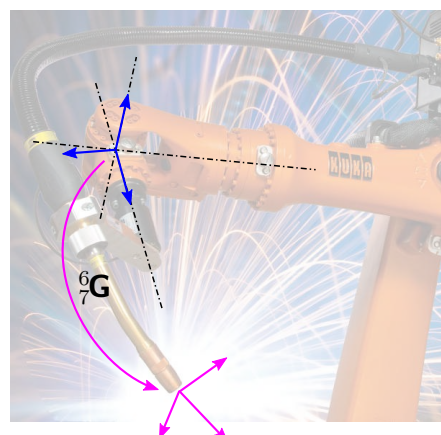


Figure 4.14: Welding tool attached to the robot arm (background image from [www.kuka.de](http://www.kuka.de))

## 4.8 Examples of underactuated systems

### 4.8.1 Two masses connected by a spring

In order to illustrate the control approach for underactuated systems we consider the minimal example: Two bodies in prismatic joints connected by a linear spring but where only one is directly actuated by the force  $F$  as illustrated in Figure 4.15.

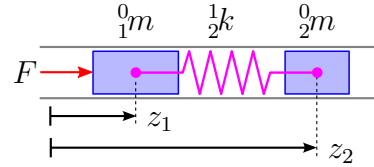


Figure 4.15: Model of two bodies connected by a spring

**Model.** We choose the absolute positions of the bodies as configuration coordinates  $\mathbf{x} = [z_1, z_2]^\top$  and their derivative as velocity coordinates  $\boldsymbol{\xi} = \dot{\mathbf{x}}$ . With this the body configurations are

$${}^0_1\mathbf{G} = \begin{bmatrix} 1 & 0 & 0 & z_1 \\ 0 & 1 & 0 & 0 \\ 0 & 0 & 1 & 0 \\ 0 & 0 & 0 & 1 \end{bmatrix}, \quad {}^0_2\mathbf{G} = \begin{bmatrix} 1 & 0 & 0 & z_2 \\ 0 & 1 & 0 & 0 \\ 0 & 0 & 1 & 0 \\ 0 & 0 & 0 & 1 \end{bmatrix}. \quad (4.136)$$

With the total mass  ${}_1^0m$ ,  ${}_2^0m$  of the individual bodies and the spring stiffness  ${}_2^1k$  the resulting equations of motion may be written as

$$\underbrace{\begin{bmatrix} {}_1^0m & 0 \\ 0 & {}_2^0m \end{bmatrix}}_M \begin{bmatrix} \ddot{z}_1 \\ \ddot{z}_2 \end{bmatrix} + \underbrace{\begin{bmatrix} {}_2^1k & -{}_2^1k \\ -{}_2^1k & {}_2^1k \end{bmatrix}}_K \begin{bmatrix} z_1 \\ z_2 \end{bmatrix} = \underbrace{\begin{bmatrix} 1 \\ 0 \end{bmatrix}}_B F. \quad (4.137)$$

**Desired closed loop.** We assume general body inertia  ${}_1^0\mathbf{M}$ , ..., damping and stiffness. The three proposed control approaches lead to identical desired closed loop dynamics:

$$\bar{\mathbf{M}}\ddot{\mathbf{e}} + \bar{\mathbf{D}}\dot{\mathbf{e}} + \bar{\mathbf{K}}\mathbf{e} = \mathbf{0}, \quad \mathbf{e} = \mathbf{x} - \mathbf{x}_R \quad (4.138)$$

where

$$\bar{\mathbf{M}} = \begin{bmatrix} {}_1^0\bar{m} + {}_2^1\bar{m} & -{}_2^1\bar{m} \\ -{}_2^1\bar{m} & {}_2^0\bar{m} + {}_1^1\bar{m} \end{bmatrix}, \quad \bar{\mathbf{D}} = \begin{bmatrix} {}_1^0\bar{d} + {}_2^1\bar{d} & -{}_2^1\bar{d} \\ -{}_2^1\bar{d} & {}_2^0\bar{d} + {}_1^1\bar{d} \end{bmatrix}, \quad \bar{\mathbf{K}} = \begin{bmatrix} {}_1^0\bar{k} + {}_2^1\bar{k} & -{}_2^1\bar{k} \\ -{}_2^1\bar{k} & {}_2^0\bar{k} + {}_1^1\bar{k} \end{bmatrix}. \quad (4.139)$$

The corresponding potential  $\bar{\mathcal{V}} = \frac{1}{2}\mathbf{e}^\top \bar{\mathbf{K}} \mathbf{e}$  has the obvious transport map  $\mathbf{Q} = \mathbf{I}_2$ .

**Matching.** The matching condition (4.79) for this example may be written as

$$\boldsymbol{\lambda} = (\boldsymbol{B}^\perp)^\top (\bar{\boldsymbol{M}} \bar{\boldsymbol{M}}^{-1} (-\bar{\boldsymbol{M}} \ddot{\boldsymbol{x}}_R + \bar{\boldsymbol{D}}(\dot{\boldsymbol{x}} - \dot{\boldsymbol{x}}_R) + \bar{\boldsymbol{K}}(\boldsymbol{x} - \boldsymbol{x}_R)) - \boldsymbol{K}\boldsymbol{x}) = \mathbf{0}. \quad (4.140)$$

Since this equation is linear in the system coordinates we can separate the into

$$(\boldsymbol{B}^\perp)^\top (\bar{\boldsymbol{M}} \ddot{\boldsymbol{x}}_R + \boldsymbol{K}\boldsymbol{x}_R) = \mathbf{0}. \quad (4.141a)$$

$$(\boldsymbol{B}^\perp)^\top \bar{\boldsymbol{M}} \bar{\boldsymbol{M}}^{-1} \bar{\boldsymbol{D}} = \mathbf{0}, \quad (4.141b)$$

$$(\boldsymbol{B}^\perp)^\top \bar{\boldsymbol{M}} \bar{\boldsymbol{M}}^{-1} (\bar{\boldsymbol{K}} - \boldsymbol{K}) = \mathbf{0}, \quad (4.141c)$$

Choosing  $\boldsymbol{B}^\perp = [0, 1]^\top$  this is explicitly

$$\ddot{z}_{2R} + \varpi(z_{2R} - z_{1R}) = 0 \quad (4.142a)$$

$$\begin{cases} {}^0\bar{m} {}^1\bar{d} - {}^1\bar{m} {}^0\bar{d} = 0 \\ {}^0\bar{m} {}^1\bar{d} + ({}^0\bar{m} + {}^1\bar{m}) {}^0\bar{d} = 0 \end{cases} \quad (4.142b)$$

$$\begin{cases} {}^0\bar{m} {}^1\bar{k} - {}^1\bar{m} {}^0\bar{k} = ({}^0\bar{m} {}^0\bar{m} + {}^0\bar{m} {}^1\bar{m} + {}^0\bar{m} {}^1\bar{m}) \varpi \\ {}^0\bar{m} {}^1\bar{k} + ({}^0\bar{m} + {}^1\bar{m}) {}^0\bar{k} = ({}^0\bar{m} {}^0\bar{m} + {}^0\bar{m} {}^1\bar{m} + {}^0\bar{m} {}^1\bar{m}) \varpi \end{cases} \quad (4.142c)$$

where  $\varpi = {}^1\bar{k}/{}^0\bar{m}$  is the sole model parameter relevant for the matching condition. The first part (4.142a) is a constraint on the reference trajectory as it is independent of tunable parameters. It can be resolved by acknowledging that  $z_2$  is a *flat output* of the system and planing the reference trajectory accordingly, i.e.

$$z_{1R} = z_{2R} - \ddot{z}_{2R}/\varpi. \quad (4.143)$$

The other conditions can be resolved by setting

$$\begin{aligned} {}^1\bar{k} &= \frac{{}^1\bar{m}}{{}^0\bar{m}} {}^0\bar{k} + \frac{{}^0\bar{m} {}^0\bar{m} + {}^0\bar{m} {}^1\bar{m} + {}^0\bar{m} {}^1\bar{m}}{{}^0\bar{m}} \varpi, & {}^0\bar{k} &= -\frac{{}^1\bar{m}}{{}^0\bar{m} + {}^1\bar{m}} {}^0\bar{k}, & {}^1\bar{d} &= \frac{{}^1\bar{m}}{{}^0\bar{m}} {}^0\bar{d}, & {}^0\bar{d} &= -\frac{{}^1\bar{m}}{{}^0\bar{m} + {}^1\bar{m}} {}^0\bar{d}, \end{aligned} \quad (4.144)$$

which leaves the 5 tuning parameters  ${}^0\bar{k}$ ,  ${}^1\bar{d}$ ,  ${}^0\bar{m}$ ,  ${}^0\bar{m}$  and  ${}^1\bar{m}$ .

The resulting control law is

$$\begin{aligned} F = {}^0\bar{m} \ddot{z}_{1R} + {}^1\bar{k}(z_{1R} - z_{2R}) + & \left( {}^1\bar{k} + \frac{{}^0\bar{m}({}^1\bar{m} {}^1\bar{k} + {}^0\bar{m}({}^0\bar{k} - {}^1\bar{k}))}{{}^0\bar{m}({}^0\bar{m} + {}^1\bar{m})} \right) e_1 \\ & - \left( {}^1\bar{k} - \frac{{}^0\bar{m}({}^1\bar{m} {}^1\bar{k} - {}^0\bar{m} {}^1\bar{k})}{{}^0\bar{m}({}^0\bar{m} + {}^1\bar{m})} \right) e_2 - \frac{{}^0\bar{m}({}^0\bar{d} + {}^1\bar{d})}{{}^0\bar{m} + {}^1\bar{m}} \dot{e}_1 + \frac{{}^0\bar{m} {}^1\bar{d}}{{}^0\bar{m} + {}^1\bar{m}} \dot{e}_2. \end{aligned} \quad (4.145)$$

**Pole placement.** Tuning the design parameters under the given matching conditions might not be intuitive for this example. To resolve this we can fall back to the classical approach of placing the eigenvalues of the closed loop system (4.138). Taking into account the matching condition (4.144), the characteristic polynomial of (4.138) is

$$\frac{\det(\bar{\boldsymbol{M}} \lambda^2 + \bar{\boldsymbol{D}} \lambda + \bar{\boldsymbol{K}})}{\det \bar{\boldsymbol{M}}} = \lambda^4 + \underbrace{\frac{{}^0\bar{d}}{{}^0\bar{m}}}_{p_3} \lambda^3 + \underbrace{\frac{{}^0\bar{k} + ({}^0\bar{m} + {}^1\bar{m}) \varpi}{{}^0\bar{m}}}_{p_2} \lambda^2 + \underbrace{\frac{\varpi {}^0\bar{d}}{{}^0\bar{m} + {}^1\bar{m}}}_{p_1} \lambda + \underbrace{\frac{\varpi {}^0\bar{k}}{{}^0\bar{m} + {}^1\bar{m}}}_{p_0}. \quad (4.146)$$

This can be solved for

$${}^0\bar{k} = \frac{{}^1\bar{m} p_0 p_3}{\varpi p_3 - p_1}, \quad {}^0\bar{d} = \frac{{}^1\bar{m} p_1 p_3}{\varpi p_3 - p_1}, \quad {}^0\bar{m} = \frac{{}^1\bar{m} p_1}{\varpi p_3 - p_1}, \quad {}^0\bar{m} = \frac{{}^1\bar{m} (p_1 p_2 - p_0 p_3 - \varpi p_1)}{\varpi (\varpi p_3 - p_1)}. \quad (4.147a)$$

and  ${}^1\bar{m} \in \mathbb{R} \neq 0$ . Choosing any Hurwitz polynomial for the coefficients  $p_i$  guarantees the asymptotic stability of the closed loop. In order to conclude  $\bar{\boldsymbol{M}} > 0$ ,  $\bar{\boldsymbol{D}} \geq 0$  and  $\bar{\boldsymbol{K}} > 0$  from the Hurwitz criterion ( $p_0, p_1, p_2, p_3, p_1 p_2 - p_0 p_3, p_1 p_2 p_3 - p_1^2 - p_0 p_3^2 > 0$ ) we need  $\text{sign } {}^1\bar{m} = \text{sign}(\varpi p_3 - p_1)$ .

**Conclusions.** The resulting controller is equivalent to one that could be designed by standard linear state-feedback methods. However, this approach here might give some *physical* insight to the resulting closed loop system. For example that the closed loop system must have an inertial coupling ( $\frac{1}{2}\bar{m} \neq 0$ ) of the two bodies, if one wants to tune all 4 poles.

### 4.8.2 PVTOL

The planar vertical take off landing aircraft (PVTOL), Figure 4.16, is a common benchmark problem discussed in e.g. [Hauser et al., 1992] or [Fliess et al., 1999].

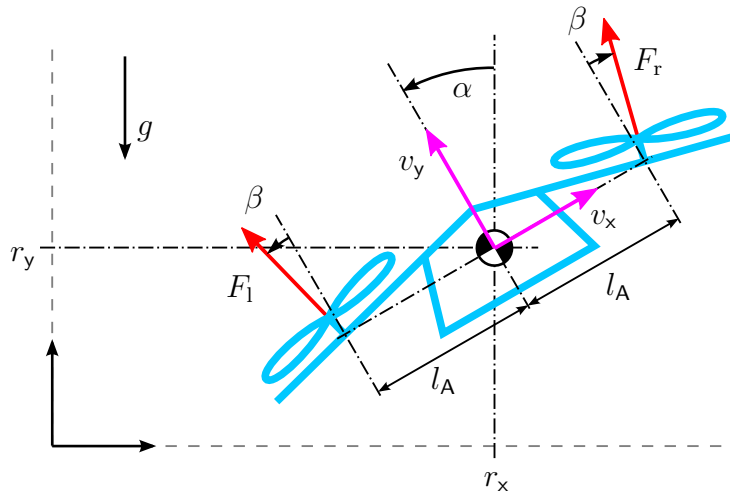


Figure 4.16: Model of the PVTOL

**Model.** We choose the position  $(r_x, r_y)$  of the center of mass and the tilt angle  $\alpha$  as configuration coordinates. So the body configuration is

$${}^0_1\mathbf{G} = \begin{bmatrix} \cos \alpha & -\sin \alpha & 0 & r_x \\ \sin \alpha & \cos \alpha & 0 & r_y \\ 0 & 0 & 1 & 0 \\ 0 & 0 & 0 & 1 \end{bmatrix}. \quad (4.148)$$

Note that in these coordinates the gravity acceleration has the components  $\mathbf{a}_G = [0, -g, 0]^\top$ , so the potential energy due to gravity is  $\mathcal{V} = mgy$ . In contrast to the sources mentioned above, we use the coefficients  $(v_x, v_y)$  of the absolute velocity w.r.t. the body fixed frame and the angular velocity  $\omega_z$  of the body tilt as velocity coordinates. The kinematic relation is

$$\frac{d}{dt} \underbrace{\begin{bmatrix} r_x \\ r_y \\ \alpha \end{bmatrix}}_x = \underbrace{\begin{bmatrix} \cos \alpha & -\sin \alpha & 0 \\ \sin \alpha & \cos \alpha & 0 \\ 0 & 0 & 1 \end{bmatrix}}_A \underbrace{\begin{bmatrix} v_x \\ v_y \\ \omega_z \end{bmatrix}}_\xi. \quad (4.149)$$

Let  $m$  be the total mass of the PVTOL and  $\Theta_z$  the moment of inertia around the center of mass. The propeller thrusts are  $F_r, F_l$  according to Figure 4.16. Overall, we have the kinetic equation

$$\underbrace{\begin{bmatrix} m & 0 & 0 \\ 0 & m & 0 \\ 0 & 0 & \Theta_z \end{bmatrix}}_M \underbrace{\begin{bmatrix} \dot{v}_x \\ \dot{v}_y \\ \dot{\omega}_z \end{bmatrix}}_{\dot{\xi}} + \underbrace{\begin{bmatrix} m(g \sin \alpha - v_y \omega_z) \\ m(g \cos \alpha + v_x \omega_z) \\ 0 \end{bmatrix}}_b = \underbrace{\begin{bmatrix} \sin \beta & -\sin \beta \\ \cos \beta & \cos \beta \\ l_A \cos \beta & -l_A \cos \beta \end{bmatrix}}_B \underbrace{\begin{bmatrix} F_r \\ F_l \end{bmatrix}}_u. \quad (4.150)$$

**Reference trajectory.** For the following we chose the left complement  $\mathbf{B}^\perp = [1, 0, -\frac{\sin \beta}{l \cos \beta}]$ . The condition for the reference from (4.80) for this example is

$$\lambda^{\text{ZeroError}} = m \left( \dot{v}_{xR} - \underbrace{\frac{\Theta_z \sin \beta}{ml_A \cos \beta} \dot{\omega}_{zR}}_\varepsilon - \omega_{zR} v_{yR} + g \sin \alpha_R \right) = 0 \quad (4.151)$$

This can be fulfilled by parameterizing the configuration through the flat output  $y_{1R} = r_{xR} - \varepsilon \sin \alpha_R$ ,  $y_{2R} = r_{yR} + \varepsilon \cos \alpha_R$  (see e.g. [Fliess et al., 1999]), i.e.

$$r_{xR} = y_{1R} - \varepsilon \frac{\ddot{y}_{1R}}{\sqrt{\ddot{y}_{1R}^2 + (\dot{y}_{1R} + g)^2}}, \quad (4.152)$$

$$r_{yR} = y_{2R} - \varepsilon \frac{\ddot{y}_{2R} - g}{\sqrt{\ddot{y}_{1R}^2 + (\dot{y}_{1R} + g)^2}}, \quad (4.153)$$

$$\alpha_R = \text{atan2}(\ddot{y}_{2R}, \dot{y}_{1R} + g). \quad (4.154)$$

Note that this parameterization fails if  $\ddot{y}_{1R} = \dot{y}_{1R} + g = 0$ , i.e. the body is in free fall.

**Closed loop.** The PVTOL model is just a planar rigid body with particular actuation. So its closed loop template coincides with the one for the planar rigid body from subsection 4.7.4, but for symmetry reasons we choose the parameters  $\bar{h}_x = \bar{l}_x = \bar{s}_x = 0$ .

**Matching.** The matching force  $\boldsymbol{\lambda}$  from (4.78) with the orthogonal complement from above takes a rather cumbersome form and is not given explicitly here. Instead we will investigate its linear approximation about any reference trajectory with  $\alpha_R = 0$ : The matrices of the linearized model and desired closed loop are

$$\mathbf{M}_0 = \begin{bmatrix} m & 0 & 0 \\ 0 & m & 0 \\ 0 & 0 & J \end{bmatrix}, \quad \bar{\mathbf{M}}_0 = \begin{bmatrix} \bar{m} & 0 & -\bar{m}\bar{s}_y \\ 0 & \bar{m} & 0 \\ -\bar{m}\bar{s}_y & 0 & \bar{\Theta}_z + \bar{m}\bar{s}_y^2 \end{bmatrix}, \quad (4.155a)$$

$$\mathbf{D}_0 = \begin{bmatrix} 0 & 0 & 0 \\ 0 & 0 & 0 \\ 0 & 0 & 0 \end{bmatrix}, \quad \bar{\mathbf{D}}_0 = \begin{bmatrix} \bar{d} & 0 & -\bar{d}\bar{l}_y \\ 0 & \bar{d} & 0 \\ -\bar{d}\bar{l}_y & 0 & \bar{\Upsilon}_z + \bar{d}\bar{l}_y^2 \end{bmatrix}, \quad (4.155b)$$

$$\mathbf{K}_0 = \begin{bmatrix} 0 & 0 & mg \\ 0 & 0 & 0 \\ 0 & 0 & 0 \end{bmatrix}, \quad \bar{\mathbf{K}}_0 = \begin{bmatrix} \bar{k} & 0 & -\bar{k}\bar{h}_y \\ 0 & \bar{k} & 0 \\ -\bar{k}\bar{h}_y & 0 & \bar{\Pi}_z + \bar{k}\bar{h}_y^2 \end{bmatrix}. \quad (4.155c)$$

The conditions for  $(\mathbf{B}^\perp)^\top (\bar{\mathbf{M}}_0 \bar{\mathbf{M}}_0^{-1} \bar{\mathbf{D}}_0 - \mathbf{D}_0) = \mathbf{0}$  and  $(\mathbf{B}^\perp)^\top (\bar{\mathbf{M}}_0 \bar{\mathbf{M}}_0^{-1} \bar{\mathbf{K}}_0 - \mathbf{K}_0) = \mathbf{0}$  for the linearized matching force from (4.82) to vanish are equivalent to

$$\bar{k}(\bar{\Theta}_z - \bar{m}(\bar{h}_y - \bar{s}_y)(\bar{s}_y - \varepsilon)) = 0, \quad (4.156a)$$

$$\bar{m}\bar{\Pi}_z(\bar{s}_y - \varepsilon) - \bar{k}\bar{h}_y(\bar{\Theta}_z - \bar{m}(\bar{h}_y - \bar{s}_y)(\bar{s}_y - \varepsilon)) = \bar{\Theta}_z \bar{m}g, \quad (4.156b)$$

$$\bar{d}(\bar{\Theta}_z - \bar{m}(\bar{l}_y - \bar{s}_y)(\bar{s}_y - \varepsilon)) = 0, \quad (4.156c)$$

$$\bar{m}\bar{\Upsilon}_z(\bar{s}_y - \varepsilon) - \bar{d}\bar{l}_y(\bar{\Theta}_z - \bar{m}(\bar{l}_y - \bar{s}_y)(\bar{s}_y - \varepsilon)) = 0. \quad (4.156d)$$

One solution for this is

$$\bar{\Theta}_z = \bar{m}(\bar{h}_y - \bar{s}_y)(\bar{s}_y - \varepsilon), \quad \bar{l}_y = \bar{h}_y, \quad \bar{\Upsilon}_z = 0, \quad \bar{\Pi}_z = \bar{m}g(\bar{h}_y - \bar{s}_y) \quad (4.157)$$

which leaves the parameters  $\bar{k}, \bar{d}, \bar{m}, \bar{h}_y, \bar{s}_y$  for tuning. The resulting matching force is

$$\tilde{\mathbf{b}} = \frac{\bar{m}(\bar{h}_y - \bar{s}_y)}{\bar{m}(\bar{h}_y - \varepsilon)} \begin{bmatrix} 1 \\ 0 \\ -\varepsilon \end{bmatrix} \lambda \quad (4.158)$$

where  $\lambda$  for the corresponding approach is

$$\lambda^{\text{ParticleBased}} = m(a_{yR} - \varepsilon\omega_{zR}^2) \sin \alpha_E \quad (4.159a)$$

$$\lambda^{\text{BodyBased}} = m(a_{yR} \sin \alpha_E - r_{xR}\omega_{zR}^2 + 2v_{yE}\omega_{zR} + (\varepsilon(1 - \cos \alpha_E) - r_{yE})\dot{\omega}_{zR}) \quad (4.159b)$$

$$\lambda^{\text{EnergyBased}} = m(a_{yR} \sin \alpha_E - r_{xR}\omega_{zR}^2 + v_{yE}\omega_{zR} + (\varepsilon(1 - \cos \alpha_E) - r_{yE})\dot{\omega}_{zR}) \quad (4.159c)$$

where  $a_{yR} = \dot{v}_{yR} + v_{xR}\omega_{zR} + g(\cos \alpha_R - 1)$ .

**Tuning.** For the energies to be positive (semi) definite, we need  $\bar{\mathbf{M}} > 0$ ,  $\bar{\mathbf{D}} \geq 0$  and  $\bar{\mathcal{V}} > 0$  which means for the remaining tuning parameters

$$\bar{k}, \bar{d}, \bar{m} > 0, \quad \bar{h}_y > \bar{s}_y > \varepsilon. \quad (4.160)$$

The characteristic polynomial of the linearized system is

$$\begin{aligned} & \det(\bar{\mathbf{M}}\lambda^2 + \bar{\mathbf{D}}\lambda + \bar{\mathbf{K}}) / \det \bar{\mathbf{M}} \\ &= (\lambda^2 + \frac{\bar{d}}{\bar{m}}\lambda + \frac{\bar{k}}{\bar{m}})(\lambda^4 + \frac{\bar{d}(\bar{h}_y - \varepsilon)}{\bar{m}(\bar{s}_y - \varepsilon)}\lambda^3 + \frac{\bar{k}(\bar{h}_y - \varepsilon) + \bar{m}g}{\bar{m}(\bar{s}_y - \varepsilon)}\lambda^2 + \frac{\bar{d}g}{\bar{m}(\bar{s}_y - \varepsilon)}\lambda + \frac{\bar{k}g}{\bar{m}(\bar{s}_y - \varepsilon)}) \end{aligned} \quad (4.161)$$

Set a desired polynomial of forth degree  $\lambda^4 + p_3\lambda^3 + p_2\lambda^2 + p_1\lambda + p_0$  we get the parameters

$$\bar{k} = \frac{\bar{m}p_0p_1}{p_1p_2 - p_0p_3}, \quad \bar{h}_y = \varepsilon + \frac{gp_3}{p_1}, \quad \bar{\Theta}_z = \frac{\bar{m}g^2(p_1p_2p_3 - p_1^2 - p_0p_3^2)}{(p_1p_2 - p_0p_3)^2}, \quad (4.162)$$

$$\bar{d} = \frac{\bar{m}p_1^2}{p_1p_2 - p_0p_3}, \quad \bar{s}_y = \varepsilon + \frac{gp_1}{p_1p_2 - p_0p_3}, \quad \bar{\Pi}_z = \frac{\bar{m}g^2(p_1p_2p_3 - p_1^2 - p_0p_3)}{p_1(p_1p_2 - p_0p_3)}, \quad (4.163)$$

Note that the Hurwitz criterion ( $p_0, p_1, p_2, p_3, p_1p_2 - p_0p_3, p_1p_2p_3 - p_1^2 - p_0p_3^2 > 0$ ) implies the positive definiteness of the inertia  $\bar{\mathbf{M}}$  and stiffness matrix  $\bar{\mathbf{K}}$ . Even though the damping matrix  $\bar{\mathbf{D}}$  is only positive semidefinite the *local* attractiveness of the nonlinear system can be concluded by Lyapunov's indirect method.

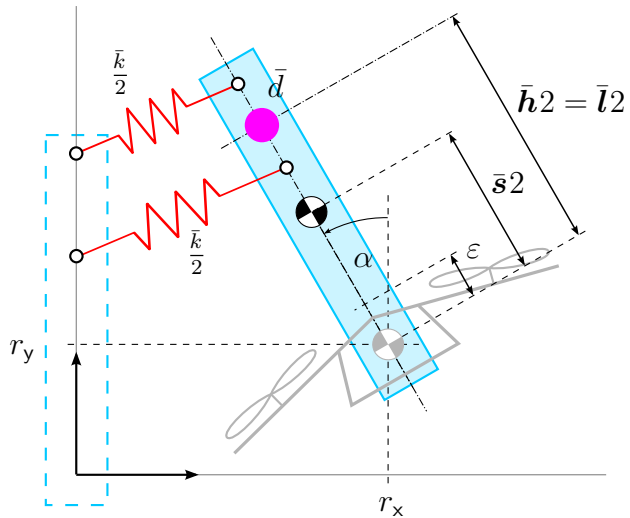


Figure 4.17: Interpretation of the controlled PVTOL as a mechanical system

**Mechanical interpretation.**

### 4.8.3 Quadcopter

Consider a Quadcopter Figure 4.18

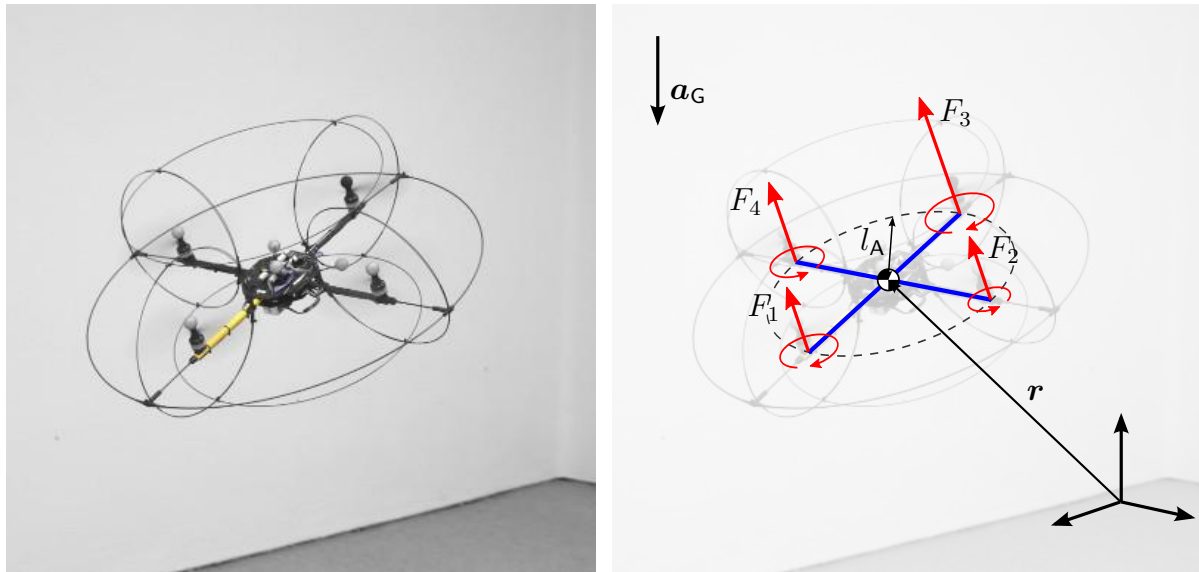


Figure 4.18: Model of the Quadcopter

**Model.** Kinematics

$$\dot{\mathbf{r}} = \mathbf{R}\mathbf{v}, \quad \dot{\mathbf{R}} = \mathbf{R} \operatorname{wed}(\boldsymbol{\omega}) \quad (4.164)$$

Kinetics

$$\underbrace{\begin{bmatrix} m & 0 & 0 & 0 & 0 & 0 \\ 0 & m & 0 & 0 & 0 & 0 \\ 0 & 0 & m & 0 & 0 & 0 \\ 0 & 0 & 0 & \Theta_y & 0 & 0 \\ 0 & 0 & 0 & 0 & \Theta_x & 0 \\ 0 & 0 & 0 & 0 & 0 & \Theta_z \end{bmatrix}}_M \underbrace{\begin{bmatrix} \dot{v}_x \\ \dot{v}_y \\ \dot{v}_z \\ \dot{\omega}_x \\ \dot{\omega}_y \\ \dot{\omega}_z \end{bmatrix}}_{\dot{\xi}} + \underbrace{\begin{bmatrix} m(v_y\omega_z - v_z\omega_y + R_x^z g) \\ m(v_x\omega_z - v_z\omega_x + R_y^z g) \\ m(v_y\omega_x - v_x\omega_y + R_z^z g) \\ (\Theta_z - \Theta_y)\omega_y\omega_z \\ (\Theta_x - \Theta_z)\omega_x\omega_z \\ (\Theta_y - \Theta_x)\omega_x\omega_y \end{bmatrix}}_b = \underbrace{\begin{bmatrix} 0 & 0 & 0 & 0 \\ 0 & 0 & 0 & 0 \\ 1 & 1 & 1 & 1 \\ 0 & l_A & 0 & -l_A \\ -l_A & 0 & l_A & 0 \\ -b_F & b_F & -b_F & b_F \end{bmatrix}}_B \underbrace{\begin{bmatrix} F_1 \\ F_2 \\ F_3 \\ F_4 \\ u \end{bmatrix}}_u \quad (4.165)$$

**Closed loop template.** The quadcopter is just a free rigid body with a particular actuation, so the closed loop templates coincide with the ones given in subsection 4.1.2, subsection 4.2.1 and subsection 4.3.3. Due to symmetry considerations we set  $\bar{s}_x = \bar{s}_y = 0$ ,  $\bar{\Theta}_{xx} = \bar{\Theta}_{yy}$ ,  $\bar{\Theta}_{xy} = \bar{\Theta}_{xz} = \bar{\Theta}_{yz} = 0$  and analog for the stiffness and damping parameters.

**Matching** An obvious left complement for  $B$  is

$$B^\perp = \begin{bmatrix} 1 & 0 \\ 0 & 1 \\ 0 & 0 \\ 0 & 0 \\ 0 & 0 \\ 0 & 0 \end{bmatrix}. \quad (4.166)$$

As the actual matching force  $\lambda$  is extremely cumbersome, we will consider its first order approximation first: The reference part is

$$\lambda^{\text{ZeroError}} = m \begin{bmatrix} \dot{v}_{xR} + v_{zR}\omega_{yR} - v_{yR}\omega_{zR} + R_{xR}^z g \\ \dot{v}_{yR} + v_{xR}\omega_{zR} - v_{zR}\omega_{xR} + R_{yR}^z g \end{bmatrix} \quad (4.167)$$

which is just the first two coefficients of (4.165). Combining this with the kinematic relation  $\dot{x}_R = A(x_R)\xi_R$  .. flat output.. see [Konz and Rudolph, 2013]

With the linearized system matrices

$$\begin{aligned} \mathbf{M}_0 &= \begin{bmatrix} m & 0 & 0 & 0 & 0 & 0 \\ 0 & m & 0 & 0 & 0 & 0 \\ 0 & 0 & m & 0 & 0 & 0 \\ 0 & 0 & 0 & \Theta_y & 0 & 0 \\ 0 & 0 & 0 & 0 & \Theta_x & 0 \\ 0 & 0 & 0 & 0 & 0 & \Theta_z \end{bmatrix}, \quad \bar{\mathbf{M}}_0 = \begin{bmatrix} \bar{m} & 0 & 0 & 0 & \bar{m}\bar{s}_z & 0 \\ 0 & \bar{m} & 0 & -\bar{m}\bar{s}_z & 0 & 0 \\ 0 & 0 & \bar{m} & 0 & 0 & 0 \\ 0 & -\bar{m}\bar{s}_z & 0 & \bar{\Theta}_y + \bar{m}\bar{s}_z^2 & 0 & 0 \\ \bar{m}\bar{s}_z & 0 & 0 & 0 & \bar{\Theta}_x + \bar{m}\bar{s}_z^2 & 0 \\ 0 & 0 & 0 & 0 & 0 & \bar{\Theta}_z \end{bmatrix}, \\ \mathbf{D}_0 &= \begin{bmatrix} 0 & 0 & 0 & 0 & 0 & 0 \\ 0 & 0 & 0 & 0 & 0 & 0 \\ 0 & 0 & 0 & 0 & 0 & 0 \\ 0 & 0 & 0 & 0 & 0 & 0 \\ 0 & 0 & 0 & 0 & 0 & 0 \\ 0 & 0 & 0 & 0 & 0 & 0 \end{bmatrix}, \quad \bar{\mathbf{D}}_0 = \begin{bmatrix} \bar{d} & 0 & 0 & 0 & \bar{d}\bar{l}_z & 0 \\ 0 & \bar{d} & 0 & -\bar{d}\bar{l}_z & 0 & 0 \\ 0 & 0 & \bar{d} & 0 & 0 & 0 \\ 0 & -\bar{d}\bar{l}_z & 0 & \bar{\Upsilon}_y + \bar{d}\bar{l}_z^2 & 0 & 0 \\ \bar{d}\bar{l}_z & 0 & 0 & 0 & \bar{\Upsilon}_x + \bar{d}\bar{l}_z^2 & 0 \\ 0 & 0 & 0 & 0 & 0 & \bar{\Upsilon}_z \end{bmatrix}, \\ \mathbf{K}_0 &= \begin{bmatrix} 0 & 0 & 0 & 0 & -mg & 0 \\ 0 & 0 & 0 & mg & 0 & 0 \\ 0 & 0 & 0 & 0 & 0 & 0 \\ 0 & 0 & 0 & 0 & 0 & 0 \\ 0 & 0 & 0 & 0 & 0 & 0 \\ 0 & 0 & 0 & 0 & 0 & 0 \end{bmatrix}, \quad \bar{\mathbf{K}}_0 = \begin{bmatrix} \bar{k} & 0 & 0 & 0 & \bar{k}\bar{h}_z & 0 \\ 0 & \bar{k} & 0 & -\bar{k}\bar{h}_z & 0 & 0 \\ 0 & 0 & \bar{k} & 0 & 0 & 0 \\ 0 & -\bar{k}\bar{h}_z & 0 & \bar{\Pi}_y + \bar{k}\bar{h}_z^2 & 0 & 0 \\ \bar{k}\bar{h}_z & 0 & 0 & 0 & \bar{\Pi}_x + \bar{k}\bar{h}_z^2 & 0 \\ 0 & 0 & 0 & 0 & 0 & \bar{\Pi}_z \end{bmatrix}. \end{aligned}$$

the linearized matching condition is

$$\bar{k}(\bar{\Theta}_x - \bar{m}\bar{s}_z(\bar{h}_z - \bar{s}_z)) = 0 \quad (4.168a)$$

$$\bar{m}(\bar{\Theta}_x g - \bar{\Pi}_x \bar{s}_z) + \bar{k}\bar{h}_z(\bar{\Theta}_x - \bar{m}\bar{s}_z(\bar{h}_z - \bar{s}_z)) = 0 \quad (4.168b)$$

$$\bar{d}(\bar{\Theta}_x - \bar{m}\bar{s}_z(\bar{h}_z - \bar{s}_z)) = 0 \quad (4.168c)$$

$$-\bar{m}\bar{s}_z\bar{\Upsilon}_x + \bar{d}\bar{l}_z(\bar{\Theta}_x - \bar{m}\bar{s}_z(\bar{l}_z - \bar{s}_z)) = 0 \quad (4.168d)$$

These terms vanish for

$$\bar{l}_z = \bar{h}_z, \quad \bar{\Theta}_x = \bar{m}\bar{s}_z(\bar{h}_z - \bar{s}_z), \quad \bar{\Upsilon}_x = 0, \quad \bar{\Pi}_x = \bar{m}g(\bar{h}_z - \bar{s}_z). \quad (4.169)$$

Even with these the ...

$$\tilde{\mathbf{b}} = \frac{1}{m\bar{h}_z} \begin{bmatrix} \bar{\Theta}_z\omega_x\omega_z - \frac{1}{2}\bar{\Pi}_z(R_z^x + R_x^z) \\ \bar{\Theta}_z\omega_y\omega_z - \frac{1}{2}\bar{\Pi}_z(R_z^y + R_y^z) \\ 0 \\ 0 \\ 0 \\ 0 \end{bmatrix} \quad (4.170)$$

#### 4.8.4 Bicopter

**Equations of motion.** The bicopter considered here is a single rigid body with two tilttable propellers as illustrated in Figure 4.18. With the same coordinates as for the previous examples, the equations of motion are identical as well up to the generalized

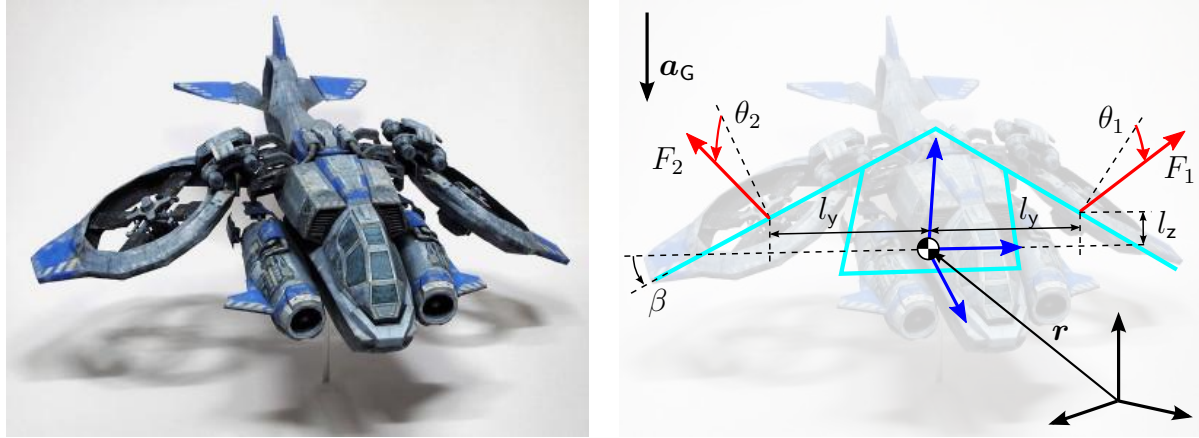


Figure 4.19: Model of a bicopter (background image: [www.poppaper.net/80155164809](http://www.poppaper.net/80155164809))

force from the propellers

$$\mathbf{f}^U = \underbrace{\begin{bmatrix} 1 & 0 & 1 & 0 \\ 0 & \sin \beta_F & 0 & -\sin \beta_F \\ 0 & \cos \beta_F & 0 & \cos \beta_F \\ 0 & l_y \cos \beta_F - l_z \sin \beta_F & 0 & -l_y \cos \beta_F + l_z \sin \beta_F \\ l_z & 0 & l_z & 0 \\ -l_y & 0 & l_y & 0 \end{bmatrix}}_B \underbrace{\begin{bmatrix} F_1 \sin \theta_1 \\ F_1 \cos \theta_1 \\ F_2 \sin \theta_2 \\ F_2 \cos \theta_2 \end{bmatrix}}_u. \quad (4.171)$$

The transformation of the actual control inputs  $F_1, F_2$  and  $\theta_1, \theta_2$  to a auxiliary input  $\mathbf{u}$  is used to achieve the linear form  $\mathbf{f}^U = \mathbf{B}\mathbf{u}$ . Within the input constraints  $2 \text{ N} \leq F_i \leq 14 \text{ N}$ ,  $-30^\circ \leq \theta_i \leq 30^\circ$ ,  $i = 1, 2$  this transformation is bijective. To account for the original constraints in transformed input  $\mathbf{u} \in \mathbb{R}^4$  a convex approximation illustrated in Figure 4.20 is used. These constraints can be written in the required form  $\mathbf{W}\mathbf{u} \leq \mathbf{l}$ .

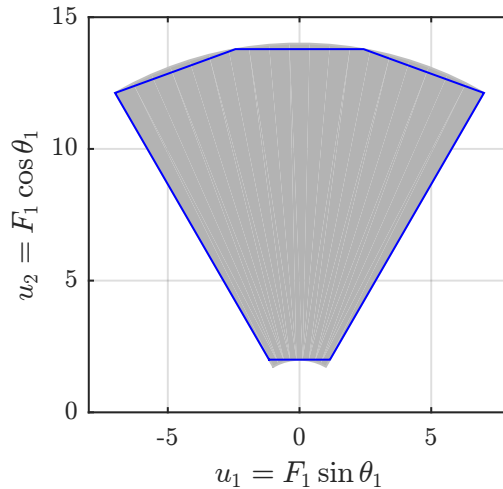


Figure 4.20: Approximation of the Bicpter input constraints

**Closed loop template.** Mechanically the bicopter is just a free rigid body, so the control template from (??) is reasonable. Due to symmetry of the mechanical model we set the center of mass on the body fixed vertical axis and set the principle axis of inertia to be parallel to the body fixed axis, i.e.  $\bar{s}_x = \bar{s}_y = 0$  and  $\bar{\Theta} = \text{diag}(\bar{\Theta}_x, \bar{\Theta}_y, \bar{\Theta}_z)$  and the same for damping and stiffness.

### Matching

$$\mathbf{B}^\perp = \begin{bmatrix} l_z & 0 & 0 & 0 & -1 & 0 \\ 0 & l_y \cos \beta_F - l_z \sin \beta_F & 0 & \sin \beta_F & 0 & 0 \end{bmatrix} \quad (4.172)$$

constraints on parameters

$$\bar{l}_z = \bar{h}_z, \quad (4.173)$$

$$\bar{\Theta}_x = \bar{m}(\bar{h}_z - \bar{s}_z)(\bar{s}_z - \varepsilon_y), \quad \bar{\Upsilon}_x = 0, \quad \bar{\Pi}_x = \bar{m}g(\bar{h}_z - \bar{s}_z), \quad (4.174)$$

$$\bar{\Theta}_y = \bar{m}(\bar{h}_z - \bar{s}_z)(\bar{s}_z - \varepsilon_x), \quad \bar{\Upsilon}_y = 0, \quad \bar{\Pi}_y = \bar{m}g(\bar{h}_z - \bar{s}_z). \quad (4.175)$$

where

$$\varepsilon_x = -\frac{\Theta_y}{ml_z}, \quad \varepsilon_y = \frac{\Theta_x \sin \beta_F}{m(l_y \cos \beta_F - l_z \sin \beta_F)}. \quad (4.176)$$

This leaves the tuning parameters  $\bar{m}$ ,  $\bar{d}$ ,  $\bar{k}$ ,  $\bar{s}_z$ ,  $\bar{h}_z$  and  $\bar{\Theta}_z$ ,  $\bar{\Upsilon}_z$ ,  $\bar{\Pi}_z$ .

The remaining matching force is

$$\tilde{\mathbf{f}} = \begin{bmatrix} 1 & 0 \\ 0 & 1 \\ 0 & 0 \\ 0 & -\varepsilon_y \\ \varepsilon_x & 0 \\ 0 & 0 \end{bmatrix} \begin{bmatrix} \frac{1}{\bar{h}_z - \varepsilon_x} (\bar{\Theta}_z - \bar{m}(\bar{h}_z - \bar{s}_z)) \left( \frac{\Theta_x - \Theta_z}{\Theta_y} \varepsilon_x - \varepsilon_y \right) \omega_x \omega_z - \frac{\bar{\Pi}_z}{2} (R_z^x + R_x^z) \\ \frac{1}{\bar{h}_z - \varepsilon_y} (\bar{\Theta}_z - \bar{m}(\bar{h}_z - \bar{s}_z)) \left( \frac{\Theta_y - \Theta_z}{\Theta_x} \varepsilon_y - \varepsilon_x \right) \omega_x \omega_z - \frac{\bar{\Pi}_z}{2} (R_z^y + R_y^z) \end{bmatrix} \quad (4.177)$$

### Simulation result.

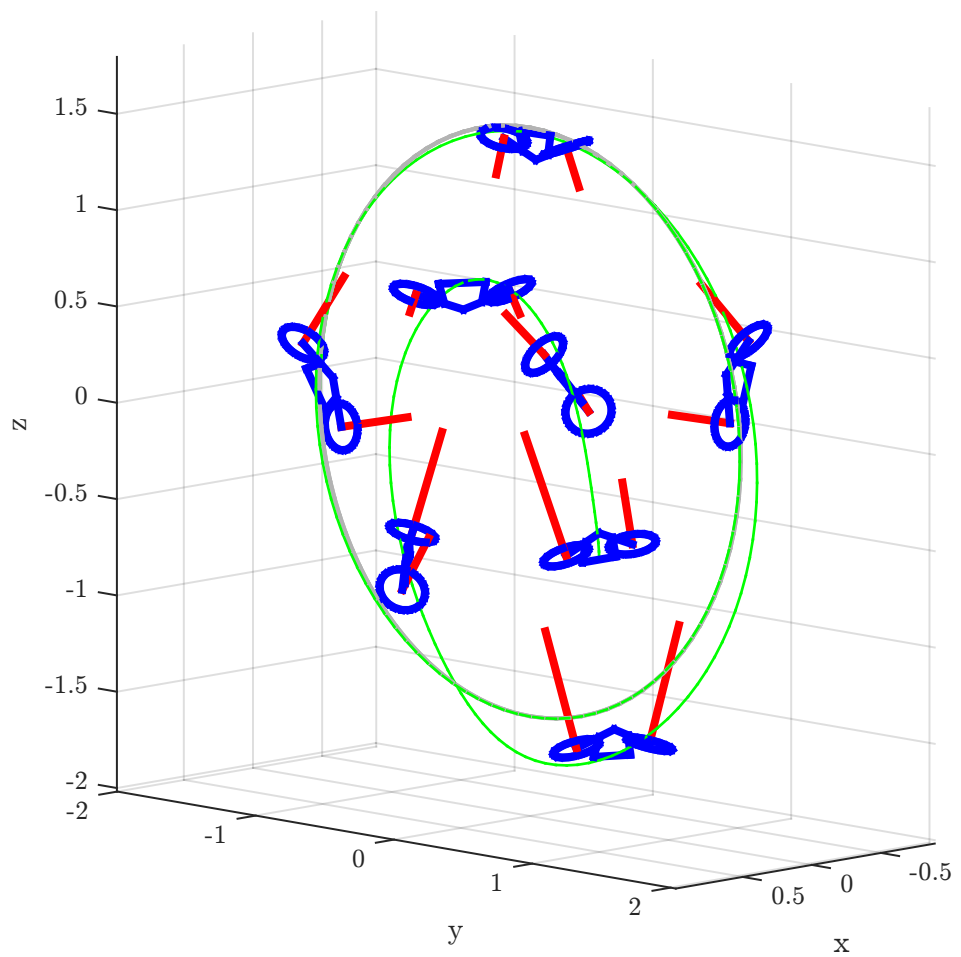


Figure 4.21: Simulation result for the Bicopter

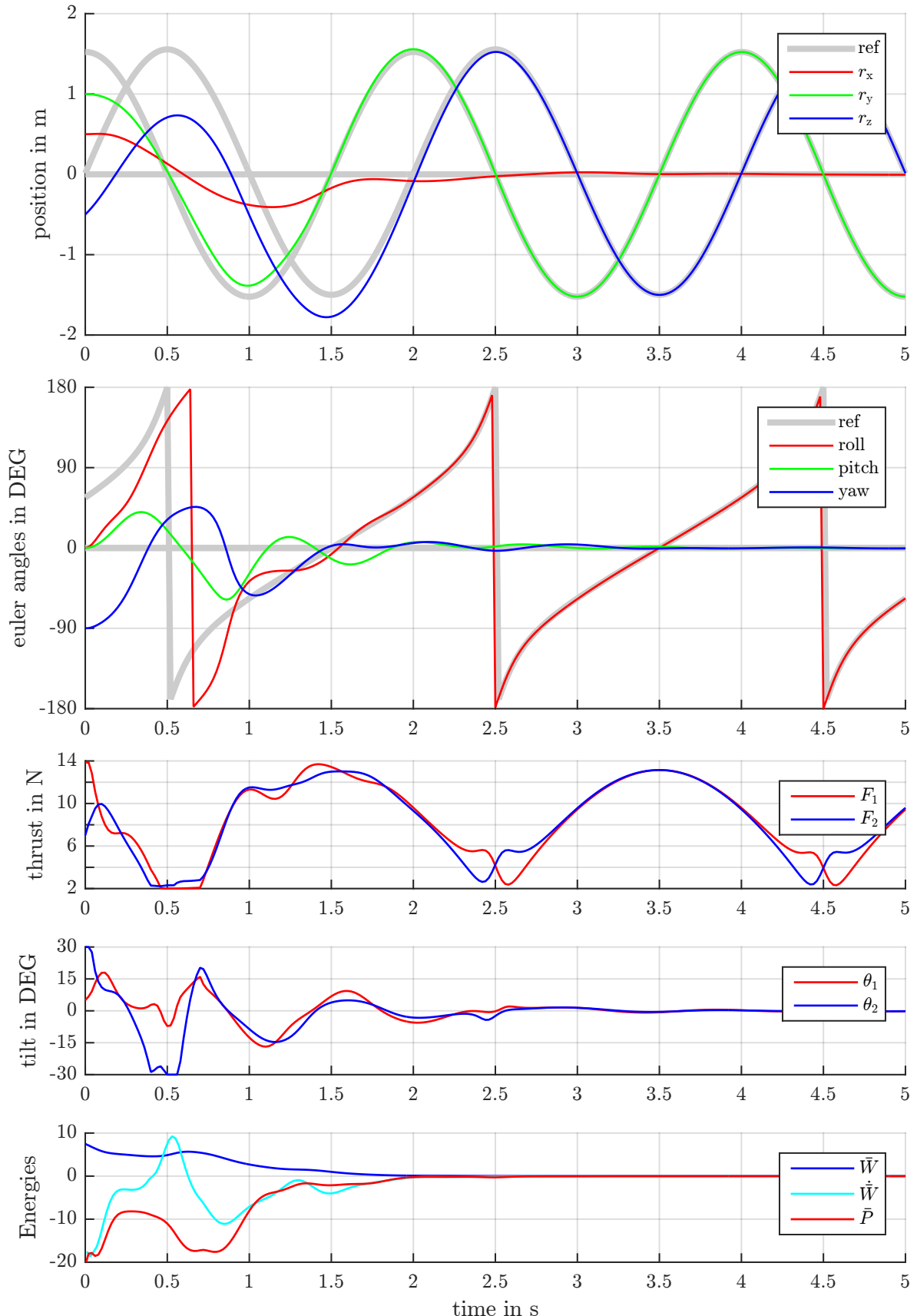


Figure 4.22: Simulation result for the Bicopter

# Chapter 5

## Multicopter control realization

This chapter describes the realization and discusses the experimental results with the LSR-Multicopters. On the highest abstraction layer they can be regarded as a single rigid body with body fixed forces (the propellers forces and torques). The tracking control of these models has been extensively discussed in the previous chapter.

- Hardware realization
  - mechanical construction,
  - actuators/Propellers, power electronics
  - sensorics
  - communication
  - framework for controller implementation
- mathematical model of the multicopters (Quadcopter, Tricopter)
  - full model: multibody, servo dynamics, propeller model, propeller motor model
  - simplified model for control design
  - model validation
- control of the actuators to generate the required generalized force on the rigid body
  - propeller control
  - servo control
  - Quadcopter force vector control
- state estimation
  - misalignment correction
  - Sensor model: IMU & Vicon
  - velocity and bias observer
  - configuration observer

- reference generation
  - for pilot supporting control
  - for position control
- rigid body controller
  - pilot supporting control
  - full configuration control
  - comparison to other controllers
- control integral action
- experiments
  - Maneuver42
  - maneuver53 (flip)
  - loop (the real loop)

## 5.1 Hardware & software realization

blah Figure 5.1

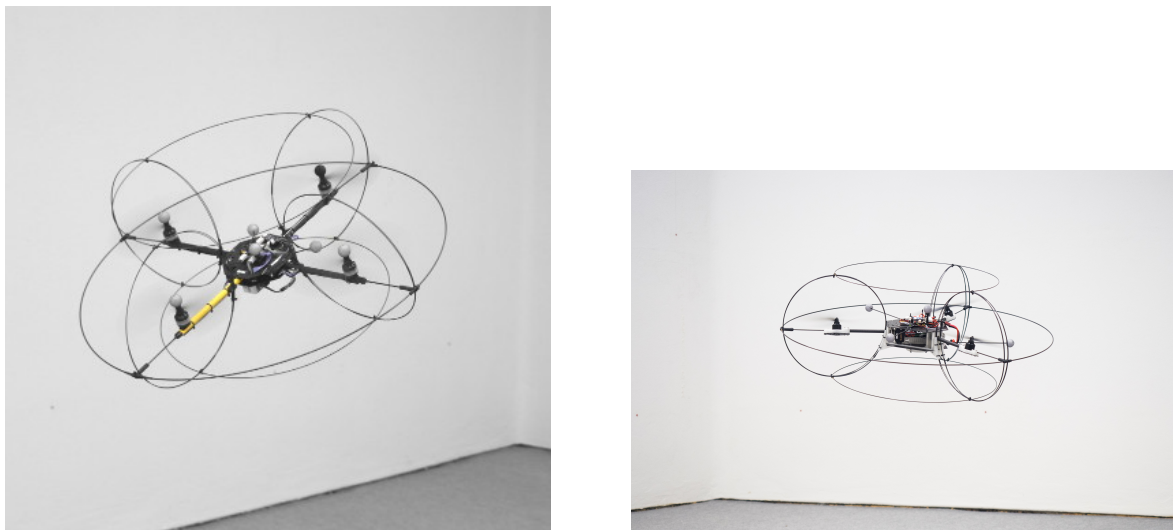


Figure 5.1: LSR-Quad- and Tricopter

The developed tricopter shown in Figure 5.1 is characterized by the three independently tiltable, propeller supporting arms. The central body and the arms are a sandwich construction of carbon-fiber plates and tubes and 3d-printed parts. The outer carbon-fiber rings serve as collision protection and landing gear. The vehicle has an outer diameter of about 0.8 m and a mass of about 1.2 kg.

The tilting mechanism is driven by a standard hobby servo motor that is connected to a gear on the arm by a toothed-belt and allows for tilt angles of  $\pm 75^\circ$ . The three 10 inch

propellers are each driven by a brushless dc-motor (BLDC) capable of angular velocities up to 120 Hz, corresponding to a maximum thrust of 8 N. As energy source the tricopter carries a 14.8 V, 2.2 Ah LiPo battery that allows for up to 15 min of autonomous flight.

Two types of sensors are used by the tricopter: An inertial measurement unit (IMU) VN100s from VECTORNAV is mounted on the central body to measure its angular velocity and acceleration and provide attitude estimates. An external camera-based motion capture system from VICON measures position and attitude by way of reflective markers on the tricopter.

A standard two-joystick remote control is used as a reliable and near real-time user interface to the vehicle while a pair of XBee S6B Wi-Fi modules provides a two-way communication link with a groundstation PC. The important hardware components are summarized in Figure 5.2.

The onboard electronics consist mainly of a custom-built mainboard and three identical motor drivers. The mainboard contains an Atmel AT32UC3C 32-bit, 66 MHz microcontroller with FPU and is tasked with executing all control algorithms. Although compact brushless-dc motor drivers are ubiquitous, available products typically lack explicit speed control. Moreover, while the rotor speed is implicitly known to the driver through electrical commutation, speed feedback necessary for an external control implementation is usually not provided. As a result, a custom module was developed that provides such a measurement while implementing an underlying current controller to drive the motor. This solution allows for rapid propeller dynamics described further in (??) that include active braking, achieved by feeding current back into the battery.

## 5.2 Multicopter Models

### 5.2.1 Actuator models

**Propeller motor.** The propellers are mounted on a small brushless DC motor (BLDC) which is controlled by dedicated BLDC driver electronics. This driver implements the electronic commutation and a digital current control with sampling frequency of 64 kHz. It gets the desired current  $i_M$  from the maincontroller with the sampling frequency of 200 Hz. Consequently we assume that all electrical dynamics of the propeller drive are negligible on the timescale of the main controller and the motor torque on the propeller is

$$\tau_M = k_M i_M. \quad (5.1)$$

friction

**Servo motor.** On the tricopter there are servo motors controlling the tilt  $\theta$  of the propellers. These are standard hobbyist servos which combine a small motor, a gearbox, a potentiometer and some digital controller which takes the desired servo angle  $\theta_R$  as input. The integrated controller is probably a fast PID controller since it handles constant loads

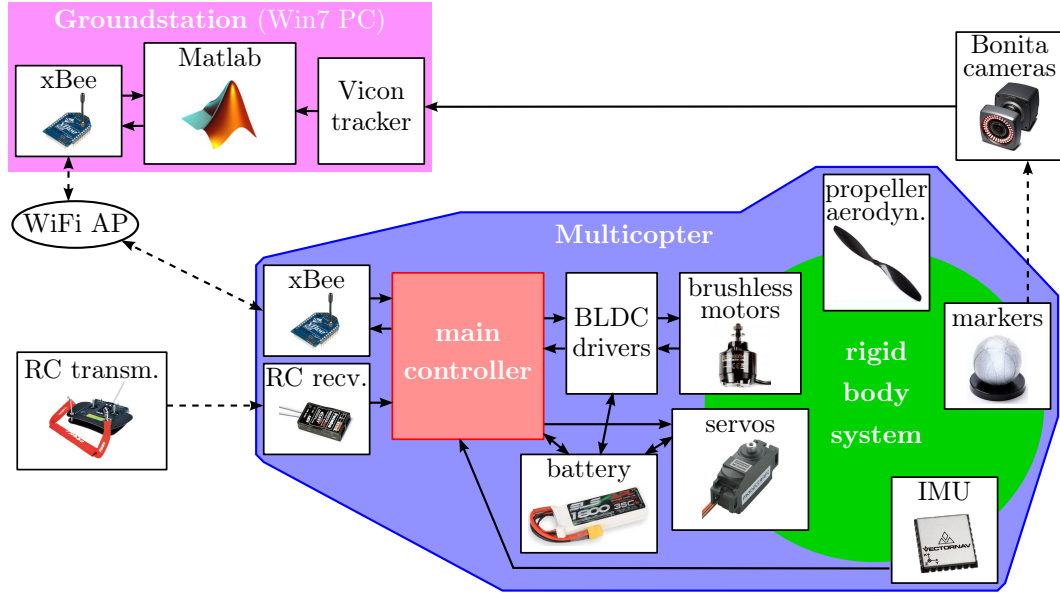


Figure 5.2: Multicopter Hardware realization

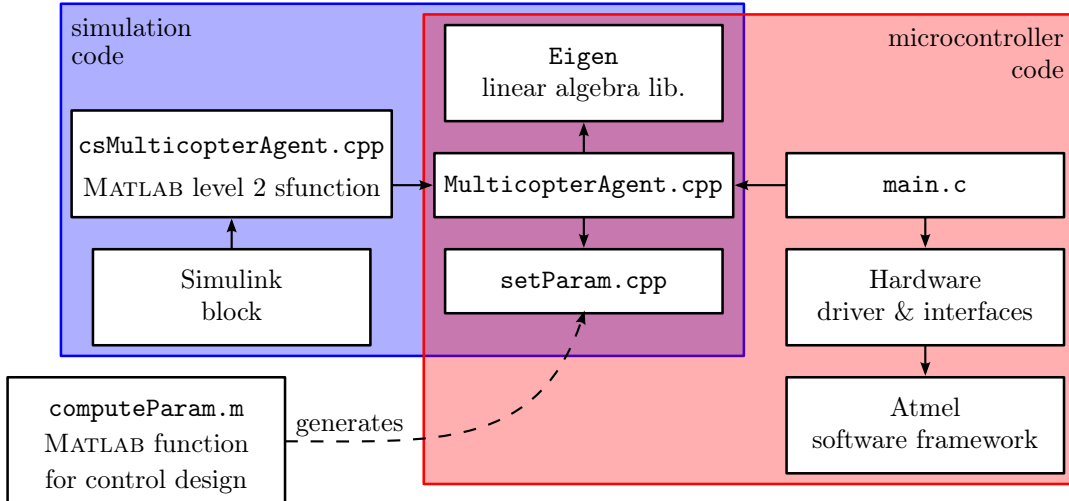


Figure 5.3: Controller code structure

as well as fast transitions quite well. However, here we assume that the servo torque arises from a simple PD-controller

$$\tau_S = k_{PS}(\theta_R - \theta) - k_{DS}\dot{\theta}. \quad (5.2)$$

**blah validation**

### 5.2.2 Propeller aerodynamics

Here we like to model the propellers, i.e. the forces and torques resulting from its rotation. A general theory of propellers is quite sophisticated, see e.g. [Johnson, 1980]. However, for the small, rigid propellers used here (and most common for multicopters of this size)

and for the working regime of this text it is sufficient to consider a very simple model:

$$F = \kappa_F \varpi^2, \quad \tau = -\kappa_T \varpi^2. \quad (5.3)$$

where  $\varpi$  is the angular velocity of the propeller. The propeller thrust  $F$  is directed along its spinning direction and the propeller drag  $\tau$  acts opposing the spinning direction. The model parameters  $\kappa_F$  and  $\kappa_T$  arise from the propeller geometry but will be identified in dedicated experiments. This model is quite common within the corresponding literature, it is also used in e.g. [Hamel et al., 2002], [Mellinger et al., 2012] or [Fritsch, 2014].

In [Bristeau et al., 2009] and [Martin and Salaun, 2010] a more sophisticated aerodynamic model for a quadcopter of about the same size as the one used here is proposed. It mainly adds dissipative forces that are bilinear in the propeller velocities  $\varpi$  and the rigid body velocities  $\mathbf{v}$  and  $\boldsymbol{\omega}$ . For this it introduces 8 additional constant model parameters. Even though their model has a nice physical derivation it does not fit to the experimental observations done for this work.

It does, however, give a physical motivation for linear drag on the multicopter body.

### 5.2.3 Dissipative forces

We assume a linear damping model for the overall multicopter

$$\begin{bmatrix} F_D \\ \tau_D \end{bmatrix} = \begin{bmatrix} D_v & D_v \text{ wed}(\mathbf{l})^\top \\ \text{wed}(\mathbf{l})D_v & \boldsymbol{\Upsilon} \end{bmatrix} \begin{bmatrix} \mathbf{v} \\ \boldsymbol{\omega} \end{bmatrix} \quad (5.4)$$

where  $D_v = \text{diag}(d_x, d_y, d_z)$ ,  $\mathbf{l} = [0, 0, l_z]^\top$ ,  $\boldsymbol{\Upsilon} = \text{diag}(\Upsilon_x, \Upsilon_y, \Upsilon_z)$ .

### 5.2.4 Rigid body model

A rigid body model for a generic multicopter with tiltable propellers has been extensively discussed in section 3.4. The rigid body model for the quadcopter and tricopter arises by setting special parameter values.

**Coordinates and Kinematics.** We choose the configuration coordinates

$$\mathbf{x} = [\mathbf{r}^\top, \text{vec}(\mathbf{R})^\top, \theta^\top, \psi^\top]^\top \in \mathbb{R}^{12+2\rho} \quad (5.5)$$

where  $\mathbf{r} \in \mathbb{R}^3$  is the position of the center body,  $\mathbf{R} \in \mathbb{SO}(3)$  its orientation matrix,  $\theta = [\theta_1, \dots, \theta_\rho]^\top \in \mathbb{R}^\rho$  the arm tilt angles and  $\psi = [\psi_1, \dots, \psi_\rho]^\top \in \mathbb{R}^\rho$  the angles of the propellers, see Figure 5.4. Note that the propellers are asymmetric, i.e. designed only for either clockwise or counter-clockwise rotation, and will only rotate in this direction during operation. The propeller angles  $\psi_k$  are defined, such that  $\dot{\psi}_k > 0$  during operation. To recover the spinning directions we use the parameter  $\varepsilon_k = 1$  for a positive/counter-clockwise and  $\varepsilon_k = -1$  for a negative/clockwise spinning propeller.

To capture the velocity state of the system we use the velocity coordinates

$$\boldsymbol{\xi} = [\mathbf{v}, \boldsymbol{\omega}, \dot{\theta}, \varpi]^\top \in \mathbb{R}^{6+2\rho}, \quad (5.6)$$

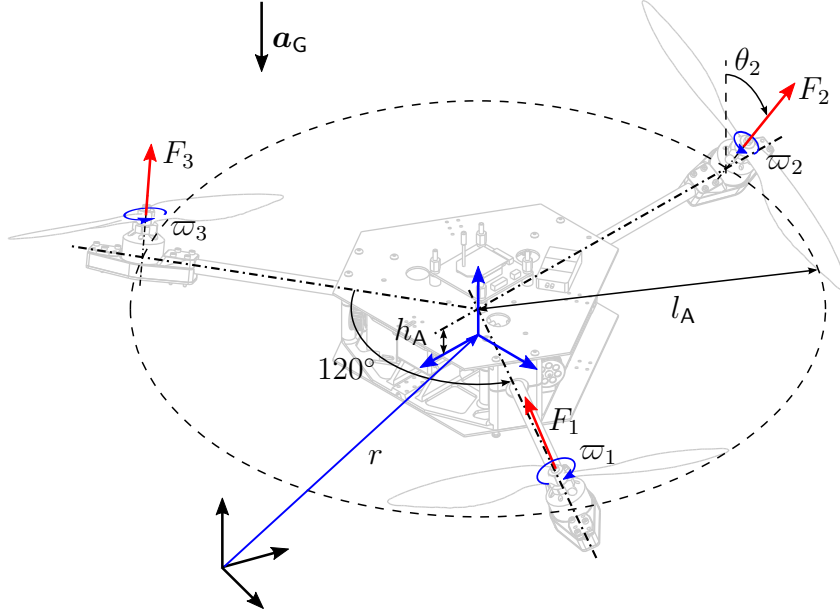


Figure 5.4: Mechanical model of the tricopter

related to the configuration coordinates by

$$\dot{\mathbf{r}} = \mathbf{R}\mathbf{v}, \quad \dot{\mathbf{R}} = \mathbf{R} \text{ wed}(\boldsymbol{\omega}), \quad \dot{\psi} = \varpi. \quad (5.7)$$

**Kinetic equation.** The algorithm proposed in section 3.4 does of course handle general mass distributions of the rigid bodies, but the resulting kinetic equations are far too cumbersome to display here explicitly. Instead we do some assumptions on the body inertia matrices that will lead to a condensed system inertia matrix: We assume that the combined center of mass of one arms and its propeller lies on the tilt axis. This already implies that the overall center of mass  $\mathbf{s} \in \mathbb{R}^3$  of the system is constant w.r.t. the body fixed frame. This was one goal during the construction process of the Tricopter. Furthermore, we assume that the combined moment of inertia of one arm and propeller is symmetric about the tilt axis. This is not the case for the real inertia parameters. However, it is justified by the fact that the overall inertia  $\boldsymbol{\Theta}$  changes only slightly depending on the arm tilts  $\theta$  or the propeller angles  $\psi$ . A crucial thing to get the overall dynamics right is to consider the rotor of the servo motor. The relevant moment of inertia  $\Theta_{Sxx}$  might be very small, but since it is located behind a gearbox with transmission ratio  $c_S = 625$  its contribution to the system inertia matrix is significant. The validity of the model with these assumptions will be discussed later by comparison to experimental data.

With the above assumptions the kinetic equation for the multicopter takes the form

$$\mathbf{M}(\theta)\dot{\boldsymbol{\xi}} + \mathbf{c}(\theta, \boldsymbol{\xi}) + \mathbf{D}\boldsymbol{\xi} + \mathbf{f}^G(\mathbf{R}) = \mathbf{f}^P(\theta, \varpi) + \mathbf{f}^U(\tau_M, \tau_S) + \mathbf{f}^B \quad (5.8)$$

where

$$\mathbf{M}(\theta) = \begin{bmatrix} m\mathbf{I}_3 & m \text{wed}(\mathbf{s})^\top & 0 & 0 \\ m \text{wed}(\mathbf{s}) & \boldsymbol{\Theta} & \Theta_{AC}H_1 & \Theta_P H_3(\theta) \text{diag}(\varepsilon) \\ 0 & \Theta_{AC}H_1^\top & \Theta_A \mathbf{I}_\rho & 0 \\ 0 & \Theta_P \text{diag}(\varepsilon)H_3^\top(\theta) & 0 & \Theta_P \mathbf{I}_\rho \end{bmatrix}, \quad (5.9a)$$

$$\mathbf{c}(\theta, \xi) = \begin{bmatrix} \text{wed}(\boldsymbol{\omega})p_v \\ \text{wed}(\mathbf{v})p_v + \text{wed}(\boldsymbol{\omega})p_\omega + \Theta_P H_4(\theta) \text{diag}(\dot{\theta}) \text{diag}(\varepsilon) \varpi \\ -\Theta_P \text{diag}(\text{diag}(\varepsilon)H_4^\top(\theta)\boldsymbol{\omega})\varpi \\ \Theta_P \text{diag}(\text{diag}(\varepsilon)H_4^\top(\theta)\boldsymbol{\omega})\dot{\theta} \end{bmatrix}, \quad (5.9b)$$

$$\mathbf{D} = \begin{bmatrix} D_v & D_v \text{wed}(\mathbf{l})^\top & 0 & 0 \\ \text{wed}(\mathbf{l})D_v & \boldsymbol{\Upsilon} & 0 & 0 \\ 0 & 0 & 0 & 0 \\ 0 & 0 & 0 & 0 \end{bmatrix}, \quad \mathbf{f}^G(\mathbf{R}) = \begin{bmatrix} m\mathbf{I}_3 \\ m \text{wed}(\mathbf{s}) \\ 0 \\ 0 \end{bmatrix} \mathbf{R}^\top(-\mathbf{a}_G), \quad (5.9c)$$

$$\mathbf{f}^P(\theta, \varpi) = \begin{bmatrix} \kappa_F H_3(\theta) \\ \kappa_F(l_A H_4(\theta) + h_A H_2(\theta)) - \kappa_T H_3(\theta) \text{diag}(\varepsilon) \\ 0 \\ -\kappa_T \mathbf{I}_\rho \end{bmatrix} \text{diag}(\varpi) \varpi, \quad (5.9d)$$

$$\mathbf{f}^U(\tau_M, \tau_S) = \begin{bmatrix} 0 \\ 0 \\ \tau_S \\ \tau_M \end{bmatrix} \quad \mathbf{f}^B = \begin{bmatrix} F_B \\ \tau_B \\ 0 \\ \tau_{MB} \end{bmatrix} \quad (5.9e)$$

with the (just for readability) substituted momenta

$$p_v = m(\mathbf{v} - \text{wed}(\mathbf{s})\boldsymbol{\omega}), \quad (5.9f)$$

$$p_\omega = m \text{wed}(\mathbf{s})\mathbf{v} + \boldsymbol{\Theta}\boldsymbol{\omega} + \Theta_{AC}H_1\dot{\theta} + \Theta_P H_3(\theta) \text{diag}(\varepsilon) \varpi. \quad (5.9g)$$

and the sub-matrices

$$H_1 = \begin{bmatrix} c_{\varphi_1} & \cdots & c_{\varphi_\rho} \\ s_{\varphi_1} & \cdots & s_{\varphi_\rho} \\ 0 & \cdots & 0 \end{bmatrix}, \quad H_2(\theta) = \begin{bmatrix} c_{\varphi_1}s_{\theta_1} & \cdots & c_{\varphi_\rho}s_{\theta_\rho} \\ s_{\varphi_1}s_{\theta_1} & \cdots & s_{\varphi_\rho}s_{\theta_\rho} \\ 0 & \cdots & 0 \end{bmatrix}, \quad (5.9h)$$

$$H_3(\theta) = \begin{bmatrix} s_{\varphi_1}s_{\theta_1} & \cdots & s_{\varphi_\rho}s_{\theta_\rho} \\ -c_{\varphi_1}s_{\theta_1} & \cdots & -c_{\varphi_\rho}s_{\theta_\rho} \\ c_{\theta_1} & \cdots & c_{\theta_\rho} \end{bmatrix}, \quad H_4(\theta) = \begin{bmatrix} s_{\varphi_1}c_{\theta_1} & \cdots & s_{\varphi_\rho}c_{\theta_\rho} \\ -c_{\varphi_1}c_{\theta_1} & \cdots & -c_{\varphi_\rho}c_{\theta_\rho} \\ -s_{\theta_1} & \cdots & -s_{\theta_\rho} \end{bmatrix} \quad (5.9i)$$

**Tricopter.** To get the rigid body model equations for the Tricopter (displayed in Figure 5.4) we can plug the following parameters into (5.9)

$$\rho = 3, \quad \varphi = \frac{\pi}{3}[1, 3, 5]^\top, \quad \varepsilon = [-1, +1, +1]^\top. \quad (5.10)$$

However, the model equations do not simplify too much and are not displayed explicitly here.

**Quadcopter.** For the Quadcopter model we have the parameters (see Figure 5.5)

$$\rho = 4, \quad \varphi = \frac{\pi}{2}[0, 1, 2, 3]^\top, \quad \varepsilon = [+1, -1, +1, -1]^\top, \quad \theta = [0, 0, 0, 0]^\top. \quad (5.11)$$

Here the model equations simplify significantly. Since the propellers do not tilt  $\theta = 0$ , the corresponding equations can be regarded as definition of reaction torques  $\tau_S$  and dropped from the model equations. Overall the model for the Quadcopter is

$$\mathbf{M} = \begin{bmatrix} m\mathbf{I}_3 & -m \text{wed}(\mathbf{s}) & 0 \\ m \text{wed}(\mathbf{s}) & \boldsymbol{\Theta} & \boldsymbol{\Theta}_{\mathbf{P}} H_3 \text{diag}(\varepsilon) \\ 0 & \boldsymbol{\Theta}_{\mathbf{P}} \text{diag}(\varepsilon) H_3^\top & \boldsymbol{\Theta}_{\mathbf{P}} \mathbf{I}_4 \end{bmatrix}, \quad (5.12a)$$

$$\mathbf{c}(\boldsymbol{\xi}) = \begin{bmatrix} \text{wed}(\boldsymbol{\omega}) & 0 & 0 \\ \text{wed}(\mathbf{v}) & \text{wed}(\boldsymbol{\omega}) & 0 \\ 0 & 0 & 0 \end{bmatrix} \mathbf{M} \boldsymbol{\xi}, \quad \mathbf{f}^G(\mathbf{R}) = \begin{bmatrix} m\mathbf{I}_3 \\ m \text{wed}(\mathbf{s}) \\ 0 \end{bmatrix} \mathbf{R}^\top (-\mathbf{a}_G), \quad (5.12b)$$

$$\mathbf{f}^P(\varpi) = \begin{bmatrix} \kappa_F H_3 \\ \kappa_F l_A H_4 - \kappa_T H_3 \text{diag}(\varepsilon) \\ -\kappa_T \mathbf{I}_4 \end{bmatrix} \text{diag}(\varpi) \varpi, \quad \mathbf{f}^U(\tau_M) = \begin{bmatrix} 0 \\ 0 \\ \tau_M \end{bmatrix} \quad (5.12c)$$

with the sub-matrices

$$H_3 = \begin{bmatrix} 0 & 0 & 0 & 0 \\ 0 & 0 & 0 & 0 \\ 1 & 1 & 1 & 1 \end{bmatrix}, \quad H_4 = \begin{bmatrix} 0 & 1 & 0 & -1 \\ -1 & 0 & 1 & 0 \\ 0 & 0 & 0 & 0 \end{bmatrix}. \quad (5.12d)$$

Note that the system inertia matrix  $\mathbf{M}$  is constant, but there is still an inertial coupling between the propeller velocities  $\varpi$  and  $\omega_z$ . The same model up to different dissipative forces has been derived in [Martin and Salaun, 2010]. In [Hamel et al., 2002] a quadcopter model is proposed which is similar ...

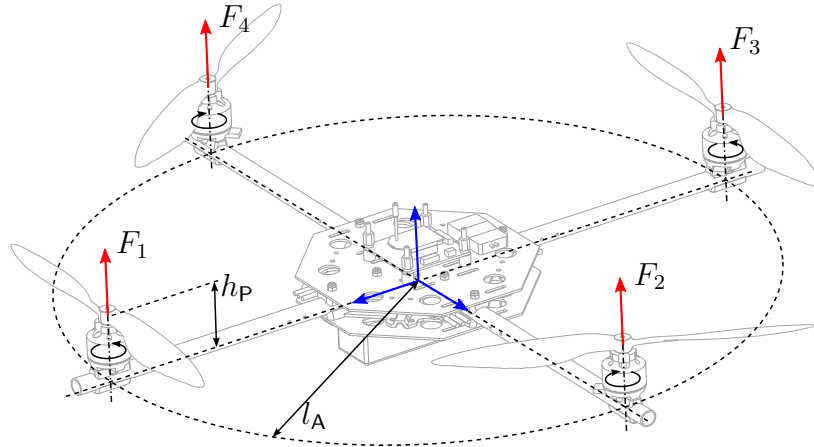


Figure 5.5: Propeller forces on the Quadcopter

### 5.2.5 Parameter identification

The preceding mathematical model for the multicopters contains various constant parameters of which only the total mass  $m$  and the arm radius  $l_A$  can be measured directly. Some crucial parameters are identified in dedicated experimental setups which will be discussed in the following. The remaining parameters are estimated by the method of least squares ...

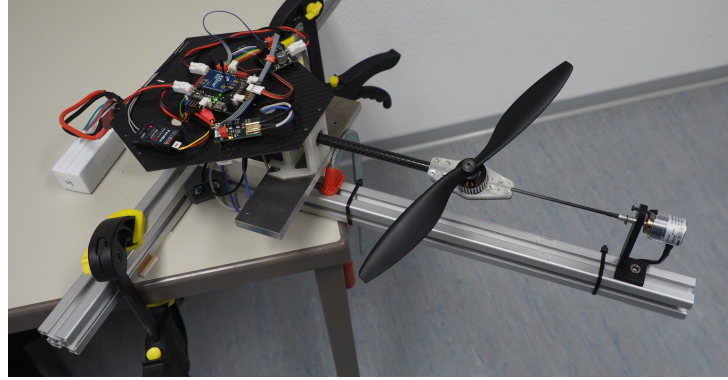


Figure 5.6: Test bench for the propeller and tilting mechanism

**Propeller and servo drive.** For the identification of the propeller drive and its tilting mechanism we use a dedicated test bench, see Figure 5.6. It is essentially one mounted Tricopter arm with additional high resolution sensors for the tilt  $\theta$  and propeller velocity  $\varpi$ .

The equations of motion for the test bench are

$$\dot{\varpi} + \underbrace{\frac{\kappa_T}{\Theta_P}}_{p_{P1}} \varpi^2 = \underbrace{\frac{k_M}{\Theta_P} i_M}_{p_{P2}} + \underbrace{\frac{\tau_{MB}}{\Theta_P}}_{p_{P3}} \quad (5.13)$$

$$\ddot{\theta} + \underbrace{\frac{k_{DS}}{\Theta_A}}_{p_{S1}} \dot{\theta} + \underbrace{\frac{k_{PS}}{\Theta_A}}_{p_{S0}} \theta = \underbrace{\frac{k_{PS}}{\Theta_A}}_{p_{S0}} \theta_U \quad (5.14)$$

The equations are normalized, yielding the parameters  $p_{P1}$ ,  $p_{P2}$ ,  $p_{P3}$  and  $p_{S0}$ ,  $p_{S1}$ , which will become mode convenient later. These parameters can be directly estimated by the method of least squares. The inertia parameters  $\Theta_P$  and  $\Theta_A$  are calculated from the detailed CAD model of the multicopters. With them one could recover the original parameters  $\kappa_T$ ,  $k_{PS}$ , etc.. The identified parameter values are summarized in Table 5.1.

The accuracy of the proposed model and its identified parameters can be seen from the results in Figure 5.12 and Figure 5.13 in section 5.4. An online estimation of the bias parameter  $p_{P3}$  by means of an observer will be discussed there as well.

**Propeller thrust.** For identification of the thrust constant  $\kappa_F$ , a propeller drive was mounted horizontally on a 1 m tall pole. The pole in turn stands on a digital scale and the “weight” was recorded at different propeller speeds  $\varpi$ . From this “weight” we can compute the corresponding propeller thrust  $F$ . The measurements are displayed in Figure 5.7 together with the model  $F = \kappa_F \varpi^2$  with the identified parameter value  $\kappa_F = 1.44 \cdot 10^{-5} \text{ N s}^2$ .

**Rigid body inertia.** For identification of the inertia parameters  $\Theta_{xx}$ ,  $\Theta_{yy}$  and  $\Theta_{zz}$  for Tri- and Quadcopter a dedicated experiment was conducted. The body was suspended by two strings as shown on the left side of Figure 5.8. The basic idea is that a rotation of the body about the vertical axis results in a upward movement of the body which is countered by gravity.

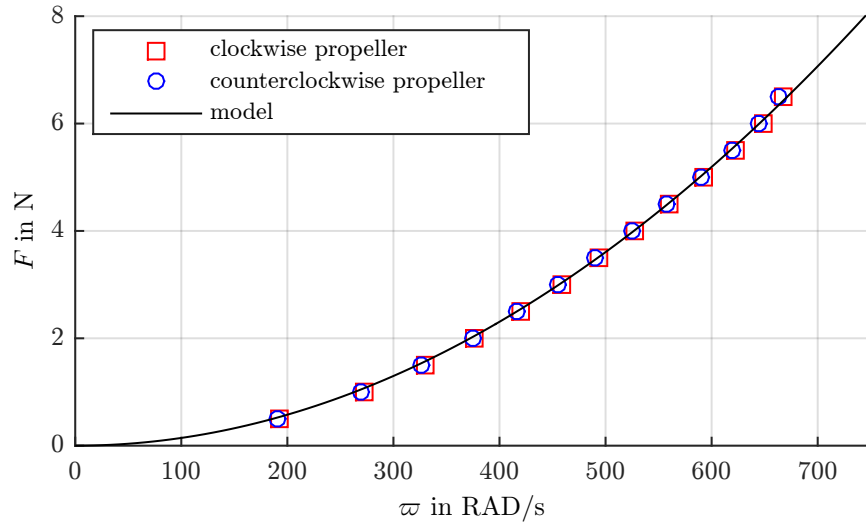
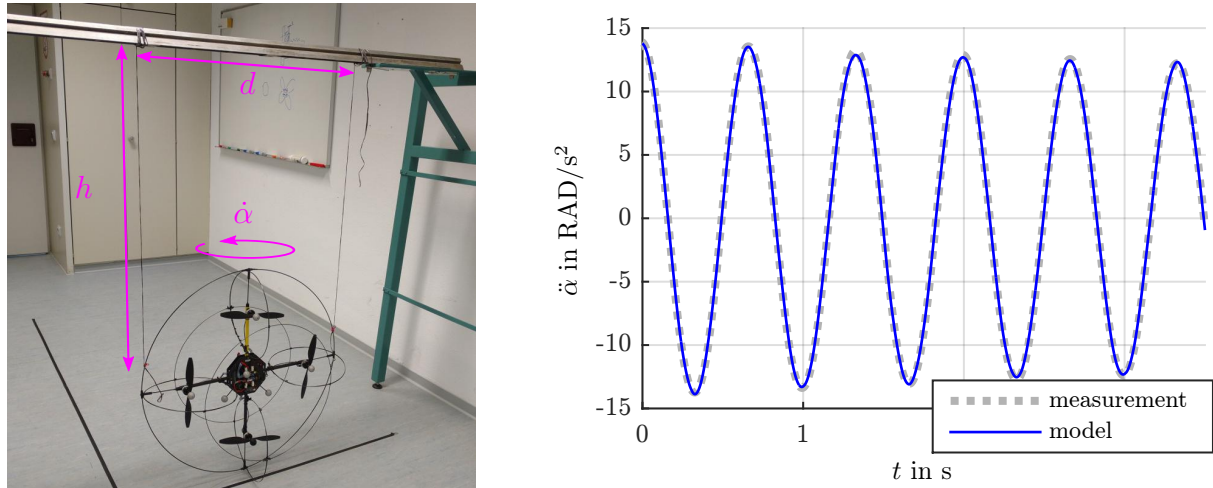


Figure 5.7: Measured propeller thrust compared to proposed model

Figure 5.8: Experimental setup and identification result for  $\Theta_{xx}$  of the Quadcopter

The equation of motion for the vertical rotation with angle  $\alpha$  in this setup is

$$\Theta \ddot{\alpha} + mg \frac{d^2 \sin \alpha}{4\sqrt{h^2 - \frac{d^2}{2}(1 - \cos \alpha)}} = 0. \quad (5.15)$$

Here  $m$  indicated the total mass of the copter,  $g = 9.81 \text{ m/s}^2$  is the gravitational acceleration,  $d$  and  $h$  are the distance and length of the strings. From the measured trajectory  $t \mapsto \alpha$  of the twist angle we can estimate the inertia  $\Theta$  about the corresponding axis. On the right side of Figure 5.8, the acceleration  $\ddot{\alpha}$  computed from the model (5.15) with the estimated parameters is plotted against the measured acceleration.

This test was conducted for all three axis, i.e. for  $\Theta_{xx}$ ,  $\Theta_{yy}$  and  $\Theta_{zz}$  for Tri- and Quadcopter and the resulting parameters are given in Table 5.1. The identified parameters match the values computed from a detailed CAD model by  $\pm 10\%$ .

**Parameter identification from flight test.** The model (5.8) still contains several so far unknown parameters: The coordinates of the center of mass  $\mathbf{s} = [s_x, s_y, s_z]^\top$ , the off-diagonal entries  $\Theta_{xy}$ ,  $\Theta_{xz}$  and  $\Theta_{yz}$  of the inertia matrix and the inertia parameter  $\Theta_{AC}$ . The translational damping  $d_x$ ,  $d_z$ , the rotational damping  $\Upsilon_x$ ,  $\Upsilon_z$  and the coordinate  $l_z$  of the center of damping.

With some auxiliary transformation ( $\tilde{l}_z = d_x l_z$ ,  $\tilde{\Upsilon}_x = \Upsilon_x + d_z l_z^2$ ) the first 6 model equations (5.8) are linear in the remaining unknown parameters. So we can identify these by the method of least squares from flight test measurements. Table 5.1 summarizes the identified parameter values from this flight test as well as the ones from the previously discussed dedicated experiments. These are the values that are used for the simulator.

From this experiment we have the first estimate for the overall center of mass  $\mathbf{s}$  of Tri- and Quadcopter. The identified value  $s_z$  is then used to adjust the body fixed frame in the vertical direction such that  $s_z = 0\text{ m}$ . For the Tricopter this determines also the parameter  $h_A$ . The values for  $s_x$  and  $s_y$  are small so we stick to the geometric center in the horizontal directions.

The damping parameter values for the Tricopter are greater than the ones for the Quadcopter. This could be explained by the model from [Martin and Salaun, 2010] and the fact that the propellers of the Tricopter nominally spin 40% faster than on the Quadcopter. Also the identified value for  $l_z$  is roughly the distance from the body fixed frame to the propeller plane which fits well to their model. On the other hand, the identified translational damping  $d_z$  in the vertical direction is greater than the horizontal damping  $d_x$ . This contradicts the model proposed in [Martin and Salaun, 2010] which would imply  $d_z = 0$ .

Table 5.1 also shows identified constant bias forces  $F_B$  and torques  $\tau_B$  for this particular experiment. These mean values probably result from small misalignments of the propellers and servos rather than constant side wind or anything similar. In the practical application the bias forces will be estimated online by means of an observer, so can vary slowly. However, the magnitudes of the displayed identified values are less than 3% compared to the maximal available propeller forces  $\mathbf{f}^P$  in the corresponding directions, so their influence on the overall identification result should be small.

Symbol	Tricopter value	Quadcopter value	Source
$m$	1.251 kg	1.001 kg	directly measured
$s_x$	$1.7 \cdot 10^{-3}$ m	$-1.8 \cdot 10^{-3}$ m	flight test
$s_y$	$0.6 \cdot 10^{-3}$ m	$0.6 \cdot 10^{-3}$ m	flight test
$s_z$	$0.0 \cdot 10^{-3}$ m	$0.0 \cdot 10^{-3}$ m	manually adjusted
$\Theta_{xx}$	$19.2 \cdot 10^{-3}$ kg m <sup>2</sup>	$17.9 \cdot 10^{-3}$ kg m <sup>2</sup>	pendulum test
$\Theta_{yy}$	$19.2 \cdot 10^{-3}$ kg m <sup>2</sup>	$18.0 \cdot 10^{-3}$ kg m <sup>2</sup>	pendulum test
$\Theta_{zz}$	$30.8 \cdot 10^{-3}$ kg m <sup>2</sup>	$30.7 \cdot 10^{-3}$ kg m <sup>2</sup>	pendulum test
$\Theta_{xy}$	$-0.8 \cdot 10^{-3}$ kg m <sup>2</sup>	$-0.7 \cdot 10^{-3}$ kg m <sup>2</sup>	flight test
$\Theta_{xz}$	$-1.2 \cdot 10^{-3}$ kg m <sup>2</sup>	$0.2 \cdot 10^{-3}$ kg m <sup>2</sup>	flight test
$\Theta_{yz}$	$-2.1 \cdot 10^{-3}$ kg m <sup>2</sup>	$0.0 \cdot 10^{-3}$ kg m <sup>2</sup>	flight test
$d_x$	0.29 kg/s	0.30 kg/s	flight test
$d_z$	0.45 kg/s	0.36 kg/s	flight test
$l_z$	$4.0 \cdot 10^{-3}$ m	$12 \cdot 10^{-3}$ m	flight test
$\Upsilon_x$	$8.5 \cdot 10^{-3}$ kg m <sup>2</sup> /s	$-1.5 \cdot 10^{-3}$ kg m <sup>2</sup> /s	flight test
$\Upsilon_z$	$14 \cdot 10^{-3}$ kg m <sup>2</sup> /s	$10 \cdot 10^{-3}$ kg m <sup>2</sup> /s	flight test
$\mathbf{a}_G$	$[0, 0, -9.81]^\top$ m/s <sup>2</sup>		god given
$l_A$	$240 \cdot 10^{-3}$ m	$240 \cdot 10^{-3}$ m	directly measured
$h_A$	$-6 \cdot 10^{-3}$ m	-	manually adjusted
$\Theta_A$	0.9 kg m <sup>2</sup>	-	CAD model
$\Theta_{AC}$	0.002 kg m <sup>2</sup>	-	prop. test bench
$k_{PS}$	1400 Nm s <sup>2</sup>	-	prop. test bench
$k_{DS}$	66 Nm s	-	prop. test bench
$\Theta_P$	$3.6 \cdot 10^{-5}$ kg m <sup>2</sup>		CAD model
$\kappa_F$	$1.44 \cdot 10^{-5}$ N s <sup>2</sup>		prop. test bench
$\kappa_T$	$2.45 \cdot 10^{-7}$ Nm s <sup>2</sup>		prop. test bench
$k_M$	0.0105 Nm/A		prop. test bench
$\tau_{MB}$	0.005 Nm		prop. test bench
$F_{Bx}$	-0.21 N	0.09 N	flight test
$F_{By}$	-0.02 N	0.02 N	flight test
$F_{Bz}$	0.03 N	-0.09 N	flight test
$\tau_{Bx}$	0.037 Nm	0.049 Nm	flight test
$\tau_{By}$	-0.024 Nm	-0.015 Nm	flight test
$\tau_{Bz}$	-0.003 Nm	-0.012 Nm	flight test

Table 5.1: Parameter values for Tri- and Quadcopter

### 5.2.6 Model validation and simplification

In the previous subsections we proposed a quite detailed model for Tri- and Quadcopter. Now we like to validate this model by comparing it to experimental data. From this quantitative analysis we can also motivate which parts of the model can be neglected to obtain a simplified model that is still accurate enough for our working domain.

**Tricopter.** Figure 5.9 shows the accelerations  $\dot{\xi}$  during a 20 s sample of a benchmark flight test for the Tricopter. The gray lines are obtained by applying a Savitzky–Golay derivative filter to the measured generalized velocities  $\xi$ . The blue lines are the accelerations  $\dot{\xi}$  computed from the model (5.8) with the parameters from (5.1) and the measured configuration, velocity and inputs. The dashed red lines are the accelerations computed in the same way but from a simplified model that will be proposed now:

For the simplified model of the Tricopter we drop all off diagonal entries in the system inertia matrix  $\mathbf{M}$ . This means in particular  $s = 0$  and  $\Theta = \text{diag}(\Theta_x, \Theta_y, \Theta_z)$ . Furthermore we drop the damping parameters  $l_z = 0$ ,  $\Upsilon_x = \Upsilon_z = 0$  and assume isotropic translational damping  $D_v = d\mathbf{I}_3$  with  $d = \frac{1}{3}(2d_x + d_z)$ . The resulting model equations are summarized as follows:

**Simplified Tricopter model.** Rigid body dynamics

$$\dot{\mathbf{r}} = \mathbf{R}\mathbf{v}, \quad m\dot{\mathbf{v}} + \text{wed}(\boldsymbol{\omega})m\mathbf{v} + d\mathbf{v} - \mathbf{R}^\top(m\mathbf{a}_G) = \mathbf{F} + \mathbf{F}_B, \quad (5.16a)$$

$$\dot{\mathbf{R}} = \mathbf{R} \text{wed}(\boldsymbol{\omega}), \quad \Theta\dot{\boldsymbol{\omega}} + \text{wed}(\boldsymbol{\omega})\Theta\boldsymbol{\omega} = \boldsymbol{\tau} + \boldsymbol{\tau}_B, \quad (5.16b)$$

Generalized force from propellers

$$\underbrace{\begin{bmatrix} F_x \\ F_y \\ F_z \\ \tau_x \\ \tau_y \\ \tau_z \end{bmatrix}}_f = \underbrace{\begin{bmatrix} 0 & 0 & 0 & \frac{\sqrt{3}}{2} & 0 & -\frac{\sqrt{3}}{2} \\ 0 & 0 & 0 & -\frac{1}{2} & 1 & -\frac{1}{2} \\ 1 & 1 & 1 & 0 & 0 & 0 \\ \frac{\sqrt{3}l_A}{2} & 0 & -\frac{\sqrt{3}l_A}{2} & \frac{h_A}{2} + \frac{\sqrt{3}\kappa_T}{2\kappa_F} & h_A & \frac{h_A}{2} + \frac{\sqrt{3}\kappa_T}{2\kappa_F} \\ -\frac{l_A}{2} & l_A & -\frac{l_A}{2} & \frac{\sqrt{3}h_A}{2} - \frac{\kappa_T}{2\kappa_F} & \frac{\kappa_T}{\kappa_F} & \frac{\kappa_T}{2\kappa_F} - \frac{\sqrt{3}h_A}{2} \\ \frac{\kappa_T}{\kappa_F} & -\frac{\kappa_T}{\kappa_F} & -\frac{\kappa_T}{\kappa_F} & -l_A & -l_A & -l_A \end{bmatrix}}_B \underbrace{\begin{bmatrix} F_1^V \\ F_2^V \\ F_3^V \\ F_1^H \\ F_2^H \\ F_3^H \end{bmatrix}}_{F^{VH}} \quad (5.16c)$$

$$F_j^V = F_j \cos \theta_j, \quad F_j^H = F_j \sin \theta_j, \quad F_j = \kappa_F \varpi_j^2, \quad j = 1, 2, 3 \quad (5.16d)$$

Propeller drive dynamics

$$\dot{\varpi}_j + p_{P1}\varpi_j^2 = p_{P2}i_M j - p_{P3}, \quad j = 1, 2, 3. \quad (5.16e)$$

Servo dynamics

$$\ddot{\theta}_j + p_{S1}\dot{\theta}_j + p_{S0}\theta_j = p_{S0}\theta_{Uj}, \quad j = 1, 2, 3. \quad (5.16f)$$

Comparing the computed accelerations flight test in Figure 5.9 leads to the following

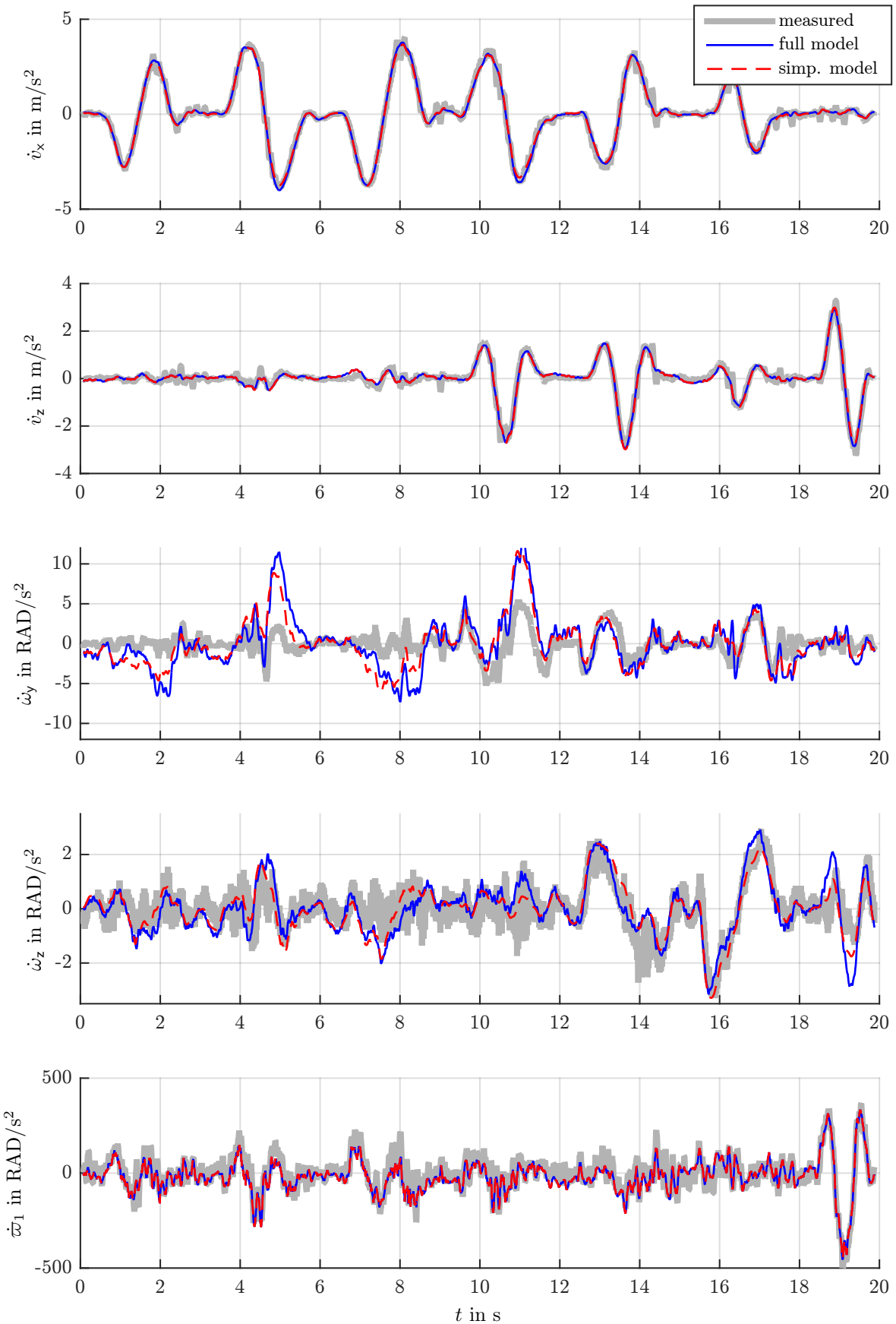


Figure 5.9: Model vs. measured accelerations for the Tricopter

conclusions: For the translational  $\dot{v}_x$ ,  $\dot{v}_z$  and the propeller acceleration  $\dot{\varpi}_1$  the two models can not be distinguished and they match the measured accelerations quite well. For the angular accelerations  $\dot{\omega}_x$  and  $\dot{\omega}_z$  the models differ slightly. Unfortunately, one cannot say that the full model matches the measured accelerations better than the simplified. This means that there are unmodeled effects that have a greater influence than the ones we dropped for the simplified model. Overall the simplified model (5.16) captures the Tricopter dynamics reasonably well and is due to its simplicity a good starting point for the model based control design.

**Quadcopter.** Neglect the inertial couplings between the center body and propeller except  $\Theta_P H_1 \dot{\varpi}$ . Assume  $s = 0$  and  $\Theta = \text{diag}(\Theta_x, \Theta_x, \Theta_z)$ .

Rigid body dynamics

$$\dot{r} = \mathbf{R} v, \quad m\dot{v} + \text{wed}(\boldsymbol{\omega})mv + d\mathbf{v} - \mathbf{R}^\top(m\mathbf{a}_G) = F_z e_3 + F_B, \quad (5.17a)$$

$$\dot{\mathbf{R}} = \mathbf{R} \text{wed}(\boldsymbol{\omega}), \quad \Theta \dot{\boldsymbol{\omega}} + \text{wed}(\boldsymbol{\omega})\Theta \boldsymbol{\omega} = \tau + \tau_B, \quad (5.17b)$$

Generalized force from propeller rotation

$$\underbrace{\begin{bmatrix} F_z \\ \tau_x \\ \tau_y \\ \tau_z \end{bmatrix}}_f = \underbrace{\begin{bmatrix} 1 & 1 & 1 & 1 \\ 0 & l_A & 0 & -l_A \\ -l_A & 0 & l_A & 0 \\ -\frac{\kappa_T}{\kappa_F} & \frac{\kappa_T}{\kappa_F} & -\frac{\kappa_T}{\kappa_F} & \frac{\kappa_T}{\kappa_F} \end{bmatrix}}_B \underbrace{\begin{bmatrix} \kappa_F \varpi_1^2 \\ \kappa_F \varpi_2^2 \\ \kappa_F \varpi_3^2 \\ \kappa_F \varpi_4^2 \end{bmatrix}}_F - \begin{bmatrix} 0 \\ 0 \\ 0 \\ \Theta_P (\dot{\varpi}_1 - \dot{\varpi}_2 + \dot{\varpi}_3 - \dot{\varpi}_4) \end{bmatrix} \quad (5.17c)$$

Propeller drive dynamics

$$\Theta_P \dot{\varpi}_j + \kappa_T \varpi_j^2 = k_{Mj} i_{Mj} - \tau_{MBj}, \quad j = 1, \dots, 4. \quad (5.17d)$$

## 5.3 Controller Structure

The structure of the model suggests a cascaded approach for the controller.

## 5.4 Control of the generalized force

1. Servo simulation
2. Propeller tracking control
3. Tricopter force filter
4. Quadcopter force filter

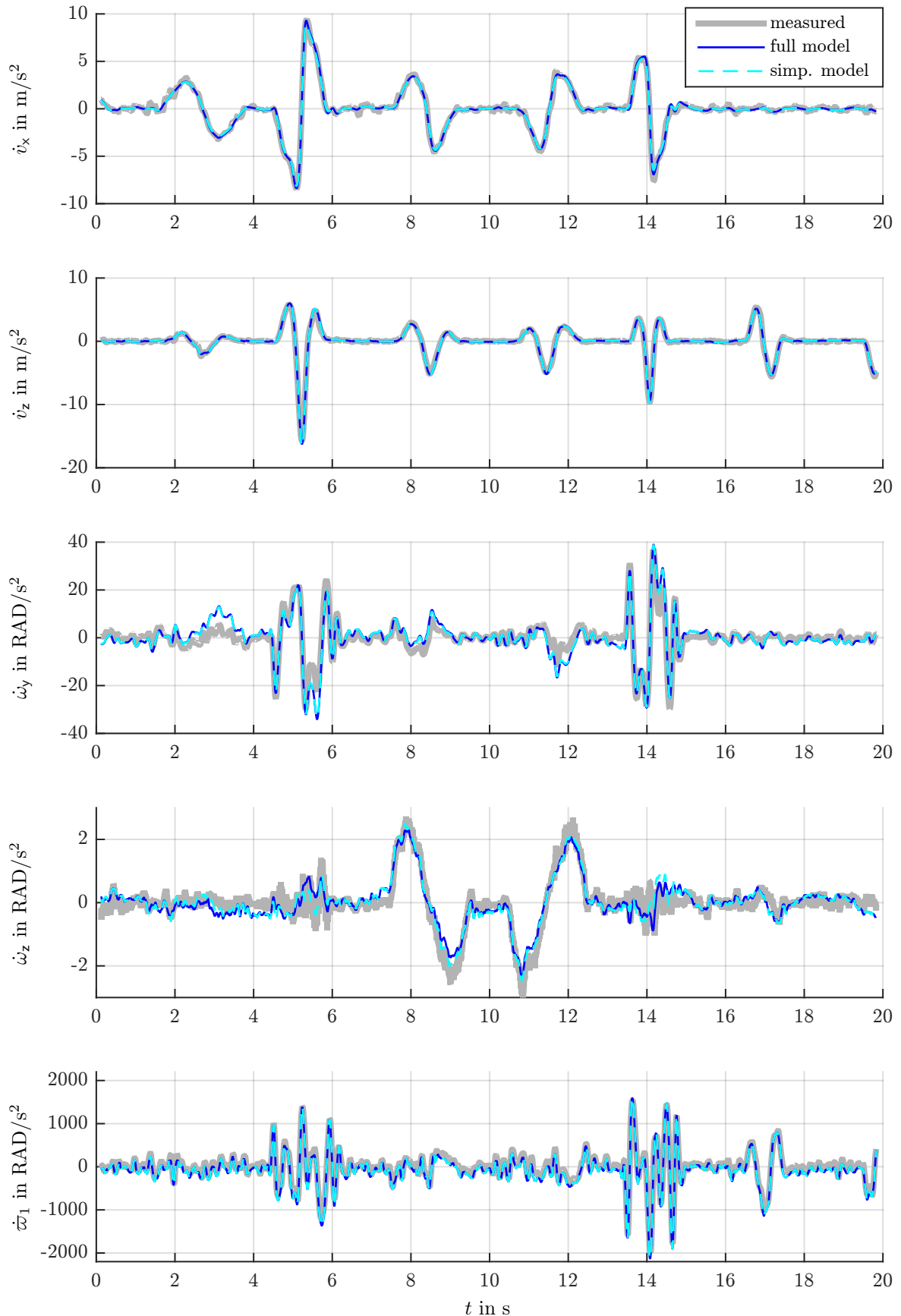


Figure 5.10: Model vs. measured accelerations on the quadcopter

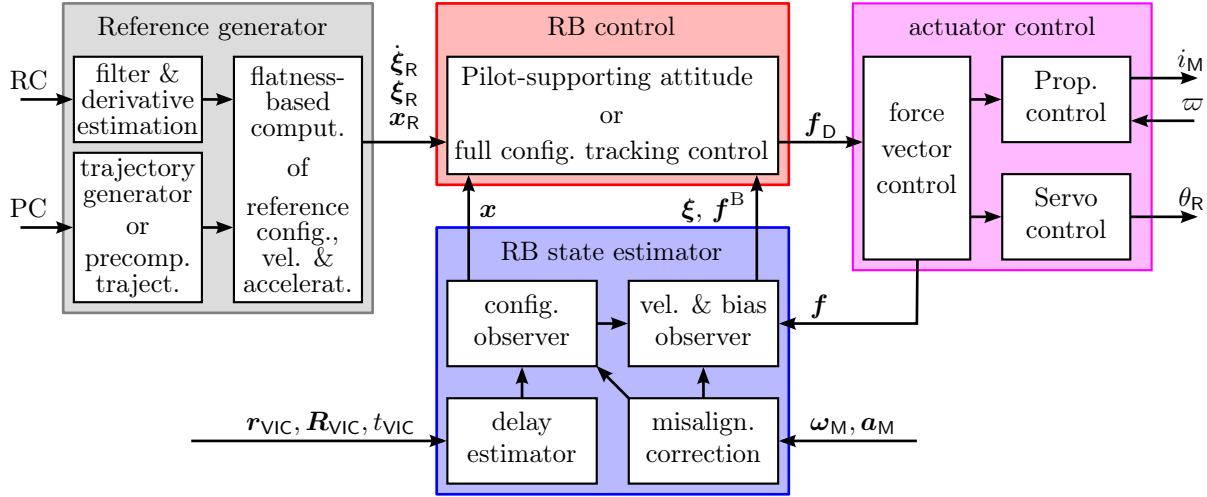


Figure 5.11: Structure of the Multicopter Agent

## 5. reconstruction of the generalized force

The rigid body controller computes a *desired* generalised force  $\mathbf{f}_D$  for the corresponding multicopter. Since the force  $\mathbf{f}$  itself is subject to its own actuator dynamics (see section 5.2), it is not possible to realize it instantaneously. However, we can pursue to realise it reasonably fast, which is the subject of this section. At the same time we need an accurate estimate for the current generalized force for the rigid body observer.

### 5.4.1 Servo simulation

The integrated servo controller uses an internal angle measurement but this is not available for the main controller. So for validation of the servo dynamics (5.16f) and identification of its parameters  $p_{S0}$  and  $p_{S1}$ , a dedicated test bench with an incremental encoder for the tilt angle  $\theta$  was used. Since the model is asymptotically stable a simple online simulation of the model is sufficient to get an estimate of the current servo angle. For this a simple forward Euler discretization of (5.16f) is implemented on the main controller

$$\hat{\theta}[k+1] = \hat{\theta}[k] + T_S \dot{\hat{\theta}}[k] \quad (5.18a)$$

$$\dot{\hat{\theta}}[k+1] = \dot{\hat{\theta}}[k] + T_S (p_{S0}(\theta_U[k] - \hat{\theta}[k]) - p_{S1}\dot{\hat{\theta}}[k]). \quad (5.18b)$$

In Figure 5.12 its result is compared to the measurement of the encoder. To be close to the real application on the Tricopter, the propeller on the test bench is spinning with about 70 Hz during the experiment. This explains the vibration seen in the encoder measurements. If the propeller is switched off, the estimation error is always less than  $\pm 0.5$  DEG.

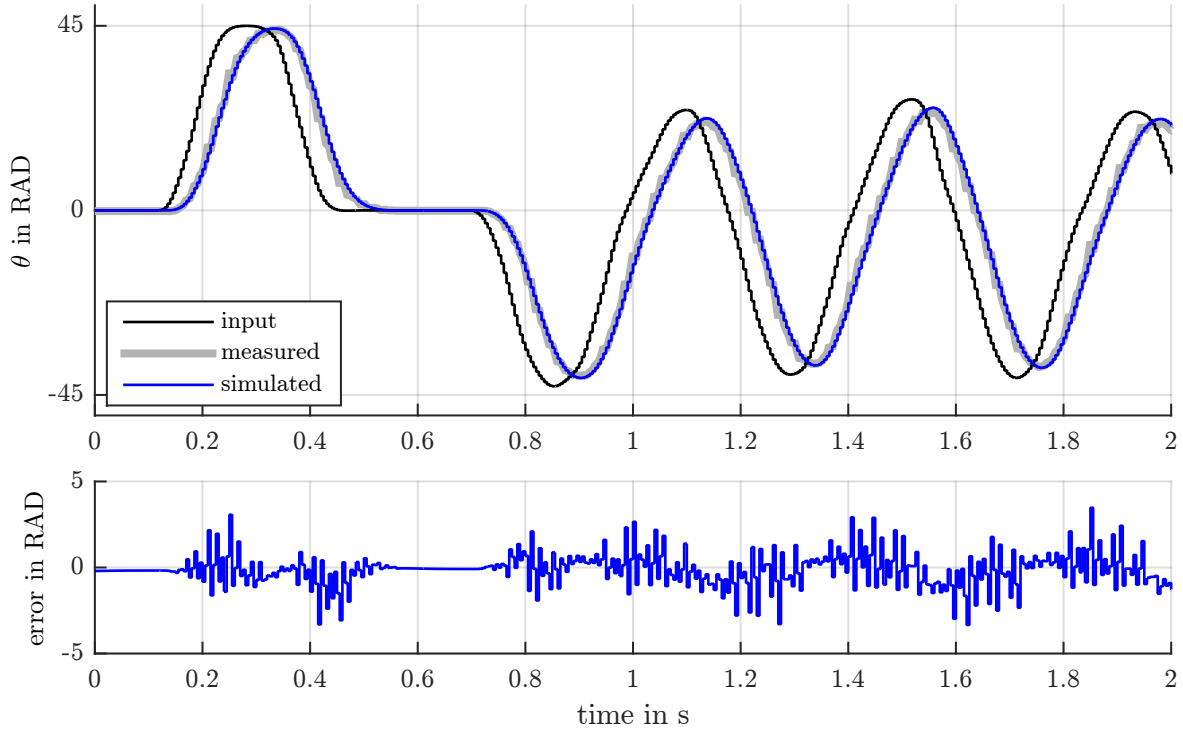


Figure 5.12: Servo simulation validation

### 5.4.2 Propeller tracking control

The forward Euler discretization of the propeller model (5.17d) is

$$\varpi[k+1] = \varpi[k] + T_S (p_{P2} i_M[k] - p_{P3} - p_{P1} (\varpi[k])^2), \quad (5.19)$$

**Measurement model.** From the commutation algorithm of the BLDC driver we get an estimate  $\varpi_M$  of the propeller velocity which relies on its *angle*  $\psi$  estimation used for the commutation, which is

$$\varpi_M[k] = \frac{1}{T_S} (\psi[k] - \psi[k-1]). \quad (5.20)$$

Assuming that the angular acceleration  $\dot{\varpi}$  is roughly constant within one sampling step, we have the relations

$$\psi[k] = \psi[k-1] + \varpi[k-1] T_S + \frac{1}{2} \dot{\varpi}[k-1] T_S^2, \quad \dot{\varpi}[k-1] = \frac{1}{T_S} (\varpi[k] - \varpi[k-1]). \quad (5.21)$$

So the estimate corresponds to the mean velocity between the current and the last sampling step, i.e.

$$\varpi_M[k] = \frac{1}{2} (\varpi[k] + \varpi[k-1]). \quad (5.22)$$

**Observer.** The velocity estimate  $\varpi_M$  from the BLDC driver is quite noisy, so it should not be used directly in a feedback. The scaled model (5.19) also contains the a friction

parameter  $p_{\text{P}3} = \frac{T_{\text{MB}}}{\Theta_p}$  which we like to estimate online for each propeller drive individually. To address these two aspects, an observer for each propeller drive is implemented on the main controller. It is essentially a copy of the discrete model (5.19) supplemented with a linear error feedback

$$e[k] = \varpi_M[k] - \frac{1}{2}(\hat{\varpi}[k] + \hat{\varpi}[k-1]) \quad (5.23a)$$

$$\hat{\varpi}[k+1] = \hat{\varpi}[k] + T_S(p_{\text{P}2}i_M[k] - \hat{p}_{\text{P}3}[k] - p_{\text{P}1}(\hat{\varpi}[k])^2 + l_{\text{P}1}e[k]), \quad (5.23b)$$

$$\hat{p}_{\text{P}3}[k+1] = \hat{p}_{\text{P}3}[k] + T_S l_{\text{P}2} e[k]. \quad (5.23c)$$

where  $l_{\text{P}1}, l_{\text{P}2} \in \mathbb{R}$  are the feedback gains. For quantitative analysis of the observer we consider the linearization of the observer error dynamics about a general expansion point  $\varpi = \bar{\varpi} > 0$ . Its characteristic polynomial is

$$\lambda^3 + \left(\frac{T_S}{2}(4p_{\text{P}1}\bar{\varpi} + l_{\text{P}1}) - 2\right)\lambda^2 + \left(1 - \frac{T_S}{2}(4p_{\text{P}1}\bar{\varpi} + T_S l_{\text{P}2})\right)\lambda - \frac{T_S}{2}(l_{\text{P}1} + T_S l_{\text{P}2}) = 0 \quad (5.24)$$

The roots  $\lambda$  for the given parameters are shown in (??).

**Tracking controller.** Assume that we have a given trajectory  $k \mapsto \hat{\varpi}_D[k]$  and we want the trajectory of the propeller velocity  $k \mapsto \varpi[k]$  (actually its estimate  $\hat{\varpi}$ ) to converge to it. Being at the sampling step  $k$  the available control input is the motor current  $i_M[k+1]$  for the *next* step. From the observer (5.23) we have estimates for the velocity  $\hat{\varpi}[k+1]$  and the friction  $\hat{p}_{\text{P}3}[k+1]$  at the next sampling step. Taking this into account we propose the control law:

$$e[k+1] = \hat{\varpi}_D[k+1] - \hat{\varpi}[k+1], \quad (5.25a)$$

$$i_M[k+1] = \frac{1}{p_{\text{P}2}}\left(\frac{\hat{\varpi}_D[k+2] - \hat{\varpi}_D[k+1]}{T_S} + p_{\text{P}1}(\hat{\varpi}_D[k+1])^2 + \hat{p}_{\text{P}3}[k+1] + k_P e[k+1]\right), \quad (5.25b)$$

It is essentially a (shifted) copy of the discrete model (5.19) supplemented with a linear error feedback with the gain  $k_P \in \mathbb{R}$ . Plugging the control law (5.25) into the model (5.19) and assuming the observer has converged, i.e.  $\hat{\varpi}[k] = \varpi[k]$  and  $\hat{p}_{\text{P}3}[k] = p_{\text{P}3}$ , yields the tracking error dynamics

$$e[k+1] + (T_S(2p_{\text{P}1}\varpi[k] + k_P) - 1)e[k] + T_S p_{\text{P}1}(e[k])^2 = 0. \quad (5.26)$$

For a the linearization about the expansion point  $e = 0$ ,  $\varpi = \bar{\varpi}$  the corresponding characteristic polynomial has the root

$$\lambda = 1 - T_S(2p_{\text{P}1}\bar{\varpi} + k_P). \quad (5.27)$$

### 5.4.3 Tricopter force control

The generalized force  $\mathbf{f}$  on the tricopter is a static transformation of the propeller velocities  $\varpi_1, \dots, \varpi_3$  and the servo angles  $\theta_1, \dots, \theta_3$  as given in (5.16c). For a given desired

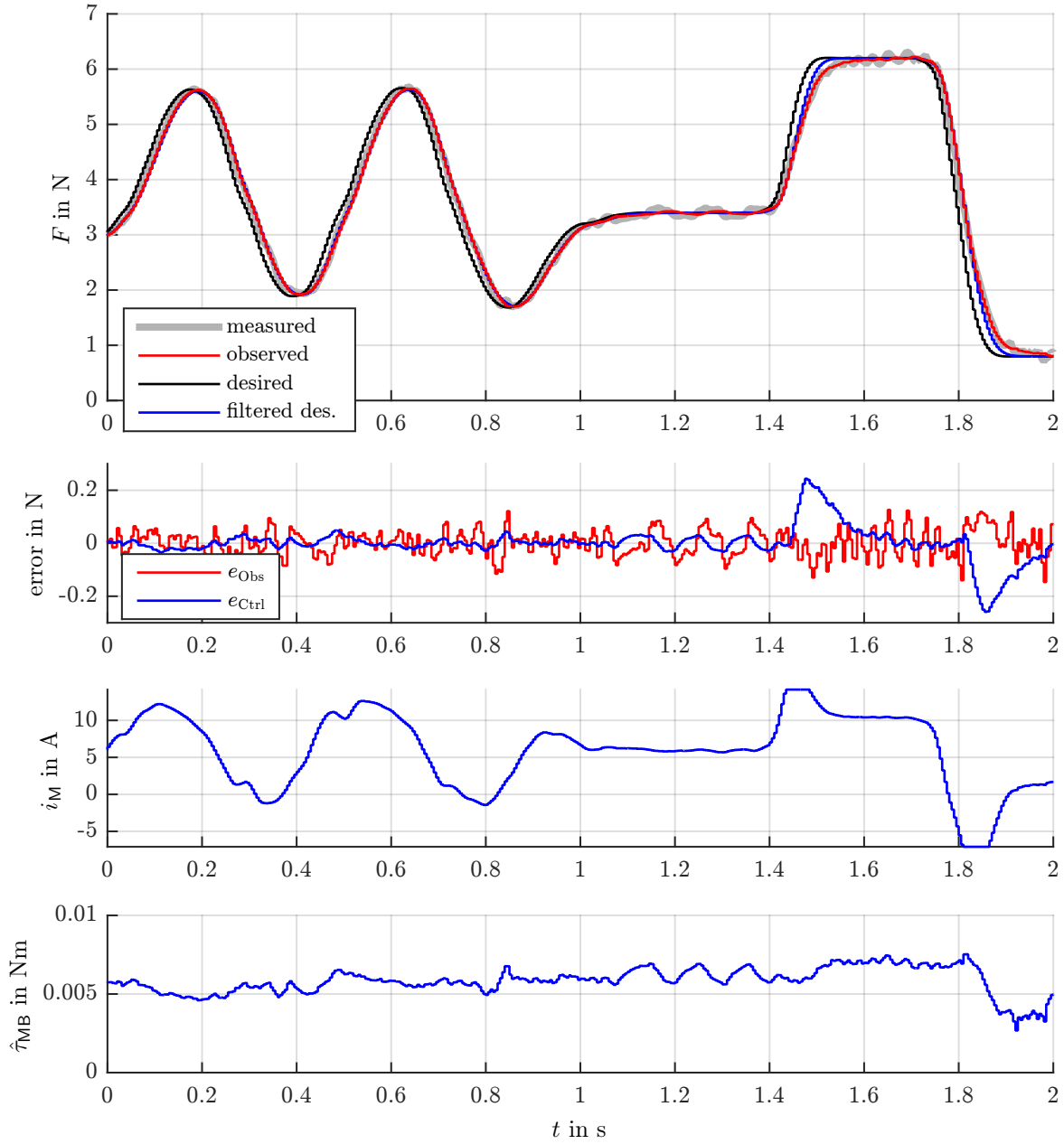


Figure 5.13: Propeller control validation

generalized force  $\mathbf{f}_D$  we can (partially) invert this relation to obtain the corresponding propeller thrusts  $F_{D1}, \dots, F_{D3}$  and servo angles  $\theta_{D1}, \dots, \theta_{D3}$  as

$$F_D^{\text{VH}} = B^{-1} \mathbf{f}_D, \quad F_{Dj} = \sqrt{(F_{Dj}^{\text{V}})^2 + (F_{Dj}^{\text{H}})^2}, \quad \theta_{Dj} = \text{atan2}(F_{Dj}^{\text{H}}, F_{Dj}^{\text{V}}), \quad j = 1, 2, 3. \quad (5.28)$$

In addition the computed values are saturated to  $0.3 \text{ N} \leq F_{Di} \leq 7.0 \text{ N}$  and  $-45^\circ \leq \theta_{Di} \leq 45^\circ, i = 1, 2, 3$  to incorporate the practical limitations of the actuators. The desired servo angles  $\theta_{Di}$  are directly forwarded to the servo controllers. In contrast, for the desired thrusts  $F_i$  a first order filter is applied:

$$\hat{F}_D[k+2] = \lambda_{\text{Filt}} \hat{F}_D[k+1] + (1 - \lambda_{\text{Filt}}) F_D[k+1], \quad \hat{\varpi}_D[k+2] = \sqrt{\hat{F}_D[k+2]/\kappa_F}. \quad (5.29)$$

This yields the desired propeller velocities  $\hat{\varpi}_{Di}[k+1]$  and  $\hat{\varpi}_{Di}[k+2]$  for the next two sampling steps which are required for the propeller *tracking* controller. After the propeller controller has converged, i.e.  $F_i = \hat{F}_{Di}$ , the thrust dynamic is completely determined by this filter.

Overall we can combine the discrete servo dynamics (5.18), the thrust filter (5.29) and the static transformations (5.16c) and (5.28) to obtain a nonlinear dynamic system with the input  $\mathbf{f}_D$  and the output  $\mathbf{f}$ , the *tricopter actuator dynamics*. For a quantitative analysis its first order approximation about a general expansion point  $(\bar{F}_1, \bar{F}_2, \bar{F}_3, \bar{\theta}_1, \bar{\theta}_2, \bar{\theta}_3)$  is considered. Using the  $z$ -transformation  $\mathcal{Z}\{\cdot\}$  the linearized dynamics between  $\mathbf{f}$  and  $\mathbf{f}_D$  can be written as

$$\mathcal{Z}\{\Delta \mathbf{f}\} = G_f(z) \mathcal{Z}\{\Delta \mathbf{f}_D\}. \quad (5.30)$$

The discrete transfer function

$$G_f(z) = J \text{diag}(G_F(z), G_F(z), G_F(z), G_\theta(z), G_\theta(z), G_\theta(z)) J^{-1} \quad (5.31)$$

consists of  $G_F(z)$ , the transfer function of the thrust filter (5.29),  $G_\theta(z)$ , the transfer function of the controlled servo (5.18):

$$G_F(z) = \frac{1 - c_F}{z - c_F}, \quad G_\theta(z) = \frac{p_{S0} T_S^2}{(z - 1)^2 + p_{S1} T_S(z - 1) + p_{S0} T_S^2}. \quad (5.32)$$

and  $J$  is the Jacobian matrix of the force transformation (5.16c) at the expansion point.

$$J = B \begin{bmatrix} \cos \bar{\theta}_1 & 0 & 0 & -\bar{F}_1 \sin \bar{\theta}_1 & 0 & 0 \\ 0 & \cos \bar{\theta}_2 & 0 & 0 & -\bar{F}_2 \sin \bar{\theta}_2 & 0 \\ 0 & 0 & \cos \bar{\theta}_3 & 0 & 0 & -\bar{F}_3 \sin \bar{\theta}_3 \\ \sin \bar{\theta}_1 & 0 & 0 & \bar{F}_1 \cos \bar{\theta}_1 & 0 & 0 \\ 0 & \sin \bar{\theta}_2 & 0 & 0 & \bar{F}_2 \cos \bar{\theta}_2 & 0 \\ 0 & 0 & \sin \bar{\theta}_3 & 0 & 0 & \bar{F}_3 \cos \bar{\theta}_3 \end{bmatrix}. \quad (5.33)$$

Note that  $\bar{F}$  cancels out in (5.31), i.e.  $G_f$  is independent of it.

From the structure of  $G_f$  in (5.31) it is clear that its entries are linear combinations of the transfer functions the the thrust and the servos,  $G_F$  and  $G_\theta$ . Also it is evident that if  $G_F = G_\theta$ , then  $G_f$  would be diagonal. Since this is not the case we do have off-diagonal

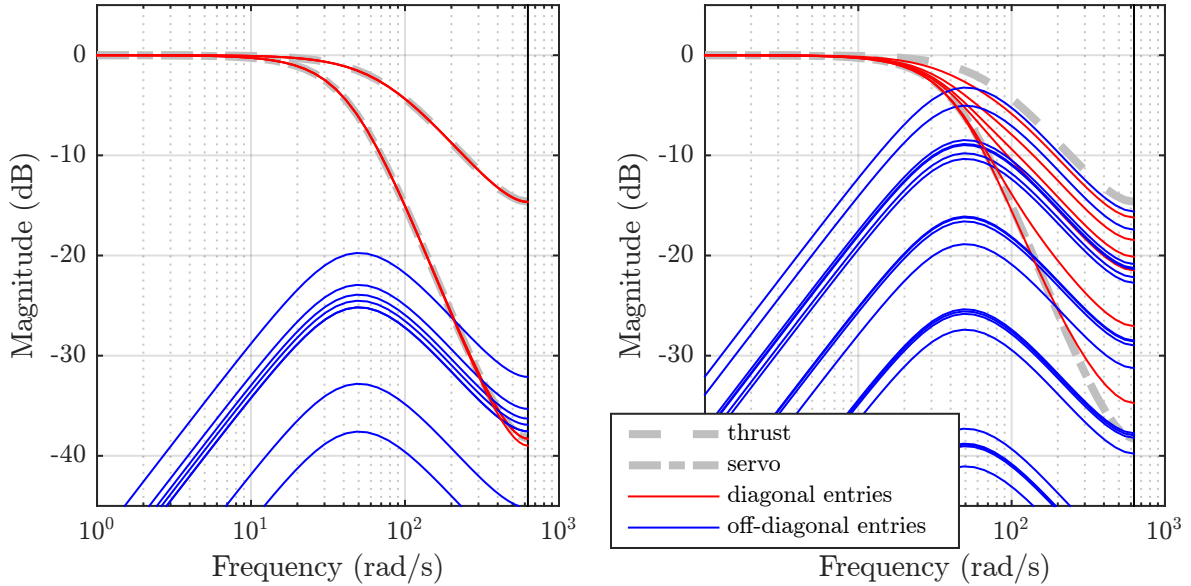


Figure 5.14: Bode magnitude plot of the normalized tricopter actuator dynamics transfer function  $\tilde{G}_f$  at different expansion points

entries in the transfer matrix  $G_f$ . This so-called crosstalk between the components of the generalized force  $\mathbf{f}$  depends mainly on the expansion point of the servo angles  $\bar{\theta}$ .

For a better quantitative analysis of the off-diagonal entries of  $G_f$ , the transfer function is normalized as  $\tilde{G}_f = S^{-1}G_fS$  where  $S = \text{diag}(F_{x,\text{Max}}, \dots, \tau_{z,\text{Max}})$  contains the maximal magnitudes of the corresponding forces and torques. Figure 5.14 shows exemplary the bode magnitude plot of  $\tilde{G}_f$  for the hover case  $\bar{\theta} = [0, 0, 0]^\top$  (left) and for a forward force with  $\bar{\theta} = [\pi/4, 0, -\pi/4]^\top$  (right). In the hover case the diagonal entries for  $F_z$ ,  $\tau_x$  and  $\tau_y$  coincide with the thrust dynamics  $G_F$ , whereas the diagonal entries for  $F_x$  and  $F_y$  coincide with the servo dynamics  $G_\theta$ . The diagonal entry for  $\tau_z$  is dominated by the servo dynamics  $G_\theta$  but also has a small influence from  $G_F$  due to the propeller drag (terms involving  $\kappa_T$  in (5.16c)). The propeller drag is also responsible for the small off-diagonal entries in the hover case. For the forward force case it is evident that the diagonal entries are linear combinations of  $G_F$  and  $G_\theta$ . Furthermore, the off-diagonal entries have a significantly larger magnitude.

#### 5.4.4 Quadcopter force vector control

**Model.** The model of the generalized force on the quadcopter from (5.17c) can be split into a static part  $f^{\text{stat}}$ , proportional to the squares of the propeller velocities  $\varpi$ , and a

dynamic part  $f^{\text{dyn}}$  proportional to the propeller accelerations  $\dot{\varpi}$ , as

$$f(\varpi, \dot{\varpi}) = \underbrace{\begin{bmatrix} \kappa_F & \kappa_F & \kappa_F & \kappa_F \\ 0 & \kappa_F l_A & 0 & -\kappa_F l_A \\ -\kappa_F l_A & 0 & \kappa_F l_A & 0 \\ -\kappa_T & \kappa_T & -\kappa_T & \kappa_T \end{bmatrix}}_{f^{\text{stat}}(\varpi)} \underbrace{\begin{bmatrix} \varpi_1^2 \\ \varpi_2^2 \\ \varpi_3^2 \\ \varpi_4^2 \end{bmatrix}}_{B} - \underbrace{\begin{bmatrix} 0 \\ 0 \\ 0 \\ \Theta_P(\dot{\varpi}_1 - \dot{\varpi}_2 + \dot{\varpi}_3 - \dot{\varpi}_4) \end{bmatrix}}_{f^{\text{dyn}}(\dot{\varpi})}. \quad (5.34)$$

**Filter dynamics.** The task here is to design a filter which outputs the desired propeller velocities  $\varpi[k]$  and  $\varpi[k+1]$  for the next two sampling steps based on the given desired generalized force  $f_D[k]$ . Note that  $f$  is *not* a flat output of (5.34), so a simple low-pass filter for  $f_D$  does not do the trick. However, the propeller velocities  $\varpi$  form a flat output and so we propose the following continuous time filter

$$\frac{d^2}{dt^2}(f^{\text{stat}}(\hat{\varpi}_D)) + K_1 \frac{d}{dt}(f^{\text{stat}}(\hat{\varpi}_D)) + K_0(f(\hat{\varpi}_D, \dot{\hat{\varpi}}_D) - f_D) = 0. \quad (5.35)$$

With introduction of the auxiliary state  $\dot{h} = \frac{d}{dt}(f^{\text{stat}}(\hat{\varpi}_D)) + K_1 f^{\text{stat}}(\hat{\varpi}_D)$  this can be rewritten in an explicit first order form

$$\dot{\hat{\varpi}}_D = \text{diag}(2\kappa_F \hat{\varpi}_D)^{-1} B^{-1} (\dot{h} - K_1 f^{\text{stat}}(\hat{\varpi}_D)), \quad (5.36a)$$

$$\dot{h} = K_0(f_D - f(\hat{\varpi}_D, \dot{\hat{\varpi}}_D)). \quad (5.36b)$$

For the time discrete implementation we add the forward Euler approximation of the derivatives

$$\hat{\varpi}_D[k+1] = \hat{\varpi}_D[k] + T_S \dot{\hat{\varpi}}_D[k], \quad \dot{h}[k+1] = \dot{h}[k] + T_S \dot{h}[k]. \quad (5.37)$$

With this representation of the filter dynamics it is very simple to add a saturation  $\varpi_{\min} \leq \hat{\varpi}_D \leq \varpi_{\max}$  to take into account the practical limitations of the propellers. The combination of (5.36) and (5.37) constitute a time discrete nonlinear system with the input  $f_D[k]$  and the output  $\hat{\varpi}_D[k]$ ,  $\hat{\varpi}_D[k+1]$ , the *quadcopter actuator dynamics*.

**Tuning.** The filter gains  $K_1$  and  $K_2$  are chosen as diagonal matrices and for symmetry considerations the gains corresponding to  $\tau_x$  and  $\tau_y$  are identical, i.e.

$$K_0 = \text{diag}(k_{\text{mag}0}, k_{\text{tilt}0}, k_{\text{tilt}0}, k_{\text{head}0}), \quad K_1 = \text{diag}(k_{\text{mag}1}, k_{\text{tilt}1}, k_{\text{tilt}1}, k_{\text{head}1}). \quad (5.38)$$

For a quantitative analysis of the actuator dynamics we consider its linearization for a general expansion point  $(\bar{\varpi}_1, \dots, \bar{\varpi}_4) \in [\varpi_{\min}, \varpi_{\max}]^4$ . Using the  $z$ -transformation we get the following transfer matrix

$$\mathcal{Z}\{\Delta f\} = G_f(z) \mathcal{Z}\{\Delta f_D\}, \quad G_f(z) = \begin{bmatrix} G_{11}(z) & 0 & 0 & 0 \\ 0 & G_{22}(z) & 0 & 0 \\ 0 & 0 & G_{33}(z) & 0 \\ G_{41}(z) & G_{42}(z) & G_{43}(z) & G_{44}(z) \end{bmatrix} \quad (5.39)$$

with the components

$$G_{11}(z) = \frac{k_{\text{mag}0}}{\left(\frac{z-1}{T_S}\right)^2 + k_{\text{mag}1}\frac{z-1}{T_S} + k_{\text{mag}0}} \quad (5.40\text{a})$$

$$G_{22}(z) = G_{33}(z) = \frac{k_{\text{tilt}0}}{\left(\frac{z-1}{T_S}\right)^2 + k_{\text{tilt}1}\frac{z-1}{T_S} + k_{\text{tilt}0}} \quad (5.40\text{b})$$

$$G_{44}(z) = \frac{k_{\text{head}0}(p_4\frac{z-1}{T_S} + 1)}{\left(\frac{z-1}{T_S}\right)^2 + (k_{\text{head}0}p_4 + k_{\text{tilt}1})\frac{z-1}{T_S} + k_{\text{head}0}} \quad (5.40\text{c})$$

$$G_{4j}(z) = \frac{p_j G_{jj}(z) \left(\frac{z-1}{T_S}\right)^2 \left(\frac{z-1}{T_S} + k_{\text{head}1}\right)}{\left(\frac{z-1}{T_S}\right)^2 + (k_{\text{head}0}p_4 + k_{\text{tilt}1})\frac{z-1}{T_S} + k_{\text{head}0}}, \quad j = 1, 2, 3 \quad (5.40\text{d})$$

and the (expansion point dependent) model parameters

$$p_1 = \frac{\Theta_P}{8\kappa_F} \left( \frac{1}{\bar{\omega}_4} - \frac{1}{\bar{\omega}_3} + \frac{1}{\bar{\omega}_2} - \frac{1}{\bar{\omega}_1} \right), \quad p_2 = \frac{\Theta_P}{4\kappa_F l_A} \left( \frac{1}{\bar{\omega}_2} - \frac{1}{\bar{\omega}_4} \right), \quad (5.41\text{a})$$

$$p_4 = \frac{\Theta_P}{8\kappa_T} \left( \frac{1}{\bar{\omega}_1} + \frac{1}{\bar{\omega}_2} + \frac{1}{\bar{\omega}_3} + \frac{1}{\bar{\omega}_4} \right), \quad p_3 = \frac{\Theta_P}{4\kappa_F l_A} \left( \frac{1}{\bar{\omega}_1} - \frac{1}{\bar{\omega}_3} \right). \quad (5.41\text{b})$$

The transfer behaviors for  $F_z$ ,  $\tau_x$  and  $\tau_y$  are uncorrelated and independent of the expansion point. Their parameters are chosen to form a second order Butterworth filter.

Unfortunately, the transfer behavior for  $\tau_z$  is not that nice: It is in general affected by all components of  $\mathbf{f}_D$  and the corresponding transfer functions  $G_{4j}, j = 1, \dots, 4$  depend on the expansion point. However, for the hover case  $\bar{\omega}_1 = \bar{\omega}_2 = \bar{\omega}_3 = \bar{\omega}_4 = \sqrt{mg/4\kappa_F}$  we have  $p_1 = p_2 = p_3 = 0$  and  $p_4 = \frac{\Theta_P}{\kappa_T} \sqrt{\kappa_F/mg}$ . We choose  $k_{\text{head}1} = 1/p_4 = \frac{\kappa_T}{\Theta_P} \sqrt{mg/\kappa_F}$  such that *at this particular expansion point* we have a pole-zero cancellation. The remaining parameter  $k_{\text{head}0}$  is then used to adjust the cut-off frequency of the filter.

Figure 5.15 shows the Bode magnitude plot of the normalized transfer matrix  $\tilde{G}_f$  coefficients from (5.40) with the used filter parameters. The left side corresponds to the most common hover case  $\bar{\omega}_1 = \bar{\omega}_2 = \bar{\omega}_3 = \bar{\omega}_4 = \sqrt{mg/4\kappa_F}$  whereas the right side captures the “worst case” expansion points where  $(\bar{\omega}_1, \dots, \bar{\omega}_4) \in \{\bar{\omega}_{\min}, \bar{\omega}_{\max}\}^4$ . Obviously the pole-zero cancellation only holds for the hover case but even for the worst case points  $G_{44}$  only differs slightly from its design. Furthermore one can see that the influence of the off-diagonal entries is restricted to high frequencies.

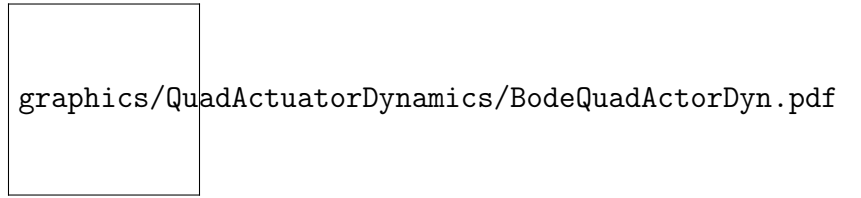


Figure 5.15: Bode magnitude plot of the normalized transfer matrix  $\tilde{G}_f$  at different expansion points

**Comparison to static approach.** The proposed filter (5.35) might seem complicated. In particular one might argue that the dynamic part  $f^{\text{dyn}}$  in the model (5.34) is neglectable, as is done in most publications on this subject.

To answer this question we can replace (5.35) by

$$\frac{d^2}{dt^2}(f^{\text{stat}}(\hat{\varpi}_D)) + K_1 \frac{d}{dt}(f^{\text{stat}}(\hat{\varpi}_D)) + K_0(f^{\text{stat}}(\hat{\varpi}_D) - f_D) = 0 \quad (5.42)$$

what essentially neglects the dynamics part  $f^{\text{dyn}}$  in the generalized force  $f = f^{\text{stat}} + f^{\text{dyn}}$ . As before we now consider the transfer matrix  $G_f$  for the linearized filter at a general expansion point. The components differing from (5.40) are

$$G_{44}(z) = \frac{k_{\text{head}0}(p_4 \frac{z-1}{T_S} + 1)}{\left(\frac{z-1}{T_S}\right)^2 + k_{\text{tilt}1} \frac{z-1}{T_S} + k_{\text{head}0}} \quad G_{4j}(z) = p_j \frac{z-1}{T_S} G_{jj}(z), \quad j = 1, 2, 3. \quad (5.43)$$

Now one can chose the gains  $K_0$  and  $K_1$  such that (5.42) forms 4 decoupled second order Butterworth filters with inputs  $f_D$  and outputs  $f^{\text{stat}}$ . However, since the real force on the quadcopter does contain the dynamic part as well the behavior from  $f_D$  to  $f = f^{\text{stat}} + f^{\text{dyn}}$  is quite different, as can be seen in (5.43). The Bode magnitude plot of the transfer functions is displayed in Figure 5.16 on the left side. Even for the hover case (thick lines) the transfer function  $G_{44}$  for  $\tau_z$  has an unacceptable overshoot.

In oder to improve the behavior we can do the same as before: adjust the parameters in  $G_{44}$ , i.e.  $k_{\text{head}0}$  and  $k_{\text{head}1}$ , such that there is a pole-zero cancelation at the hover expansion point. The resulting Bode magnitude plot is shown on the right side of Figure 5.16. It is already a significant improvement compared to the right side but is much worse as the previous result shown in Figure 5.15. Moreover, the magnitude of the off-diagonal transfer functions at low frequencies is much higher for both cases in Figure 5.16 than in Figure 5.15.

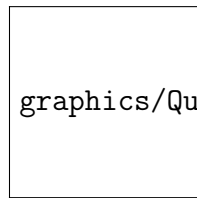


Figure 5.16: Bode magnitude plot of the normalized transfer matrix  $\tilde{G}_f$  at different expansion points (static approach)

Overall this discussion should justify the filter design in (5.35) and justify the consideration of the dynamic model (5.34) for the present case. For other quadcopters with smaller ratios  $\Theta_P/\kappa_T$  or less aggressively tuned multicopters like the previously discussed tricopter, however, the situation can be different.

## 5.5 State estimation

Rigid body model

$$m(\ddot{\mathbf{r}} - \mathbf{a}_G) + d\dot{\mathbf{r}} = R_{\text{quat}}(\mathbf{q})(F + F_B) \quad (5.44)$$

$$\dot{\mathbf{q}} = A_{\text{quat}}(\mathbf{q}) \boldsymbol{\omega}, \quad \Theta \dot{\boldsymbol{\omega}} + \text{wed}(\boldsymbol{\omega}) \Theta \boldsymbol{\omega} = \boldsymbol{\tau} + \boldsymbol{\tau}_B \quad (5.45)$$

measurements

$$\mathbf{r}_{\text{VIC}} = \mathbf{r}, \quad \mathbf{q}_{\text{VIC}} = \mathbf{q} \quad (5.46)$$

$$\boldsymbol{\omega}_M = \boldsymbol{\omega} + \boldsymbol{\omega}_N, \quad \mathbf{a}_M = R^\top(\ddot{\mathbf{r}} - \mathbf{a}_G) + \mathbf{a}_B + \mathbf{a}_N \quad (5.47)$$

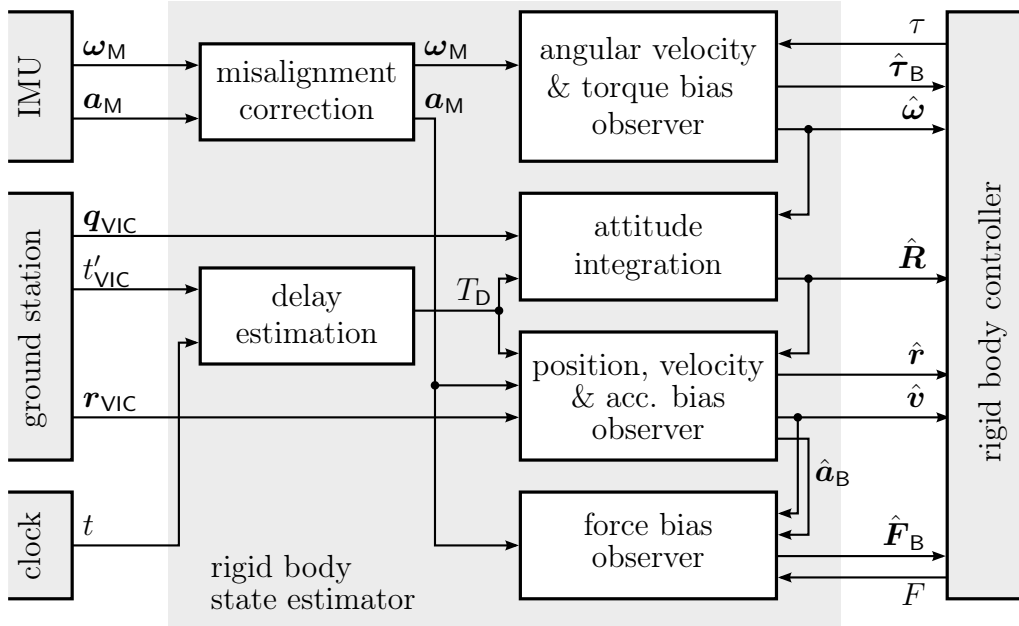


Figure 5.17: Overall structure of the state estimation

sadsadv Figure 5.17.

### 5.5.1 IMU model and misalignment correction

Onboard the multicopters there is an inertial measurement unit (IMU), the model VN100 from VECTORNAV. The IMU contains a 3-axis accelerometer, gyroscope and magnetometer connected to microcontroller which implements an extended Kalman-filter to estimate the attitude quaternion and gyroscope biases.

By construction the IMU has a small misalignment  $\mathbf{R}_{\text{IMU,BR}} \in \mathbb{SO}(3)$  to the body fixed frame. Also the reference frame of the IMU is aligned with the gravity direction and the direction to magnetic north. The lab frame  $(\mathbf{h}_1, \mathbf{h}_2, \mathbf{h}_3)$  is also aligned with the gravity  $\mathbf{a}_G = [0, 0, -9.81]^\top$  but the  $\mathbf{h}_1$  and  $\mathbf{h}_2$  axis are aligned with the walls for convenience, yielding a misalignment  $\mathbf{R}_{\text{IMU,BL}} \in \mathbb{SO}(3)$ .

Overall the relation of the IMU measurements  $(\mathbf{R}_{\text{IMU}}, \boldsymbol{\omega}_M, \mathbf{a}_M)$  and the real system variables  $(\mathbf{R}, \boldsymbol{\omega}, \ddot{\mathbf{r}})$  is assumed as

$$\mathbf{R} = \mathbf{R}_{\text{IMU,BL}} \mathbf{R}_{\text{IMU}} \mathbf{R}_{\text{IMU,BR}}^\top \quad (5.48a)$$

$$\boldsymbol{\omega} = \mathbf{R}_{\text{IMU,BR}} (\boldsymbol{\omega}_M + \boldsymbol{\omega}_N) \quad (5.48b)$$

$$\mathbf{R}^\top(\ddot{\mathbf{r}} - \mathbf{a}_G) = \mathbf{R}_{\text{IMU,BR}} (\mathbf{a}_M + \mathbf{a}_B + \mathbf{a}_N). \quad (5.48c)$$

**Identification of mounting misalignment and accelerometer bias.** For identification of the misalignment  $\mathbf{R}_{\text{IMU},\text{BR}}$  and the accelerometer bias  $\mathbf{a}_B$  a multicopter is placed ( $\mathbf{r} = \text{const.}$ ) in different random orientations  $\mathbf{R} = \text{const.}$  while the accelerometer measurements  $\mathbf{a}_M$  are recorded. Since the robot is not moving the acceleration that *should* be measured is  $a = -\mathbf{R}^\top \mathbf{a}_G$ . We record measurements over 10 s (2000 samples) and take the mean values to eliminate the noise  $\mathbf{a}_N$ . At the same time the attitude  $\mathbf{R} = \mathbf{R}_{\text{VIC}}$  captured with the Vicon system. Between the measurements we have the relation

$$-\mathbf{R}_{\text{VIC}}^\top \mathbf{a}_G = \mathbf{R}_{\text{IMU},\text{BR}}(\mathbf{a}_M + \mathbf{a}_B). \quad (5.49)$$

We assume that the misalignment  $\mathbf{R}_{\text{IMU},\text{BR}}$  is small, so

$$\mathbf{R}_{\text{IMU},\text{BR}} = \exp(\text{wed}(\boldsymbol{\varepsilon}_{\text{IMU},\text{BR}})) \approx \mathbf{I}_3 + \text{wed}(\boldsymbol{\varepsilon}_{\text{IMU},\text{BR}}), \quad \boldsymbol{\varepsilon}_{\text{IMU},\text{BR}} \in \mathbb{R}^3. \quad (5.50)$$

Now can write (5.49) in a form that is *linear* in the parameters

$$(-\mathbf{R}_{\text{VIC}}^\top \mathbf{a}_G)^\wedge \boldsymbol{\varepsilon}_{\text{IMU},\text{BR}} - \mathbf{a}_B = \mathbf{a}_M + \mathbf{R}_{\text{VIC}}^\top \mathbf{a}_G \quad (5.51)$$

and use a least squares approximation to identify values for  $\boldsymbol{\varepsilon}_{\text{IMU},\text{BR}}$  and  $\mathbf{a}_B$ .

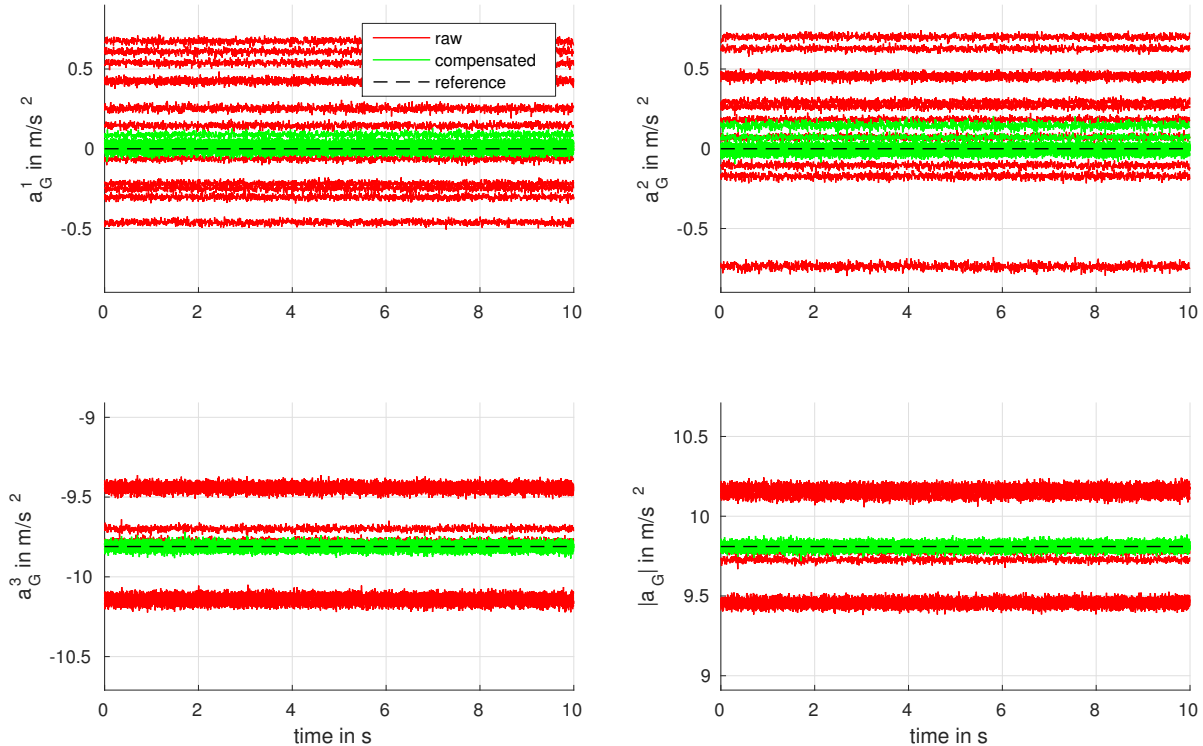


Figure 5.18: Accelerometer measurements and identification result

For validation Figure 5.18 displays the measured gravity coefficients  $\mathbf{a}_G$  within the 20 experiments with different orientations. The red lines are the raw measurements  $\mathbf{a}_G = \mathbf{R}_{\text{VIC}} \mathbf{a}_M$ , the green lines incorporate the identified values  $\mathbf{a}_G = \mathbf{R}_{\text{VIC}} \mathbf{R}_{\text{IMU},\text{BR}}(\mathbf{a}_M + \mathbf{a}_B)$  and the black line is the reference value  $\mathbf{a}_G = [0, 0, -9.81]^\top$ . Most notably one can see that even the magnitude  $\|\mathbf{a}_G\|$  of the raw acceleration is off by about 5% for some experiments whereas the compensated values are all within a window of about 0.2%.

### 5.5.2 Angular velocity and torque bias

The model for the rotational kinetics and the gyroscope measurement are

$$\Theta \dot{\omega} + \text{wed}(\omega) \Theta \omega = \tau + \tau_B, \quad \omega_M = \omega + \omega_N. \quad (5.52)$$

Luenberger Observer

$$\hat{\omega}[k+1] = \hat{\omega}[k] + T_S \Theta^{-1} (\tau[k] + \hat{\tau}_B[k] - \text{wed}(\hat{\omega}[k]) \Theta \hat{\omega}[k]) + L_\omega (\omega_M[k] - \hat{\omega}[k]) \quad (5.53a)$$

$$\hat{\tau}_B[k+1] = \hat{\tau}_B[k] + L_\tau (\omega_M[k] - \hat{\omega}[k]) \quad (5.53b)$$

Introducing the error quantities  $e_\omega = \omega - \hat{\omega}$  and  $e_\tau = \tau_B - \hat{\tau}_B$  and subtracting the observer (5.53) from the discretized model we find the *observer error dynamics*:

$$\begin{bmatrix} e_\omega[k+1] \\ e_\tau[k+1] \end{bmatrix} = \begin{bmatrix} \mathbf{I}_3 - L_\omega - S(\omega[k]) & T_S \Theta^{-1} \\ -L_\tau & \mathbf{I}_3 \end{bmatrix} \begin{bmatrix} e_\omega[k] \\ e_\tau[k] \end{bmatrix} + \begin{bmatrix} T_S \Theta^{-1} \text{wed}(e_\omega[k]) \Theta e_\omega[k] \\ 0 \end{bmatrix} - \begin{bmatrix} L_\omega \\ L_\tau \end{bmatrix} \omega_N \quad (5.54)$$

where

$$S(\omega[k]) = T_S \Theta^{-1} (\text{wed}(\omega[k]) \Theta - \text{wed}(\Theta \omega[k])). \quad (5.55)$$

Note that the term quadratic in  $e_\omega$  is negligible if assuming small errors. The term  $S(\omega[k])$  contains the time-variant part of the error dynamics. However, for a reasonable gain  $L_\omega$  and typical working conditions (e.g.  $\|\omega\| < 10$  rad/s) the gain  $L_\omega$  dominates over the time-variant part and the error dynamics are asymptotically stable. Furthermore, for the linearization about the hover case,  $\omega \approx 0$ , the matrix  $S$  drops out completely. This is used to compute the gains  $L_\omega = \text{diag}(l_{\omega_x}, l_{\omega_y}, l_{\omega_z})$  and  $L_\tau = \text{diag}(l_{\tau_x}, l_{\tau_y}, l_{\tau_z})$  corresponding to given desired closed loop poles at this expansion point.

### 5.5.3 Configuration measurement delay

the configuration measurement ( $r_{\text{VICON}}$ ,  $q_{\text{VICON}}$ ) is done by a VICON motion capturing system. This measurement relies on the optical tracking of reflective markers fixed on the multi-copters by infrared cameras mounted at the walls of the lab and connected to the ground station PC. The groundstation software runs a timer at  $T'_S = 0.1$  ms which reads the measurement, validates it and forwards it to the XBee radio module. Finally the multicopter microcontroller receives the measurements through its radio module.

MATLAB is not a real-time system and the radio modules are transmitting and receiving other data at the same time. Thus the frequency at which the configuration measurements are available to the multicopter is *not* constant, but varies by several main sampling steps  $T_S$ , see Figure 5.21 for actual measurements. Furthermore the process is not performed instantaneously but takes some, again variable, time. Overall we assume a *variable time delay*  $T_D[k']$  for each measurement.

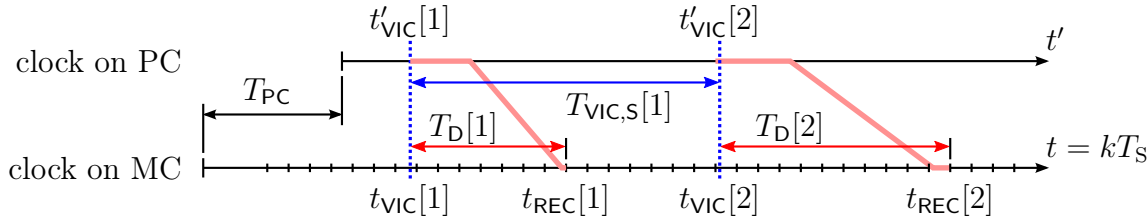


Figure 5.19: Illustration of the measurement time at the PC and when it is available on the microcontroller (MC)

To get an estimate  $\hat{T}_D[k']$  for this delay we utilize the clocks on the ground station PC,  $t'$ , and the microcontroller,  $t$ . The clocks are assumed to be synchronous but have an unknown offset  $T_{\text{PC}} = t - t' = \text{const.}$  depending on when each clock was started. Figure 5.19 illustrates the time  $t'_{\text{VIC}}[k']$  at which a measurement was taken and the time  $t_{\text{REC}}[k']$  at which it is received/available on the microcontroller. Taking a large enough sample of these times we have the relation

$$\text{mean}(t_{\text{REC}}[1, \dots, K'] - t'_{\text{VIC}}[1, \dots, K']) = T_{\text{PC}} + \text{mean}(T_D[1, \dots, K']), \quad K' \gg 1. \quad (5.56)$$

Whereas  $T_{\text{PC}}$  changes whenever the ground station or the microcontroller restarts, the average delay  $\bar{T}_D = \text{mean}(T_D[1, \dots, K'])$  remains constant.

**Experimental average delay identification.** The Identification of the average delay  $\bar{T}_D$  is done in a dedicated experiment: The vehicle is mounted on an incremental encoder that serves as a reference for the yaw-angle. The encoder signal and the yaw-angle from the motion capture system are recorded by the multicopter microcontroller. The experimental data here is about 1 min long and captures about  $K' = 600$  VICON frames. Now we can plot the reference encoder angle  $\varphi[k]$  at the sampling points  $t = kT_S$  and the yaw angle  $\varphi_{\text{VIC}}[k']$  received from the Vicon system at the shifted time  $t'_{\text{VIC}}[k'] + \text{mean}(t_{\text{REC}}[1, \dots, K'] - t'_{\text{VIC}}[1, \dots, K'])$ . If the previous assumption (5.56) hold these signals should be similar up to a shift of the mean delay  $\bar{T}_D$ .

Figure 5.20 shows a small sample of the measured yaw angle and the correlations of the two measurements. The identified average delay is where the cross-correlation has its maximum at  $\bar{T}_D = 0.034$  s. In order to achieve this resolution the measurements were up-sampled to 1 ms by cubic interpolation.

**Clock offset estimation.** For the realtime implementation, (5.56) is approximated by a slow ( $c_{\text{PC}} = 0.99$ ) low-pass filter

$$\hat{T}_{\text{PC}}[k'] = c_{\text{PC}}\hat{T}_{\text{PC}}[k'-1] + (1 - c_{\text{PC}})(t_{\text{REC}}[k'] - t'_{\text{VIC}}[k'] - \bar{T}_D) \quad (5.57)$$

yielding the estimate  $\hat{T}_{\text{PC}}$  for the constant clock offset  $T_{\text{PC}}$ . Finally, the estimated delay of the  $k'$ -th Vicon measurement is

$$\hat{T}_D[k'] = t_{\text{REC}}[k'] - (t'_{\text{VIC}}[k'] + \hat{T}_{\text{PC}}[k']). \quad (5.58)$$

Figure 5.21 shows the estimated clock offset  $\hat{T}_{\text{PC}}$  and the resulting estimated delay  $\hat{T}_D$  for the previous example measurement.

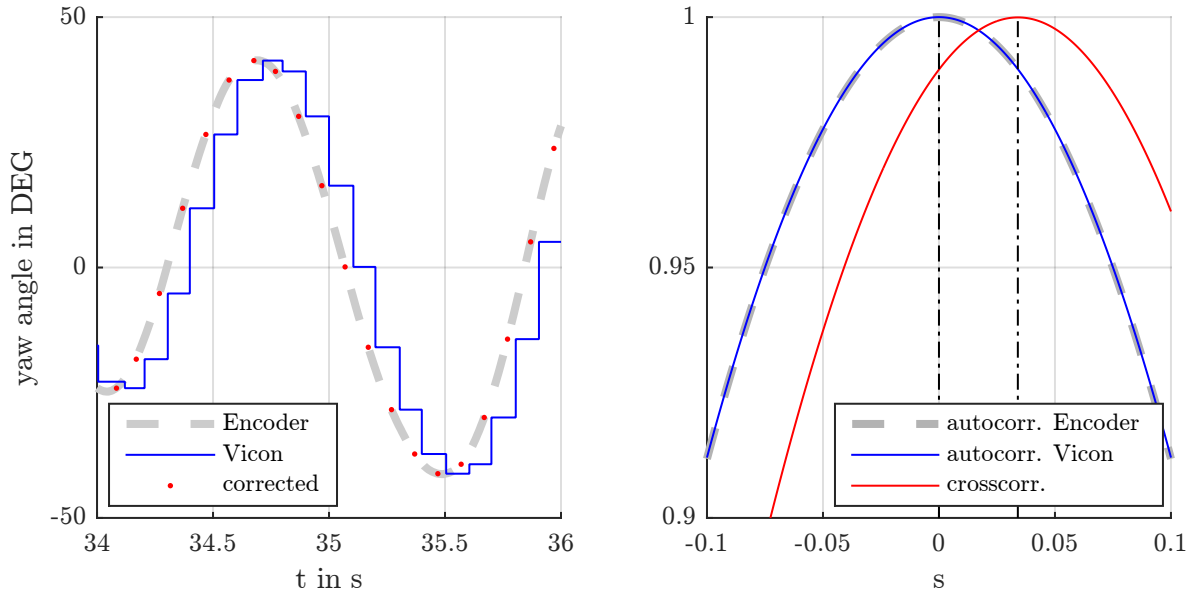


Figure 5.20: A small sample of the yaw-angle measurements (left) and the correlations (right) of the complete 60 s measurements for the identification of the average time delay

### 5.5.4 Attitude

The attitude measurement for the Vicon system is given in terms of an attitude quaternion  $\mathbf{q}_{\text{VIC}}$ . **delay**

**Attitude quaternion.** A unit quaternion is the quadruple  $\mathbf{q} = [q_w, q_x, q_y, q_z]^\top \in \mathbb{R}^4$  with the geometric constraint

$$\phi(\mathbf{q}) = \|\mathbf{q}\|^2 - 1 = q_w^2 + q_x^2 + q_y^2 + q_z^2 - 1 = 0. \quad (5.59)$$

What makes it an attitude quaternion is the relation to the rotation matrix

$$R_{\text{quat}}(\mathbf{q}) = \begin{bmatrix} 1 - 2(q_y^2 + q_z^2) & 2(q_y q_x - q_w q_z) & 2(q_z q_x + q_w q_y) \\ 2(q_y q_x + q_w q_z) & 1 - 2(q_x^2 + q_z^2) & 2(q_y q_z - q_w q_x) \\ 2(q_z q_x - q_w q_y) & 2(q_y q_z + q_w q_x) & 1 - 2(q_x^2 + q_y^2) \end{bmatrix} \in \mathbb{SO}(3). \quad (5.60)$$

The kinematic relation between the quaternion  $\mathbf{q}$  and the angular velocity  $\boldsymbol{\omega}$  arises from

$$\frac{d}{dt}(R_{\text{quat}}(\mathbf{q})) = R_{\text{quat}}(\mathbf{q}) \text{wed}(\boldsymbol{\omega}) \quad \Leftrightarrow \quad \dot{\mathbf{q}} = A_{\text{quat}}(\mathbf{q})\boldsymbol{\omega}. \quad (5.61)$$

Adding a stabilization term for the constraint, motivated in ??, the explicit relations are

$$\underbrace{\frac{d}{dt} \begin{bmatrix} q_w \\ q_x \\ q_y \\ q_z \end{bmatrix}}_{\dot{\mathbf{q}}} = \frac{1}{2} \underbrace{\begin{bmatrix} -q_x & -q_y & -q_z \\ q_w & -q_z & q_y \\ q_z & q_w & -q_x \\ -q_y & q_x & q_w \end{bmatrix}}_{A_{\text{quat}}(\mathbf{q})} \underbrace{\begin{bmatrix} \omega_x \\ \omega_y \\ \omega_z \end{bmatrix}}_{\boldsymbol{\omega}} - \frac{1}{2} \underbrace{\begin{bmatrix} q_w \\ q_x \\ q_y \\ q_z \end{bmatrix}}_{\underbrace{\left( \frac{\partial \phi}{\partial \mathbf{q}}(\mathbf{q}) \right)^+} \lambda \underbrace{(\|\mathbf{q}\|^2 - 1)}_{\phi(\mathbf{q})}}. \quad (5.62)$$

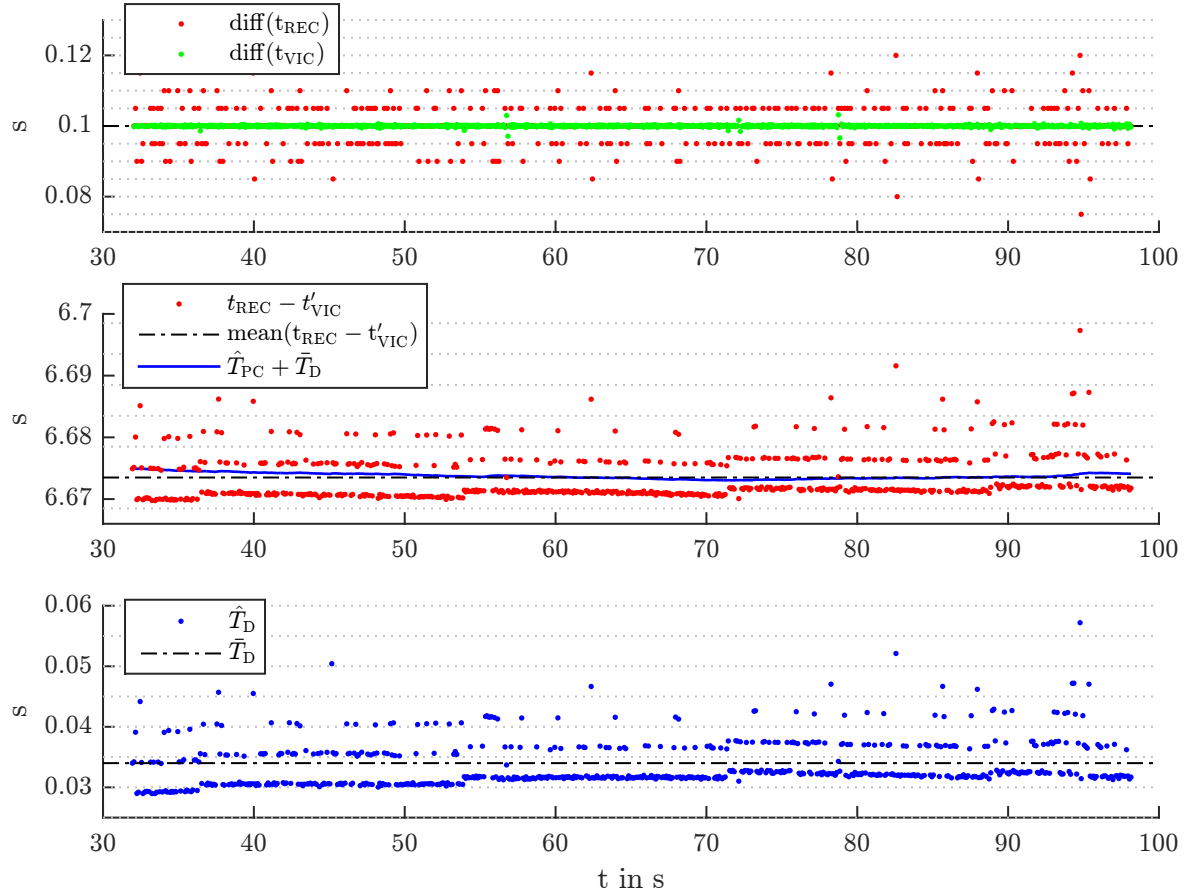


Figure 5.21: Measured timings

The forward Euler discretization with the stabilization gain chosen as  $\lambda = 2/T_S$  is

$$\mathbf{q}[k+1] = \mathbf{q}[k] + T_S A_{\text{quat}}(\mathbf{q}[k]) \boldsymbol{\omega}[k] - (\|\mathbf{q}[k]\|^2 - 1)\mathbf{q}[k]. \quad (5.63)$$

Note that with this particular gain the stabilization coincides with an approximation of the normalization

$$\mathbf{q} \mapsto \mathbf{q}/\|\mathbf{q}\| \stackrel{\|\mathbf{q}\| \approx 1}{\approx} \mathbf{q} - (\|\mathbf{q}\|^2 - 1)\mathbf{q}.$$

In contrast to the exact normalization, the approximation avoids computation of a square root and division.

**Attitude integration.** From the previous subsection we know the micro controller time  $t_{\text{VIC}}[k'] = t_{\text{REC}}[k'] - \hat{T}_{\text{D}}[k']$  at which the received attitude measurement  $\mathbf{q}_{\text{VIC}}[k']$  was taken. To get the an estimate  $\hat{\mathbf{q}}[k]$  for the current attitude we *integrate* the attitude quaternion kinematics (5.63) using the measurement  $\mathbf{q}_{\text{VIC}}[k']$  as initial value and the (ring) buffered angular velocity estimates  $\hat{\boldsymbol{\omega}}[k - \text{floor}(\hat{T}_{\text{D}}[k']/T_S)], \dots, \hat{\boldsymbol{\omega}}[k]$ . Since the delay  $\hat{T}_{\text{D}}[k']$  is usually not a multiple of the micro controller sampling time  $T_S$  a linear interpolation of the angular velocity  $\hat{\boldsymbol{\omega}}(t_{\text{VIC}}[k'])$  is used.

### 5.5.5 Position, velocity and accelerometer bias

For the translational dynamics we have a similar situation as for the attitude kinematics: We have a down-sampled and delayed position measurement  $\mathbf{r}_{\text{VIC}}$  and a biased and noisy measurement of the acceleration  $\mathbf{a}_M$ . From this we want to estimate the current position  $\mathbf{r}$  and velocity  $\dot{\mathbf{r}}$  required for the controller implementation.

The relation between position and accelerometer measurement and the differential equation for a constant accelerometer bias are

$$\mathbf{a}_M = \mathbf{R}^\top (\ddot{\mathbf{r}} - \mathbf{a}_G) + \mathbf{a}_B + \mathbf{a}_N, \quad \dot{\mathbf{a}}_B = 0 \quad (5.64)$$

Introducing the state  $z = [\mathbf{r}^\top, \dot{\mathbf{r}}^\top, \mathbf{a}_B^\top]^\top$  and neglecting the accelerometer noise  $\mathbf{a}_N = 0$ , this can be written as

$$\underbrace{\frac{d}{dt} \begin{bmatrix} \mathbf{r} \\ \dot{\mathbf{r}} \\ \mathbf{a}_B \end{bmatrix}}_{z} = \underbrace{\begin{bmatrix} 0 & \mathbf{I}_3 & 0 \\ 0 & 0 & -\mathbf{R} \\ 0 & 0 & 0 \end{bmatrix}}_A \underbrace{\begin{bmatrix} \mathbf{r} \\ \dot{\mathbf{r}} \\ \mathbf{a}_B \end{bmatrix}}_z + \underbrace{\begin{bmatrix} 0 \\ \mathbf{I}_3 \\ 0 \end{bmatrix}}_B \underbrace{(\mathbf{a}_G + \mathbf{R}\mathbf{a}_M)}_u \quad (5.65)$$

**Estimator implementation.** The implemented estimation algorithm on the microcontroller works as follows: After having received 2 subsequent position measurements  $\mathbf{r}_{\text{VIC}}[1]$ ,  $\mathbf{r}_{\text{VIC}}[2]$  and their reconstructed time  $t_{\text{VIC}}[1]$ ,  $t_{\text{VIC}}[2]$  with  $T'_S[1] = t_{\text{VIC}}[2] - t_{\text{VIC}}[1]$  we set the initial value for the estimator state  $\hat{z} = [\hat{\mathbf{r}}^\top, \hat{\dot{\mathbf{r}}}^\top, \hat{\mathbf{a}}_B^\top]^\top$  as

$$\hat{\mathbf{r}}(t_{\text{VIC}}[2]) = \mathbf{r}_{\text{VIC}}[2], \quad \hat{\dot{\mathbf{r}}}(t_{\text{VIC}}[2]) = \frac{\mathbf{r}_{\text{VIC}}[2] - \mathbf{r}_{\text{VIC}}[1]}{T'_S[1]} \quad \mathbf{a}_B(t_{\text{VIC}}[2]) = 0. \quad (5.66)$$

Then a discrete approximation of the accelerometer dynamics (5.65):

$$\underbrace{\begin{bmatrix} \hat{\mathbf{r}}[k+1] \\ \hat{\dot{\mathbf{r}}}[k+1] \\ \hat{\mathbf{a}}_B[k+1] \end{bmatrix}}_{\hat{z}[k+1]} = \underbrace{\begin{bmatrix} \mathbf{I}_3 & T_S \mathbf{I}_3 & -\frac{T_S^2}{2} \hat{\mathbf{R}}[k] \\ 0 & \mathbf{I}_3 & -T_S \hat{\mathbf{R}}[k] \\ 0 & 0 & \mathbf{I}_3 \end{bmatrix}}_{\hat{A}_S[k]} \underbrace{\begin{bmatrix} \hat{\mathbf{r}}[k] \\ \hat{\dot{\mathbf{r}}}[k] \\ \hat{\mathbf{a}}_B[k] \end{bmatrix}}_{\hat{z}[k]} + \underbrace{\begin{bmatrix} \frac{T_S^2}{2} \mathbf{I}_3 \\ T_S \mathbf{I}_3 \\ 0 \end{bmatrix}}_{B_S} \underbrace{(\mathbf{a}_G + \hat{\mathbf{R}}[k]\mathbf{a}_M[k])}_{\hat{u}[k]} \quad (5.67)$$

is used to integrate the current position and velocity. Note that the measurement time  $t_{\text{VIC}}[2]$  usually does not coincide with a sampling step, see Figure 5.19. Consequently the value  $T_S$  in (5.67) has to be adjusted to match the time from the initial value to the subsequent sampling step. Furthermore the accelerometer measurement  $\mathbf{a}_M$  is linearly interpolated to approximate the acceleration at the initial time  $t_{\text{VIC}}[2]$ . The attitude  $\mathbf{R}$  at the initial point is  $R_{\text{quat}}(\mathbf{q}_{\text{VIC}}[2])$  which is received simultaneously with  $\mathbf{r}_{\text{VIC}}[2]$ .

After this initial procedure, (5.67) is computed once every sampling step with the most recent accelerometer measurement  $\mathbf{a}_M[k]$  yielding the most recent predictions for the position and velocity. The position estimates  $\hat{\mathbf{r}}[k]$  for the last 64 sampling steps are stored in a ring buffer.

When a new configuration measurement  $(\mathbf{r}_{\text{VIC}}[k'], \mathbf{R}_{\text{VIC}}[k'])$  and its timestamp  $t_{\text{VIC}}[k']$  are available, the corresponding estimate  $\hat{\mathbf{r}}(t_{\text{VIC}}[k'])$  is interpolated. This is used to correct

the estimate *at the measurement time*  $t_{\text{VIC}}[k']$ , i.e.

$$\underbrace{\begin{bmatrix} \hat{\mathbf{r}}(t_{\text{VIC}}[k']) \\ \hat{\dot{\mathbf{r}}}(t_{\text{VIC}}[k']) \\ \hat{\mathbf{a}}_B(t_{\text{VIC}}[k']) \end{bmatrix}}_{\hat{z}(t_{\text{VIC}}[k'])} \leftarrow \underbrace{\begin{bmatrix} \hat{\mathbf{r}}(t_{\text{VIC}}[k']) \\ \hat{\dot{\mathbf{r}}}(t_{\text{VIC}}[k']) \\ \hat{\mathbf{a}}_B(t_{\text{VIC}}[k']) \end{bmatrix}}_{\hat{z}(t_{\text{VIC}}[k'])} + \underbrace{\begin{bmatrix} L_r[k'] \\ L_v[k'] \\ L_a[k'](\mathbf{R}_{\text{VIC}}[k'])^\top \end{bmatrix}}_{L[k']} (\mathbf{r}_{\text{VIC}}[k'] - \hat{\mathbf{r}}(t_{\text{VIC}}[k'])). \quad (5.68)$$

After the correction the prediction for the current sampling step is again integrated from (5.67). Note that this also requires a (ring) buffer for the last accelerometer measurements.

**Error dynamics and tuning.** To chose reasonable correction gains  $L_r$ ,  $L_v$  and  $L_a$  we investigate the resulting error dynamics of the proposed estimator. Here we do the coarse assumption that the attitude is constant and perfectly known  $\hat{\mathbf{R}} = \bar{\mathbf{R}}$ . Then the dynamic matrix  $A$  in the continuous model (5.65) is constant and is denoted by  $\bar{A}$ .

From measurement time  $t_{\text{VIC}}[k']$  till the next one at  $t_{\text{VIC}}[k'+1]$  there are several prediction steps (5.67): The first from the measurement time till the subsequent sampling step with integration time  $T_l$ . Then several steps with integration time  $T_s$  till the sampling step before  $t_{\text{VIC}}[k'+1]$ , and finally a step integration time  $T_F$  till  $t_{\text{VIC}}[k'+1]$ . Overall this results in the dynamic matrix

$$\bar{A}'_S = \exp(\bar{A} T_l) \exp(\bar{A} T_S) \cdots \exp(\bar{A} T_S) \exp(\bar{A} T_F) = \exp(\bar{A} T'_S), \quad (5.69)$$

where  $T'_S[k'] = T_l[k'] + T_S + \dots + T_S + T_F[k'] = t_{\text{VIC}}[k'] - t_{\text{VIC}}[k'-1]$ . Since  $T'_S[k']$  is known and exploiting this property of the exponential map, we do not need to worry about the different integration times of the predictions.

Finally we add one correction step (5.68) and subtract the estimator from the discretization of the model (5.65) to obtain the relation for the error  $e = z - \hat{z}$  at one correction/measurement time  $t_{\text{VIC}}[k']$  to the next one at  $t_{\text{VIC}}[k'+1]$  as

$$e(t_{\text{VIC}}[k'+1]) = \underbrace{(\mathbf{I}_9 - \bar{L}[k']C)\bar{A}'_S[k']}_{\bar{A}'_e[k']} e(t_{\text{VIC}}[k']) \quad (5.70)$$

where

$$\bar{A}'_S[k'] = \begin{bmatrix} \mathbf{I}_3 & T'_S[k']\mathbf{I}_3 & -\frac{(T'_S[k'])^2}{2}\bar{\mathbf{R}} \\ 0 & \mathbf{I}_3 & -T'_S[k']\bar{\mathbf{R}} \\ 0 & 0 & \mathbf{I}_3 \end{bmatrix}, \quad \bar{L}[k'] = \begin{bmatrix} L_r[k'] \\ L_v[k'] \\ L_a[k']\bar{\mathbf{R}}^\top \end{bmatrix}, \quad C = [\mathbf{I}_3 \ 0 \ 0] \quad (5.71)$$

and finally

$$\bar{A}'_e[k'] = \begin{bmatrix} \mathbf{I}_3 - L_r[k'] & T'_S(\mathbf{I}_3 - L_r[k']) & \frac{(T'_S[k'])^2}{2}(L_r[k'] - \mathbf{I}_3)\bar{\mathbf{R}} \\ -L_v[k'] & \mathbf{I}_3 - T'_S[k']L_v[k'] & T_S\left(\frac{T'_S[k']}{2}L_v[k'] - \mathbf{I}_3\right)\bar{\mathbf{R}} \\ -L_a[k']\bar{\mathbf{R}}^\top & -T'_S[k']L_a[k']\bar{\mathbf{R}}^\top & \mathbf{I}_3 + \frac{T'_S[k']^2}{2}L_a[k'] \end{bmatrix} \quad (5.72)$$

Scaling the gains with the variable integration time  $T'_S[k']$  between two correction steps as

$$L_r[k'] = l_r \mathbf{I}_3, \quad L_v[k'] = \frac{l_v}{T'_S[k']} \mathbf{I}_3, \quad L_a[k'] = \frac{2l_a}{(T'_S[k'])^2} \quad (5.73)$$

yields the characteristic polynomial with constant coefficients

$$\det(\lambda \mathbf{I}_9 - \bar{A}'_e[k']) = \left( \lambda^3 + (l_r + l'_v - l'_a - 3)\lambda^2 + (3 - 2l_r - l'_v - l'_a)\lambda + l_r - 1 \right)^3. \quad (5.74)$$

However, it should be noted here that constant eigenvalues of the time varying matrix  $\bar{A}'_e[k']$  can not conclude stability of the time-varying system.

In practice the eigenvalues  $\text{eig}(\bar{A}'_e) = \{0, 0.5, 0.9\}$  and the resulting gains  $l_r = 1, l_v = 0.575, l_a = -0.025$  did result in quite good estimation performance. These rather fast eigenvalues also reflect a high confidence in the position measurement.

### 5.5.6 Force bias

Recall the translational multicopter dynamics and the accelerometer measurement  $\mathbf{a}_M$  equation

$$m(\ddot{\mathbf{r}} - \mathbf{a}_G) + d\dot{\mathbf{r}} = \mathbf{R}(F + F_B), \quad \mathbf{a}_M = \mathbf{R}^\top(\ddot{\mathbf{r}} - \mathbf{a}_G) + \mathbf{a}_N + \mathbf{a}_B. \quad (5.75)$$

Solving these equations for the force bias  $F_B$  and elimination of the acceleration  $\ddot{\mathbf{r}}$  yields

$$F_B = m(\mathbf{a}_M - \mathbf{a}_N - \mathbf{a}_B) + d\mathbf{R}^\top\dot{\mathbf{r}} - F. \quad (5.76)$$

From the previous subsections we have estimates for the attitude  $\hat{\mathbf{R}}$ , velocity  $\hat{\mathbf{r}}$  and the accelerometer bias  $\hat{\mathbf{a}}_B$ . From the previous section on the actuator dynamics we have a an estimate for the multicopter force  $\hat{\mathbf{F}}$ . However, the accelerometer measurement  $\mathbf{a}_M$  contains the significant, unknown noise  $\mathbf{a}_N$ . In order to suppress this noise we use a simple low-pass to obtain the estimate  $\hat{\mathbf{F}}_B$  for the force bias

$$\hat{\mathbf{F}}_B[k+1] = l_F \hat{\mathbf{F}}_B[k] + (1 - l_F)(m(\mathbf{a}_M[k] - \hat{\mathbf{a}}_B[k]) + d(\hat{\mathbf{R}}[k])^\top \hat{\mathbf{r}}[k] - \hat{\mathbf{F}}[k]). \quad (5.77)$$

In practice the low-pass gain  $l_F = 0.98$  did yield reasonable results.

## 5.6 Experimental results

In this section we finally discuss results of flight tests. The task for the experiments is to track different given reference trajectories.

**Error quantization.** In order to quantify the tracking performance we use the scalar quantities

$$e_r = \|\hat{\mathbf{r}} - \mathbf{r}_R\|, \quad (5.78a)$$

$$e_R = \cos^{-1}\left(\frac{1}{2}(\text{tr } \mathbf{R}_E - 1)\right), \quad \mathbf{R}_E = \mathbf{R}_R^\top \hat{\mathbf{R}}, \quad (5.78b)$$

$$e_\varphi = |\text{atan2}(R_{xE}^y - R_{yE}^x, R_{xE}^x + R_{yE}^y)|. \quad (5.78c)$$

The position error  $e_r$  is the Euclidean distance between estimated position  $\hat{\mathbf{r}}$  and its reference  $\mathbf{r}_R$ . The attitude error  $e_R$  is the angle of the rotation matrix  $\mathbf{R}_E$  which rotates

the reference attitude  $\mathbf{R}_R$  to the estimated attitude  $\hat{\mathbf{R}}$ . The heading error  $e_\varphi$  is the magnitude of the heading angle of  $\mathbf{R}_E$  resulting from the decomposition discussed in ??.

There are two reasons for considering the heading error  $e_\varphi$  in addition to the attitude error  $e_R$ : Firstly the copters behave differently for the tilting degree of freedom and the heading. This is also reflected by the different controller parameters for the respective directions. Secondly, for the quadcopter, the tilting is used to compensate a horizontal position error. A horizontal bias force implies a tilt error and consequently an attitude error. Based on the arguments from ?? one could say that the heading error  $e_\varphi$  captures the part of the attitude error that is “orthogonal” to the tilt error. Note that there is the relation  $e_R \geq e_\varphi$ .

To quantify the errors for an experiment containing  $N$  sampling steps we use the root-mean-square

$$\text{rms}(e_r) = \sqrt{\frac{1}{N} \sum_{k=1}^N (e_r[k])^2}. \quad (5.79)$$

As an indicator for the dynamic of the reference trajectory for one experiment we consider the maximal velocity

$$\max(\|\mathbf{v}_R\|) = \max (\|\mathbf{v}_R[1]\|, \dots, \|\mathbf{v}_R[N]\|) \quad (5.80)$$

and in the same way the maximal acceleration  $\max(\|\dot{\mathbf{v}}_R\|)$ , the maximal angular velocity  $\max(\|\boldsymbol{\omega}_R\|)$  and the maximal angular acceleration  $\max(\|\dot{\boldsymbol{\omega}}_R\|)$ . The resulting values for the following four experiments are collected in Table 5.2.

	tricopter transitions	quadcopter transitions	quadcopter looping	quadcopter flip
$\max(\ \mathbf{v}_R\ )$ in $\frac{\text{m}}{\text{s}}$	2.2	3.4	4.2	2.3
$\max(\ \dot{\mathbf{v}}_R\ )$ in $\frac{\text{m}}{\text{s}^2}$	3.9	8.2	17.1	17.5
$\max(\ \boldsymbol{\omega}_R\ )$ in $\frac{\text{deg}}{\text{s}}$	318	271	537	736
$\max(\ \dot{\boldsymbol{\omega}}_R\ )$ in $\frac{\text{deg}}{\text{s}^2}$	497	1380	1610	2480
$\text{rms}(e_r)$ in m	0.013	0.017	0.027	0.026
$\text{rms}(e_R)$ in deg	1.1	1.3	2.5	2.1
$\text{rms}(e_\varphi)$ in deg	0.95	0.3	1.2	0.8

Table 5.2: Statistical values for the multicopter experiments

**Tricopter transitions.** Figure 5.23 shows measurements of the tricopter tracking polynomial transitions between constant configurations. A video of this experiment is available here<sup>1</sup>.

In the first 10 s the tricopter does some horizontal movement while maintaining the attitude and height. For the next 10 s it tracks similar trajectories, but this time using

<sup>1</sup><https://youtu.be/oS5PHe6HOK4>

the body tilt to generate the necessary horizontal force. The difference between the approaches is obvious in the trajectories for the servo angles for the first case and the roll and pitch angle for the second case. Furthermore a  $90^\circ$  heading transition is added to the last two position transitions. In the last third of the maneuver the tricopter tilts while maintaining its position. One can see that for a body tilt of  $15^\circ$  the servos have to tilt more than  $30^\circ$ . The last transition is a  $360^\circ$  heading rotation and 1 m height transition in 2 s. This is the part where we have the maximal attitude error of about  $5^\circ$ . Here in particular one can see that the heading error  $e_\varphi$  is the mayor part of the attitude error  $e_R$ .

Comparing the performance of this tricopter experiment with the following quadcopter experiments, see Table 5.2, one can see that the tricopter has the lowest position and attitude error. However, the comparison is not really fair since the quadcopter trajectories are much more dynamic.

**Quadcopter transitions.** Figure 5.24 shows measurements of the quadcopter tracking polynomial transitions between constant configurations. A video of this and the following experiments is available here<sup>2</sup>.

The reference trajectories are very similar to the previous transitions for the tricopter, but with reduced transitions times. The maximal velocity and acceleration, see Table 5.2, are achieved at about 12 s, for a 2 m horizontal transition in 1.5 s. Since the tilt here is almost  $45^\circ$  it is evident that the acceleration must be almost  $\|a_G\|$ . The last transition is a  $360^\circ$  heading rotation in 4 s, which is much slower as the corresponding maneuver for the tricopter due to the limited control torque of the quadcopter. On the other hand the heading error  $e_\varphi$  during this maneuver is much better as with the tricopter. This might be a positive result of the sophisticated thrust controller from section 5.4.

**Quadcopter looping.** Figure 5.25 shows measurements of the quadcopter tracking four looping trajectories. The reference trajectory for  $r_x$  and  $r_z$  is essentially a vertical circle with 2 m diameter, see Figure 5.22. The individual looping takes about 3 s from rest to rest.

This is the first maneuver which involves that the quadcopter is upside down, i.e.  $R_R e_z = -e_z$ , so an appropriate method for the heading reference generation is required here. Though the accelerations are quite high as well, this experiment has in comparison to the others the highest translational velocity. The fact that it has largest position and attitude errors could suggest that there are large model errors and/or unknown disturbances related to higher translational velocity.

**Quadcopter flip.** Figure 5.26 shows measurements of the quadcopter tracking six flip trajectories about different axis. A flip is a trajectory where the quadcopter does a  $360^\circ$  tilt transition while trying to minimize translational movement. The maneuver here requires a vertical clearance of less than 1 m and just a few centimeters horizontally. The individual flip takes less than 2 s from rest to rest.

---

<sup>2</sup><https://youtu.be/x66sua3M6RQ>

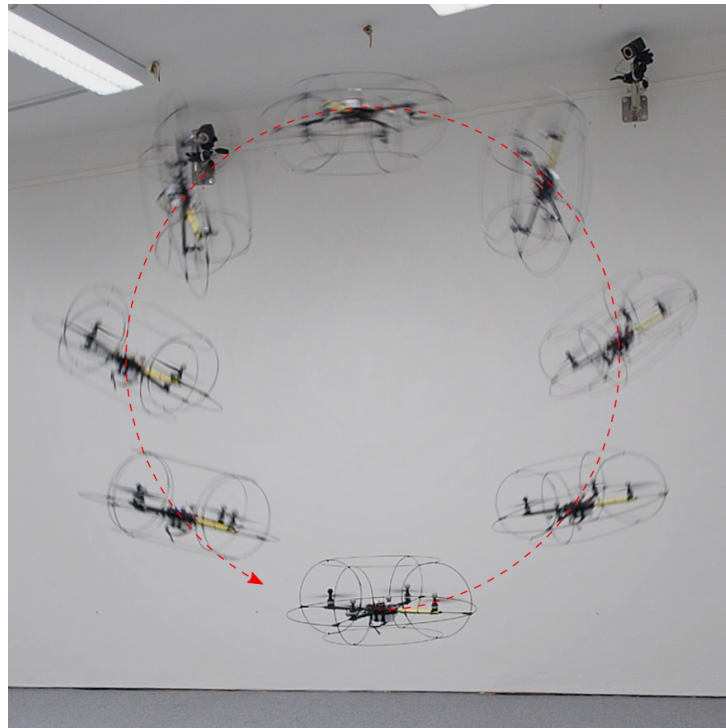


Figure 5.22: Snapshots of the quadcopter tracking the loop trajectory

This maneuver contains the largest translational and angular accelerations of the four experiments. The maximal linear acceleration of  $17.5 \frac{\text{m}}{\text{s}^2}$  obviously appears when the quadcopter is upside down. Here gravity pulls it with  $9.81 \frac{\text{m}}{\text{s}^2}$  and the propellers generate significant thrust in the same direction.

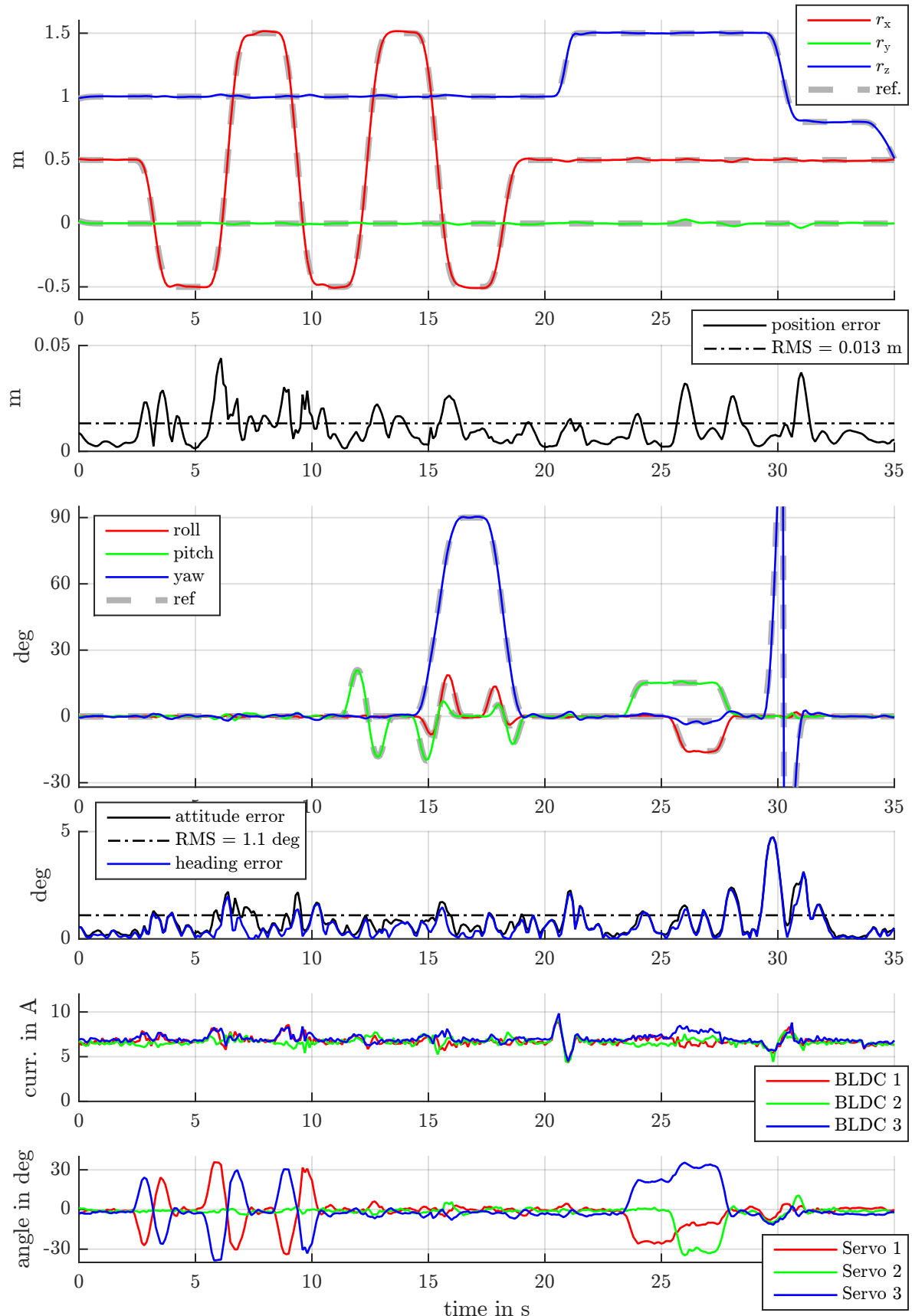


Figure 5.23: Tricopter flight test result for polynomial transition trajectories

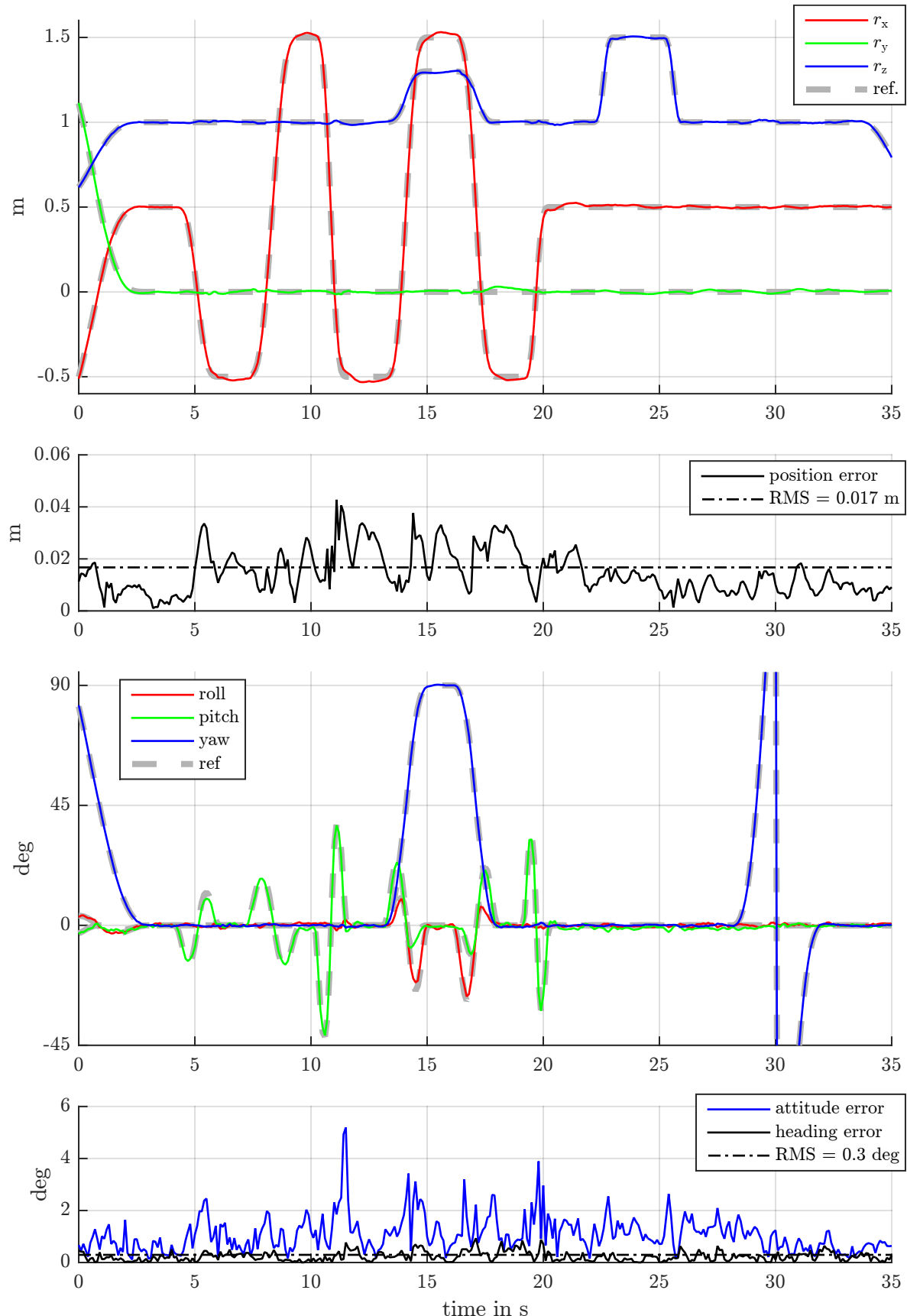


Figure 5.24: Quadcopter flight test result for polynomial transition trajectories

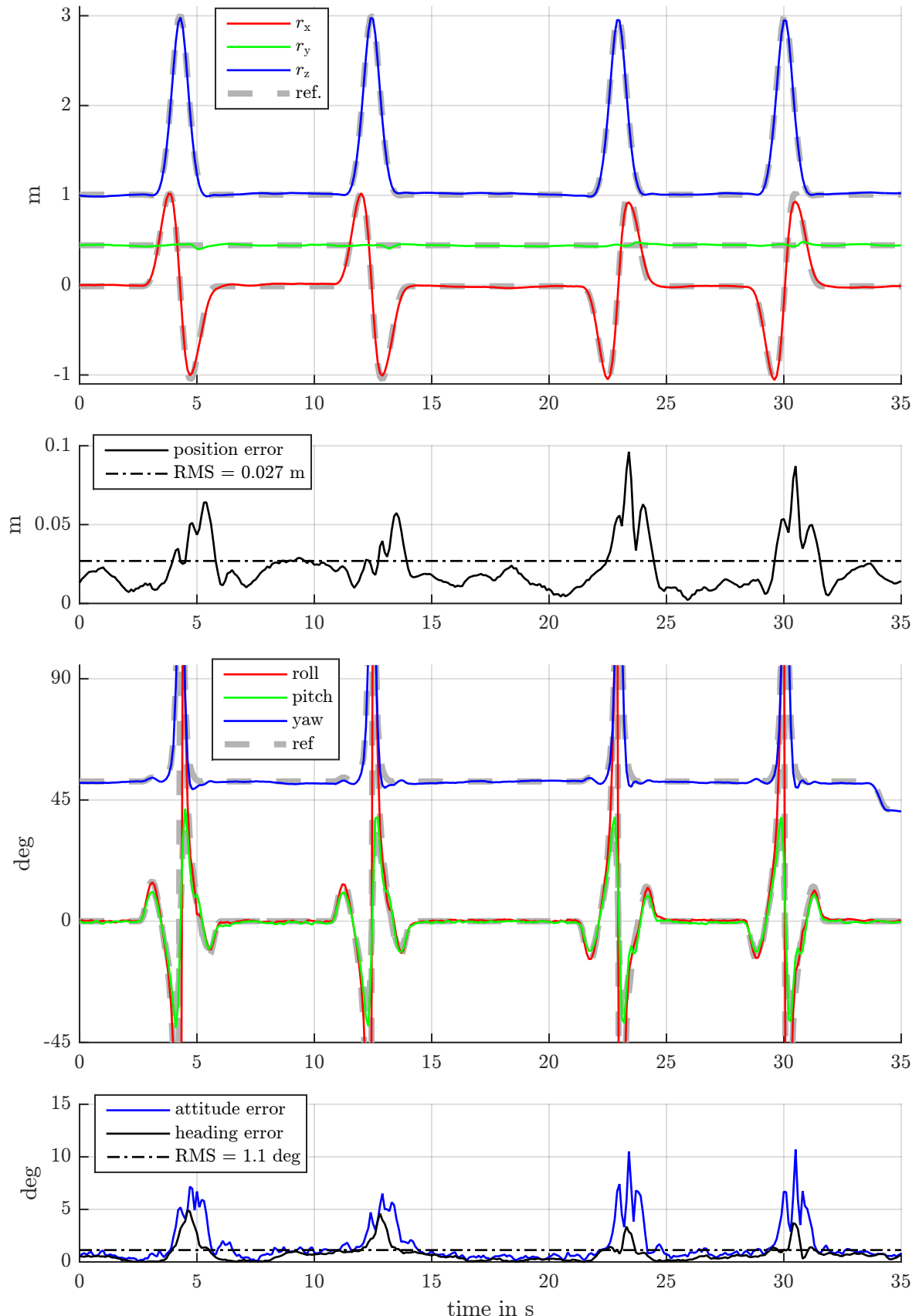


Figure 5.25: Quadcopter flight test result for looping trajectories

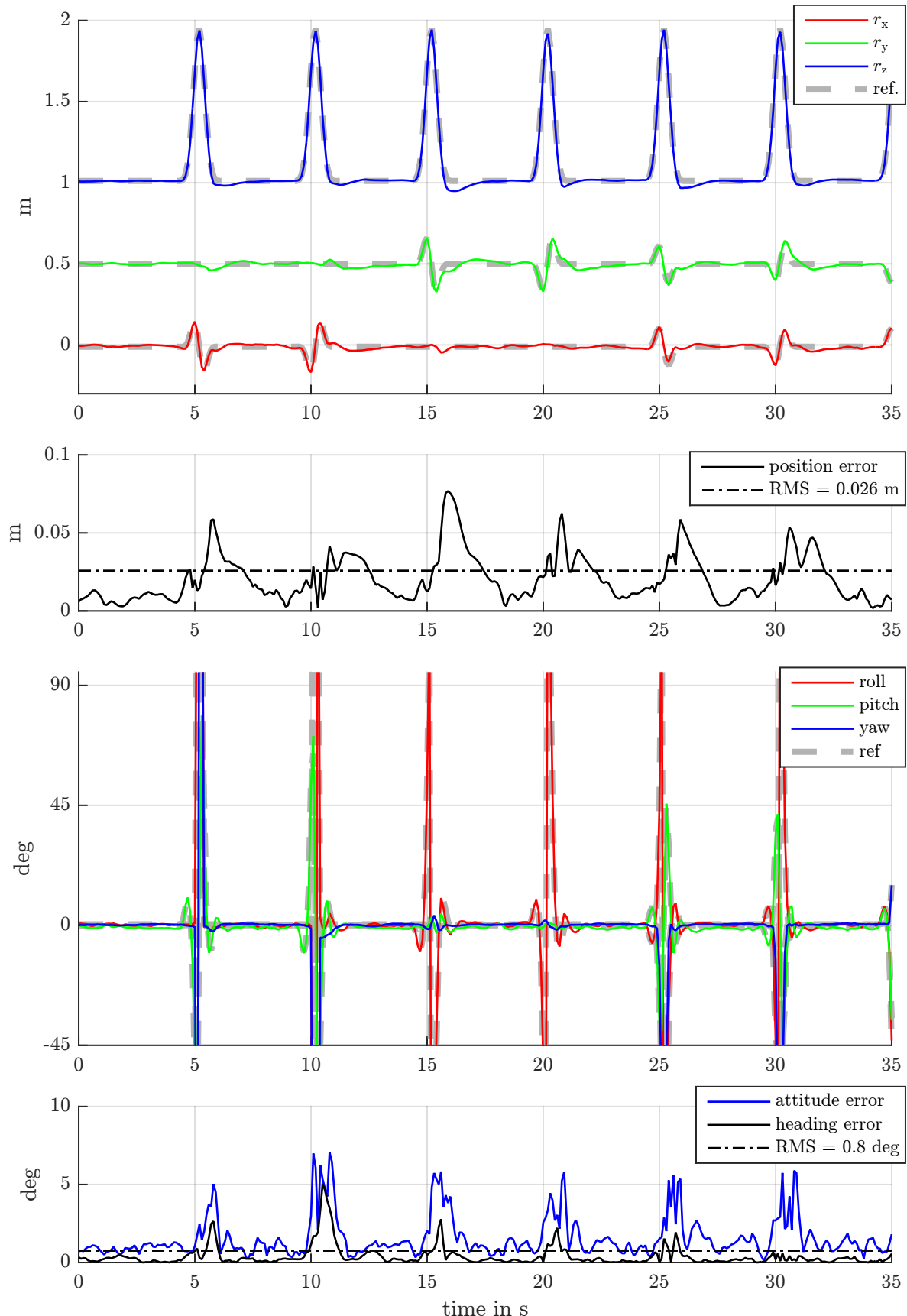


Figure 5.26: Quadcopter flight test result for the flip trajectories

# Appendix A

## Some math

### A.1 Linear algebra

#### A.1.1 Matrix sets

Define the following sets of real matrices that are frequently used in the work:

$$(\text{symmetric}) \quad \mathbb{S}\mathbb{Y}\mathbb{M}(n) = \{\mathbf{A} \in \mathbb{R}^{n \times n} \mid \mathbf{A} = \mathbf{A}^\top\}, \quad (\text{A.1a})$$

$$(\text{symmetric, pos. def.}) \quad \mathbb{S}\mathbb{Y}\mathbb{M}^+(n) = \{\mathbf{A} \in \mathbb{S}\mathbb{Y}\mathbb{M}(n) \mid \mathbf{x}^\top \mathbf{A} \mathbf{x} > 0 \forall \mathbf{x} \in \mathbb{R}^n \setminus \{\mathbf{0}\}\}, \quad (\text{A.1b})$$

$$(\text{sym., pos. semi-def.}) \quad \mathbb{S}\mathbb{Y}\mathbb{M}_0^+(n) = \{\mathbf{A} \in \mathbb{S}\mathbb{Y}\mathbb{M}(n) \mid \mathbf{x}^\top \mathbf{A} \mathbf{x} \geq 0 \forall \mathbf{x} \in \mathbb{R}^n \setminus \{\mathbf{0}\}\}, \quad (\text{A.1c})$$

$$(\text{unit sphere}) \quad \mathbb{S}^n = \{\mathbf{a} \in \mathbb{R}^n \mid \mathbf{a}^\top \mathbf{a} = 1\}, \quad (\text{A.1d})$$

$$(\text{orthogonal}) \quad \mathbb{O}(n) = \{\mathbf{A} \in \mathbb{R}^{n \times n} \mid \mathbf{A}^{-1} = \mathbf{A}^\top\}, \quad (\text{A.1e})$$

$$(\text{special orthogonal}) \quad \mathbb{SO}(n) = \{\mathbf{R} \in \mathbb{O}(n) \mid \det \mathbf{R} = +1\}, \quad (\text{A.1f})$$

$$(\text{special Euclidean}) \quad \mathbb{SE}(n) = \left\{ \begin{bmatrix} \mathbf{R} & \mathbf{r} \\ \mathbf{0} & 1 \end{bmatrix} \mid \mathbf{r} \in \mathbb{R}^n, \mathbf{R} \in \mathbb{SO}(n) \right\}, \quad (\text{A.1g})$$

$$(\text{skew symmetric}) \quad \mathfrak{so}(n) = \{\boldsymbol{\Omega} \in \mathbb{R}^{n \times n} \mid \boldsymbol{\Omega}^\top = -\boldsymbol{\Omega}\}, \quad (\text{A.1h})$$

$$\mathfrak{se}(n) = \left\{ \begin{bmatrix} \boldsymbol{\Omega} & \mathbf{v} \\ \mathbf{0} & 0 \end{bmatrix} \mid \boldsymbol{\Omega} \in \mathfrak{so}(n), \mathbf{v} \in \mathbb{R}^n \right\}. \quad (\text{A.1i})$$

#### A.1.2 Trace

The *trace* of a quadratic matrix  $\mathbf{A} \in \mathbb{R}^{n \times n}$  is the sum of its diagonal entries

$$\text{tr } \mathbf{A} = \sum_{i=1}^n A_{ii} \quad (\text{A.2})$$

Some properties of the trace are

$$\mathbf{A}, \mathbf{B} \in \mathbb{R}^{n \times n}, \lambda \in \mathbb{R} : \quad \text{tr}(\mathbf{A} + \mathbf{B}) = \text{tr} \mathbf{A} + \text{tr} \mathbf{B}, \quad (\text{A.3a})$$

$$\text{tr}(\lambda \mathbf{A}) = \lambda \text{tr} \mathbf{A}, \quad (\text{A.3b})$$

$$\text{tr} \mathbf{A}^\top = \text{tr} \mathbf{A}, \quad (\text{A.3c})$$

$$\mathbf{A} \in \mathbb{R}^{n \times m}, \mathbf{B} \in \mathbb{R}^{m \times n} : \quad \text{tr}(\mathbf{AB}) = \text{tr}(\mathbf{BA}), \quad (\text{A.3d})$$

$$\mathbf{A}, \mathbf{P} \in \mathbb{R}^{n \times n}, \det \mathbf{P} \neq 0 : \quad \text{tr}(\mathbf{P}^{-1} \mathbf{AP}) = \text{tr} \mathbf{A}. \quad (\text{A.3e})$$

$$\mathbf{K} \in \text{SYM}(n), \boldsymbol{\Omega} \in \mathfrak{so}(n) : \quad \text{tr}(\mathbf{K}\boldsymbol{\Omega}) = 0. \quad (\text{A.3f})$$

For matrices  $\mathbf{A}, \mathbf{B} \in \mathbb{R}^{n \times n}, n \geq 2$  we may define the bijective mapping

$$\mathbf{B} = \text{tr}(\mathbf{A})\mathbf{I}_n - \mathbf{A} \quad \Leftrightarrow \quad \mathbf{A} = \frac{1}{n-1} \text{tr}(\mathbf{B})\mathbf{I}_n - \mathbf{B}. \quad (\text{A.4})$$

which is due to  $\text{tr} \mathbf{B} = (n-1) \text{tr} \mathbf{A}$ .

### A.1.3 Inner product

**Inner product.** For matrices  $\mathbf{A}, \mathbf{B} \in \mathbb{R}^{n \times m}$  and a symmetric, positive definite matrix  $\mathbf{K} \in \text{SYM}^+(n)$ , define an *inner product* as

$$\langle \mathbf{A}, \mathbf{B} \rangle_{\mathbf{K}} = \text{tr}(\mathbf{A}^\top \mathbf{K} \mathbf{B}). \quad (\text{A.5})$$

For  $\mathbf{A}, \mathbf{B}, \mathbf{C} \in \mathbb{R}^{n \times m}$  and  $\lambda \in \mathbb{R}$  we have the basic properties

$$(\text{linearity}) \quad \langle \lambda \mathbf{A}, \mathbf{B} \rangle_{\mathbf{K}} = \lambda \langle \mathbf{A}, \mathbf{B} \rangle_{\mathbf{K}} = \langle \mathbf{A}, \lambda \mathbf{B} \rangle_{\mathbf{K}}, \quad (\text{A.6a})$$

$$\langle \mathbf{A} + \mathbf{C}, \mathbf{B} \rangle_{\mathbf{K}} = \langle \mathbf{A}, \mathbf{B} \rangle_{\mathbf{K}} + \langle \mathbf{C}, \mathbf{B} \rangle_{\mathbf{K}} \quad (\text{A.6b})$$

$$(\text{symmetry}) \quad \langle \mathbf{B}, \mathbf{A} \rangle_{\mathbf{K}} = \langle \mathbf{A}, \mathbf{B} \rangle_{\mathbf{K}} \quad (\text{A.6c})$$

$$(\text{positive definiteness}) \quad \langle \mathbf{A}, \mathbf{A} \rangle_{\mathbf{K}} \geq 0, \quad \langle \mathbf{A}, \mathbf{A} \rangle_{\mathbf{K}} = 0 \Leftrightarrow \mathbf{A} = \mathbf{0}. \quad (\text{A.6d})$$

Setting  $\mathbf{K} = \mathbf{I}_n$  in the definition (A.5) is called the *Frobenius inner product* in [Horn and Johnson, 1985, sec. 5.2] or *Hilbert-Schmidt inner product* in [Hall, 2015, sec. A.6]. Furthermore, for  $\mathbf{A}, \mathbf{B} \in \mathbb{R}^{n \times 1}$  it coincides with the common *dot product*.

**Norm.** The induced norm is

$$\|\mathbf{A}\|_{\mathbf{K}} = \sqrt{\langle \mathbf{A}, \mathbf{A} \rangle_{\mathbf{K}}}. \quad (\text{A.7})$$

For  $\mathbf{A}, \mathbf{B} \in \mathbb{R}^{n \times m}$  and  $\lambda \in \mathbb{R}$  we have the basic properties

$$(\text{triangle inequality}) \quad \|\mathbf{A} + \mathbf{B}\|_{\mathbf{K}} \leq \|\mathbf{A}\|_{\mathbf{K}} + \|\mathbf{B}\|_{\mathbf{K}} \quad (\text{A.8a})$$

$$(\text{absolute homogeneity}) \quad \|\lambda \mathbf{A}\|_{\mathbf{K}} = |\lambda| \|\mathbf{A}\|_{\mathbf{K}}, \quad (\text{A.8b})$$

$$(\text{positive definiteness}) \quad \|\mathbf{A}\|_{\mathbf{K}} \geq 0, \quad \|\mathbf{A}\|_{\mathbf{K}} = 0 \Leftrightarrow \mathbf{A} = \mathbf{0}. \quad (\text{A.8c})$$

**Metric.** The induced metric is

$$d_{\mathbf{K}}(\mathbf{A}, \mathbf{B}) = \|\mathbf{A} - \mathbf{B}\|_{\mathbf{K}}. \quad (\text{A.9})$$

For  $\mathbf{A}, \mathbf{B}, \mathbf{C} \in \mathbb{R}^{n \times m}$  and  $\lambda \in \mathbb{R}$  we have the basic properties

$$(\text{triangle inequality}) \quad d_{\mathbf{K}}(\mathbf{A}, \mathbf{B}) \leq d_{\mathbf{K}}(\mathbf{A}, \mathbf{C}) + d_{\mathbf{K}}(\mathbf{B}, \mathbf{C}) \quad (\text{A.10a})$$

$$(\text{symmetry}) \quad d_{\mathbf{K}}(\mathbf{A}, \mathbf{B}) = d_{\mathbf{K}}(\mathbf{B}, \mathbf{A}), \quad (\text{A.10b})$$

$$(\text{positive definiteness}) \quad d_{\mathbf{K}}(\mathbf{A}, \mathbf{B}) \geq 0, \quad d_{\mathbf{K}}(\mathbf{A}, \mathbf{B}) = 0 \Leftrightarrow \mathbf{A} = \mathbf{B}. \quad (\text{A.10c})$$

#### A.1.4 Vee & wedge

Define the wed operator for vectors as

$$\text{wed} : \mathbb{R}^3 \rightarrow \mathfrak{so}(3) : \begin{bmatrix} \omega_1 \\ \omega_2 \\ \omega_3 \end{bmatrix} \mapsto \begin{bmatrix} 0 & -\omega_3 & \omega_2 \\ \omega_3 & 0 & -\omega_1 \\ -\omega_2 & \omega_1 & 0 \end{bmatrix}, \quad (\text{A.11a})$$

$$\text{wed} : \mathbb{R}^6 \rightarrow \mathfrak{se}(3) : \begin{bmatrix} \mathbf{v} \\ \boldsymbol{\omega} \end{bmatrix} \mapsto \begin{bmatrix} \text{wed } \boldsymbol{\omega} & \mathbf{v} \\ \mathbf{0} & 0 \end{bmatrix}, \quad (\text{A.11b})$$

The corresponding inverse operator is denoted vee.

Furthermore, define the vee2 operator through

$$\text{tr}(\mathbf{A}(\text{wed } \boldsymbol{\xi})^\top) = \boldsymbol{\xi}^\top \text{vee2}(\mathbf{A}). \quad (\text{A.12})$$

The particular important cases for this work are

$$\text{vee2} : \mathbb{R}^{3 \times 3} \rightarrow \mathbb{R}^3 : \begin{bmatrix} * & A_{12} & A_{13} \\ A_{21} & * & A_{23} \\ A_{31} & A_{32} & * \end{bmatrix} \mapsto \begin{bmatrix} A_{32} - A_{23} \\ A_{13} - A_{31} \\ A_{21} - A_{12} \end{bmatrix}, \quad (\text{A.13a})$$

$$\text{vee2} : \mathbb{R}^{4 \times 4} \rightarrow \mathbb{R}^6 : \begin{bmatrix} \mathbf{A} & \mathbf{b} \\ * & * \end{bmatrix} \mapsto \begin{bmatrix} \mathbf{b} \\ \text{vee2 } \mathbf{A} \end{bmatrix}. \quad (\text{A.13b})$$

Note that for  $\boldsymbol{\Omega} \in \mathfrak{so}(3) \subset \mathbb{R}^{3 \times 3}$  we have  $\text{vee2}(\boldsymbol{\Omega}) = 2 \text{vee}(\boldsymbol{\Omega})$ , thus giving the motivation for the name.

For matrices define the Vee through the relation

$$\text{vee2}(\text{wed } \boldsymbol{\xi} \mathbf{A}) = \text{Vee}(\mathbf{A})\boldsymbol{\xi}. \quad (\text{A.14})$$

The particular important cases for this work are

$$\text{Vee} : \mathbb{R}^{3 \times 3} \rightarrow \mathbb{R}^{3 \times 3} : \mathbf{A} \mapsto \text{tr}(\mathbf{A})\mathbf{I}_3 - \mathbf{A}, \quad (\text{A.15a})$$

$$\text{Vee} : \mathbb{R}^{4 \times 4} \rightarrow \mathbb{R}^{6 \times 6} : \begin{bmatrix} \mathbf{A} & \mathbf{b} \\ \mathbf{c}^\top & d \end{bmatrix} \mapsto \begin{bmatrix} d\mathbf{I}_3 & (\text{wed } \mathbf{b})^\top \\ \text{wed } \mathbf{c} & \text{Vee } \mathbf{A} \end{bmatrix}, \quad (\text{A.15b})$$

The corresponding inverse operator is denoted Wed. Combining (A.13) and (A.15) yields

$$\text{tr}(\text{wed } \boldsymbol{\xi} \mathbf{A}(\text{wed } \boldsymbol{\eta})^\top) = \boldsymbol{\eta}^\top \text{Vee}(\mathbf{A})\boldsymbol{\xi}. \quad (\text{A.16})$$

## A.2 SVD and polar decomposition

### A.2.1 Singular value decomposition (SVD)

Any matrix  $\mathbf{A} \in \mathbb{R}^{n \times m}$  can be decomposed into  $\mathbf{A} = \mathbf{X}\Sigma\mathbf{Y}^\top$ , where  $\mathbf{X} \in \mathbb{O}(n)$ ,  $\mathbf{Y} \in \mathbb{O}(m)$  and  $\Sigma \in \mathbb{R}^{n \times m}$  with  $\Sigma_{ii} \geq 0, i = 1, \dots, \min(n, m)$ ,  $\Sigma_{ij} = 0, i \neq j$ .

- The columns of  $\mathbf{X}$  are eigenvectors of  $\mathbf{A}\mathbf{A}^\top = \mathbf{X}(\Sigma\Sigma^\top)\mathbf{X}^\top$ .
- The columns of  $\mathbf{Y}$  are eigenvectors of  $\mathbf{A}^\top\mathbf{A} = \mathbf{Y}(\Sigma^\top\Sigma)\mathbf{Y}^\top$ .

It is common practice to place the singular values in descending order, i.e.  $\Sigma_{ii} \geq \Sigma_{jj}, i > j$ , thus making  $\Sigma$  unique. The matrices  $\mathbf{X}$  and  $\mathbf{Y}$  are unique up to orthogonal transformations of the subspaces of each singular value and the kernel and co-kernel of  $\mathbf{A}$ .

### A.2.2 Polar decomposition

Any square matrix  $\mathbf{A} \in \mathbb{R}^{n \times n}$  can be decomposed into  $\mathbf{A} = \mathbf{U}\mathbf{K}$ , where  $\mathbf{U} \in \mathbb{O}(n)$ ,  $\mathbf{K} \in \mathbb{SYM}_0^+(n)$ . The matrix  $\mathbf{K}$  is uniquely defined while  $\mathbf{U}$  is only unique if  $\mathbf{A}$  is invertible. The same holds for the decomposition  $\mathbf{A} = \mathbf{L}\mathbf{V}$ , where  $\mathbf{V} \in \mathbb{O}(n)$ ,  $\mathbf{L} \in \mathbb{SYM}_0^+(n)$ . The relation to the singular value decomposition  $\mathbf{A} = \mathbf{X}\Sigma\mathbf{Y}^\top$  is

$$\mathbf{U} = \mathbf{X}\mathbf{Y}^\top, \quad \mathbf{K} = \mathbf{Y}\Sigma\mathbf{Y}^\top \quad \text{and} \quad \mathbf{L} = \mathbf{X}\Sigma\mathbf{X}^\top, \quad \mathbf{V} = \mathbf{X}\mathbf{Y}^\top. \quad (\text{A.17})$$

### A.2.3 Special singular decomposition

One problem when dealing with rigid body attitudes, i.e.  $\mathbb{SO}(3)$ , is that the singular value decomposition and orthogonal decomposition return orthogonal matrices, i.e.  $\det \mathbf{X}, \det \mathbf{Y} = \pm 1$ , which might not be pure rotations. A way to mend this was proposed in [Kabsch, 1976]: Consider the SVD  $\mathbf{A} = \mathbf{X}\Sigma\mathbf{Y}^\top$  and define

$$\bar{\mathbf{X}} = \mathbf{X} \operatorname{diag}(1, \dots, 1, \det \mathbf{X}) \in \mathbb{SO}(n), \quad (\text{A.18a})$$

$$\bar{\mathbf{Y}} = \mathbf{Y} \operatorname{diag}(1, \dots, 1, \det \mathbf{Y}) \in \mathbb{SO}(n), \quad (\text{A.18b})$$

$$\bar{\Sigma} = \operatorname{diag}(\Sigma_{1,1}, \dots, \Sigma_{n-1,n-1}, \Sigma_{n,n} \det \mathbf{X} \det \mathbf{Y}). \quad (\text{A.18c})$$

i.e. flip the directions corresponding to the smallest singular value  $\Sigma_{n,n}$  if the original orthonormal matrix contains a reflection. We have a possibly different decomposition  $\mathbf{A} = \bar{\mathbf{X}}\bar{\Sigma}\bar{\mathbf{Y}}^\top$ .

For the following we restrict to *square matrices*  $\mathbf{A}$  and consequently  $\bar{\Sigma}$ . Since  $\bar{\Sigma}_{n,n} = \Sigma_{n,n} \det \mathbf{X} \det \mathbf{Y}$  might be negative, the matrix  $\bar{\Sigma}$  is, in general, indifferent. Nevertheless, since only the smallest singular value might be flipped, the matrix  $\operatorname{Vee}(\bar{\Sigma}) = \bar{\Lambda}$  is positive semidefinite.

In the following we call  $\mathbf{A} = \bar{\mathbf{X}} \operatorname{Wed}(\bar{\Lambda}) \bar{\mathbf{Y}}^\top$  with  $\bar{\mathbf{X}}, \bar{\mathbf{Y}} \in \mathbb{SO}(n)$  and  $\bar{\Lambda} \in \mathbb{R}^{n \times n}$  with  $\bar{\Lambda}_{ii} \geq 0, i = 1, \dots, n$ ,  $\bar{\Lambda}_{ij} = 0, i \neq j$  the *special* singular value decomposition. Note that the property of the SVD  $\bar{\Sigma}_{1,1} \geq \dots \geq \bar{\Sigma}_{n-1,n-1} \geq |\bar{\Sigma}_{n,n}| \geq 0$  implies  $\bar{\Lambda}_{1,1} \geq \dots \geq \bar{\Lambda}_{n-1,n-1} \geq \bar{\Lambda}_{n,n} \geq 0$ . The uniqueness of  $\bar{\mathbf{X}}, \bar{\Lambda}, \bar{\mathbf{Y}}$  is the same as for the SVD.

### A.2.4 Special polar decomposition

Using the special singular value decomposition above we may write

$$\mathbf{A} = \bar{\mathbf{X}} \underbrace{\bar{\mathbf{Y}}^\top \bar{\mathbf{Y}}}_{\mathbf{I}_n} \text{Wed}(\bar{\mathbf{A}}) \bar{\mathbf{Y}}^\top = \underbrace{\bar{\mathbf{X}} \bar{\mathbf{Y}}^\top}_{\mathbf{U} \in \mathbb{SO}(n)} \text{Wed} \left( \underbrace{\bar{\mathbf{Y}} \bar{\mathbf{A}} \bar{\mathbf{Y}}^\top}_{\mathbf{K} \in \mathbb{SYM}_0^+(n)} \right) \quad (\text{A.19a})$$

$$= \bar{\mathbf{X}} \text{Wed}(\bar{\mathbf{A}}) \underbrace{\bar{\mathbf{X}}^\top \bar{\mathbf{X}} \bar{\mathbf{Y}}^\top}_{\mathbf{I}_n} = \text{Wed} \left( \underbrace{\bar{\mathbf{X}} \bar{\mathbf{A}} \bar{\mathbf{X}}^\top}_{\mathbf{L} \in \mathbb{SYM}_0^+(n)} \right) \underbrace{\bar{\mathbf{X}} \bar{\mathbf{Y}}^\top}_{\mathbf{U} \in \mathbb{SO}(n)} \quad (\text{A.19b})$$

Since this only involves proper rotations this is potentially useful in physics where we can't have reflections.

These special versions of the singular value and polar decomposition are not established in the literature to the best of the authors knowledge.

## A.3 Attitude potential

We are interested in the extrema of the function

$$\mathcal{V}(\mathbf{R}) = -\text{tr}(\mathbf{P}\mathbf{R}), \quad \mathbf{R} \in \mathbb{SO}(3) \quad (\text{A.20})$$

with the constant parameter  $\mathbf{P} \in \mathbb{R}^{3 \times 3}$ . Similar functions appear in the context of attitude control [Koditschek, 1989] or in the so-called Wahba's problem [Wahba, 1965].

**Coordinate transformation.** A crucial ingredient for the solution is what we called the *special singular value decomposition* above: Let  $\mathbf{P} = \bar{\mathbf{X}} \text{Wed}(\bar{\mathbf{A}}) \bar{\mathbf{Y}}^\top$  with  $\bar{\mathbf{X}}, \bar{\mathbf{Y}} \in \mathbb{SO}(3)$  and  $\bar{\mathbf{A}} = \text{diag}(\lambda_1, \lambda_2, \lambda_3)$ ,  $\lambda_1 \geq \lambda_2 \geq \lambda_3 \geq 0$ . With this we define the transformed function

$$\mathcal{V}(\mathbf{R}) = -\text{tr}(\bar{\mathbf{X}} \text{Wed}(\bar{\mathbf{A}}) \bar{\mathbf{Y}}^\top \mathbf{R}) = -\text{tr}(\text{Wed}(\bar{\mathbf{A}}) \underbrace{\bar{\mathbf{Y}}^\top \mathbf{R} \bar{\mathbf{X}}}_{\bar{\mathbf{R}}}) =: \bar{\mathcal{V}}(\bar{\mathbf{R}}) \quad (\text{A.21})$$

Since the SVD is not unique in general, the transformed function  $\bar{\mathcal{V}}$  is neither. However, since the coordinate transformation  $\mathbf{R} = \bar{\mathbf{Y}} \bar{\mathbf{R}} \bar{\mathbf{X}}^\top$  is bijective, no information is lost here.

**Critical points.** The first and second differential of the transformed function are

$$\nabla \bar{\mathcal{V}}(\bar{\mathbf{R}}) = \text{vee2}(\text{Wed}(\bar{\mathbf{A}}) \bar{\mathbf{R}}), \quad (\text{A.22})$$

$$\nabla^2 \bar{\mathcal{V}}(\bar{\mathbf{R}}) = \text{Vee}(\text{Wed}(\bar{\mathbf{A}}) \bar{\mathbf{R}})^\top. \quad (\text{A.23})$$

So, for a critical point  $\bar{\mathbf{R}}_0 : \nabla \bar{\mathcal{V}}(\bar{\mathbf{R}}_0) = \mathbf{0}$  we need the matrix  $\text{Wed}(\bar{\mathbf{A}}) \bar{\mathbf{R}}_0$  to be symmetric. An obvious critical point is  $\bar{\mathbf{R}}_0 = \mathbf{I}_3$  which is a minimum if  $\nabla^2 \bar{\mathcal{V}}(\mathbf{I}_3) = \bar{\mathbf{A}}$  is positive definite. Depending on the actual constellation of  $\lambda_1 \geq \lambda_2 \geq \lambda_3 \geq 0$  we have more critical points or submanifolds which are analysed in the following:

- Distinct eigenvalues:  $\lambda_3 > \lambda_2 > \lambda_1 > 0$ : We have the critical points

$$\bar{\mathbf{R}}_0 = \mathbf{I}_3 : \quad \mathcal{V}(\bar{\mathbf{R}}_0) = -\frac{\lambda_1}{2} - \frac{\lambda_2}{2} - \frac{\lambda_3}{2}, \quad \text{eig}(\nabla^2 \bar{\mathcal{V}}(\bar{\mathbf{R}}_0)) = \{\lambda_3, \lambda_2, \lambda_1\} \quad (\text{A.24a})$$

$$\bar{\mathbf{R}}_1 = \text{diag}(1, -1, -1) : \quad \mathcal{V}(\bar{\mathbf{R}}_1) = \frac{3\lambda_1 - \lambda_2 - \lambda_3}{2}, \quad \text{eig}(\nabla^2 \bar{\mathcal{V}}(\bar{\mathbf{R}}_1)) = \{\lambda_3 - \lambda_1, \lambda_2 - \lambda_1, -\lambda_1\} \quad (\text{A.24b})$$

$$\bar{\mathbf{R}}_2 = \text{diag}(-1, 1, -1) : \quad \mathcal{V}(\bar{\mathbf{R}}_2) = \frac{3\lambda_2 - \lambda_1 - \lambda_3}{2}, \quad \text{eig}(\nabla^2 \bar{\mathcal{V}}(\bar{\mathbf{R}}_2)) = \{\lambda_3 - \lambda_2, \lambda_1 - \lambda_2, -\lambda_2\} \quad (\text{A.24c})$$

$$\bar{\mathbf{R}}_3 = \text{diag}(-1, -1, 1) : \quad \mathcal{V}(\bar{\mathbf{R}}_3) = \frac{3\lambda_3 - \lambda_1 - \lambda_2}{2}, \quad \text{eig}(\nabla^2 \bar{\mathcal{V}}(\bar{\mathbf{R}}_3)) = \{\lambda_2 - \lambda_3, \lambda_1 - \lambda_3, -\lambda_3\} \quad (\text{A.24d})$$

so  $\bar{\mathbf{R}}_0$  is a minimum,  $\bar{\mathbf{R}}_1$  and  $\bar{\mathbf{R}}_2$  are saddle points, and  $\bar{\mathbf{R}}_3$  is a maximum.

- Double eigenvalue:  $\lambda_3 > \lambda_2 = \lambda_1 > 0$ : We have a minimum at  $\bar{\mathbf{R}}_0$ , a maximum at  $\bar{\mathbf{R}}_3$  and a saddle on the circular manifold

$$\bar{\mathbf{R}}_4 = \begin{bmatrix} -c & s & 0 \\ s & c & 0 \\ 0 & 0 & -1 \end{bmatrix}, \quad c^2 + s^2 = 1 : \quad \mathcal{V}(\bar{\mathbf{R}}_4) = \lambda_1 - \frac{\lambda_3}{2}, \quad \text{eig}(\nabla^2 \bar{\mathcal{V}}(\bar{\mathbf{R}}_4)) = \{\lambda_3 - \lambda_1, 0, -\lambda_1\} \quad (\text{A.24e})$$

which includes the points  $\bar{\mathbf{R}}_1$  and  $\bar{\mathbf{R}}_2$ .

- Double eigenvalue:  $\lambda_3 = \lambda_2 > \lambda_1 > 0$ : Analog to above we have a minimum at  $\bar{\mathbf{R}}_0$ , a saddle at  $\bar{\mathbf{R}}_4$  and a maximum on the circular manifold

$$\bar{\mathbf{R}}_5 = \begin{bmatrix} -1 & 0 & 0 \\ 0 & c & s \\ 0 & s & -c \end{bmatrix}, \quad c^2 + s^2 = 1 : \quad \mathcal{V}(\bar{\mathbf{R}}_5) = \lambda_2 - \frac{\lambda_1}{2}, \quad \text{eig}(\nabla^2 \bar{\mathcal{V}}(\bar{\mathbf{R}}_5)) = \{0, \lambda_1 - \lambda_2, -\lambda_2\} \quad (\text{A.24f})$$

which includes the points  $\bar{\mathbf{R}}_2$  and  $\bar{\mathbf{R}}_3$ .

- Triple eigenvalue:  $\lambda_3 = \lambda_2 = \lambda_1 > 0$ : Minimum at  $\bar{\mathbf{R}}_0$  and a maximum on the spherical manifold

$$\bar{\mathbf{R}}_6 = \begin{bmatrix} q_x^2 - q_y^2 - q_z^2 & 2q_x q_y & 2q_x q_z \\ 2q_x q_y & q_y^2 - q_x^2 + q_z^2 & 2q_y q_z \\ 2q_x q_z & 2q_y q_z & q_z^2 - q_x^2 - q_y^2 \end{bmatrix}, \quad q_x^2 + q_y^2 + q_z^2 = 1 : \quad \mathcal{V}(\bar{\mathbf{R}}_6) = \frac{\lambda_1}{2}, \quad \text{eig}(\nabla^2 \bar{\mathcal{V}}(\bar{\mathbf{R}}_6)) = \{0, 0, -\lambda_1\} \quad (\text{A.24g})$$

which includes the points  $\bar{\mathbf{R}}_1$ ,  $\bar{\mathbf{R}}_2$  and  $\bar{\mathbf{R}}_3$  and the circles  $\bar{\mathbf{R}}_4$  and  $\bar{\mathbf{R}}_5$ . It corresponds to a  $180^\circ$  rotation about an arbitrary axis  $[q_x, q_y, q_z]^\top \in \mathbb{S}^2$ .

- One zero eigenvalue:  $\lambda_3 > \lambda_2 > \lambda_1 = 0$ : We have a minimum on the circular manifold

$$\bar{\mathbf{R}}_7 = \begin{bmatrix} 1 & 0 & 0 \\ 0 & c & -s \\ 0 & s & c \end{bmatrix}, \quad c^2 + s^2 = 1 : \quad \mathcal{V}(\bar{\mathbf{R}}_7) = -\frac{\lambda_2 + \lambda_3}{2}, \quad \text{eig}(\nabla^2 \bar{\mathcal{V}}(\bar{\mathbf{R}}_7)) = \{\lambda_3, \lambda_2, 0\} \quad (\text{A.24h})$$

which includes  $\bar{\mathbf{R}}_0$  and  $\bar{\mathbf{R}}_1$ . Furthermore we have a saddle point at  $\bar{\mathbf{R}}_2$  and a maximum at  $\bar{\mathbf{R}}_3$ .

- Double eigenvalue and zero eigenvalue:  $\lambda_3 = \lambda_2 > \lambda_1 = 0$ : We have a minimum on  $\bar{\mathbf{R}}_7$  and a maximum on  $\bar{\mathbf{R}}_5$ .
- Two zero eigenvalues:  $\lambda_3 > \lambda_2 = \lambda_1 = 0$ : We have a minimum on the spherical manifold

$$\bar{\mathbf{R}}_8 = \begin{bmatrix} q_w^2 + q_x^2 - q_y^2 & 2q_x q_y & 2q_w q_y \\ 2q_x q_y & q_w^2 - q_x^2 + q_y^2 & -2q_w q_x \\ -2q_w q_x & 2q_w q_x & q_w^2 - q_x^2 - q_y^2 \end{bmatrix}, \quad q_w^2 + q_x^2 + q_y^2 = 1 : \\ \mathcal{V}(\bar{\mathbf{R}}_8) = -\frac{\lambda_3}{2}, \quad \text{eig}(\nabla^2 \bar{\mathcal{V}}(\bar{\mathbf{R}}_8)) = \{\lambda_3, 0, 0\} \quad (\text{A.24i})$$

which includes  $\bar{\mathbf{R}}_0$ ,  $\bar{\mathbf{R}}_1$  and  $\bar{\mathbf{R}}_2$  and corresponds to an arbitrary rotation about an axis  $[q_x, q_y, 0]^\top$ . Furthermore we have a maximum at  $\bar{\mathbf{R}}_3$ .

- All zero Eigenvalues:  $\lambda_3 = \lambda_2 = \lambda_1 = 0$ : for this we have  $\bar{\boldsymbol{\Sigma}} = \mathbf{P} = \mathbf{0}$  and the function is  $\mathcal{V} = 0$ .

We may conclude that the function  $\bar{\mathcal{V}}$  has a minimum at  $\bar{\mathbf{R}}_0 = \mathbf{I}_3$  and a maximum at  $\bar{\mathbf{R}}_3 = \text{diag}(-1, -1, 1)$ , though they may not be strict. The minimum is strict if and only if  $\lambda_1 > 0$ . The maximum is strict if and only if  $\lambda_3 > \lambda_2$ .

It should also be noted that the results of this paragraph would be much more “symmetric” if we would not have required the descending order of the singular values  $\sigma_i$ . This did however reduce the number of cases to distinguish.

**Original coordinates.** The original function  $\mathcal{V}$  has a minimum at  $\mathbf{R}_0 = \bar{\mathbf{Y}} \bar{\mathbf{X}}^\top$ . The minimum  $\mathbf{R}_0$  is strict, if, and only if,  $\lambda_i > 0, i = 1, 2, 3$  or equivalently if  $\mathbf{K}$  is positive definite:

$$\mathbf{K} = \nabla^2 \mathcal{V}(\mathbf{R}_0) = \text{Vee}(\mathbf{P} \mathbf{R}_0) = \bar{\mathbf{X}} \boldsymbol{\Lambda} \bar{\mathbf{X}}^\top. \quad (\text{A.25})$$

Note that the minimum  $\mathbf{R}_0$  and the Hessian  $\mathbf{K}$  coincide with the special orthogonal decomposition  $\mathbf{P}^\top = \mathbf{R}_0 \text{Wed}(\mathbf{K})$  introduced above.

**Prototype for a positive definite function.** Subtracting the minimal value  $\mathcal{V}(\mathbf{R}_0)$  from the function we obtain

$$\begin{aligned} \hat{\mathcal{V}}(\mathbf{R}) &= \mathcal{V}(\mathbf{R}) - \mathcal{V}(\mathbf{R}_0) \\ &= -\text{tr}(\bar{\mathbf{X}} \text{Wed}(\boldsymbol{\Lambda}) \bar{\mathbf{Y}}^\top \mathbf{R}) + \frac{1}{2} \text{tr}(\boldsymbol{\Lambda}) \\ &= -\text{tr}(\bar{\mathbf{X}} \text{Wed}(\boldsymbol{\Lambda}) \bar{\mathbf{X}}^\top \mathbf{R}_0^\top \mathbf{R}) + \text{tr}(\text{Wed}(\mathbf{K})) \\ &= \text{tr}(\text{Wed}(\mathbf{K})(\mathbf{I}_3 - \mathbf{R}_0^\top \mathbf{R})) \end{aligned} \quad (\text{A.26a})$$

$$\begin{aligned} &= \frac{1}{2} \text{tr}(\text{Wed}(\mathbf{K})(\mathbf{R} - \mathbf{R}_0)^\top (\mathbf{R} - \mathbf{R}_0)) \\ &= \frac{1}{2} \|\mathbf{R} - \mathbf{R}_0\|_{\text{Wed}(\mathbf{K})}^2. \end{aligned} \quad (\text{A.26b})$$

We have the properties

$$\mathbf{K} \geq 0 \Leftrightarrow \hat{\mathcal{V}}(\mathbf{R}) \geq 0 \quad (\text{A.27a})$$

$$\mathbf{K} > 0 \Leftrightarrow \hat{\mathcal{V}}(\mathbf{R}) \geq 0 \wedge \hat{\mathcal{V}}(\mathbf{R}) = 0 \Leftrightarrow \mathbf{R} = \mathbf{R}_0. \quad (\text{A.27b})$$

The form (A.26a) is called the *navigation function* for  $\mathbb{SO}(3)$  in [Koditschek, 1989]. From its properties  $\hat{\mathcal{V}}$  is an  $\mathbb{SO}(3)$  analogon to  $\frac{1}{2}(\mathbf{x} - \mathbf{x}_0)^\top \mathbf{K}(\mathbf{x} - \mathbf{x}_0)$ ,  $\mathbf{x}, \mathbf{x}_0 \in \mathbb{R}^3$ .

## A.4 On error coordinates

**Error coordinates.** Introduce (possibly redundant) error coordinates  $\mathbf{e} \in \mathbb{R}^{\nu_e}$  as

$$\mathbf{e} = \boldsymbol{\chi}_{\text{E}}(\mathbf{x}, \mathbf{x}_{\text{R}}), \quad \dot{\boldsymbol{\phi}}_{\text{E}}(\mathbf{e}) = 0. \quad (\text{A.28})$$

and require that this relation is invertible with  $\mathbf{x} = \boldsymbol{\chi}(\mathbf{e}, \mathbf{x}_{\text{R}})$ , i.e.  $\boldsymbol{\chi}(\boldsymbol{\chi}_{\text{E}}(\mathbf{x}, \mathbf{x}_{\text{R}}), \mathbf{x}_{\text{R}}) = \mathbf{x} \forall \mathbf{x} \in \mathbb{X}$ . The inverse function theorem now implies that the differential  $\nabla \boldsymbol{\chi}_{\text{E}} = \frac{\partial \boldsymbol{\chi}_{\text{E}}}{\partial \mathbf{x}} \mathbf{A}$  has full rank:  $\text{rank}(\nabla \boldsymbol{\chi}_{\text{E}}) = \dim \mathbb{X} = n$ .

Let  $\boldsymbol{\Phi}_{\text{E}}$  be the linear independent rows of  $\partial \boldsymbol{\phi}_{\text{E}} / \partial \mathbf{e}$ . Then the derivative of the geometric constraint  $\dot{\boldsymbol{\phi}}_{\text{E}} = 0$  implies

$$\boldsymbol{\Phi}_{\text{E}} \nabla \boldsymbol{\chi}_{\text{E}} = 0, \quad \boldsymbol{\Phi}_{\text{E}} \nabla_{\text{R}} \boldsymbol{\chi}_{\text{E}} = 0, \quad (\text{A.29})$$

Since the matrices  $\nabla \boldsymbol{\chi}_{\text{E}}$  and  $\boldsymbol{\Phi}_{\text{E}}$  have full rank, their pseudo-inverses are

$$(\nabla \boldsymbol{\chi}_{\text{E}})^+ = ((\nabla \boldsymbol{\chi}_{\text{E}})^\top (\nabla \boldsymbol{\chi}_{\text{E}}))^{-1} (\nabla \boldsymbol{\chi}_{\text{E}})^\top, \quad (\nabla \boldsymbol{\chi}_{\text{E}})^+ (\nabla \boldsymbol{\chi}_{\text{E}}) = \mathbf{I}_n \quad (\text{A.30})$$

$$\boldsymbol{\Phi}_{\text{E}}^+ = \boldsymbol{\Phi}_{\text{E}}^\top (\boldsymbol{\Phi}_{\text{E}} \boldsymbol{\Phi}_{\text{E}}^\top)^{-1}, \quad \boldsymbol{\Phi}_{\text{E}} \boldsymbol{\Phi}_{\text{E}}^+ = \mathbf{I}_{\nu_e - n}. \quad (\text{A.31})$$

Furthermore, due to the orthogonality  $\boldsymbol{\Phi}_{\text{E}} \nabla \boldsymbol{\chi}_{\text{E}} = 0$  we have

$$(\nabla \boldsymbol{\chi}_{\text{E}}) (\nabla \boldsymbol{\chi}_{\text{E}})^+ + \boldsymbol{\Phi}_{\text{E}}^+ \boldsymbol{\Phi}_{\text{E}} = \mathbf{I}_{\nu_e}. \quad (\text{A.32})$$

**Error potential.** We require that the potential  $\bar{\mathcal{V}}$  can be expressed as a function  $\bar{\mathcal{V}}_{\text{E}}$  of the error coordinates  $\mathbf{e}$  alone, i.e.

$$\bar{\mathcal{V}}(\mathbf{x}, \mathbf{x}_{\text{R}}) = \bar{\mathcal{V}}_{\text{E}}(\boldsymbol{\chi}_{\text{E}}(\mathbf{x}, \mathbf{x}_{\text{R}})). \quad (\text{A.33})$$

Now the requirement (4.43) for the transport map  $\mathbf{Q}$  can be written as

$$\begin{aligned} \nabla_{\text{R}} \bar{\mathcal{V}} + \mathbf{Q}^\top \nabla \bar{\mathcal{V}} &= (\nabla_{\text{R}} \boldsymbol{\chi}_{\text{E}} + \nabla \boldsymbol{\chi}_{\text{E}} \mathbf{Q})^\top \frac{\partial \bar{\mathcal{V}}_{\text{E}}}{\partial \mathbf{e}} \\ &= \underbrace{((\nabla \boldsymbol{\chi}_{\text{E}}) (\nabla \boldsymbol{\chi}_{\text{E}})^+ + \boldsymbol{\Phi}_{\text{E}}^+ \boldsymbol{\Phi}_{\text{E}})}_{\mathbf{I}_{\nu_e}} \nabla_{\text{R}} \boldsymbol{\chi}_{\text{E}} + \nabla \boldsymbol{\chi}_{\text{E}} \mathbf{Q} \Big|^\top \frac{\partial \bar{\mathcal{V}}_{\text{E}}}{\partial \mathbf{e}} \\ &= ((\nabla \boldsymbol{\chi}_{\text{E}})^+ (\nabla_{\text{R}} \boldsymbol{\chi}_{\text{E}}) + \mathbf{Q})^\top (\nabla \boldsymbol{\chi}_{\text{E}})^\top \frac{\partial \bar{\mathcal{V}}_{\text{E}}}{\partial \mathbf{e}} + \boldsymbol{\Phi}_{\text{E}}^+ \underbrace{\boldsymbol{\Phi}_{\text{E}} \nabla_{\text{R}} \boldsymbol{\chi}_{\text{E}}}_{0} \frac{\partial \bar{\mathcal{V}}_{\text{E}}}{\partial \mathbf{e}} = 0 \end{aligned} \quad (\text{A.34})$$

which has the simple solution

$$\mathbf{Q} = -(\nabla \boldsymbol{\chi}_{\text{E}})^+ (\nabla_{\text{R}} \boldsymbol{\chi}_{\text{E}}). \quad (\text{A.35})$$

**Error kinematics.** With the same approach as above we can derive a kinematic relation between the error coordinates  $\boldsymbol{e}$  and the error velocity  $\boldsymbol{\xi}_E = \boldsymbol{\xi} - Q\boldsymbol{\xi}_R$  as

$$\begin{aligned}\dot{\boldsymbol{e}} &= (\nabla \boldsymbol{\chi}_E) \boldsymbol{\xi} + (\nabla_R \boldsymbol{\chi}_E) \boldsymbol{\xi}_R \\ &= (\nabla \boldsymbol{\chi}_E) \boldsymbol{\xi} + \underbrace{((\nabla \boldsymbol{\chi}_E)(\nabla \boldsymbol{\chi}_E)^+ + \boldsymbol{\Phi}_E^+ \boldsymbol{\Phi}_E)}_{\mathbf{I}_{\nu_e}} \nabla_R \boldsymbol{\chi}_E \boldsymbol{\xi}_R \\ &= (\nabla \boldsymbol{\chi}_E) \underbrace{(\boldsymbol{\xi} + (\nabla \boldsymbol{\chi}_E)^+ (\nabla_R \boldsymbol{\chi}_E) \boldsymbol{\xi}_R)}_{\boldsymbol{\xi}_E} + \boldsymbol{\Phi}_E^+ \underbrace{\boldsymbol{\Phi}_E (\nabla_R \boldsymbol{\chi}_E)}_0 \boldsymbol{\xi}_R\end{aligned}\quad (\text{A.36})$$

## A.5 A possible generalization of the rigid body energies

Note that any symmetric, positive matrix  $\mathbf{K} \in \mathbb{SYM}^+(6)$  can be decomposed into

$$\mathbf{K} = \begin{bmatrix} \mathbf{I}_3 & \mathbf{0} \\ \mathbf{H} & \mathbf{I}_3 \end{bmatrix} \begin{bmatrix} \mathbf{K}_r & \mathbf{0} \\ \mathbf{0} & \mathbf{K}_R \end{bmatrix} \begin{bmatrix} \mathbf{I}_3 & \mathbf{H}^\top \\ \mathbf{0} & \mathbf{I}_3 \end{bmatrix} = \begin{bmatrix} \mathbf{K}_r & \mathbf{K}_r \mathbf{H}^\top \\ \mathbf{H} \mathbf{K}_r & \mathbf{K}_R + \mathbf{H} \mathbf{K}_r \mathbf{H}^\top \end{bmatrix} \quad (\text{A.37})$$

where  $\mathbf{K}_r, \mathbf{K}_R \in \mathbb{SYM}^+(3)$  and  $\mathbf{H} \in \mathbb{R}^{3 \times 3}$ . For variables  $\mathbf{x}_i \in \mathbb{R}^3$  and  $\mathbf{Y}_i \in \mathbb{R}^{3 \times 3}$  collected in the square matrix  $\boldsymbol{\Xi}_i = [\begin{smallmatrix} \mathbf{Y}_i & \mathbf{x}_i \\ \mathbf{0} & 1 \end{smallmatrix}]$  define the inner product as

$$\langle \boldsymbol{\Xi}_1, \boldsymbol{\Xi}_2 \rangle_{\mathbf{K}} = \tilde{\mathbf{x}}_1^\top \mathbf{K}_r \tilde{\mathbf{x}}_2 + \text{tr}(\mathbf{Y}_1 \text{Vee}(\mathbf{K}_R) \mathbf{Y}_2^\top), \quad (\text{A.38})$$

where  $\tilde{\mathbf{x}}_i = \mathbf{x}_i + \frac{1}{2} \mathbf{Y}_i \text{vee2}(\mathbf{H}) + \frac{1}{4} (\mathbf{H} + \mathbf{H}^\top) \text{vee2}(\mathbf{Y}_i)$ . To prove that this is indeed an inner product one can use the same argument as in ?? and note that positive definiteness of  $\mathbf{K}_R$  implies positive definiteness of  $\text{Vee}(\mathbf{K}_R)$ . For the special parameters  $\mathbf{K}_r = k\mathbf{I}_3$  and  $\mathbf{H} = \text{wed}(\mathbf{h})$ ,  $\mathbf{h} \in \mathbb{R}^3$  this inner product coincides with the definition of (A.5). For the special arguments  $\mathbf{Y}_i = \text{wed}(\mathbf{y}_i)$ ,  $\mathbf{y}_i \in \mathbb{R}^3$  we have the following simplifications  $\tilde{\mathbf{x}}_i = \mathbf{x}_i + \mathbf{H}^\top \mathbf{y}_i$  and  $\text{tr}(\text{wed}(\mathbf{y}_1) \text{Vee}(\mathbf{K}_R) \text{wed}(\mathbf{y}_2)^\top) = \mathbf{y}_1^\top \mathbf{K}_R \mathbf{y}_2$ . So, for the case  $\boldsymbol{\Xi}_i = \text{wed}(\boldsymbol{\xi}_i)$ ,  $\boldsymbol{\xi}_i = [\mathbf{x}_i^\top, \mathbf{y}_i^\top]^\top$  the inner product (A.38) simplifies to

$$\langle \text{wed}(\boldsymbol{\xi}_1), \text{wed}(\boldsymbol{\xi}_2) \rangle_{\mathbf{K}} = \boldsymbol{\xi}_1^\top \mathbf{K} \boldsymbol{\xi}_2. \quad (\text{A.39})$$

For any inner product we may define an induced norm and metric as

$$\|\boldsymbol{\Xi}\|_{\mathbf{K}} = \sqrt{\langle \boldsymbol{\Xi}, \boldsymbol{\Xi} \rangle_{\mathbf{K}}}, \quad d_{\mathbf{K}}(\boldsymbol{\Xi}_1, \boldsymbol{\Xi}_2) = \|\boldsymbol{\Xi}_1 - \boldsymbol{\Xi}_2\|_{\mathbf{K}}. \quad (\text{A.40})$$

Note that the same inner product, norm and metric can also be defined for elements of the form  $\boldsymbol{\Xi}_i = [\begin{smallmatrix} \mathbf{Y}_i & \mathbf{x}_i \\ \mathbf{0} & 1 \end{smallmatrix}]$ .

With this we may define the following energies as the square of the metrics

$$\mathcal{V} = \frac{1}{2} d_{\mathbf{K}}^2(\mathbf{G}, \mathbf{G}_R), \quad \mathbf{K} \in \mathbb{SYM}^+(6), \quad (\text{A.41a})$$

$$\mathcal{R} = \frac{1}{2} d_{\mathbf{D}}^2(\dot{\mathbf{G}}, \dot{\mathbf{G}}_R), \quad \mathbf{D} \in \mathbb{SYM}^+(6), \quad (\text{A.41b})$$

$$\mathcal{T} = \frac{1}{2} d_{\mathbf{M}}^2(\ddot{\mathbf{G}}, \ddot{\mathbf{G}}_R), \quad \mathbf{M} \in \mathbb{SYM}^+(6). \quad (\text{A.41c})$$

For the special parameters  $\mathbf{K}_r = k\mathbf{I}_3$  and  $\mathbf{H} = \text{wed}(\mathbf{h})$ ,  $\mathbf{h} \in \mathbb{R}^3$  this coincides with the energies defined in (4.11). Alternatively, using  $\mathbf{G}_E = \mathbf{G}_R^{-1} \mathbf{G}$ , we may define

$$\mathcal{V} = \frac{1}{2} d_{\mathbf{K}}^2(\mathbf{G}_E, \mathbf{I}_4), \quad \mathbf{K} \in \mathbb{SYM}^+(6), \quad (\text{A.42a})$$

$$\mathcal{R} = \frac{1}{2} d_{\mathbf{D}}^2(\dot{\mathbf{G}}_E, \mathbf{0}), \quad \mathbf{D} \in \mathbb{SYM}^+(6), \quad (\text{A.42b})$$

$$\mathcal{T} = \frac{1}{2} d_{\mathbf{M}}^2(\ddot{\mathbf{G}}_E, \mathbf{0}), \quad \mathbf{M} \in \mathbb{SYM}^+(6), \quad (\text{A.42c})$$

For the special parameters mentioned above, this coincides with the energies defined in (4.20).

The inner product and its induced norm and metric can be regarded as a generalization of the inner product (with 10 parameters) proposed in ?? in the sense that it incorporates all 21 independent coefficients of the symmetric matrix  $\mathbf{K} \in \text{SYM}^+(6)$ . This results in more tuning parameters for the control design. On the downside, the translation invariance (??) and the physical interpretation of the parameters are lost for the general case.

# Bibliography

- [Arnold, 1989] Arnold, V. I. (1989). *Mathematical Methods of Classical Mechanics*, volume 60 of *Graduate Texts in Mathematics*. Springer, New York.
- [Bloch et al., 2000] Bloch, A. M., Leonard, N. E., and Marsden, J. E. (2000). Controlled Lagrangians and the stabilization of mechanical systems. I. The first matching theorem. *IEEE Trans. on Automatic Control*, 45(12):2253–2270.
- [Boltzmann, 1897] Boltzmann, L. (1897). *Vorlesungen ueber die Pincipe der Mechanik*. Johann Ambrosius Barth.
- [Boltzmann, 1902] Boltzmann, L. (1902). Über die Form der Lagrangeschen Gleichungen für nichtholonom, generalisierte Koordinaten. In *Wissenschaftliche Abhandlungen*, volume 3, pages 682–692. Johann Ambrosius Barth.
- [Bremer, 2008] Bremer, H. (2008). *Elastic Multibody Dynamics: A Direct Ritz Approach*. Springer.
- [Bristeau et al., 2009] Bristeau, P.-J., Martin, P., Salaün, E., and Petit, N. (2009). The role of propeller aerodynamics in the model of a quadrotor uav. In *Proc. ECC 2009*, pages 683–688.
- [Bullo and Murray, 1999] Bullo, F. and Murray, R. M. (1999). Tracking for fully actuated mechanical systems: A geometric framework. *Automatica*, 35(1):17–34.
- [Courant and Hilbert, 1924] Courant, R. and Hilbert, D. (1924). *Methoden der Mathematischen Physik*. Julius Springer.
- [Desloge, 1987] Desloge, E. A. (1987). Relationship between Kane’s equations and the Gibbs-Appell equations. *Journal of Guidance, Control, and Dynamics*, 10(1):120–122.
- [Fliess et al., 1999] Fliess, M., Levine, J., Martin, P., and Rouchon, P. (1999). A Lie-Bäcklund approach to equivalence and flatness of nonlinear systems. *IEEE Trans. Automat. Contr.*, 44(5):922–937.
- [Fliess et al., 1995] Fliess, M., L’evine, J., and Rouchon, P. M. M. (1995). Flatness and defect of non-linear systems: introductory theory and examples. *International Journal of Control*, 61(6):1327–1361.
- [Fritsch, 2014] Fritsch, O. (2014). *Energiebasierte Lage- und Positionsfolgeregelung für einen Quadrocopter*. PhD thesis, Technische Universität München.

- [Galilei, 1638] Galilei, G. (1638). *Discorsi e dimostrazioni matematiche intorno a due nuove scienze.*
- [Gauß, 1829] Gauß, C. F. (1829). Über ein neues allgemeines Grundgesetz der Mechanik. *Journal für die reine und angewandte Mathematik.*
- [Goldstein, 1951] Goldstein, H. (1951). *Classical Mechanics.* Addison-Wesley.
- [Graffarend and Kühnel, 2011] Graffarend, E. W. and Kühnel, W. (2011). A minimal atlas for the rotation group  $\text{SO}(3)$ . *GEM-International Journal on Geomathematics*, 2(1):113–122.
- [Hall, 2015] Hall, B. (2015). *Lie Groups, Lie Algebras, and Representations*, volume 222 of *Graduate Texts in Mathematics*. Springer, 2nd edition.
- [Hamel, 1904] Hamel, G. (1904). Die Lagrange-Eulerschen Gleichungen der Mechanik. *Z. für Mathematik u. Physik*, 50:1–57.
- [Hamel, 1949] Hamel, G. (1949). *Theoretische Mechanik.* Springer.
- [Hamel et al., 2002] Hamel, T., Mahony, R., Lozano, R., and Ostrowski, J. (2002). Dynamic Modelling and configuration stabilization for an X4-Flyer. In *Proc. 15th Triennial IFAC World Congress*, pages 217–222.
- [Hauser et al., 1992] Hauser, J., Sastry, S., and Meyer, G. (1992). Nonlinear control design for slightly non-minimum phase systems: Application to V/STOL aircraft. *Automatica*, 28(4):664–679.
- [Hooke, 1678] Hooke, R. (1678). *Lectures De Potentia Restitutiva, or of Spring. Explaining the Power of Springing Bodies.* Printed for John Martyn Printer to the Royal Society.
- [Horn and Johnson, 1985] Horn, R. A. and Johnson, C. R. (1985). *Matrix Analysis.* Cambridge University Press.
- [Johnson, 1980] Johnson, W. (1980). *Helicopter Theory.* Princeton University Press.
- [Kabsch, 1976] Kabsch, W. (1976). A solution for the best rotation to relate two sets of vectors. *Acta Crystallographica*, A32(5):922.
- [Kane and Levinson, 1985] Kane, T. R. and Levinson, D. A. (1985). *Dynamics.* McGraw Hill.
- [Koditschek, 1989] Koditschek, D. E. (1989). The Application of Total Energy as a Lyapunov Function for Mechanical Control Systems. In Marsden, J. E., Krishnaprasad, P. S., and Simo, J. C., editors, *Dynamics and Control of Multibody Systems*, volume 97 of *Contemporary Mathematics*, pages 131–157. American Mathematical Society.
- [Konz and Rudolph, 2013] Konz, M. and Rudolph, J. (2013). Quadrotor tracking control based on a moving frame. In *Proc. 9th IFAC Symposium on Nonlinear Control Systems*, pages 80–85.

- [Konz and Rudolph, 2016] Konz, M. and Rudolph, J. (2016). Beispiele für einen direkten Zugang zu einer globalen, energiebasierten Modellbildung und Regelung von Starrkörperpersystemen. *at - Automatisierungstechnik*, 64(2):96–109.
- [Lanczos, 1986] Lanczos, C. (1986). *The Variational Principles of Mechanics*. Dover Publications, 4 edition.
- [Landau and Lifshitz, 1960] Landau, L. D. and Lifshitz, E. M. (1960). *Mechanics*, volume 1 of *Course of Theoretical Physics*. Pergamon Press.
- [Lee, 2003] Lee, J. M. (2003). *Introduction to Smooth Manifolds*. Springer.
- [Lesser, 1992] Lesser, M. (1992). A geometric interpretation of kane's equations. *Proceedings of the Royal Society of London*, 436(1896):69–87.
- [Luenberger and Ye, 2015] Luenberger, D. G. and Ye, Y. (2015). *Linear and Nonlinear Programming*. Springer, 4th edition.
- [Lurie, 2002] Lurie, A. I. (2002). *Analytical Mechanics*. Springer.
- [Martin et al., 1997] Martin, P., Murray, R. M., and Rouchon, P. (1997). Flat systems, equivalence and trajectory generation. In *Mini-course ECC'97*.
- [Martin and Salaun, 2010] Martin, P. and Salaun, E. (2010). The true role of accelerometer feedback in quadrotor control. In *IEEE Int. Conf. on Robotics and Automation*, pages 1623–1629.
- [Mellinger et al., 2012] Mellinger, D., Michael, N., and Kumar, V. (2012). Trajectory Generation and Control for Precise Aggressive Maneuvers with Quadrotors. *Int. J. Rob. Res.*, 31(5):664–674.
- [Misner et al., 1973] Misner, C. W., Thorne, K. S., and Wheeler, J. A. (1973). *Gravitation*. W. H. Freeman and Company.
- [Murray et al., 1994] Murray, R. M., Li, Z., and Sastry, S. S. (1994). *A Mathematical Introduction to Robotic Manipulation*. CRC Press.
- [Murray et al., 1995] Murray, R. M., Rathinam, M., and Sluis, W. (1995). Differential flatness of mechanical control systems: A catalog of prototype systems. In *Proceedings of the ASME International Congress and Exposition*.
- [Neimark and Fufaev, 1972] Neimark, J. I. and Fufaev, N. A. (1972). *Dynamics of Nonholonomic Systems*. Amer. Mathem. Society.
- [Newton, 1687] Newton, I. (1687). *Philosophiae naturalis principia mathematica*. Jussu Societatis Regiae ac Typis Josephi Streater.
- [Newton, 1846] Newton, I. (1846). *The Mathematical Principles of Natural Philosophy, Translated into English by A. Motte and N. W. Chittenden*. Daniel Adee.
- [Nocedal and Wright, 2006] Nocedal, J. and Wright, S. J. (2006). *Numerical Optimization*. Springer, 2nd edition.

- [Olfati-Saber, 2001] Olfati-Saber, R. (2001). *Nonlinear Control of Underactuated Mechanical Systems with Applications to Robotics and Aerospace Vehicles*. PhD thesis, Massachusetts Institute of Technology, Cambridge, MA.
- [Papastavridis, 2002] Papastavridis, J. G. (2002). *Analytical Mechanics*. World Scientific.
- [Penrose, 1955] Penrose, R. (1955). A generalized inverse for matrices. *Mathematical proceedings of the Cambridge philosophical society*, 51(3):406–413.
- [Pfeiffer and Glocker, 1996] Pfeiffer, F. and Glocker, C. (1996). *Multibody Dynamics with unilateral contacts*. Wiley-VCH.
- [Päsler, 1968] Päsler, M. (1968). *Prinzip der Mechanik*. Walter de Gruyter & Co.
- [Rathinam and Murray, 1998] Rathinam, M. and Murray, R. M. (1998). Configuration flatness of lagrangian systems underactuated by one control. *SIAM Journal of Control and Optimization*, 36(1):164–179.
- [Rayleigh, 1877] Rayleigh, J. W. S. B. (1877). *The Theory of Sound*. Macmillan and Co.
- [Roberson and Schwertassek, 1988] Roberson, R. E. and Schwertassek, R. (1988). *Dynamics of Multibody Systems*. Springer.
- [Schlacher and Schöberl, 2007] Schlacher, K. and Schöberl, M. (2007). Construction of flat outputs by reduction and elimination. *CD Proceedings IFAC Symposium on Non-linear Control Systems*, pages 666–671.
- [Shabana, 2005] Shabana, A. A. (2005). *Dynamics of Multibody Systems*. Cambridge University Press, 3 edition.
- [Slotine and Li, 1991] Slotine, J.-J. and Li, W. (1991). *Applied Nonlinear Control*. Springer.
- [Spong et al., 2006] Spong, M. W., Hutchinson, S., and Vidyasagar, M. (2006). *Robot Modeling and Control*. Wiley.
- [Szabó, 1956] Szabó, I. (1956). *Höhere Technische Mechanik*. Springer.
- [Wahba, 1965] Wahba, G. (1965). A least squares estimate of satellite attitude. *SIAM Review*, 7(3):409.
- [Wittenburg, 2008] Wittenburg, J. (2008). *Dynamics of Multibody Systems*. Springer, 2 edition.

# Appendix B

## Templates

### B.1 Math fonts

#### Latin alphabet in math mode

default	$A B C D E F G H I J K L M N O P Q R S T U V W X Y Z$ $a b c d e f g h i j k l m n o p q r s t u v w x y z$
mathrm	$A B C D E F G H I J K L M N O P Q R S T U V W X Y Z$ $a b c d e f g h i j k l m n o p q r s t u v w x y z$
mathsf	$A B C D E F G H I J K L M N O P Q R S T U V W X Y Z$ $a b c d e f g h i j k l m n o p q r s t u v w x y z$
mathtt	$A B C D E F G H I J K L M N O P Q R S T U V W X Y Z$ $a b c d e f g h i j k l m n o p q r s t u v w x y z$
boldsymbol	$A B C D E F G H I J K L M N O P Q R S T U V W X Y Z$ $a b c d e f g h i j k l m n o p q r s t u v w x y z$
mathbf	$A B C D E F G H I J K L M N O P Q R S T U V W X Y Z$ $a b c d e f g h i j k l m n o p q r s t u v w x y z$
mathfrak	$\mathfrak{A} \mathfrak{B} \mathfrak{C} \mathfrak{D} \mathfrak{E} \mathfrak{F} \mathfrak{G} \mathfrak{H} \mathfrak{I} \mathfrak{J} \mathfrak{K} \mathfrak{L} \mathfrak{M} \mathfrak{N} \mathfrak{O} \mathfrak{P} \mathfrak{Q} \mathfrak{R} \mathfrak{S} \mathfrak{T} \mathfrak{U} \mathfrak{V} \mathfrak{W} \mathfrak{X} \mathfrak{Y} \mathfrak{Z}$ $\mathfrak{a} \mathfrak{b} \mathfrak{c} \mathfrak{d} \mathfrak{e} \mathfrak{f} \mathfrak{g} \mathfrak{h} \mathfrak{i} \mathfrak{j} \mathfrak{k} \mathfrak{l} \mathfrak{m} \mathfrak{n} \mathfrak{o} \mathfrak{p} \mathfrak{q} \mathfrak{r} \mathfrak{s} \mathfrak{t} \mathfrak{u} \mathfrak{v} \mathfrak{w} \mathfrak{x} \mathfrak{y} \mathfrak{z}$
mathcal	$\mathcal{A} \mathcal{B} \mathcal{C} \mathcal{D} \mathcal{E} \mathcal{F} \mathcal{G} \mathcal{H} \mathcal{I} \mathcal{J} \mathcal{K} \mathcal{L} \mathcal{M} \mathcal{N} \mathcal{O} \mathcal{P} \mathcal{Q} \mathcal{R} \mathcal{S} \mathcal{T} \mathcal{U} \mathcal{V} \mathcal{W} \mathcal{X} \mathcal{Y} \mathcal{Z}$
mathbb	$\mathbb{A} \mathbb{B} \mathbb{C} \mathbb{D} \mathbb{E} \mathbb{F} \mathbb{G} \mathbb{H} \mathbb{I} \mathbb{J} \mathbb{K} \mathbb{L} \mathbb{M} \mathbb{N} \mathbb{O} \mathbb{P} \mathbb{Q} \mathbb{R} \mathbb{S} \mathbb{T} \mathbb{U} \mathbb{V} \mathbb{W} \mathbb{X} \mathbb{Y} \mathbb{Z}$

### Greek alphabet in math mode

default	$\Gamma \Delta \Theta \Lambda \Xi \Pi \Sigma \Upsilon \Phi \Psi \Omega$
$\alpha \beta \gamma \delta \epsilon \zeta \eta \theta \iota \kappa \lambda \mu \nu \xi \circ \pi \rho \sigma \tau \upsilon \phi \chi \psi \omega$	
var	$A B \Gamma \Delta E Z H \Theta I K \Lambda M N \Xi O \Pi P \Sigma T \Upsilon \Phi X \Psi \Omega$
	$\varepsilon \vartheta \varpi \varrho \varsigma \varphi$
boldsymbol	$\Gamma \Delta \Theta \Lambda \Xi \Pi \Sigma \Upsilon \Phi \Psi \Omega$
$\alpha \beta \gamma \delta \epsilon \zeta \eta \theta \iota \kappa \lambda \mu \nu \xi \circ \pi \rho \sigma \tau \upsilon \phi \chi \psi \omega$	
var	$A B \Gamma \Delta E Z H \Theta I K \Lambda M N \Xi O \Pi P \Sigma T \Upsilon \Phi X \Psi \Omega$
	$\varepsilon \vartheta \varpi \varrho \varsigma \varphi$
mathsf	$A B \Gamma \Delta E Z H \Theta I K \Lambda M N \Xi O \Pi P \Sigma T \Upsilon \Phi X \Psi \Omega$
$\alpha \beta \gamma \delta \epsilon \zeta \eta \theta \iota \kappa \lambda \mu \nu \xi \circ \pi \rho \sigma \tau \upsilon \phi \chi \psi \omega$	
mathbf	$\mathbf{A} \mathbf{B} \mathbf{\Gamma} \mathbf{\Delta} \mathbf{E} \mathbf{Z} \mathbf{H} \mathbf{\Theta} \mathbf{I} \mathbf{K} \mathbf{\Lambda} \mathbf{M} \mathbf{N} \mathbf{\Xi} \mathbf{O} \mathbf{\Pi} \mathbf{P} \mathbf{\Sigma} \mathbf{T} \mathbf{\Upsilon} \mathbf{\Phi} \mathbf{X} \mathbf{\Psi} \mathbf{\Omega}$

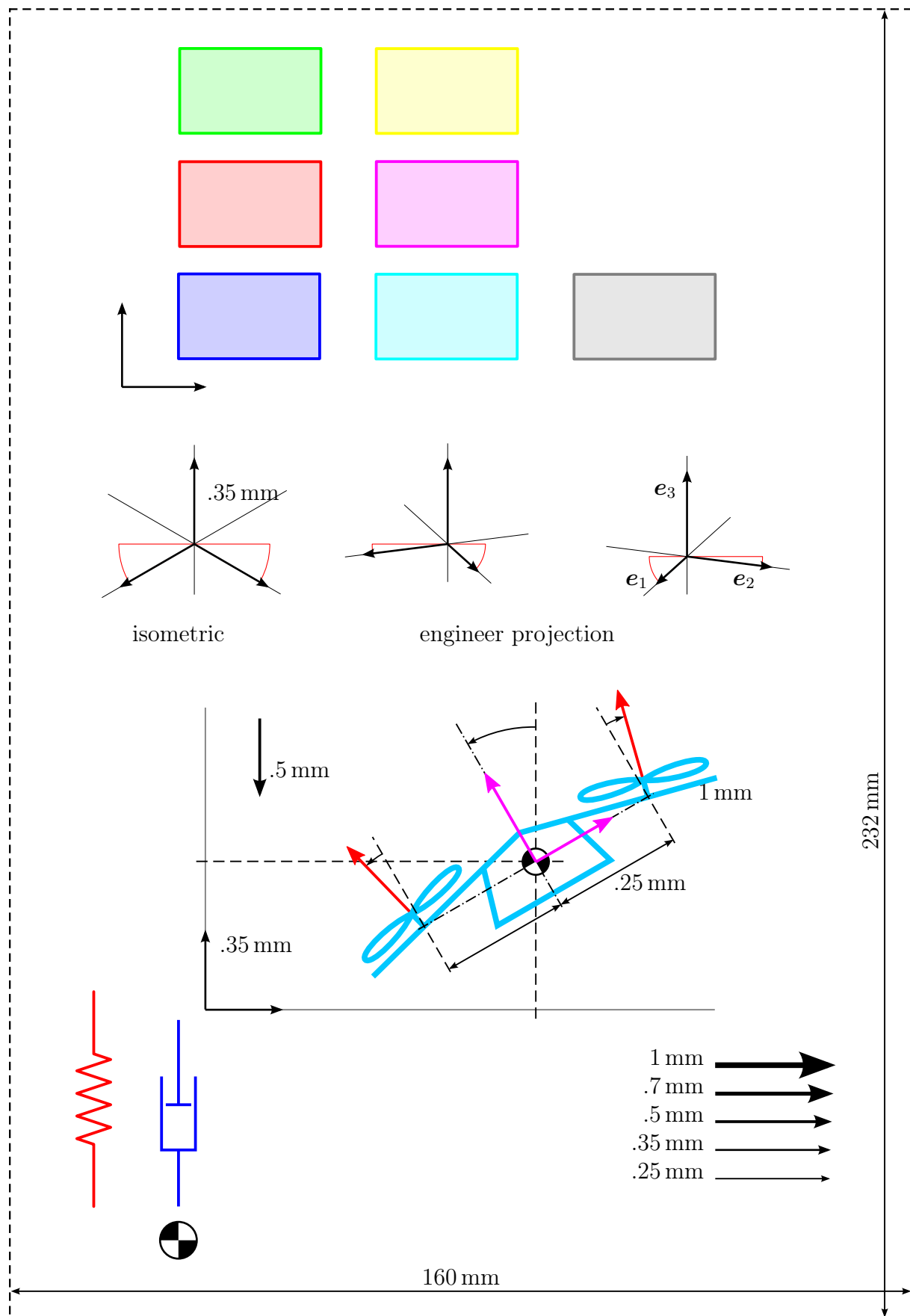


Figure B.1: Inkscape figure template